UNCLASSIFIED

CONFIDENTIAL

Classification Changed to
UNCLASSIFIED
Authority
LETTER FROM W. E. HANSEN MGR. SECURITY + PLANT PROTECTION SECTION TO NASA
Date
8-8-72
By
G. Lemon
LANGLEY RESEARCH CENTER
REF. JPL-751: LRL: cd
NOV. 4, 1970

Space Programs Summary No. 37-27, Volume I

for the period March 1, 1964 to April 30, 1964

The Lunar Program

(Title Unclassified)

JET PROPULSION LABORATORY
LIBRARY
JUN 16 1964
00606
Copy No.

CALIFORNIA INSTITUTE OF TECHNOLOGY

JET PROPULSION LABORATORY
CALIFORNIA INSTITUTE OF TECHNOLOGY
PASADENA, CALIFORNIA

May 31, 1964

CONFIDENTIAL

GROUP 4 Downgraded at 3 year intervals; declassified after 12 years.

UNCLASSIFIED

Preface

The *Space Programs Summary* is a six volume, bimonthly publication designed to report on JPL space exploration programs, and related supporting research and advanced development projects. The subtitles of all volumes of the *Space Programs Summary* are:

Vol. I. The Lunar Program (Confidential)

Vol. II. The Planetary–Interplanetary Program (Confidential)

Vol. III. The Deep Space Network (Unclassified)

Vol. IV. Supporting Research and Advanced Development (Unclassified)

Vol. V. Supporting Research and Advanced Development (Confidential)

Vol. VI. Space Exploration Programs and Space Sciences (Unclassified)

The *Space Programs Summary,* Volume VI consists of an unclassified digest of appropriate material from Volumes I, II, and III and a reprint of the space science instrumentation studies of Volumes I and II.

Beginning with the *Space Programs Summary 37-27* series, the Space Flight Operations Facility development progress, previously reported in Volume VI, will be reported in Volume III. The scope of Volume III is being expanded to incorporate the activities of the Deep Space Network.

W. H. Pickering, *Director*
Jet Propulsion Laboratory

Space Programs Summary No. 37-27, Volume I

Copyright © 1964, Jet Propulsion Laboratory, California Institute of Technology

Prepared under Contract No. NAS 7-100, National Aeronautics & Space Administration

This document contains information affecting the national defense of the United States, within the meaning of the Espionage Laws, Title 18, U.S.C., Sections 793 and 794, the transmission or revelation of which in any manner to an unauthorized person is prohibited by law. [redacted]

Contents

I. *Ranger* Project 1
A. Introduction 1
B. Systems 3
C. Guidance and Control 5
D. Propulsion 7
E. Supporting Activities and Engineering Facilities 8
References 10

II. *Ranger* TV Subsystem, Block III 11
A. System Engineering 11
B. Cameras 14
C. Telecommunications 14
D. Power 14
E. Thermal Control 15
F. Electrical Power Supply 15

III. *Surveyor* Project 16
A. Introduction 16
B. Systems 16
C. Space Sciences 18
References 21

IV. *Surveyor* Spacecraft System 22
A. System Engineering 24
B. Scientific Payload 26
C. System Analysis 35
D. Flight Control 44
E. Electronics 49
F. Electrical Power Supply 59
G. Thermal Control 67
H. Engineering Mechanics 75
I. Propulsion 84
J. Spacecraft Vehicle and Mechanisms for Basic Bus 90
K. Reliability, Quality Assurance and System Test 93
L. Mission Operations 126
M. Study on Block II *Surveyor* 137

I. *Ranger* Project

A. Introduction

The *Ranger* Project was established to develop a space flight technology for transporting engineering and scientific instruments to the Moon and planets. Nine *Ranger* launchings, using *Atlas D–Agena B* vehicles, are now planned; six of these flights have been made.

Rangers 1 and *2* (Block I) were not lunar-oriented, but were engineering evaluation flights to test the basic systems to be employed in later lunar and planetary missions. Several scientific experiments were carried on a non-interference basis. Indications are that both spacecraft performed satisfactorily within the constraints of the obtained satellite orbit. *Rangers 3, 4,* and *5* (Block II) carried a gamma-ray instrument, a TV camera, and a rough-landing seismometer capsule; all three of these flights experienced failures.

The objective of the *Ranger* Block III (*Rangers 6* through *9*) flights is to obtain TV pictures of the lunar surface which will be of benefit to both the scientific program and the U.S. manned lunar flight program. The *Ranger 6* spacecraft, which was launched from Cape Kennedy, Florida, on January 30, 1964, and impacted the Moon on target on February 2, 1964, did not accomplish the primary flight objective due to a failure of the TV subsystem to transmit pictures. An extensive failure analysis was conducted, resulting in JPL Engineering Planning Document 205, which covered the findings as well as recommendations for inclusion in the *Ranger 7* through *9* configuration.

The *Ranger 7* spacecraft was shipped to Cape Kennedy on January 29; however, as a result of the investigation on *Ranger 6*, the TV subsystem was returned to RCA and the spacecraft bus to JPL. Assembly of the *Ranger 8* spacecraft was complete and system tests had been performed. Assembly of *Ranger 9* was under way. The *Ranger 8* TV subsystem was returned to RCA.

This reporting period has seen an intense effort to implement the modifications indicated by the *Ranger 6* failure review. RCA has been working on a 7-day, 24-hr

basis for the redesign, rework, testing, and integration of the TV subsystem for both the proof test model (PTM) and *Ranger* 7. A JPL task team, consisting of 25 to 30 engineering personnel, took up residence at RCA for the detailed review and monitoring of the design, implementation, and testing of the preventive measures taken to preclude what are believed to be the most probable causes of the *Ranger 6* failure. Also, an additional team at JPL undertook a detailed review of other areas of the TV subsystem for assurance that there are no other areas of concern.

Modifications to the spacecraft bus were very minor and were accomplished without difficulty. During this period the PTM TV subsystem was modified, tested, and shipped to JPL for assembly with the PTM bus. An extensive testing program was started and is continuing. The *Ranger* 7 TV subsystem was modified and tested; a comprehensive assessment of acceptability for shipment was under way during the last days of this reporting period.

Ranger Block IV, planned as a series of three flights, was cancelled by the Office of Space Sciences, NASA, on July 12, 1963, due to budgetary constraints.

Ranger Block V, planned as a six-flight series, was cancelled on December 13, 1963, by the Office of Space Sciences, NASA. By reassignment, appropriate JPL and contractor Block V personnel were placed in direct support of *Ranger* Block III and *Mariner* Projects.

B. Systems

1. Spacecraft Design Integration, Block III

The required design changes for the *Ranger* spacecraft have been restricted to those changes that provide a significant improvement in reliability. The basic *Ranger* bus will remain the same as that of *Ranger 6*, with the most significant changes being those required to interface with the TV subsystem.

The bus changes required to accommodate the TV subsystem consist of: (1) rewiring the hydraulic timer to provide a TV enable function at separation + 30 min, (2) rewiring the solar panel actuation microswitch to provide redundant enabling to the TV subsystem, and (3) modifying the spacecraft wiring to be compatible with the new TV enabling functions. In order to provide further separation between the two sides of the TV subsystem, the Real-Time Command (RTC) 7 relay has been rewired to utilize one set of contacts to turn on one side of the TV subsystem and a second set to turn on the other side.

As a result of the temperature data obtained from the *Ranger 6* flight, a thermal control shield has been added to reduce the temperature of the Earth sensor.

An insulation breakdown of the midcourse-motor chamber temperature transducer was observed during the *Ranger 6* flight. This breakdown can unbalance the data-encoder temperature bridge and cause the invalidation of eight other temperature measurements. Since the temperature transducer performs no flight function and is monitored only during the midcourse portion of the mission, this transducer will be removed.

A review of the Sun-reacquire backup function (RTC-8) revealed that the connection of the reset side of the central computer and sequencer (CC&S) motor start relay to the output of the B + 30 relay driver will provide the CC&S with reset capability such that a midcourse maneuver can be re-initiated after being inhibited by RTC-8. Since the modification required to provide the additional capability was relatively minor, the change was made.

The launch complex and system test complex wiring changes required to provide the proper interface for the TV subsystem are being incorporated. The launch complex change consisted of adding to the umbilical J-box a separate full-power inhibit for both sides of the TV subsystem. The system test complex change consisted of moving a wire from one pin to another in the system test J-box to provide compatibility between the spacecraft and the TV operational support equipment.

As a safeguard to the spacecraft during test, isolation resistors have been added in the operational-support-equipment power monitor J-box.

2. Space Flight Operations

The *Ranger* Block III space flight operations (SFO) have been moved from JPL Buildings 125, 190, and 202 to the new Space Flight Operations Facility (SFOF), Building 230. The *Ranger* Block III Test Plan (Engineering Planning Document 170) was revised to reflect the change from Building 125 operations control to the SFOF centralized control. The SFO Plan for *Ranger* Block III is being revised and will be published on May 4, 1964. The *Ranger 6* SFO Memorandum will be published by mid-May 1964.

The first *Ranger* test in the new SFOF, held April 2, 1964, was designed to prove the compatibility of the new SFOF computer system and the *Ranger* data. The test was scheduled for approximately 4 hr, and all tracking, telemetry, and science data were processed through the computer system. The few program errors which were detected were easily corrected, and, as of April 2, 1964, all programs have been approved by the *Ranger* SFO director.

3. Ranger Block III Proof Test Model

Following the *Ranger 6* flight, the Block III schedule was revised as shown in Table 1. After the *Ranger 6* mission, the proof test model (PTM) was used in several special tests which were performed in an effort to answer questions resulting from the analysis of the *Ranger 6* mission. After the tests were completed, the TV subsystem was sent to the Astro-Electronics Division of RCA for rework. On March 16, 1964, the PTM was disassembled and inspected in order to bring it as near as possible to the Block III configuration and to produce a spacecraft which can successfully pass the planned environmental tests. During this period, the electronic assemblies were removed, microscopically inspected, and modified as required. The bus structure was inspected, and the ring harness was reworked for TV modifications. Both attitude-control nitrogen-gas systems were removed to repair leaks.

The PTM TV subsystem arrived at JPL from RCA on March 1. Postshipment checks showed the subsystem to be in good condition. The TV telemetry calibrations were performed by April 7, and the TV subsystem and bus were mated on April 10.

The attitude-control gas system leak test was performed during the week of April 7. The leak rate for the system was evaluated at 60 ± 10 cm³/hr.

A system test was performed on the spacecraft on April 13 to establish proper operation of the spacecraft prior to the vibration tests. Preparation for the vibration tests was accomplished April 14 and 15, and the spacecraft was transported to the JPL Environmental Test Laboratory on April 15. The vibration tests, conducted April 16 to 24, included x-, y-, and z-axis vibrations and also a torsional vibration on the Lockheed Missiles and Space Company (LMSC) adapter. Fig. 1 illustrates the configuration for the y-axis vibration. The following problems occurred during these tests: (1) a capacitor failure in the power sync module, (2) a Sun sensor failure and the gyro saturation problem during the z-axis shake, and (3) an out-of-tolerance indication in the three-phase inverter power monitor during the lower-noise-level z-axis test. These problems are still under investigation.

Prior to and following the vibration sequence, a modal fitness survey was performed. All indications were that no damage or change occurred in the spacecraft structure.

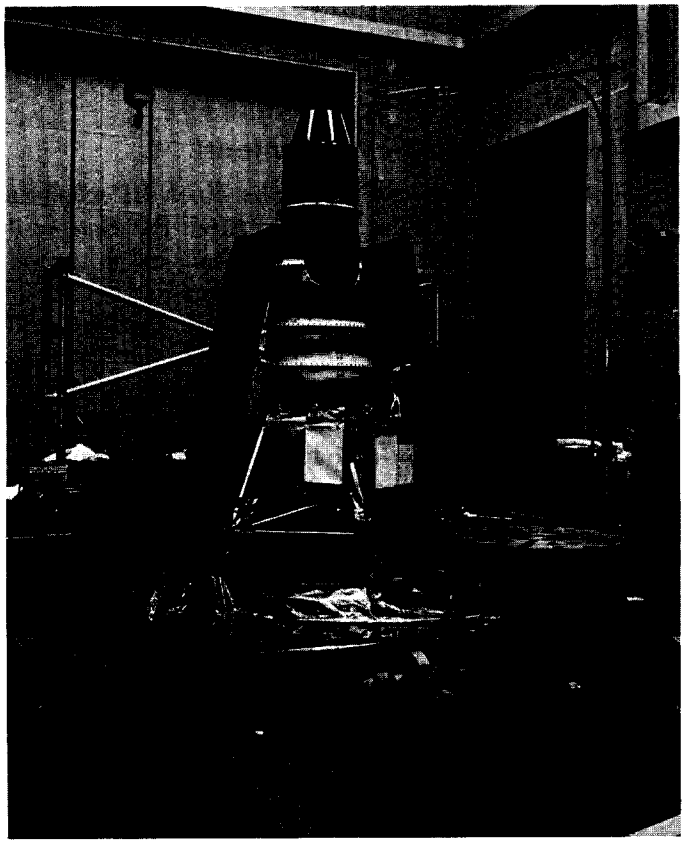

Fig. 1. Configuration for y-axis vibration of the PTM

4. Ranger 7 Assembly and Test Operations

Due to the revision of the *Ranger* Block III schedule (Table 1), the TV subsystem was shipped back to RCA for rework. The TV subsystem is presently being reassembled at RCA and is due to arrive at JPL on May 2.

The *Ranger 7* bus was shipped from the Atlantic Missile Range (AMR) and arrived at JPL on March 28. Changes in the flight hardware and rework on the *Ranger 7* bus consisted of the following:

(1) Both attitude-control nitrogen-gas systems were replaced because of contamination and leak-rate problems.

(2) Two Engineering Change Requirements were incorporated in the central computer and sequencer, including the addition of a capacitor and the removal of a diode to enable a maneuver to be rerun in the event of a Real-Time Command 8 maneuver inhibit. The central computer and sequencer was then reinstalled on the bus.

(3) Both solar panels were replaced because hinges had been damaged.

(4) The ring harness and backup command timer were reworked because of TV modifications and were then reinstalled on the bus.

A flight pressure leak test was conducted on the attitude-control gas system in the JPL Building 179 pit area. The test was completed on April 10, and preliminary results indicated a leak rate well within specification.

All changes were checked out in subsystem tests, and a system test was performed April 22 without the TV subsystem. There were no spacecraft problems during the test.

5. Ranger 8 Assembly and Test Operations

At the beginning of this reporting period, the revised Block III schedule was not yet available. All electronic assemblies were removed from the *Ranger 8* bus to be reworked, and Engineering Change Requirements were incorporated. Both attitude-control nitrogen-gas systems were removed from the spacecraft, the filter assemblies were replaced, and the gas systems were then reassembled to the bus. The electronic assemblies were reinstalled on the bus, and the bus was then assembled to the LMSC test adapter. A spring constant determination was begun on March 6 to provide additional information on the spring constant test, which was conducted during the previous reporting period. The test was completed

Table 1. *Ranger* Block III Spacecraft Assembly Facility assembly and operations schedule[a]

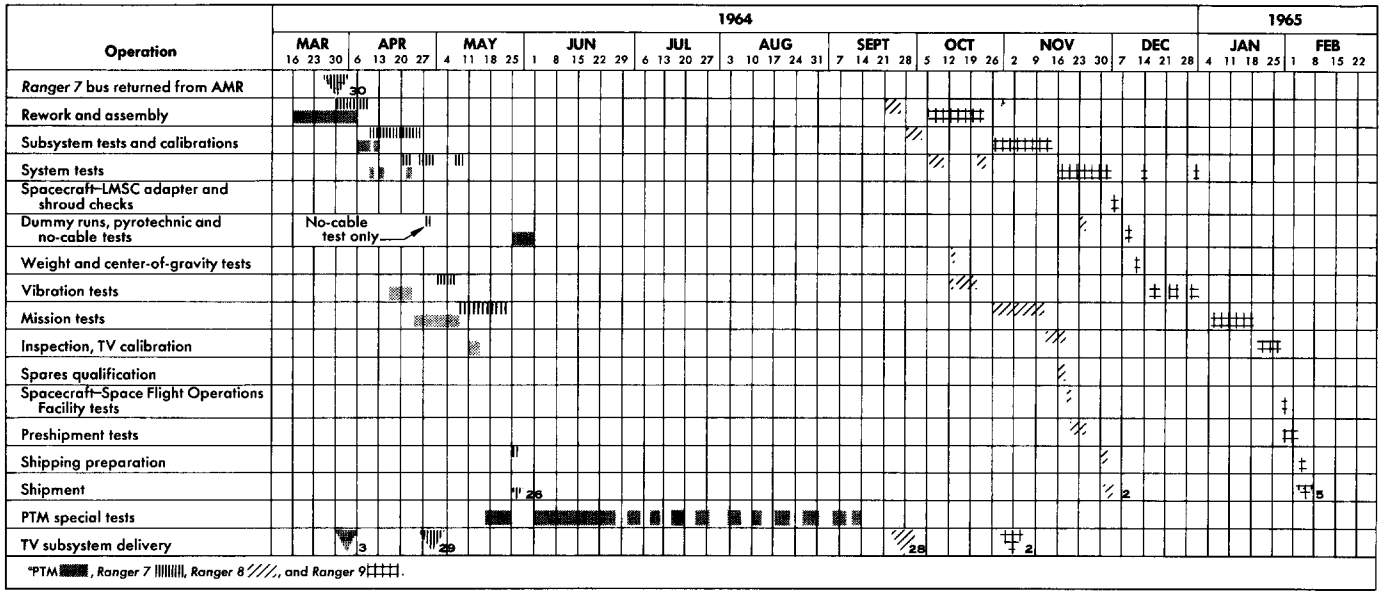

March 9, and preliminary evaluation of the data indicated that the earlier problem was with the LMSC flight adapter.

All further operations on the *Ranger* 8 and 9 buses have now been suspended until the latter part of 1964.

The *Ranger* 8 TV subsystem and all TV spares were returned to RCA for rework on March 2.

b. Compatibility testing. A series of compatibility tests with user subsystems has recently been conducted to determine peak power requirements as a function of all operational modes. This type of information is not normally obtainable in a spacecraft systems test configuration; however, comparatively accurate readings are obtainable under laboratory conditions. The area of margin testing is also being explored. Voltages to the units are varied beyond normal ranges to establish absolute operational limits. To date, results have been very satisfactory.

C. Guidance and Control

1. Flight Power Subsystem Testing

a. Proof-test-model (PTM) testing. The power subsystem was tested during the recent spacecraft PTM testing program. During the vibration testing, a malfunction caused a loss of output from the three-phase inverter, 4A14. Troubleshooting revealed the problem to be a loss of drive from the power synchronizer, 4A12. Further investigation in the laboratory indicated that an intermittent capacitor in the Schmitt trigger circuit was at fault. The unit was repaired, and the failed component was forwarded to the Component Parts Evaluation Group for appropriate followup action. The initial analysis revealed a workmanship problem internal to the capacitor.

2. Electrical Conversion

a. Status of power conversion hardware. At the present time all *Ranger* 7 flight modules and the data normally accompanying these units have been delivered to the Spacecraft Assembly Facility. The spare units are all available, except for the command converter, 4A5; this unit is out for a recent JPL Engineering Change Requirement (ECR) modification, which is discussed below. The spare units will be recoated.

b. Hardware performance investigation. A recent ECR modification is being incorporated in the flight command converter unit, 4A5. The action was partly brought about by a requirement of a former ECR for high-reliability parts, which changed the value of capacitors on the 28 v

dc outputs. Afterward, the presence of a 100-kc (approximate) oscillation was noted on the outputs of some modules. A detailed investigation indicated that the voltage regulator was unstable. Two ECRs were incorporated to correct the problem. The value of the output capacitors was raised from 33 to 56 μf. Also, three 0.01-μf emitter bypass capacitors were removed, and a 0.01-μf capacitor was placed from the collector to the base of a differential amplifier employed in the regulator. With this modification of frequency response, the unit has appeared stable in all testing performed to date. A type-approval test will also be performed on the unit.

3. Solar Panels

All flight panels are again undergoing flight-acceptance testing in conjunction with a recent structural ECR. Subsequent to an evaluation of the raised hinge joints, a decision was made to replace the solar panel hinges with solid machined units. No problems have been encountered thus far, and the delivery of the *Ranger 7* flight units is expected to be on schedule.

4. Inflight Performance of the Ranger 6 Attitude-Control System

a. System description. The attitude-control system is designed to control the orientation of the spacecraft with respect to the Sun and Earth and to point the high-gain antenna toward the Earth. Angular orientation errors with respect to the reference bodies are sensed by optical Sun sensors and an Earth sensor. Separate Sun sensors control the pitch and yaw axes; the Earth sensor controls the roll axis and the hinge orientation of the high-gain antenna. System damping is provided by rate signals from three single-axis floated gyroscopes with torque rebalance loops.

Control torques about the spacecraft axes are produced by a cold nitrogen-gas expulsion system. This system utilizes four gas expulsion jets per axis, two for the clockwise direction and two for the counterclockwise direction, for a system total of twelve jets. Gas flow through individual jets is controlled by solenoid valves. Each solenoid valve pair is operated by a signal from a switching amplifier having a bistable output switch. The switching amplifier inputs are the rate and position signals for the respective vehicle axes. When the sum of the rate and position signals exceeds a predetermined value, or "deadband," the amplifier actuates the pair of solenoid valves that will produce a torque opposing the direction of the rate-plus-position error. A controlled hysteresis in the bistable output switches prevents the valves from turning off until the error signal reaches a prescribed level below the turn-on level. This hysteresis establishes a minimum impulse that is imparted to the vehicle on each valve actuation and thus prevents possible valve chatter.

Reorientation of the spacecraft for the midcourse velocity correction is accomplished by a roll–pitch turn sequence in response to commands from the central computer and sequencer. This command disables the Sun and Earth sensors and connects a command current generator to the respective gyro torquer; the gyro senses the difference between the command rate and the actual vehicle rate. Position error is obtained by inserting an integrating capacitor in the gyro rebalance loop. When the turn command is removed, the gyro retains the position reference.

A midcourse autopilot maintains the spacecraft orientation during the midcourse-motor firing. Vehicle rate and position are sensed by the gyros, and control torques are produced by jet vane control of midcourse-motor thrust.

b. Inflight performance. The inflight performance of the *Ranger 6* attitude-control system was normal in all respects and is summarized below.

Acquisition. Upon receipt of the Sun-acquisition command, the vehicle tumbling rates were 5.0, −9.6, and 2.6 mrad/sec in pitch, yaw, and roll, respectively. The spacecraft acquired in pitch and yaw within 4 min after receipt of the acquisition command. The roll rate was reduced to 0.9 mrad/sec within 10 sec.

Upon receipt of the Earth-acquisition command, the vehicle accelerated to a roll search rate of −3.8 mrad/sec. After a 20-min, 40-sec roll search, the Earth sensor detected Earth light, and it completed the acquisition 25 min after receipt of the command. It is estimated that the spacecraft rolled through a 270-deg angle in the roll search.

Cruise. The system stabilized the spacecraft position within the nominal ±2.8-mrad deadband in pitch and yaw. Roll position stabilization was within the normal deadband limits, which vary with the distance from Earth. The limit cycle velocity increment was within the design maximum of 90 μrad/sec. An external pitch torque of −170 dyne-cm was determined from the limit cycle data. No steady external torques were evident from the roll and yaw data.

Midcourse maneuver. The midcourse maneuver required for the trajectory correction consisted of a 54-sec negative polarity roll turn and a 328-sec negative polarity pitch turn. The limit cycle positions at the start of the roll turn

were: roll, 2.8 mrad; and pitch, 0.0 mrad. Both turns were executed in a normal manner, and the rate transients compared well with the expected values. The predominant source of error in the midcourse maneuver is the initial roll limit cycle position. Since this initial condition was small compared to its maximum predicted value of 8.8 mrad, a very small midcourse pointing error resulted.

The autopilot transients compared well with predicted values from an analog computer study.

Reacquisition. Upon receipt of the Sun-reacquisition command, the spacecraft accelerated to a pitch rate of 4.9 mrad/sec and reacquired the Sun in 5 min. The yaw rate and position remained at null during the reacquisition.

At the end of the midcourse-motor burn, the residual roll rate was 100 μrad/sec. This rate reduced roll position error relative to the Earth from 11.4 deg (introduced by the midcourse roll turn) to approximately −1 deg at the time of Earth reacquisition. The Earth sensor detected the Earth as soon as it was turned on, and the reacquisition was completed within 80 sec.

Antenna hinge control. The hinge system tracked the Earth within the 1.25-deg deadband of the hinge angle servo during cruise operation. During Sun acquisition the antenna was extended to the preset angle of 135 deg inserted before launch. During the midcourse maneuver sequence, the antenna moved to the 180-deg exit angle and then to the 122-deg reacquire angle at Sun reacquisition in a normal manner.

Gas system. The control acceleration of the gas system was within the specification range of 0.54 to 0.66 mrad/sec^2. Based on the observed 60- to 90-μrad/sec velocity increment, the gas consumption is estimated to be 0.1 to 0.4 lb, which is insignificant compared to the 1.15-lb calculated worst-case value. No measurement of the actual consumption is possible due to the 0.08-lb accuracy of the telemetered measurements and the uncertainty of the gas reservoir temperatures.

Earth sensor. The measured Earth brightness was consistently 2 to 4 times the expected value. This is accounted for by the difference in color temperature between the calibration source and the Earth and by the accuracy of the calibration meters. There is also an uncertainty in the predicted Earth brightness because of variation of the Earth's albedo.

D. Propulsion

Successful accomplishment of the *Ranger* mission requires that the spacecraft be capable of undergoing a single midcourse propulsion maneuver to remove or reduce *Agena* injection dispersion errors. This maneuver is accomplished through the use of a small monopropellant–hydrazine propulsion system delivering 50-lb thrust to the spacecraft. The propulsion system is capable of delivering a variable total impulse in response to signals from an integrating accelerometer circuit. It is functionally a regulated-gas-pressure–fed constant-thrust rocket. Principal system components include a high-pressure gas reservoir, a gas pressure regulator, a propellant tank and bladder, a rocket engine, and an ignition cartridge containing a small amount of nitrogen tetroxide to initiate propellant decomposition. A detailed description of the propulsion system, including design philosophy and a system schematic, is reported initially in Ref. 1. Development progress is reported in subsequent issues of the *SPS*.

1. Ranger 6 Postflight Analysis

The propulsion system parameters telemetered to Earth during the firing of the midcourse propulsion system include: (1) the high-pressure nitrogen reservoir pressure, (2) the fuel tank pressure, (3) the nitrogen tank temperature, (4) the hydrazine reaction chamber wall temperature, and (5) the fuel tank temperature. The first four parameters are available at a high sampling rate of from 6 to 300 readings/min, whereas the last parameter is scanned once every 1000 sec (16⅔ min).

Shortly after the ignition of the propulsion system during the *Ranger 6* midcourse maneuver, the reaction chamber wall temperature transducer underwent a shift and shorted when the chamber reached steady-state temperature. The temperature–time history until the shift occurred indicated that a normal ignition had been obtained. The nitrogen tank temperature and chamber temperature measurements utilize the same reference circuitry in the telemetry system. Thus, the loss of the chamber temperature transducer caused the invalidation of the nitrogen tank temperature measurement, since the reference bridge had been severely unbalanced.

Therefore, only the two pressure measurements were available during most of the motor-burn period. The variation of these two parameters during this period is illustrated in Fig. 2. The fuel tank pressure undergoes an abrupt change at ignition since high-pressure nitrogen gas is released to the pressure regulator at this time.

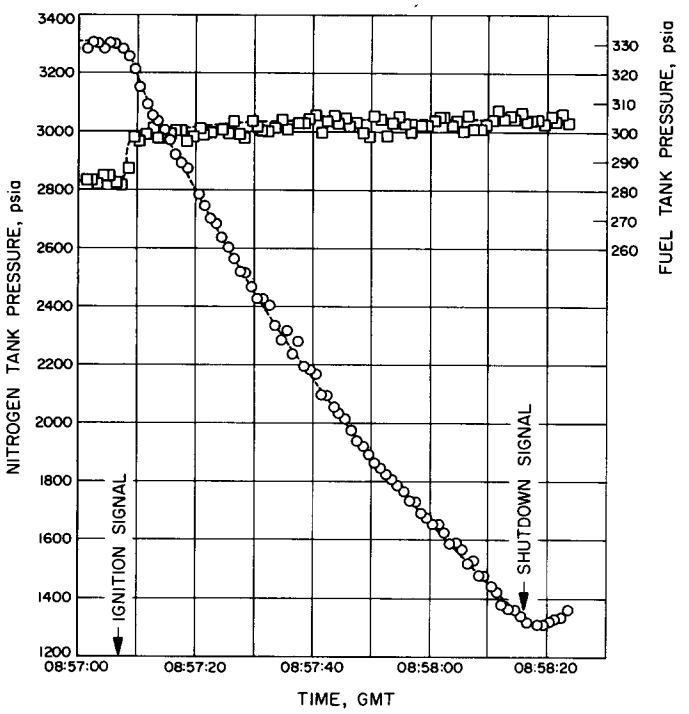

Fig. 2. Variation of propulsion system pressures during motor-burn period of midcourse maneuver

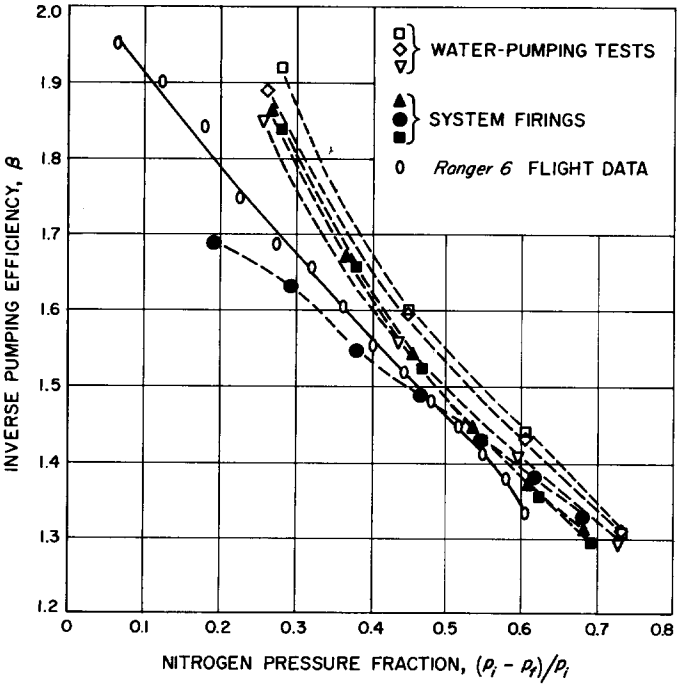

Fig. 3. Experimentally determined inverse pumping efficiencies for several pumping tests

Regulated pressure is normally very stable; the scattered data points are believed to be caused by instrumentation noise which is typical of the high-sampling-rate parameters. The nitrogen tank pressure decay curve is typical of such a process, with limited heat transfer occurring between the gas and its surroundings during the blowdown process.

The relationship between nitrogen volume requirements and the operating parameters of the system may be expressed as follows:

$$\beta \equiv \frac{V_R\,(p_i - p_f)}{p_R\,V_p} - \frac{\dfrac{V_x}{V}\left(1 - \dfrac{p_x}{p_R}\right)}{\left(1 - \dfrac{V_x}{V}\right)} = \gamma - \frac{Q_{in}\,(\gamma - 1)}{p_R\,(V - V_x)},$$

where β, an inverse pumping efficiency parameter, is a measure of the heat transfer taking place during the gas expansion process; V_R is the reservoir volume; p_i, initial reservoir pressure; p_f, final reservoir pressure; p_R, regulated pressure; V_p, volume of expelled propellant; V_x, ullage volume; V, sum of the volume of expelled propellant and the ullage volume; p_x, ullage prepressurization; γ, effective specific heat ratio of the gas; and Q_{in}, added heat from surroundings. Details of the development of this expression can be found in Ref. 2. For any given ullage fraction, V_x/V, and prepressurization fraction, p_x/p_R, the volume of compressed gas required for a given application is linearly proportional to the β-value of the system. For an expansion involving no heat transfer, the process is adiabatic and β equals the specific heat ratio of the gas (in this case, approximately 1.4 for nitrogen). For an isothermal process, β approaches unity; values of β less than unity could be obtained if sufficient heat were added from an external source.

Experimentally determined β-values for several *Ranger* Block III propellant expulsion tests are presented in Fig. 3 along with the *Ranger 6* flight values, which are based on the actual pressures from Fig. 2 and the predicted propellant flow rate based on preflight calibration. An excellent correlation was obtained; the data indicate that the test-result β-values are slightly conservative when compared to the *Ranger 6* flight values.

E. Supporting Activities and Engineering Facilities

1. Environmental Test Program

From February 15 to April 15, 1964, 73 experimental, 14 type-approval, and 18 flight-acceptance tests associated

Table 2. *Ranger* Block III usage of environmental test facilities from February 15 to April 15, 1964

Facility	Number of tests
Vibration	61
Low-frequency vibration (hydraulic shaker)	0
Acoustic	3
Centrifuge	3
Shock	1
Handling shock	2
Temperature	17
Explosive atmosphere	0
Vacuum	18
Space Simulator (25 ft)	0
Total	105

with the *Ranger* Block III Project were performed by the JPL Environmental Test Laboratory (Table 2).

2. 25-ft Space Simulator

The Eppley Laboratory, Inc., Mark IV filter wheel (Fig. 4), which is used to calibrate the spectrum and to detect possible spectrum shifts between spacecraft tests, was recently tested for the first time. The information supplied by the wheel is required to assure good solar simulation as it is applied to spacecraft thermal design. The first run was performed to verify the mechanical operation of the device under vacuum, to measure (using the 12 narrow-band filters) the spectrum in air and in vacuum for correlation purposes, to ascertain the instru-

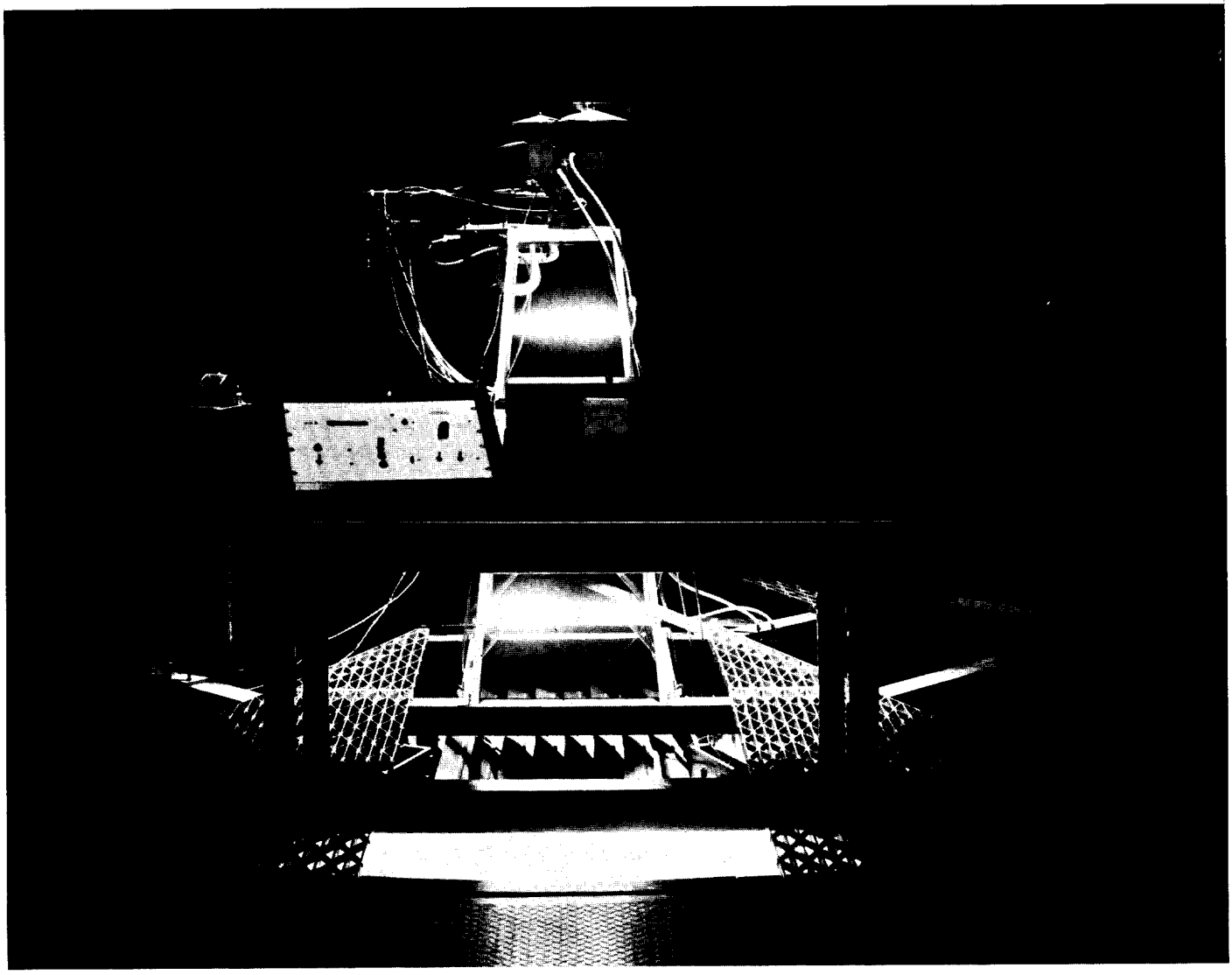

Fig. 4. Test of the Eppley Mark IV filter wheel in the 25-ft Space Simulator

ment sensitivity to temperature and pressure variations, and to yield spectral information.

The spectral distribution, as expected, revealed that the simulation of solar flux is higher in the ultraviolet, slightly lower in the visible, and slightly higher in the infrared than the Johnson (Ref. 3) or Nicolet (Ref. 4) values for solar distribution. The effects on the radiometer sensitivity of differences in pressure and temperature were tested by varying the chamber pressure and/or shroud temperature. The effect was found to be negligible within the pressure range of the radiometer (i.e., 10^{-4} torr), but was significant for large temperature variations. However, in the -100 to $-270°$F range, the effect is small.

References

1. "Propulsion," *SPS 37-3*, pp. 31–33, Jet Propulsion Laboratory, Pasadena, California, June 1, 1960 (Secret).

2. "Advanced Liquid Propulsion System," *SPS 37-14*, Vol. II, pp. 281, 282, Jet Propulsion Laboratory, Pasadena, California, April 1, 1962 (Confidential).

3. Johnson, F. S., "The Solar Constant," *Journal of Meteorology*, Vol. II, No. 6, p. 431, December 1954.

4. *Archiv für Meteorologie, Geophysik und Bioklimatologie*, Series A, Vol. III, pp. 209–219, Vienna, Austria, 1951.

II. *Ranger* TV Subsystem, Block III

The primary objective of *Rangers 6–9* (Block III) is to produce high-resolution TV pictures of the lunar surface. To implement this objective, a TV subsystem has been developed by RCA under contract to JPL. The subsystem mates with the JPL bus, as did the lunar capsule of the *Ranger 3–5* (Block II) series.

The subsystem structure consists of three major assemblies: (1) the central box which houses the main electronic components, (2) the camera subassembly with associated bracketry and equipment, and (3) the thermal shield. A view aperture for the cameras is provided in the thermal shield.

The following material relating to the subsystem development is abstracted from the RCA report: *Ranger TV Subsystem, Block III, Sixteenth Bimonthly Progress Report,* April 1, 1964, covering the period from January 16, 1964, to March 15, 1964.

A. System Engineering

1. Flight Model III-1

Final tests on Flight Model (FM) III-1 were performed at the Atlantic Missile Range (AMR). The data obtained from the last camera calibration did not agree with those obtained during the calibration at JPL, partly because of a 10% error in the calibration of the Pritchard photometer. The prefinal subsystem command checkout disclosed that there were no outputs from Telemetry Points 3 and 4 of the Channel 8 telemetry. The temperature sensor assembly was replaced, and normal operation was restored. The rest of the subsystem command checkout test demonstrated satisfactory operation of the subsystem. System operation was satisfactory during the final system test, and, although the complex noise increased to 120 mv during the test, TV operation was normal.

Flight-analysis support was supplied during launch and was continued during the post-launch analysis of the *Ranger 6* mission. Analysis of the mission led to recommendations for redesign of the TV subsystem command-and-control circuitry, telemetry, and various interfaces. These recommendations are centering on a complete redesign of the command-and-control functions of the subsystem and the routing of these functions through the JPL bus and the *Agena* stage. Also recommended are modifications to the telemetry to provide a broader base of facts for evaluation of future missions. The design of the mounting has been completed for the following new components: the command control unit, two current sensing units, and one current sensing amplifier. Concurrent with the redesign effort, an extensive inspection and quality-assurance program has been implemented.

A complete discussion of the design study will be presented in the forthcoming RCA FM III-1 Flight Evaluation Report and Design Study Report. For this reason, discussions of this effort as related to the assemblies of the controls group, the telemetry group, the sequencer, the video combiner, and the high-current voltage regulator are not included here.

2. *Flight Model III-2*

On January 15, 1964, tests were performed on the TV subsystem to evaluate noise levels and sources of this noise in the cameras. Also, the P-channel communications chain assigned to FM III-2 was returned to JPL. After installation, the P-channel was tuned for actual flight use.

As a result of further investigation on camera noise, camera grounds on the P1- and P4-cameras were removed. These modifications improved camera performance by reducing the noise level. Following the noise investigations, the P4-camera was refocused to achieve optimum focus.

On January 16, the other camera levels were checked and readjusted as required. During testing, the output of the 225-kc voltage-controlled oscillator (VCO), Serial No. 1032P, was found to be low. Although the output level was within tolerance, this VCO was removed and replaced with Serial No. 003 in order to provide a nominal output of 1.5 v peak-to-peak.

It was determined on January 17 that gain settings on the cameras were incorrect because of improper calibration of the JPL photometer. The gain levels were reset to the proper levels using an RCA photometer calibrated by the National Bureau of Standards. Resetting of the camera levels was completed on January 18, and calibration of the subsystem was started at that time.

On January 20, final mechanical preparation of the subsystem for launch began. On the following day, a short electrical checkout of the subsystem was performed before the shrouds were installed for a spacecraft test. The subsystem was operated on the spacecraft on January 22, and System Test 6 was performed on January 23.

Packing for shipment of the subsystem to AMR was completed on January 24. After arrival at AMR, the subsystem was inspected and a brief electrical test was performed; it was concluded that no damage occurred during shipping. Final mechanical inspection and preparations for launch were completed by February 6. On February 7, a backup-function system test was performed. Review of the post-shipment test data indicated that two noisy telemetry frames existed on the Channel 8 telemetry.

The TV subsystem was demated from the spacecraft, and both were put in storage awaiting schedule information. On February 11, information was received from the JPL *Ranger* Project Office that the *Ranger* 7 launch would be rescheduled. The TV subsystem was then shipped back to RCA on February 12. After its arrival, an electrical test was performed on the subsystem with satisfactory results. FM III-2 was prepared for rework on February 14 in conjunction with the anticipated *Ranger* redesign. As of March 15, all components have been released for evaluation, updating, and redesign, where necessary.

3. *Flight Model III-3*

The P-channel communications equipment from FM III-2 and the transmitter power supply from the life test model were installed in FM III-3 and were tuned. On January 24, a subsystem command checkout without the P2-camera was conducted, and the results of this test were satisfactory. The subsystem without the P2-camera was mated with the *Ranger* 8 bus on January 24, and System Test 1 was conducted with satisfactory results.

On January 27, the P2-camera, Serial No. 39, and P2-camera electronics, Serial No. 33, were installed in the subsystem, and calibration was completed on January 28. After retuning the subsystem to flight configuration, a subsystem test was conducted. Satisfactory performance of the subsystem was observed during this test.

The subsystem was again mated with the *Ranger* 8 bus on January 30, and System Test 2 was conducted. The F-channel unexpectedly turned on in warmup 15 min after turn-on of external power. The F-channel was subsequently turned off, and the test continued in the normal cruise-mode operation. It was concluded that the clock-start relay in the distribution control unit had not been reset after the previous operations; therefore, a step was added to the procedures to send a Real-Time Command 5 (TV clock off) following application of power to the subsystem.

The backup-function system test and RFI tests were conducted on February 3 and 4, respectively. Both tests indicated satisfactory performance of the subsystem. The omni-cable and -antenna were then installed in prepara-

tion for match-mate tests. A subsystem verification test conducted February 5 indicated proper operation of the subsystem.

On February 6, a system test was performed during which two abnormal conditions were observed:

(1) The F-channel turned on in warmup when power was switched from external to internal. It appears that this was caused by a transient turn-on of the high-current voltage regulator by the initial application of voltage to the silicon-controlled rectifier (SCR) cathode.

(2) The P-channel went to full power approximately 2 min early. This appeared to be a sequencer failure; however, the problem was still evident after the sequencer and sequencer power supply were replaced. Further investigation revealed that the problem was associated with the ground support equipment, although the specific source of the noise that caused the early full-power turn-on could not be isolated.

Match-mate tests were performed from February 10 through 17 with satisfactory results. Two preshipment electrical tests were conducted on February 28. Performance during the second test was normal; however, two problems were encountered during the first test:

(1) The P-channel RF output ceased when the central computer and sequencer warmup command was released at the test console. This failure could not be explained, and subsequent tests showed normal operation for the P-channel.

(2) The emergency-telemetry amplitude was approximately 50% below normal. It was determined that this was a ground-support-equipment problem.

The subsystem was shipped from JPL to RCA on March 2. Special tests were conducted from March 9 through 15 to observe transient voltages at the SCRs; the results of these tests will be reported at a later date.

4. Flight Model III-4

Camera calibration for FM III-4 was completed on January 19. On January 21, the first subsystem test was performed, and operation of the subsystem was verified to be satisfactory. The start of environmental testing was delayed to permit the following adjustments in order to obtain refinements in picture quality of the cameras:

(1) The F_b-camera was removed from the subsystem, and its electrical settings were optimized to provide improvement in vidicon-beam stability and increased resolution in excess of the originally measured 5% response at 650 TV lines.

(2) Although the electrical noise level for the P-cameras was well below the allowable limit, this characteristic appeared as some coarseness in the picture background. This situation was improved significantly after a circuit modification was made to the video amplifier section of each P-camera electronics assembly. After reinstallation of the P-cameras, operational levels were reset and abbreviated camera verifications were performed to establish the new performance levels.

A vibration test conducted on January 31 consisted of sinusoidal and random vibrations applied along the x-axis of the TV subsystem. Two sine sweeps were made to determine the resonant frequency of the structure. The resonant frequency, monitored at Accelerometer 4, occurred at 35 cps during the first sweep and at 35.5 cps during the second sine sweep. The other accelerometers indicated no unusual performance throughout the test. A subsystem command checkout test performed both before and after vibration testing indicated no mechanical or electrical degradation attributable to the vibration testing.

Environmental testing of FM III-4 was supported up to the time of suspension of testing, which occurred after vibration and during thermal-vacuum testing. The subsystem is now in storage, pending rescheduling of the modifications and tests to be performed.

5. Proof Test Model

The proof test model (PTM) bus and TV subsystem were set up in the *Ranger 7* area at JPL on January 27. A system test was conducted the following day in preparation for a dual mission coincident with the *Ranger 6* mission. All subsystem operations were normal, except that the Channel 8 telemetry exhibited a noisy output from the commutator.

After the *Ranger 6* mission, the PTM was used in several special tests which were performed in an effort to answer questions resulting from the analysis of the *Ranger 6* mission. On February 17, the PTM was returned to RCA. The assemblies and subassemblies were removed

for modification and inspection. All assemblies have now been released for evaluation, updating, and/or redesign. The structure was reworked to the latest flight configuration and now includes all adaptions and changes necessary to permit the incorporation of revised and new equipment. The PTM structure was inspected and statically load tested prior to reassembly to provide assurance of structural integrity.

B. Cameras

All phases of the camera optimization program have been completed, except for a report on the results of the vidicon-life test. The cameras and camera electronic assemblies from the PTM and FM III-2 subsystems and the spares are being entered into the rework program. Design changes resulting from dimensional variation of the camera electronics assemblies have been completed.

The checkout and testing of two of the three focus-and-alignment collimators have been completed. The remaining collimator has been received from the vendor and will be available during the next reporting period.

Both the General Electrodynamics Corporation (GEC) and the Westinghouse Corporation have completed deliveries of developmental vidicons as required under the terms of their respective subcontracts. Four of the GEC tubes were tested in a *Ranger* camera assembly. Except for their sensitivity, these tubes were found to be acceptable, and the sensitivity problem is now being investigated.

As part of the investigation into reducing the shock transmitted to the vidicon, a standard *Ranger* shutter was modified to include the new urethane bumper material. Comparative tests of the reduction in transmitted shock and the consequent effect on vidicon microphonics were made between the operations of a regular and a modified shutter. By observing the modulated output of the vidicon, it appeared that there was little reduction in the microphonics.

C. Telecommunications

The life test model telemetry equipment was subjected to and satisfactorily met the requirements of a complete requalification test program for operation during boost. It should be noted that the equipment was operated in the full-power mode throughout the various phases of the entire test program; during thermal-vacuum testing, the equipment was in operation throughout the pumpdown from ambient pressure to 10^{-4} torr.

Four new sets of commutators successfully completed acceptance testing and were designated as spares.

All telecommunications assemblies and subassemblies are being subjected to the rework program. Except for the conformal coating of all terminals, no modifications were made to the transmitter, power amplifier, telemetry processor, and strip-line four-port hybrid. A few of the components of the $\times 12$ multiplier will now be enclosed by potting compound; no other changes were made in this unit.

Modifications are being made to the transmitter power supplies for the PTM and all FMs to provide several of the transistors and diodes with a second layer of insulation from ground in the event of a failure in the chassis finish. Also, two of the resistors are being changed to increase the dielectric strength between the elements of the resistor and ground from 1000 to 1250 v rms. These new resistors have also demonstrated higher reliability.

D. Power

During this reporting period, fifteen Model 202 batteries were received from the vendor, acceptance tested, and released for use as system-test batteries. Originally, only seven of these were to be used as system-test batteries, while the remaining eight were to be used as flight batteries (six for FM III-2 and two for FM III-3). However, because of the rescheduling of the *Ranger* launch dates and a 90-day age limit requirement on flight batteries, these eight batteries were reclassified as system-test batteries. There are now sufficient system-test batteries to meet the normal requirements of the remainder of the *Ranger* Program. However, if the Program extends beyond the 6- to 9-month age limit on system-test batteries, new units for system testing may be needed.

To comply with the 90-day age limit, a total of 18 flight batteries are needed to meet the requirements of the Program. Ten units now at the manufacturer's facilities

are being held at the point of activation, awaiting instruction from RCA; eight additional new batteries will have to be ordered.

E. Thermal Control

Thermal-vacuum testing of FM III-2 was completed at JPL. The tests, performed as real-time simulated missions, were conducted in the 25-ft vacuum chamber located in JPL Building 150. During Tests 1 and 2, the subsystem was operated on internal power at an average cruise temperature of 34°C, followed by 10 min of full-power operation. In Test 3, the subsystem was operated on external power at an average cruise temperature of 12°C, followed by 10 min of full-power operation of the F-channel and then 10 min of simultaneous full-power operation of both the F- and the P-channels. During all three tests, all temperatures were within the tolerances specified by JPL for the cruise balance. No unusual temperatures were recorded during full-power operation in Tests 1 and 3; in Test 2, however, the temperature of the P-channel power amplifier was observed to be 27°F higher than that of the F-channel power amplifier after 10 min of full-power operation. A camera malfunction lasting only 30 sec occurred in Test 1 and necessitated another mission test at 93°F.

Thermal-vacuum testing of FM III-4 was conducted at RCA in an effort to duplicate the *Ranger 6* mission and to verify the thermal configuration of FM III-4. The test results proved that calculations made to produce a desired average temperature drop of 10°C from the temperatures experienced during the *Ranger 6* mission were valid. Paints will be mixed which will provide energy inputs during solar illumination that will permit this average drop in temperature.

The thermal shrouds for the PTM have been refinished, painted, and strip-coated for use in the testing of the modified PTM. Shrouds for FMs III-2, -3, and -4 are in a polished, strip-coated condition. The paint on the fins of FM III-2 will be stripped off because further buildup would cause unpredictable operation.

F. Ground Support Equipment

The ground support equipment (GSE) located at Goldstone Tracking Station supported the *Ranger 6* mission by providing the Channel 8 telemetry data during the tracking periods. Both the Echo and Pioneer Stations GSE were fully operational and aligned from initial acquisition of the spacecraft until impact.

About 12 to 13 hr prior to the acquisition of *Ranger 6* during its first pass, the high-voltage power supply in the film recorder, Serial No. 1, failed. A spare power supply was immediately installed, and the film recorder was recalibrated without interference to normal operation. The power supply which failed was returned to RCA for repair. It was determined that there was insufficient spacing between the R17 resistor in the anode supply and the V4 tube in the focus supply to prevent arcing between the two components. The spacing between these components has been sufficiently increased to eliminate the problem in this power supply, and modifications will be made to all other high-voltage power supplies.

The Serial No. 2 GSE, the blockhouse control panel, and the system test console from AMR have been returned to RCA to support the additional integration and testing efforts of the rework program. The redesign of the command-and-control circuitry is resulting in modifications to the system test console and the blockhouse control panel. These modifications are scheduled for completion in sufficient time that this equipment will be available for the PTM and FM testing at RCA, JPL, and AMR.

III. *Surveyor* Project

A. Introduction

The *Surveyor* Project will take the next step in advancing lunar technology by making soft landings on the Moon, beginning in 1965 with a group of four test missions whose objective is to demonstrate successful soft landing by post-landing spacecraft operation. An engineering payload including elements of redundancy, increased diagnostic telemetry, touchdown instrumentation, and survey TV will be used.

The general objective after 1965 is to perform operations on the Moon contributing new scientific knowledge and basic data in support of manned lunar landings. A group of four flights planned for 1966 will carry a scientific payload selected from the following experiments: two-camera TV, micrometeorite ejecta, single-axis seismometer, alpha-particle scattering, soil properties (surface sampler), and touchdown dynamics.

In 1965 and 1966, the 2150-lb (separated weight) spacecraft will be injected into the lunar trajectory by direct ascent, using single-burn *Atlas–Centaur* vehicles. The midcourse correction capability will be 50 m/sec in 1965 and 30 m/sec in 1966.

Hughes Aircraft Company is under contract to develop and manufacture the first seven spacecraft.

B. Systems

1. Preliminary Estimate of the Surveyor Spacecraft Payload Gained by Using 90-hr Transfer Trajectories

A preliminary study has been made to determine the increase in spacecraft payload weight which can be obtained by using 90-hr transfer trajectories for the *Surveyor* mission instead of the currently planned 66-hr transfer trajectories.

At present, the *Atlas–Centaur* launch vehicle is guaranteed to have the performance capability of injecting a 2150-lb spacecraft into a transfer trajectory under the following conditions: (1) launch azimuth of 108 deg, (2) injection true anomaly of −5 deg, and (3) geocentric energy of −0.85 km²/sec². Fig. 1 presents *Atlas–Centaur* performance data which were obtained by adjusting data contained in Ref. 1 to make them compatible with the guaranteed performance. The launch window for the 66-hr transfers presented in Fig. 1 opens when the injected spacecraft weight capability reaches 2150 lb and closes at the maximum launch azimuth constraint of 114 deg. It was shown that, for one launch day, a launch window of the same duration (46 min) can be obtained for the 90-hr transfers by using a 2376-lb spacecraft. Therefore, for this launch day, the injected spacecraft weight can be increased by 226 lb by using 90-hr transfers with no loss of launch window. It has not yet been determined whether this performance gain is representative of that for all launch days. There are two factors which contribute to this gain: (1) The geocentric energy required for the 90-hr transfers is less than that required for the 66-hr transfers; and (2) the perigee to target central angle is greater for the 90-hr transfers than for the 66-hr transfers, permitting a more efficient use of the allowable launch azimuth range.

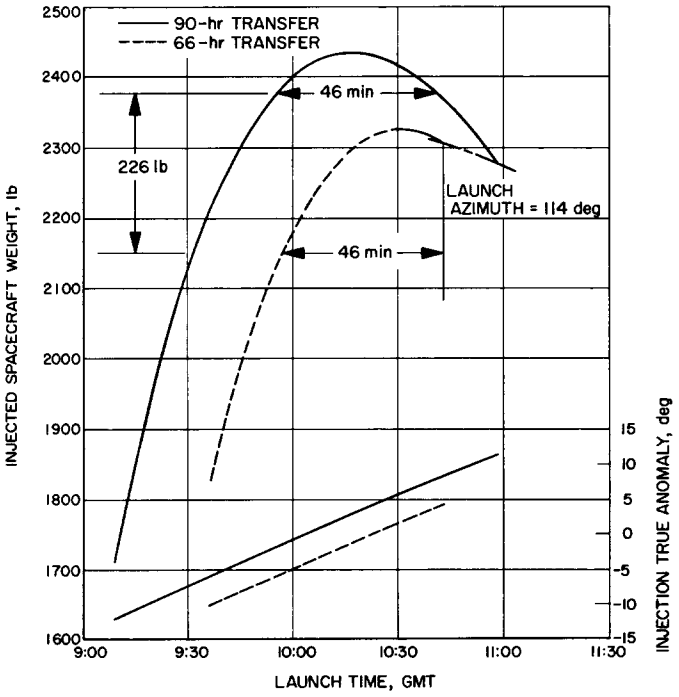

Fig. 1. Comparison of 66- and 90-hr transfer trajectories for *Surveyor* arrival date: September 14, 1964

Some of the gain in injected spacecraft weight must be allocated to the additional midcourse and terminal descent propellant requirements of the heavier spacecraft. Therefore, in general, the increase in spacecraft landed weight will be considerably less than the increase in injected weight. Fig. 2 illustrates the relationship between the increase in landed weight and the increase in injected weight. In determining this relationship, it was assumed that the maximum midcourse velocity increment was 44.4 m/sec for both the 66- and 90-hr transfers and that the sequence of events during the terminal descent was similar to that presently planned for the 66-hr transfers. Note that, for no increase in injected weight, the landed weight increases by 42 lb using a 90-hr transfer. This is because the unbraked impact velocity is less for the 90-hr transfer than for the 66-hr transfer. Hence, for a given spacecraft weight, less propellant is required for the 90-hr transfer.

It is seen that, if the increase in spacecraft injected weight is 226 lb, the spacecraft landed weight increases by 126 lb. However, not all of the increase in landed weight is available for additional spacecraft payload since the spacecraft power and insulation requirements are greater for 90-hr transfers. It has been estimated[1] that the additional spacecraft requirements will cost about 42 lb, leaving only 84 lb for additional payload (based on the 226-lb performance gain).

[1] Cloud, J. D., *Spacecraft Changes Required for a 90 Hour Trajectory*, Hughes Aircraft Company letter to members of the *Surveyor* Mission Analysis Panel.

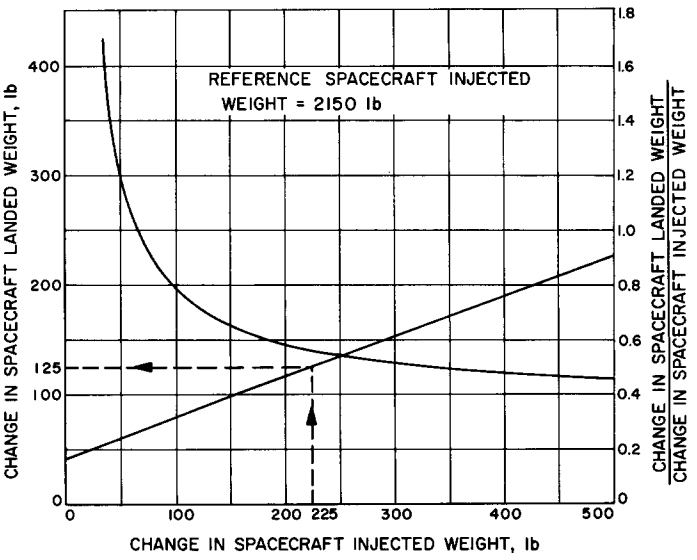

Fig. 2. Change in spacecraft landed weight vs change in spacecraft injected weight

It is concluded that the *Surveyor* spacecraft payload can be increased significantly by using 90-hr transfer trajectories. This study was based on the arrival date used in Ref. 1, i.e., September 14, 1964. At present, a detailed study is being initiated to rigorously determine the feasibility and desirability of 90-hr transfer trajectories for the *Surveyor* mission.

2. Space Flight Operations

During the period from March 1 to April 30, 1964, some key steps toward the implementation of the space flight operations (SFO) development program have been taken. Most of the activities have involved generation and revision of various *Surveyor* SFO documents and the continued planning of SFO.

A preliminary version of the *Surveyor* Project Deep Space Network (DSN) Interface Document was prepared in April. This document will provide a detailed description of all technical interfaces between the *Surveyor* Project and the DSN. Other published documents include the Deep Space Instrumentation Facility (DSIF) Tracking and Instruction Manual, the SFO System Functional Design Specifications, and the SFO Facility *Surveyor* Capabilities Document. Published revisions to existing documents include Revision 1 of the *Surveyor* SFO Plan and the SFO Test Plan. Discussions have been held between Hughes Aircraft Company and JPL personnel to finalize the format and contents of the *Surveyor* Spacecraft–SFO Interface Document. All functions and procedures documents containing technical-group operational procedures are scheduled for publication in the next reporting period. These will be included and controlled in the *Surveyor* SFO Facility Standard Operating Procedures Document at a later date.

Functional requirements have been generated for additional SFO Facility displays and a *Surveyor* spacecraft model compatible with the existing SFO Facility gimbal configuration. These requirements are presently being converted to detailed hardware specifications. Functional requirements have also been established for two computer programs which will process spacecraft data at the DSIF sites and provide spacecraft simulated data to be used extensively during future testing of the SFO System.

The DSN proposal for the mission-independent on-site computer configuration was reviewed and extended to include all *Surveyor* mission-dependent requirements. Implementation of the over-all on-site data-processing system design is proceeding. Communication line usage under various operational conditions has been established, and spacecraft data alarm monitoring techniques have been defined.

Meetings of the *Surveyor* SFO Design Team have been held on a regular basis to advance the System Development Plan.

C. Space Sciences

1. Surveyor Single-Axis Short-Period Seismometer

The *Surveyor* single-axis short-period seismometer sensor with lunar springs, available since mid-1962, has been tested for period and damping characteristics (Ref. 2). An auxiliary spring fixture, compensating for 5% of the mass weight, was used for these tests. During November 1963, the sensor was refitted with Earth springs and was mated with an engineering prototype amplifier and power supply. The seismometer sensor is shown in Fig. 3 with a microscope used to center the seismic mass. The amplifier and power supply electronics breadboard unit is shown in Fig. 4. The springs which were used produced a natural frequency of the seismic mass of 1.22 cps. The

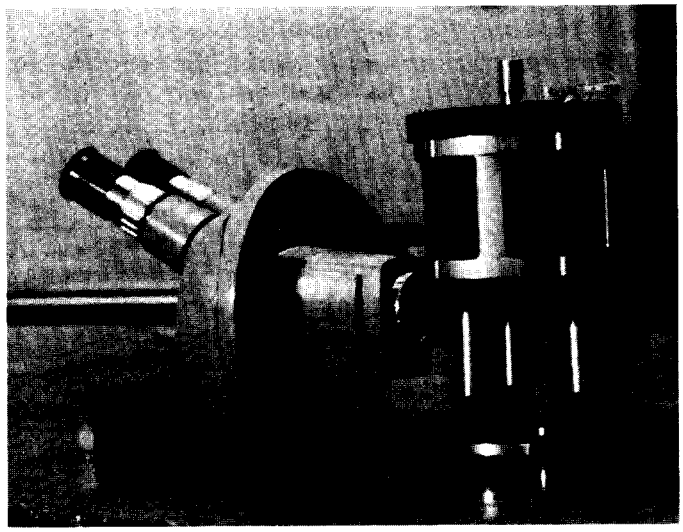

Fig. 3. *Surveyor* single-axis short-period seismometer with centering microscope

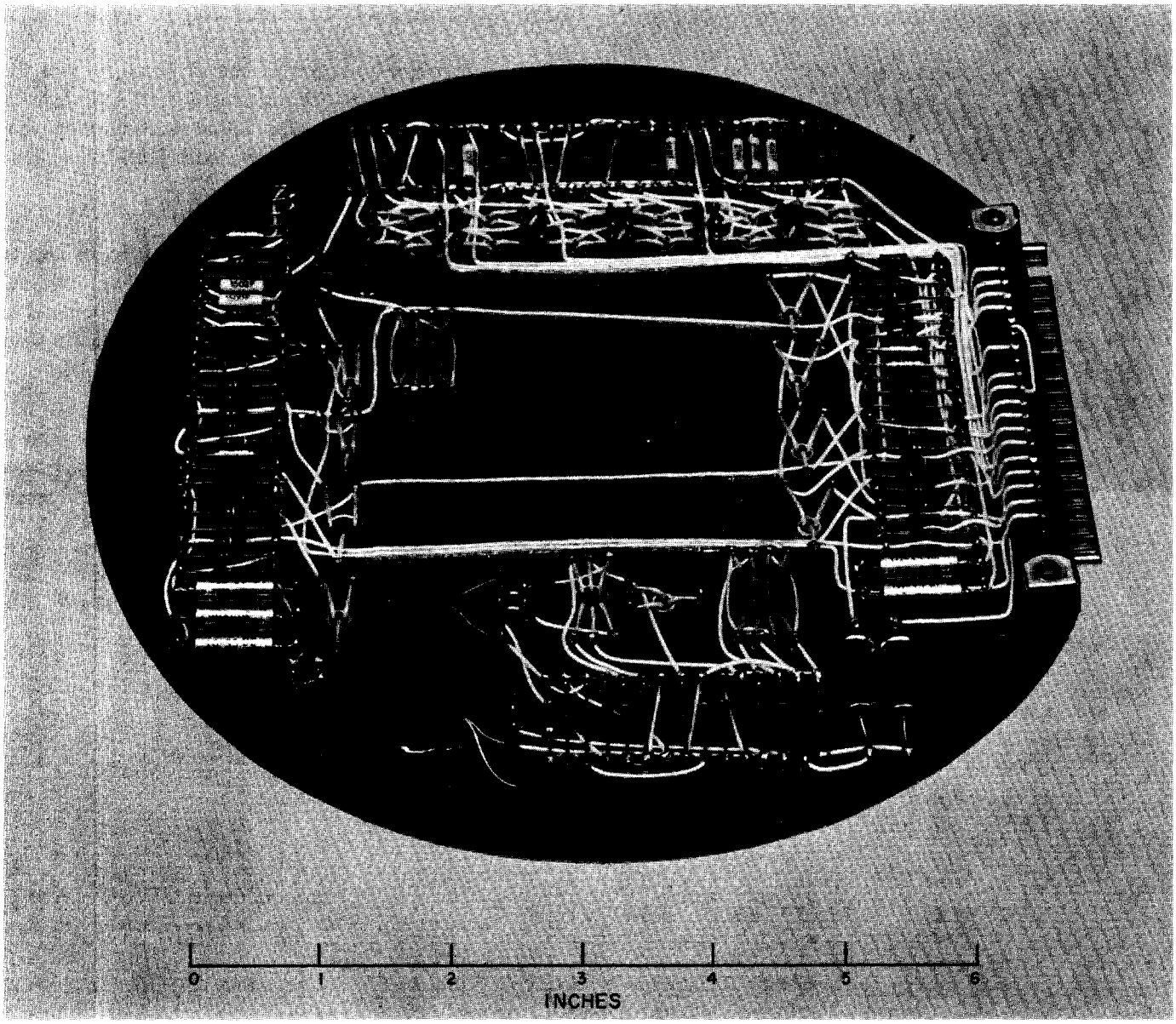

Fig. 4. Seismometer amplifier and power supply electronics breadboard unit

electromagnetic damping is set near critical. This then produces, in the Earth's gravitational field, conditions similar to those in which the lunar seismometer will operate.

The sensor was placed on the Lamont Geological Observatory seismic pier at Palisades, New York, and the output was recorded on a helical drum recorder (Fig. 5) with a drum speed of 4 rph. On the deployed recording (Fig. 6), successive traces correspond to a 15-min time interval. Intervals of 1 min are indicated by the time marks on the recording. Time notations refer to eastern standard time.

Two events recorded on December 17, 1963, at 7:48:40 and 7:59:20 p.m. correspond to the arrival of a PKP wave (i.e., a compression wave that travelled partially through the Earth's core). The quakes originated in the Tonga Island region (South Pacific, 173-deg west longitude, 20-deg south latitude). The first quake, the larger of the two, had a magnitude of 7¼ to 7½; the second had an indefinite magnitude. The travel time from Tonga to Palisades was 18.5 min. This represents an arc of 115.5 deg (111.2 km/deg), or an arc length of 12,850 km (7980 miles).

The December 18, 1963, record shows progressive buildup of the microseism level (storm). Two prominent

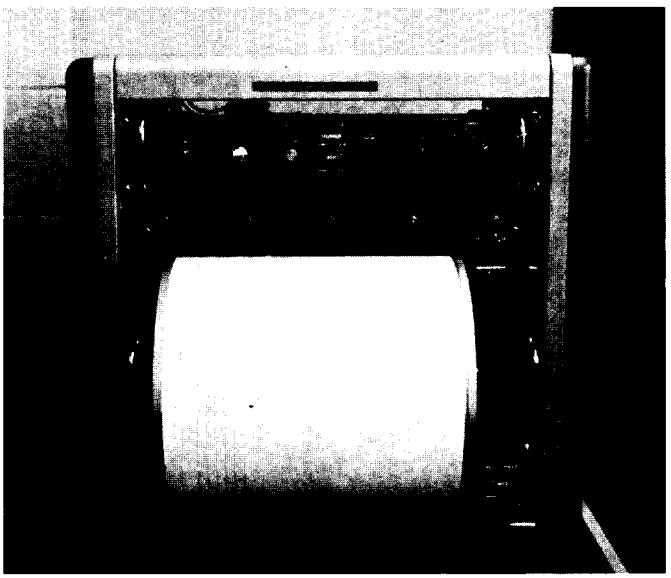

Fig. 5. Helical drum recorder

disturbances at 2:12:30 and 4:56:30 p.m. are believed to have been caused by quarry blasts some 100 km (60 miles) away. The short duration of the disturbances and the high frequencies are two characteristics that help to distinguish these from quakes. Other short-duration high-frequency perturbations were traced to someone walking or working near the pier.

Other tests were made with the breadboard unit to establish the ultimate sensitivity of the sensor. A 0.1-mμ (1-A) displacement at 1 cps was found to correspond to a signal-to-noise ratio of 1; a 1-mμ displacement will yield a signal that is easily detected.

Tests will be conducted in the near future with a prototype sensor (Fig. 7) and electronics. The design improvements incorporated in the prototype should result in improvements in over-all sensitivity.

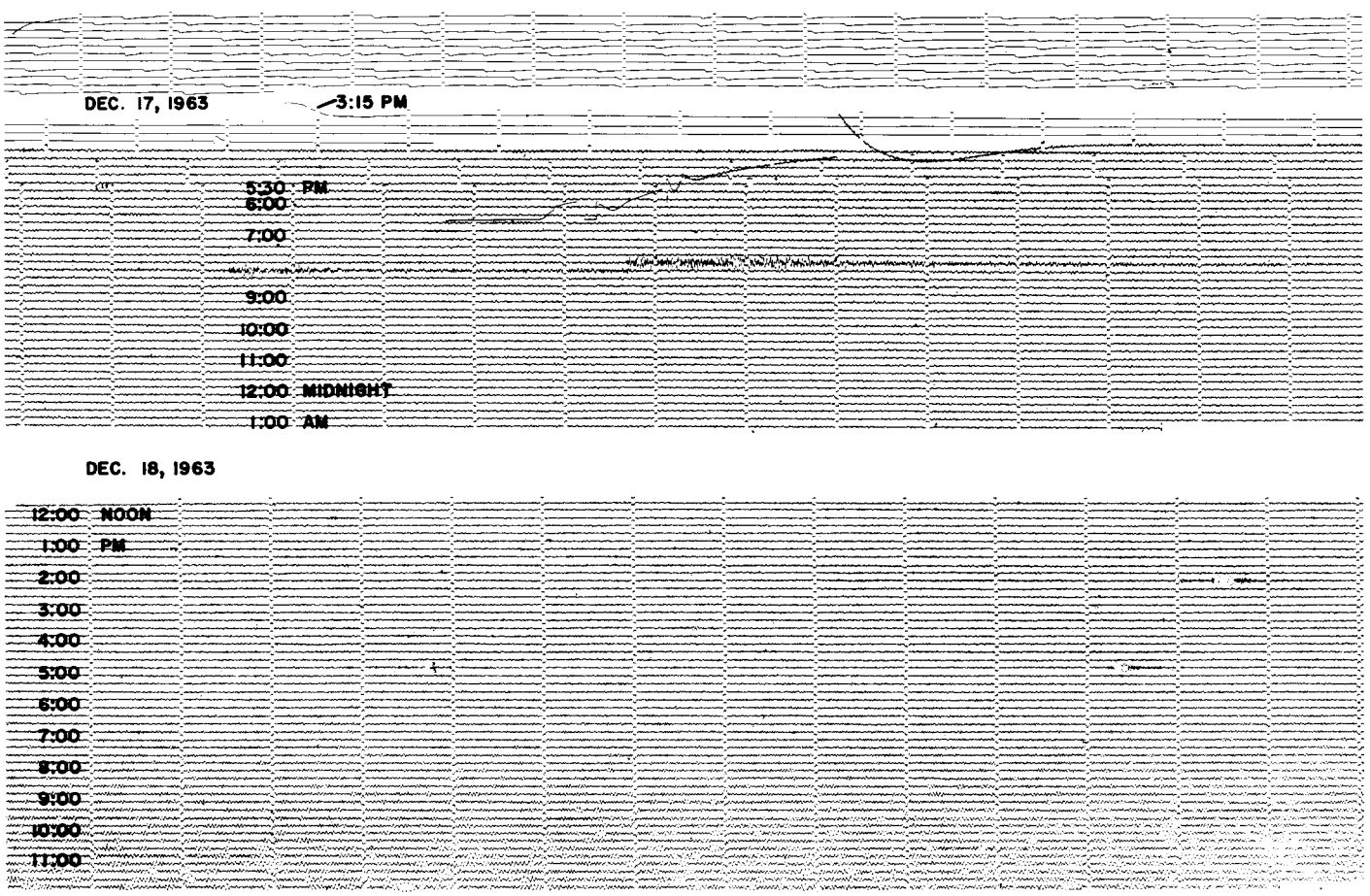

Fig. 6. Seismic recording

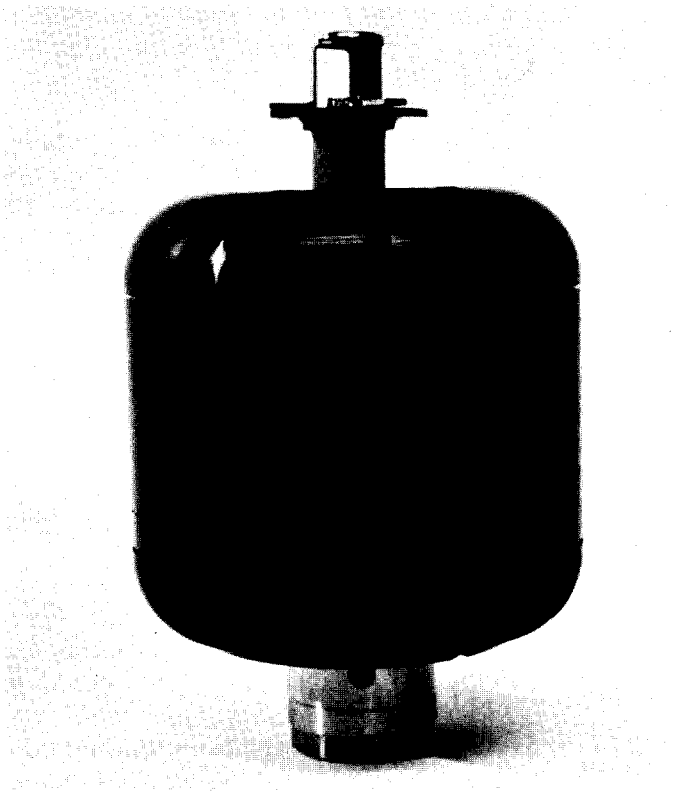

Fig. 7. Prototype single-axis short-period seismometer sensor

References

1. Griffith, G., and Swanson, P. C., *A Brief Analysis of 90 Hour Lunar Trajectories for Atlas/Centaur/Surveyor*, Report CA-FM-62, General Dynamics/Astronautics, San Diego, California, October 2, 1963.

2. "Seismograph," *SPS 37-20*, Vol. VI, pp. 90, 91, Jet Propulsion Laboratory, Pasadena, California, April 30, 1963.

IV. *Surveyor* Spacecraft System

The following material relating to the *Surveyor* spacecraft system was prepared by the Hughes Aircraft Company:

System engineering. A three-volume functional description of the A-21 spacecraft has been completed. The SD-4 type approval model of the *Surveyor* dynamic vehicle for use in *Centaur* tests successfully completed testing and was shipped to Lewis Research Center in February 1964.

Scientific payload. The engineering change proposals for incorporation of scientific instruments in the A-21A spacecraft were approved by JPL, and spacecraft/instrument interface specifications were revised accordingly. Instrument test plans and equipment are being re-evaluated. As a result of experience with the survey camera in T-21 system testing, changes are being made to prevent oscillations in the mirror drive circuit and undesirable interactions among the camera, transmitter, and central command decoder. The variable-focal-length lens design was modified to prevent a shift-of-focus and decentration problem.

System analysis. Study of earlier switching of the transmitter to the high power mode to provide added telemetry prior to *Centaur* separation indicated that high-power operation cannot be started prior to shroud ejection; the restraints due to the resulting temperature rise in Compartment A were evaluated. The program for postlanding spacecraft attitude determination was formulated. A computer routine has been designed for generating simulated spacecraft telemetry data for use in system checkout.

Flight control. In structural coupling tests with the S-2 vehicle, no inertial control loop instability was encountered under simulated vernier engine vibration inputs. Acceptance tests were completed on the first flight models of the secondary Sun sensor, inertial reference unit, and electronics unit. Type approval testing of the gas jet valves and the inertial reference unit was completed.

Electronics. Coverage of the single omnidirectional antenna as mounted on the spacecraft dynamic test vehicles was measured with a full-scale model. Steps are being taken to prevent excessive heating and cooling of the altitude marking radar under mission conditions. Investigation of vibration problems encountered in type approval tests of the radar altimeter and doppler velocity sensor is continuing; an improvement was made in the klystron to meet the 250-hr life requirement. Circuit improvements were made in the electrical converter unit for the central command decoder in order to reduce waveform spikes in the switching transistors and various outputs.

Electrical power supply. Type approval testing of the solar panel was successfully completed, and flight acceptance testing of the first flight panel has begun. A statistical analysis of performance at Table Mountain, California, indicates that the solar panel output meets requirements. Structurally improved battery cells were vibration tested

with satisfactory results, and main batteries incorporating the changes are scheduled for testing in early May. Three auxiliary batteries passed type approval tests.

Thermal control. An overall design review of thermal control provisions was held on March 31. Compartment design changes resulting from S-2 vibration test experience were evaluated with respect to thermal control. Thermal design requirements for the alternate vernier thrust chamber assemblies were studied. Thermal provisions for simulated lunar day and night testing of the T-21 spacecraft have been defined.

Engineering mechanics. In the touchdown dynamics program, data from the S-2 drop tests are being used to upgrade the rigid-body mathematical model; the improved model will increase the accuracy of the elastic-vehicle computer program. Modifications were incorporated in the landing gear shock absorber due to the failure of a developmental model in drop tests; two type approval units exhibited satisfactory strength in further drop tests. Two structural failures occurred in drop testing of the S-2 vehicle; the vehicle, presently being upgraded to incorporate structural improvements and to represent the current spacecraft configuration, will be retested.

Propulsion. The main retro-engines were successfully fired with the thermal gradients expected in a mission. Burst tests of two engine cases confirmed satisfactory design margins. The retro-engine design was frozen, and qualification tests will be conducted in July. Development of the vernier thrust chamber at the Thiokol Chemical Corporation, Reaction Motors Division, was terminated, and an evaluation of alternate thrust chamber assemblies was completed. A tank development program, including welding processes for aluminum tanks and manufacture of titanium tanks, is under way. The S-7 vernier propulsion test vehicle completed vibration tests and was shipped to the Air Force Missile Development Center (AFMDC) for further tests involving the use of propellants.

Spacecraft vehicle and mechanisms for basic bus. A new spacecraft for T-21A is being built to replace the one reassigned to the S-8 buzz test vehicle; A-21A substructure design work has started in accordance with the recent decisions on the scientific payload. S-8 substructure fabrication has begun, and preparations have been made to reinforce the Aerobee tower for the buzz tests. The lightweight landing gear successfully completed the dynamic portion of type approval tests. Two structural improvements in the omnidirectional Antenna A mechanism are being made as a result of hardware failures in type approval tests. Increased strength is also being built into the antenna/solar panel positioner so that it will be able to withstand the loads encountered in vibration tests of the S-2 vehicle.

Reliability, quality assurance, and system test. Reliability estimates were upgraded, and vendor surveillance was maintained continuously. Reliability margin testing of pyrotechnic devices is under way. Various thermal coatings and repair procedures were evaluated. Quality assurance activities included improvement in documentation of standard fabrication practices, implementation of quality audits in all Hughes work areas, and continuing audit of subcontractor effort. Two additional series of T-2 horizontal static firing tests were completed to evaluate acoustic shields on the radar antennas and radar reaction with the spacecraft footpads; descent dynamics tests of the T-2 vehicle in drops from a tethered balloon will begin during the next report period. The first pass through type approval functional testing of the T-21 spacecraft (except for vernier propulsion, television, and telecommunications systems) is nearly complete, and the spacecraft will be upgraded early in the next report period. A high-frequency vibration test on T-21, with inputs at the vernier engine brackets, was made to obtain realistic vibration test parameters for the radar altimeter and doppler velocity sensor (RADVS) system.

Mission operations. Procedures were formulated for the spacecraft readiness tests to be performed at the launch complex prior to removal of the gantry from the launch vehicle. The overall launch complex operations were described in the Launch Complex Operations Directive released during this report period. Operation of the programmed automatic telemetry evaluator in conjunction with the command and data handling console (CDC) was demonstrated. The Launch Operations Plan, the primary document for coordination of all operations and tests required for a *Surveyor* launch, was released. The CDC for the Goldstone Tracking Station was shipped on April 9.

Study on Block II Surveyor. A study was completed on the Block II *Surveyor*, proposed for soft landing lunar payloads in the period from 1967 to 1969. Minimum change from the A-21/A-21A (Block I) basic bus was assumed. Payload capability was determined for various combinations of alternatives, including spacecraft injected weight, vernier propulsion throttle range, main retro case material and propellant type, and transit trajectory class. Payload weights varied from 157 to 318 lb in the 18 configurations compared in this study. Use of a radioisotope thermoelectric generator in the power system and an increase in landing area and accuracy were also considered.

A. System Engineering

1. A-21 Spacecraft Configuration

The general arrangement of the A-21 spacecraft as described in *Space Programs Summary No. 37-25,* Vol. I, is essentially unchanged. However, certain changes affecting the vernier system installation and integration may be required as a result of changes in the vernier thrust chamber assemblies.

A detailed weight and balance status report is not available at this time because evaluation of the effects of vernier system changes, as well as evaluation of structural changes in the antenna/solar panel mast and compartment supports, has not been completed.

2. Functional Description for A-21 System

Functional schematic diagrams of the A-21 spacecraft system have been prepared to show the detailed system functional interrelationships and to assist in system test, mission operations, postflight evaluation, failure mode analysis, and spacecraft familiarization. The second revision of the functional description document was released on April 1, 1964. The title of this publication has been changed and is now called the *Surveyor* Functional Description, A-21. This three-volume publication contains functional descriptions and the theory of operation for each functional area of the A-21 spacecraft and complements the functional schematic diagrams. The functional descriptions are divided into sections, each section corresponding to a single diagram.

3. Dynamic Vehicle Models (SD-1, -2, and -4)

The SD-1 and SD-2 vehicles are to be used on *Centaur* launches AC-5 and AC-6. SD-4, the type approval test vehicle, completed testing successfully and was shipped to Lewis Research Center in February (Fig. 1).

Models SD-1 and SD-2 will be provided with S-band transponders to permit tracking of each vehicle after separation from the *Centaur*. The transponder subsystem was described in *Space Programs Summary No. 37-26,* Vol. I. The omnidirectional antenna and mast assembly designed for use with the S-band transponder on SD-1 and SD-2 were mounted on SD-4 prior to the type approval test vibration and withstood the test satisfactorily.

A recent change order authorizes addition of filtering in the accelerometer and strain gage channels to provide compatible inputs to the telepaks in the retro motor simulator. Filter parameters were determined and orders were placed with Genisco, Inc. Engineering required for installation and interconnection of the filters has been completed.

A transponder compartment has been delivered and installed on SD-1 (Fig. 2) with dummy weights simulating the subassemblies. A modal vibration survey is under way. A second transponder compartment is available for integration with the first transponder and system. Integration and system test will start early in the next reporting period.

Omnidirectional antenna radiation pattern measurements were made on a full scale model of the dynamic test vehicle with the antenna mounted on a mast at the

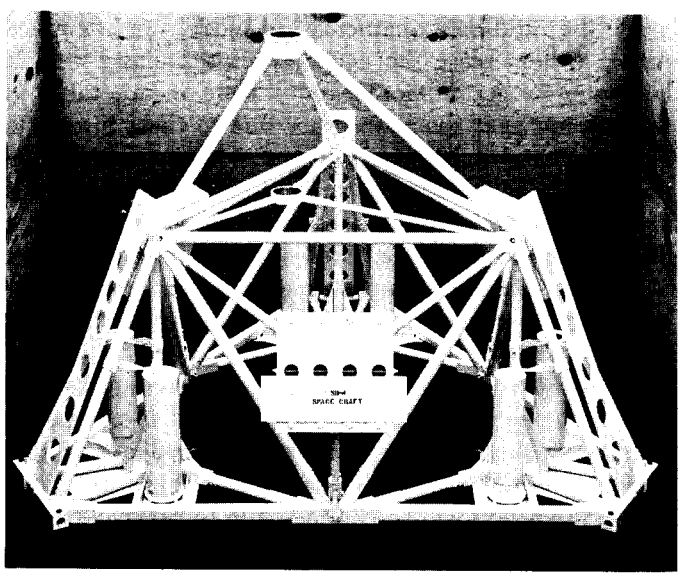

Fig. 1. SD-4 type approval test vehicle

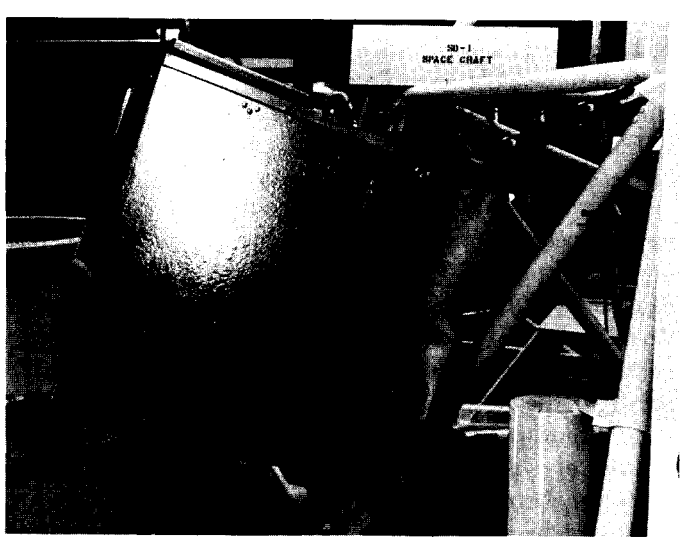

Fig. 2. S-band transponder compartment on SD-1

top of the vehicle similar to the manner in which it will be mounted on the flight vehicles. Test results are to be used in the dynamic vehicle Deep Space Instrumentation Facility (DSIF) acquisition study.

Specifications for system functional test have been prepared. The transponder test equipment requirements were established. The major item of test equipment is an rf system test equipment assembly (rf STEA). Other items peculiar to the dynamic vehicle are:

(1) 560-cps discriminator for demodulating the static phase error signal.

(2) Regulated power supply to provide external power to the transponder during all phases of test.

(3) Control panel containing the command pulse generator and selector switch for transponder operation. The commands are System ON, System OFF, High Power-External, High Power-*Centaur*, and Low Power. The control panel also contains a switch for selection of test points to be monitored during test. The test points are brought out from the subassemblies and accessible for system evaluation and fault isolation.

(4) Test cabling and junction box.

Fabrication of an additional rf STEA for use on the dynamic vehicle program is under way. The special items of test equipment, including cabling, have been purchased or fabricated. The completed test setup will be assembled and checked out prior to the beginning of system test.

4. Spacecraft Interconnections

An investigation was conducted to find the best method of twisting wires in the spacecraft harness to provide maximum electromagnetic compatibility and minimize switching transients. The power distribution and squib firing circuits were analyzed in detail. Tests showed that a 2- to 3-db improvement in minimizing switching transients can be achieved by changing the twisting procedure. Each of the individual leads should be twisted with its return, instead of twisting all leads of the multiple group together.

A second study was made to analyze the spacecraft harness shielding system. Drawings were made of all shielded wires used in the harness and an analysis was made to determine the appropriate shield terminations for each individual circuit. It had been determined earlier that the major contribution to the electromagnetic compatibility problem was the electronics conversion unit (ECU), which fed excessive noise back on the 22- and 29-v power lines. Tests were made to evaluate the effectiveness of terminating shields at one end compared with terminating shields at both ends. A 1-v peak-to-peak signal was placed on two twisted pairs with a common shield, and the crosstalk was measured across an unshielded pair with a 50-ohm load terminated at each end. Results proved that the advantage of grounding one end over grounding both ends varied from 7.9 db at 2 mc to 6 db at the upper limit of 5 mc. In some cases, the shield terminated at both ends would connect the spaceframe ground to the 29-v return. This problem was solved by terminating power distribution shields at only one end, which eliminated some ground loops.

Buzz test program. During this period, most of the engineering for the spaceframe components of the S-8 vehicle was released and fabrication started. The required vehicle instrumentation has been determined and special accelerometer amplifiers are being designed. Final scheduling of the completion date is dependent on vernier thrust chamber assembly availability. The suspension is discussed in Section K of this report.

B. Scientific Payload

1. Payload System Engineering

a. Systems integration. During this report period, authorization to incorporate the provisions of pending engineering change proposals (ECP) into the spacecraft system was received from JPL. As a result, the scientific instrument/spacecraft interface specifications were revised to provide for a hard mounted single-axis seismometer (instead of a deployable sensor), to add instrumentation to the surface sampler, to define a single-sensor micrometeorite ejecta detector, and to establish new parameters for a deployable alpha scattering instrument. Instrument, instrument auxiliary, mechanism, and overall system design is being undertaken on the basis of this payload redefinition.

In addition, JPL has recently proposed changes in the surface sampler and alpha scattering instrument interface specifications to allow for a modified operational capability. After the alpha scattering instrument sensor head has been initially deployed to the lunar surface, the deployment mechanism provides the capability to allow the sensor head to be lifted, moved, and replaced on the lunar surface by the surface sampler. In addition it is proposed that the sensor head be capable of being repositioned by the surface sampler to at least one location that has been prepared by the surface sampler. The sensor head in all possible deployed locations is to be within an unobstructed view of at least one of the television cameras.

The initial conceptual design for the alpha scattering instrument deployment mechanism consisted of a two-bar parallelogram-type linkage system to lower the sensor head to the lunar surface. This mechanism was restricted from azimuthal motion. The change proposed would require the addition of an azimuth pivot capability in the deployment mechanism after initial deployment of the sensor head, reorientation of the surface sampler and the alpha scattering instrument, and the addition of a device on top of the sensor head to allow pickup by the surface sampler.

Technical coordination meetings have been held between Hughes and JPL to review the proposed change. The submittal of a formal ECP regarding this matter is pending JPL evaluation of the Hughes preliminary analysis.

2. Payload System Laboratory

Efforts on the payload system during the report period were as follows:

(1) Re-evaluating test requirements, test plans, and test configuration design for each experiment in light of ECP approval.

(2) Completing a test requirements document for each experiment.

(3) Completing a preliminary test plan for each experiment.

(4) Reviewing with JPL, Goddard Space Flight Center, and Marshall Laboratories the requirements for the micrometeorite ejecta detector stimulus.

(5) Completing the design of such test equipment items as a modularized junction box and a test configuration auxiliary common function panel.

(6) Investigating seismic ambient noise levels in the payload system testing area.

(7) Starting special test equipment fabrication.

a. Test requirements and test plans. Test requirements have been completed for each experiment subsystem. These requirements reflect inputs from all known documents relating to each experiment, e.g., functional, design, and interface specifications, JPL test specifications, etc. Table 1 illustrates the format of these test requirements.

A preliminary test plan for each scientific experiment subsystem has been completed and conforms in general to the outline shown in Table 2.

b. Micrometeorite ejecta detector stimulus. Instrument checkout and experiment subsystem testing of both the payload systems and the spacecraft systems require the use of a standardized micrometeorite ejecta detector stimulus. To avoid unnecessary engineering and design and to assure standardization throughout the program (experimenter, instrument vendor, JPL Space Sciences, payload systems, and spacecraft systems test), JPL was requested to consider having NASA and/or their instrument vendor (Marshall Laboratory) provide a standard stimulus for integration into both the payload system and spacecraft system test equipment. A proposed panel layout is depicted in Fig. 3.

c. Payload system test junction boxes. An interconnecting junction box and rack assembly has been designed for the payload system simulated spaceframe. Fabrication is expected to start in April.

The assembly will be mounted on the spaceframe in place of spacecraft Leg 1 as illustrated in Fig. 4. Seven $5 \times 7 \times 15$ in. junction boxes will be provided to accomplish easy interconnection between experiments and remote payload system test equipment. One junction box

Table 1. Example of test requirement format

Test requirement number	Test phase	Parameter or function to be tested	Requirement	Reference
A517	Instrument functional operation	Spacecraft clock signals	(1) Alpha clock: 550 cps ±0.1% square wave +11 v dc ±2 v dc high state +0.2 v dc ±0.2 v low state less than 10 μsec rise and fall times. (2) Proton clock: 2200 cps (±0.1%) square wave; same as (1) above.	Interface specification — alpha scattering instrument 239303
A518	Instrument functional test	Command inputs 1 through 11	Monitor command input pulses: width: 21 ±4 msec rise time: 0.1 to 2 msec fall time: 0.1 to 5 msec base line: 0 to —0.01 v with 1 k-ohm load.	Interface specification — alpha scattering instrument 239303
A519	Instrument functional test	No trigger test voltage	Monitor test pulse as follows: 4-v peak in series with 1000 ohms rise and fall time: 20 μsec (maximum) pulse width: 20 ±5 msec pulse rate: 25 pps (maximum)	Interface specification — alpha scattering instrument 239303
A520	Instrument functional test	Command response	(1) Application of detector ON and OFF commands to instrument result in correct lamp indication on control panel. (2) Instrument shall not respond to command pulse as specified in A519.	Interface specification — alpha scattering instrument 239303
A521	Instrument functional test	Electronic unit functional test	Apply fixed pulse width signals to electronics unit to simulate sensor head outputs for various channel numbers. Data input signals for alpha and proton shall be as specified in 239303. zero word: 100000000 126 word: 111111100	Interface specification — alpha scattering instrument 239303

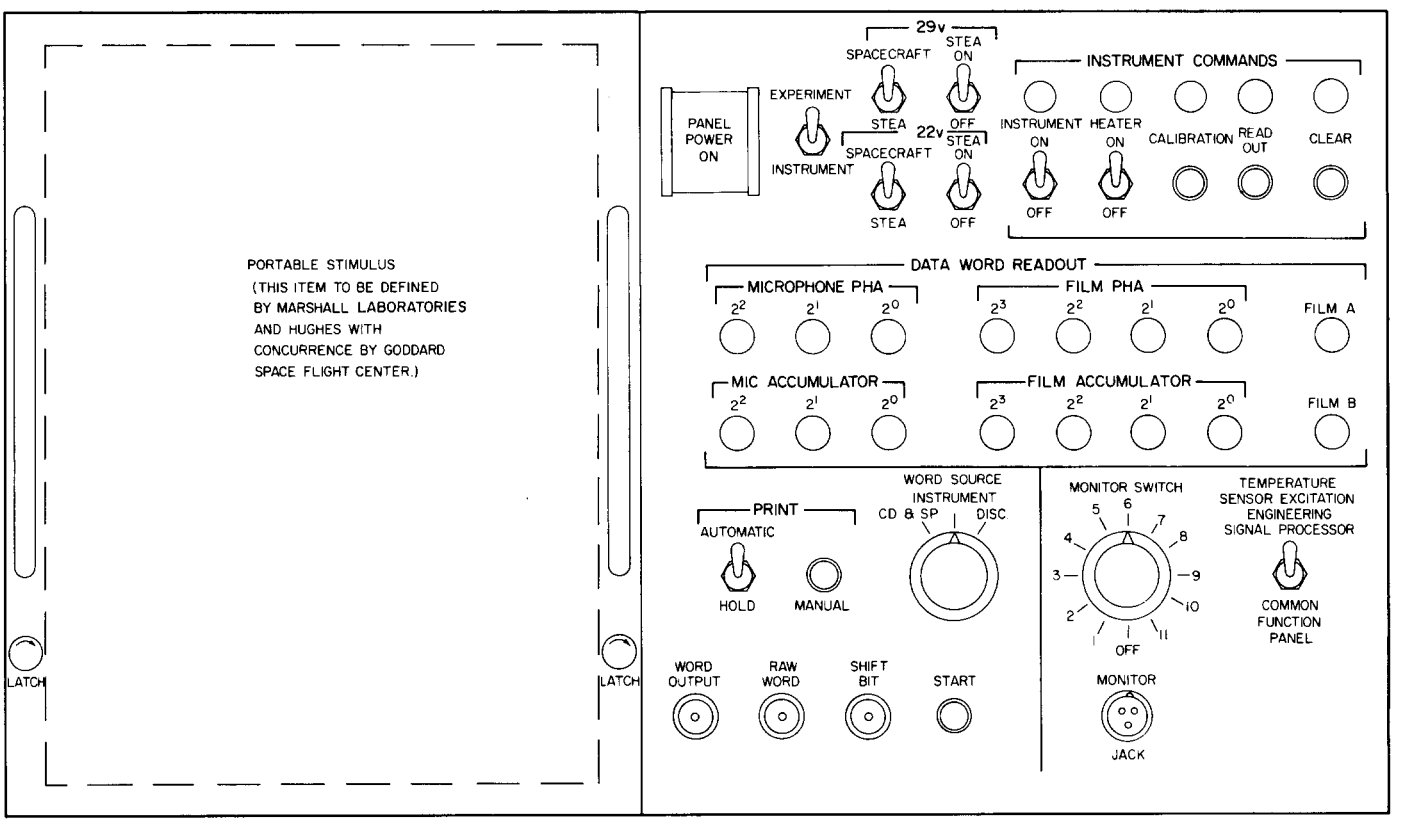

Fig. 3. Micrometeorite ejecta detector experiment panel

will be used to supply all common spacecraft and experiment power and signals to and from the individual junction boxes which are provided for each experiment. The experiment junction boxes containing T-connections, test points, switching functions, and test panel interconnections are easily removed and disassembled for rapid repair, modification, or replacement with minimum expense and equipment downtime. Payload changes can be accommodated by utilizing the two spare junction boxes or replacing a deleted experiment J-box, test equipment panel, and associated interconnecting cables.

d. Auxiliary common function panel. A preliminary panel layout design of the auxiliary common function panel is shown in Fig. 5. A functional diagram depicting the control and monitor functions provided by the panel is shown in Fig. 6. The engineering and central signal processor control and monitor functions have been described in previous reports. Among the additional test features provided are the following:

(1) Test of engineering mechanisms auxiliary (EMA) prior to use in an experiment.

(2) Change of simulated squib load to a circuit breaker selected to trip within 10 msec with normal current pulse applied from EMA, a fixed 1-ohm resistor for investigating a squib "no fire," and a test lamp for low current level continuity test of each squib circuit.

(3) Substitution of EMA with experiment 22-v dc source for low current level testing of experiment auxiliary.

(4) Current shunts for monitoring pulse waveforms.

The solenoid actuator provides for the operation and control of various experiment mechanism release solenoids, used in test in lieu of pyrotechnic squib release devices. A 60-msec, 30-amp pulse is applied to the selected solenoid upon depression of the actuate switch on the panel. The squib-circuits-test portion of the panel provides the required control and monitor points for testing the engineering mechanism auxiliary and all experiment squib circuits. When squib circuits are not being directly tested, stray voltage monitors will be installed at all experiment squib connectors in lieu of actual squibs as a safety factor and to determine unsafe voltage levels during normal test procedure.

e. Seismic ambient noise level tests. As a prerequisite to complete development of test methods and procedures for the seismometer experiment subsystem, it was required that the ambient seismic noise level in the payload system test area be measured. Appropriate geophones were obtained from JPL for this purpose. Data obtained (horizontal and vertical motion detected with the sensors placed on the laboratory floor) is shown in Fig. 7.

This test data indicated an ambient noise level of approximately 0.002 in./sec (peak-to-peak) in the vertical direction and approximately 0.001 in./sec (peak-to-peak) in the horizontal plane. Under these conditions, the *Surveyor* seismometer amplifier would saturate even at its lowest gain setting. (The sensor would produce approximately 30 mv at a noise level of 0.002 in./sec based on the *Surveyor* prototype sensor sensitivity of 15 v in./sec.)

Table 2. Preliminary test plan outline

I. Testing objectives		
II. Experiment system functional description		
III. Test requirements		
IV. Test description	(1) Test sequence	
	(2) Test configuration (functional block diagrams and descriptions)	
V. Test facilities		
Special test equipment	(1) Test fixtures	
	(2) Test racks and panels	
	(3) Stimulus	
	(4) Data logging and recording	
Commercial test equipment (type and specifications)		
Location and space		
VI. Schedule		
VII. Evaluation/reports	(1) Evaluation/analysis	
	(2) Failure data	
	(3) Repair plan	
	(4) Data sheets	

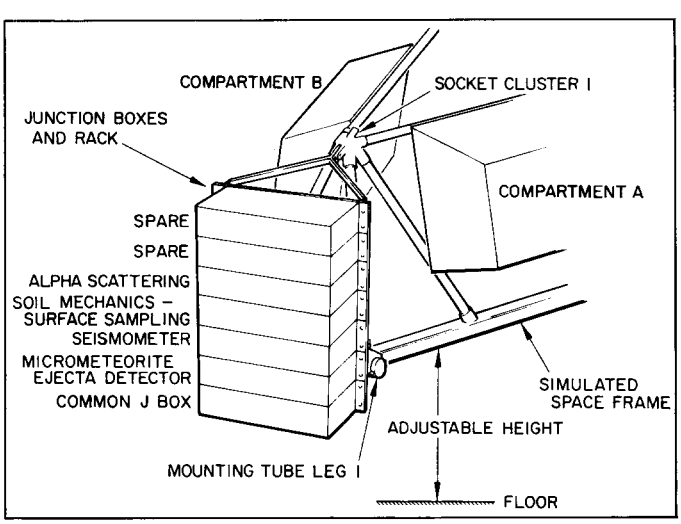

Fig. 4. Payload system junction box installation

To overcome this problem it is planned that a calibrated attenuator be placed between the seismometer sensor and its associated amplifier during test.

Similar tests are being repeated where spacecraft system test on T-21A will be conducted.

f. Fabrication of special test equipment. Fabrication of a portion of the test equipment which will have general usage for all planned experiments has been started. Completion is expected in mid-May.

3. Television Subsystem

a. T-21 survey camera. Two discrepancies in this camera were discovered during system testing in February 1964: (1) there were oscillations in the mirror drive circuit, and (2) the spacecraft transmitter was not responsive to a transmitter OFF command generated by the central command decoder (CCD) when the T-21 survey camera was connected to the spacecraft harness and not energized by 22-v dc and 29-v dc power.

The mirror drive circuits were determined to be oversensitive to the second step of the two-step mirror commands. Each step occasionally triggered the other, resulting in oscillations. The circuit modifications required to correct this discrepancy are discussed in paragraph *e* below. Immediate incorporation of these changes would have substantially delayed return of the camera to system test. The second step of both the two-step mirror right and the two-step mirror left commands was therefore disabled so that partial system test could resume. This discrepancy will be corrected during the 4-wk upgrade period which is scheduled to start in April 1964.

The second problem is concerned with interaction among the spacecraft transmitter, central command decoder, and survey camera. The problem appeared when the survey camera was connected to the spacecraft harness but the camera was not turned on. Under these conditions the transmitter could not be commanded OFF. When the camera was disconnected from the harness or when the camera was turned ON this problem was not present. Loading of the command line by a decade resistor disclosed that an impedance of less than 1700 ohms caused the problem to reappear.

Investigation of the camera transmitter OFF command circuitry (see Fig. 8)shows that a positive pulse at junction 180 J1-34 was subjected to an impedance slightly greater than 1500 ohms. This impedance was presented by the series combination of the forward impedance of CR4, the forward base-to-emitter impedance of Q5, and resistance R15 (1500 ohms). This path is presented by

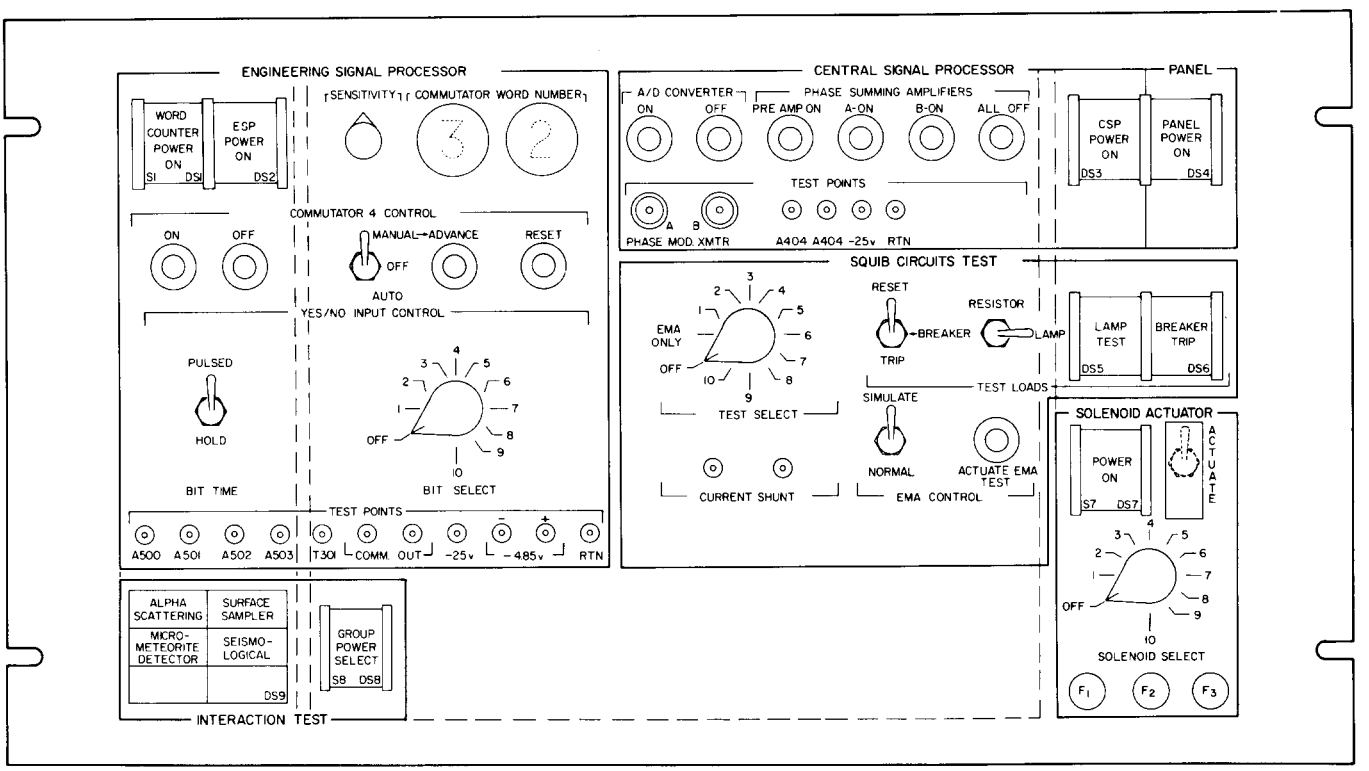

Fig. 5. Auxiliary common function control panel

the vidicon thermal control circuits inside the camera. When the camera is turned ON, transistor Q5 is biased in such a manner that this circuit no longer presents a problem.

Addition of a diode as shown in Fig. 8 places a high impedance in series with this circuit as seen from 180 J1-34. Thus, the command pulse generated by the CCD sees an impedance greater than 100,000 ohms but the camera generated pulse finds a low impedance path to the transmitter. This modification has been accomplished and will also be incorporated in all flight cameras.

After the repairs were incorporated into the camera, it was reinstalled on the T-21 vehicle. When testing was resumed, it was noticed that five of the thirteen telemetered frame ID signals were not received by the test console. Additional fault isolation, group, and telecommunication integration testing is in process and will be completed prior to the upgrade period.

b. T-21 approach camera. Special testing was accomplished during March to determine the camera susceptibility to spacecraft generated noise. Tests were performed with the following general conditions: (1) central power control turned on, camera operating from external power supplies; and (2) central power control turned on, camera operating from central power control (spacecraft) power.

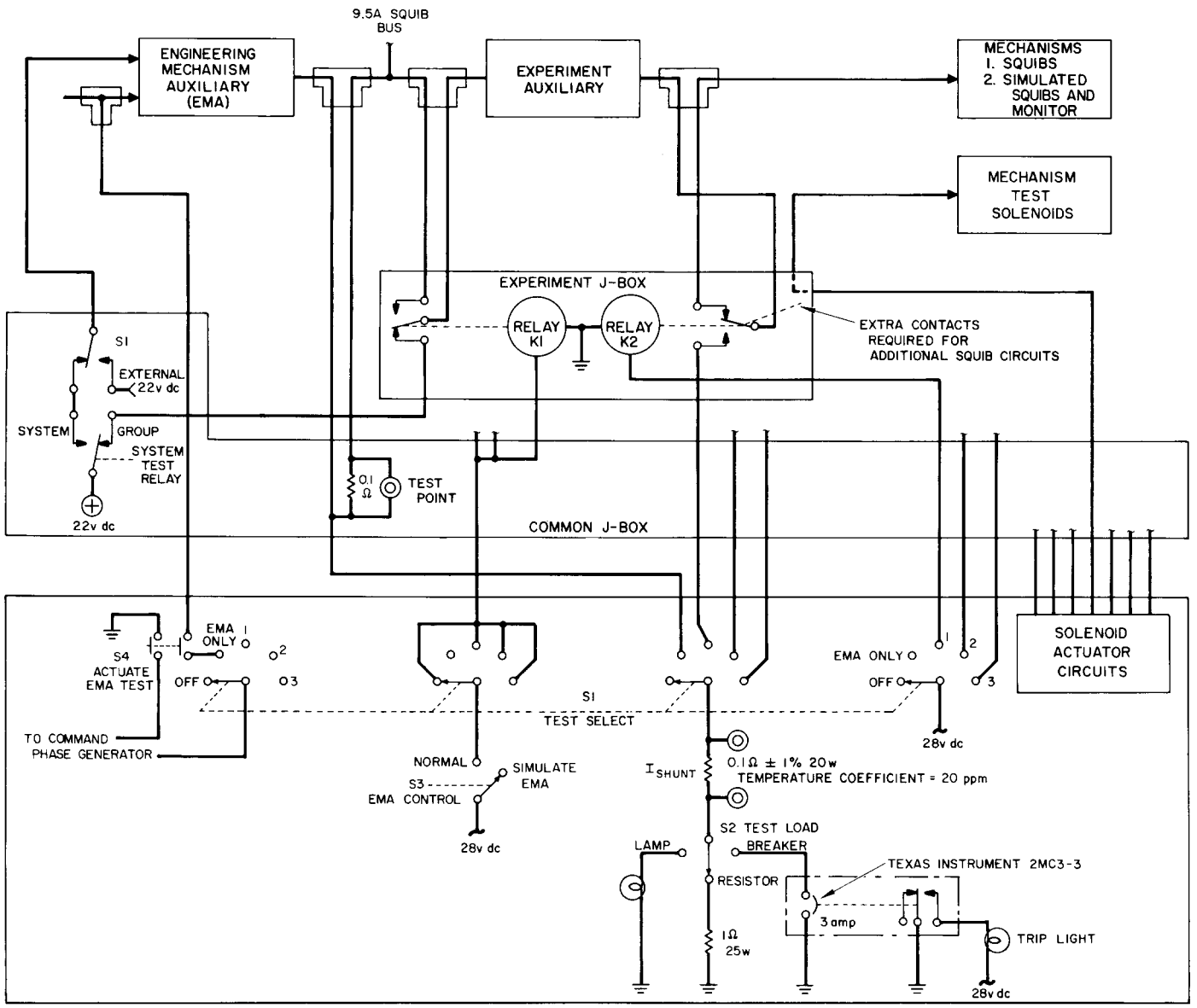

Fig. 6. Auxiliary common function panel

During both of the above test conditions the noise level radiated into the camera is excessive; however, no substantial difference exists between the two conditions.

The third test condition of interest consisted of operating the approach TV camera from the central power control system and with the radar altimeter and doppler velocity sensor (RADVS) in the ON condition. Doing so raised the noise to approximately 4 v peak-to-peak, a level which precludes obtaining a usable picture from the TV system. During the conduct of a mission, approach TV pictures will be taken starting at a nominal altitude of 1000 mi to a nominal altitude of 80 mi, all without the RADVS on. It is further desired that approximately two approach TV pictures be taken after retroengine firing, and it would be under this condition that the RADVS would be on.

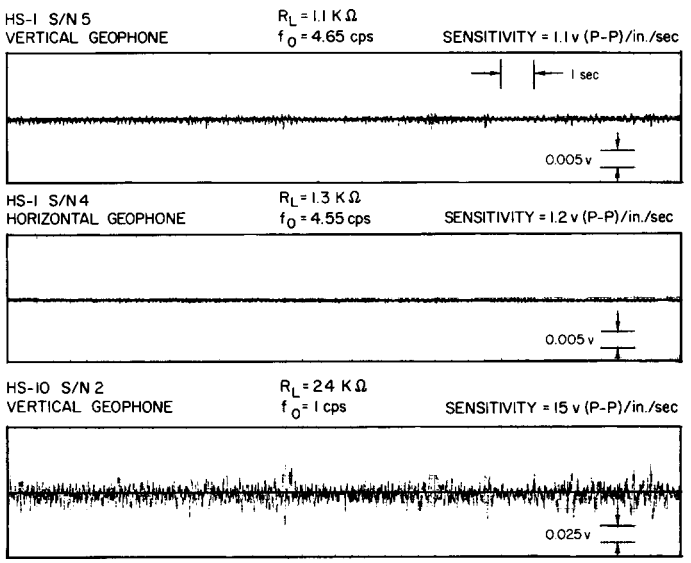

Fig. 7. Payload system-test-area seismic ambient noise

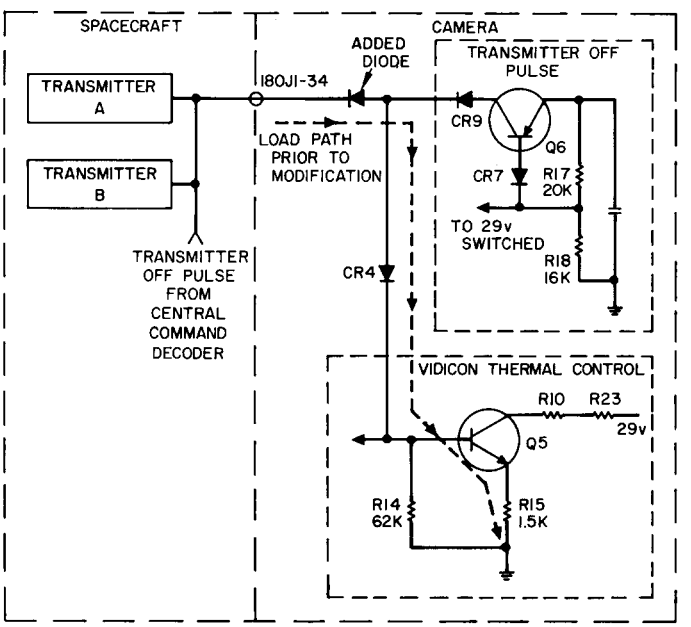

Fig. 8. Command "transmitter off" circuitry

c. Survey camera, S/N-11. This camera, intended for initial functional testing on SC-1, has been assembled and will start flight acceptance testing in April. In its present configuration, this camera does not incorporate the modification discussed in paragraph *e*, below, but will be retrofitted in August 1964 and assigned to SC-2. No unexpected difficulties have been encountered with this camera.

d. Approach camera, S/N-11. This camera is also intended for initial functional testing on SC-1 and has undergone some of the unit-level functional testing. This functional testing has revealed several discrepancies, including those described in the paragraph below; these discrepancies are being investigated and corrected so that initial camera delivery is expected to occur on May 1, 1964. As in the case of the survey camera S/N-11, this camera will be retrofitted in August 1964 and assigned to SC-2.

The discrepancies noted during functional flight acceptance testing were: (1) excessive noise was caused by the thermal control circuit and evidenced in the video output; (2) horizontal and vertical relative response was out of specification limits except at the corners of the format and varied with input line voltage; and (3) camera sensitivity increased at lower light levels rather than decreased. Test equipment problems were also evidenced and have been corrected. The camera was very susceptible to magnetic fields generated by test equipment in the laboratory but not associated with TV testing. Also, the video amplifier oscillated whenever the vidicon heaters were turned on. This problem was traced to excessive capacitance in the test equipment caused by an oscilloscope in the video line and was eliminated by suitable isolation.

e. Survey camera for type approval testing. As described in previous reports, the TV camera intended for type approval testing (TAT) exhibits command interaction failures at both low and nominal voltages and at temperature extremes. Until recently it was planned to conduct a limited TAT prior to incorporating the modifications described in paragraph *f* below, subsequently incorporate the modifications, and then conduct those portions of the type approval test not previously run. Recently, however, the vidicon in this camera was damaged so that functional testing could not be accomplished. The current plan is as follows:

(1) The camera will be used to measure and record conducted and radiated interference generated by the camera, as well as measure and record susceptibility of the camera to conducted and radiated noise from other spacecraft subsystems. This testing will occur during April.

(2) Thereafter, the camera will be upgraded with circuit modifications conforming to those to be incorporated in the SC-1 camera. Simultaneously the vidicon will be replaced.

(3) The formal TAT will start in the third week in July and will include all of the type approval test requirements.

This plan will complete type approval testing at the end of August prior to the start of system functional testing of the SC-1 spacecraft.

f. Circuit modifications. Several of the failures described above can be classified as command interaction failures. These are either (1) command responses to spurious or "no trigger" commands at low line voltages or extremes of temperatures, or (2) responses on command lines other than the intended command lines. These deficiencies, in general, occur in circuits which have been determined to be functionally marginal in operation at low temperature. The solution to these various discrepancies takes the form of one type of circuit modification. A qualitative discussion of the failure and the design solution follows using as an example one of the typical circuits that is affected. Fig. 9 is such a typical command module.

Under normal operation, transistor Q1 is conducting while transistor Q2 is not conducting. A trigger pulse is applied to the base of transistor Q2 which causes Q2 to turn on and Q1 to turn off. Subsequently, transistors Q3, Q4, and Q5 turn on for a time interval governed by the time constant $t=R_1C$, which controls the operation of the function, e.g., mirror azimuth step.

The command interaction occurs in the following manner. When transistor Q4 turns on, a current, ΔI_L, flows, which causes the 29-v line voltage to fall an amount $\Delta E = \Delta I_L R_3$. Since other camera circuits also derive their line voltage from this bus, an error signal, ΔE, is applied to these other circuits. The command interaction failure occurs when ΔE is large enough to trigger these other circuits.

When the line voltage drops by ΔE, current will flow from point A to B. The only path which can supply this current is path CDA. The base drive current of transistor Q1 is lowered causing Q2 to turn on, resulting in an erroneous switching of circuits. The voltage ΔE necessary to trigger the circuit is

$$\Delta E = R_2(I_{R_1} - I_{bQ_1})$$

where

I_{R_1} = current through resistor R_1

I_{bQ_1} = required base current of transistor Q1

Command interaction occurs when the line voltage drop, $\Delta I_L \times R_3$, is greater than ΔE.

Several circuit changes are required to ensure solution of the command interaction problem. First, the line drop is lowered by decreasing R_3. This causes smaller error signal voltages. Second, the voltage necessary to cause triggering, ΔE, is made as large as possible. Since $\Delta E = R_2(I_{R_1} - I_{bQ_1})$, I_{R_1} is increased and I_{bQ_1} is decreased. I_{R_1} is increased by lowering the resistance of R_1; however, to maintain the time constant, C must be increased the same proportion. I_{bQ_1}, the required base drive, is decreased by replacing Q1 with a transistor with a higher β.

The low temperature failure is solved simultaneously with the command interaction problem. Circuit analysis

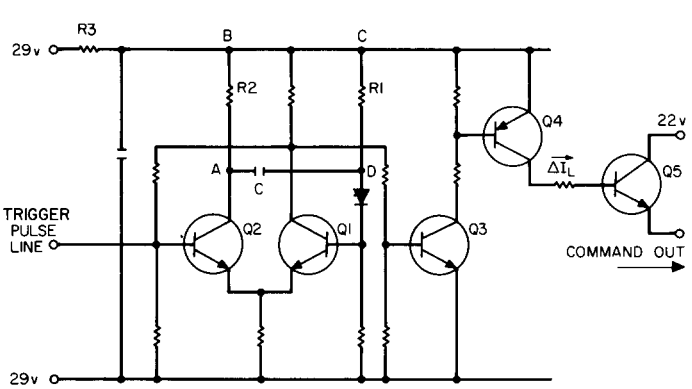

Fig. 9. Typical command module circuit

shows that this failure occurs when the base current, I_{bQ_1}, drops at low temperatures, causing Q2 to turn on. Changing the transistors Q1 and Q2 to those of higher β ensures that lower base current is required to keep Q1 on, while lowering the resistance of R_1 allows for increased base current.

These circuit changes, together with others described in previous reports, will be incorporated in all cameras starting with those intended for SC-1.

g. Optical alignment of camera subassemblies. An analysis was conducted to determine the maximum possible misalignment between the entrance pupil of the television camera and the center of the vidicon faceplate. The entrance pupil is the intersection of the azimuth and elevation axes of the scanning mirror. The local geometry is shown in Fig. 10. In a camera designed for recovery of photogrammetric information, it is desirable to maintain the angle θ as small as possible.

The camera components involved in alignment of the mirror with the faceplate are mechanically connected through a series of mating cylindrical surfaces. A dimensional analysis of these cylindrical fits yielded the following figures for lateral displacement of the center of the vidicon faceplate with respect to the entrance pupil: maximum displacement = 0.0313 in. and rms displacement = 0.0125 in. The maximum angular misalignment is

$$\theta_{max} = \tan^{-1}\frac{0.0313}{10.595} = 0^\circ\ 10'$$

This analysis indicates that satisfactory alignment can be achieved through control of dimensional tolerances.

Optical alignment of subassemblies within the camera also requires that certain other conditions exist. Typical of these conditions and the means by which they are achieved are as follow:

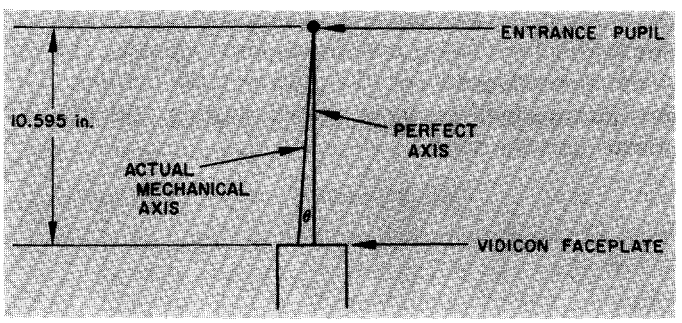

Fig. 10. Vidicon geometry

(1) The vidicon faceplate and the camera azimuth axis must be perpendicular. To achieve this, the vidicon is suspended by three arms approximately 120 deg apart on a machined spider. The perpendicularity requirement is met by raising or lowering these three arms by means of shims and thereafter fastening them into permanent positions by means of bolts.

(2) The distance between the lens mounting face and the vidicon faceplate is critical because the vidicon faceplate represents the plane on which the lens image focuses. This adjustment is performed on each camera assembly and thereafter the tube is held in place by means of a screw-on cap.

(3) The elevation axis of the mirror must be located on the reflecting surface of the mirror so that the image will be centered and the elevation and azimuth axes of the mirror intersect. This is accomplished by assembling the mirror to its elevation drive mechanisms in a holding fixture that locates the reflecting surface on the elevation axis to within 0.005 in. The two drive axes are located in the same holding fixture to within 0.010 in.

h. Variable focal length lens. It was previously reported that a modification to the lens assembly was in process of being implemented in order to preclude what is referred to as a shift-of-focus and decentration problem. This shift-of-focus problem is evidenced by a loss in resolution greater than allowed by the specification when shifting from one focal length extreme to the other focal length extreme. The decentration problem is evidenced in a similar fashion when varying either the focal length or the focus setting. The former is caused by an off-center location of a lens triplet; the latter is caused when one or more of the individual lens elements is not optically aligned with the remainder of the lens elements.

The optical elements of the lens system consist of 12 individual lens elements arranged in four distinct groups, as shown in Fig. 11. The optical axis of each element and of each group of elements must be colinear and must remain so since the relative location of the elements changes when focal length or focus setting is changed. The focus cell rotates and translates on screw threads

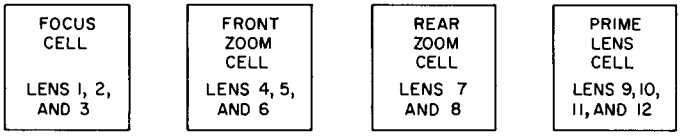

Fig. 11. Lens group

relative to the other elements. This allows the lens to remain in focus for object distances from 4 ft to infinity. The front zoom cell rotates and translates on a hyperbolic cam. Only the extremes representing focal lengths of 25 and 100 mm are of critical interest. The function of the rear zoom cell is to maintain the lens system in focus between the critical extremes of the front zoom cell. This is a safeguard against possible malfunctions of the front zoom cell at positions other than the extremes. The prime lens cell is a basic image-forming pair of doublets with a fixed location.

The following two sets of design modifications were incorporated and represent a solution to both problems simultaneously.

(1) The tolerances specified in the manufacture of the hyperbolic cam slot were tightened to 0.0005 in. Tolerances as close and repeatable as 0.001 in. were found to be detrimental.

(2) Provisions were made to hold Lens Element 1, the first element in the focus triplet, and Lens Element 5, the second element in the zoom triplet, by means of split annular rings. The rings and their respective lens elements could then be adjusted relative to the other lens elements by means of set screws. In effect, this allows an off-center location of these elements of as little as 0.0005 in. as compared to the previous design which allowed as much as 0.0015 in. These two lens elements were selected because their effective resolution sensitivities are three times greater than that of any of the other elements.

These design modifications have been incorporated into five lens subassemblies, each of which yielded average resolution greater than 95 optical line pairs per millimeter. Specification requirements call for average resolution greater than 88 optical line pairs per millimeter.

Lens-level type approval tests had previously been started on Lens S/N-2. In view of the design modifications, however, this test was stopped prior to any environmental tests so the modifications could be incorporated in the test unit. The lens now being used for type approval testing is designated Y-5; functional type approval tests started in March. Type approval test completion is scheduled for the last week in June; to date, no difficulties have been encountered.

i. TV mirror unit. As previously reported, the present TV mirror drive mechanisms are not capable of repeatedly positioning the mirror in azimuth and elevation to the required accuracy of ± 6 min of arc under all combinations of input voltages and temperature extremes.

A detailed analytical and design study was initiated to determine the mechanical and electrical redesign that would be needed to meet this requirement. The proposed elements of the new design are:

(1) Redesign both elevation and azimuth gear trains using spur gears and incorporating a Geneva mechanism to perform positive positioning, locking, controlled acceleration, and a large tolerance on the starting and ending position of the driver.

(2) Change existing drive motors to three-phase variable reluctance, high frequency stepper motors. This would necessitate redesign of the existing power supply.

(3) Incorporate preloaded ball bearings into the main azimuth bearing to reduce friction and control positioning.

(4) Preload the bearings between the proposed Geneva mechanism and the mirror to eliminate any play that might exist.

(5) Revise the mirror interface with the camera so that no disassembly of components is required after the mirror is once calibrated.

Steps are presently being taken to implement this design modification so that the redesigned drive mechanisms will be available for SC-5.

One mirror design modification was incorporated in the TV mirror unit during this past reporting period. The modification provides a positive mechanical stop for the azimuth rotation, so that during a mission it will no longer be required to rely on the telemetered azimuth position or on the preprogrammed command sequence to prevent the mirror from being overdriven and damaging the azimuth potentiometer or the mirror unit harness. This modification will be incorporated starting with the TV mirror unit for SC-1.

C. System Analysis

1. Introduction

The analytical work reported in this section covers four main categories: (1) spacecraft guidance and trajectory, (2) trajectory computer programming, (3) mission analysis, and (4) system performance. The first category includes a study of tracking system and *Centaur* interfaces with the spacecraft. Mission analysis includes a study of operational requirements and sequences, mission management requirements, and engineering data needs. System performance analysis includes maintenance of system specifications, determination of certain system test requirements, and formulation of emergency-mode operations.

2. Early High Power Transmitter Operation

a. Introduction and summary. In the initial spacecraft design, it was planned to operate the spacecraft transmitter in its low power mode throughout boost, injection, and Deep Space Instrumentation Facility (DSIF) acquisition. It would not be switched to high power operation until after DSIF acquisition was completed and then only when sensitivity considerations required it for the high bit rate data. Subsequent DSIF acquisition studies indicated the necessity of having the spacecraft transmitter on high power during acquisition to provide a sufficiently high probability of acquisition. Because the spacecraft transmitter cannot operate at high power without arcing at certain critical bands of atmospheric pressure between sea level and vacuum, and because of the necessity to minimize the length of time the spacecraft transmitter operates continuously in its high power mode, it was decided to switch the transmitter to high power operation just prior to *Centaur* separation by a command from the *Centaur*. The desire to minimize the transmitter high power "on" time results from thermal overheat considerations in Compartment A in which the high power transmitter is housed.

It has recently become desirable to turn on the transmitter in its high power mode earlier to provide additional S-band telemetry data prior to *Centaur* separation. In response to a JPL request, the considerations and constraints regarding early turn-on of the high power transmitter were studied and are described below.

In summary, it was concluded that:

(1) High power transmitter operation cannot be started prior to shroud ejection, at the very earliest, without risk of permanent damage to the transmitter as a result of arcing. Even this capability should be verified by test before its implementation.

(2) Proper operation of the transmitter and other electronics in Compartment A cannot be guaranteed when thermal tray temperatures exceed 125° F. However, it is felt that tray temperatures up to 140° F can probably be tolerated for short periods of time without causing any permanent damage.

(3) Thermal tray bulk temperatures will reach 125° F level between 53 and 120 min after the beginning of high power operation, depending on the amount of solar input to the compartment.

(4) High power operation should not be initiated any earlier than that time necessary to assure acquisition of the signal by the ground receiving station prior to the actual *Centaur*/spacecraft separation.

b. Arcing considerations. The spacecraft transmitter and rf equipment have been designed to operate in the high power mode only at vacuum conditions or sea level pressure conditions but not in between. There are three areas in which arcing at intermediate altitudes must be considered: the traveling-wave tube (TWT) high voltage supply circuits, the rf circuits (including the coaxial cables, rf switches, and diplexer), and the omnidirectional antenna. To date, there has been no consideration given to this problem, as operation at intermediate altitudes has not been required. A cursory examination of this area has indicated the following.

In the TWT high voltage supply area, the maximum dc voltage is 1200 v and this voltage occurs across a minimum spacing of $\frac{1}{16}$ in. Under these conditions, arcing is certain to occur at atmospheric pressures on the order of 0.1 to 1.0 mm of Hg. In the rf circuits area, the voltage gradients in the diplexer are such that arcing in this area is also assured at these critical pressures. In the case of the antenna, the spacing and voltage gradients are such that arcing at certain pressures is expected; however, the geometry is sufficiently complex that analysis of the arcing conditions has not been done. The transmitter and portions of the rf circuits have been tested at pressures of 10^{-5} mm of Hg and less and demonstrated no arcing under those conditions. No vacuum tests have yet been run on the antenna or certain portions of the rf circuits; however, no problems are expected in this area at pressures of 10^{-5} mm of Hg or less.

Curves showing the altitude and atmospheric pressure as a function of time after liftoff are shown in Fig. 12 for a typical direct ascent trajectory. The pressure versus altitude relationship was obtained from the standard ARDC atmosphere of 1959. Also shown on the figure are certain discrete events of interest (shroud ejection, injection, separation, etc.). From this curve and the above data, it is evident that:

(1) High power operation without arcing can be guaranteed only at altitudes above 71 nm, assuming negligible vacuum lag (pressure equals 10^{-5} mm of Hg).

(2) High power operation at altitudes down to shroud ejection can probably be tolerated without arcing.

(3) Additional low pressure testing must be performed before any more quantitative statements can be made.

It should be noted that these pressures are the pressures of the surrounding atmosphere and not necessarily the same as those in the confined areas where arcing might occur. The extent of the possible vacuum lag is unknown at this time.

c. Thermal considerations. The spacecraft transmitters are installed in Compartment A with the other equipment listed in Table 3. This equipment is thermally mounted to a thermal tray which distributes the heat throughout the compartment. The compartment is in turn isolated from its surroundings,and its radiation to and from space is controlled by several thermal switches that vary the conductance between the compartment and an external radiating surface. These thermal switches automatically provide a conductive path to the radiating surface when needed to permit power dissipation from within the compartment while maintaining a maximum thermal tray temperature of 125° F. Thus the equipment in these compartments is designed and tested for operation at tray temperatures up to but not exceeding 125° F.

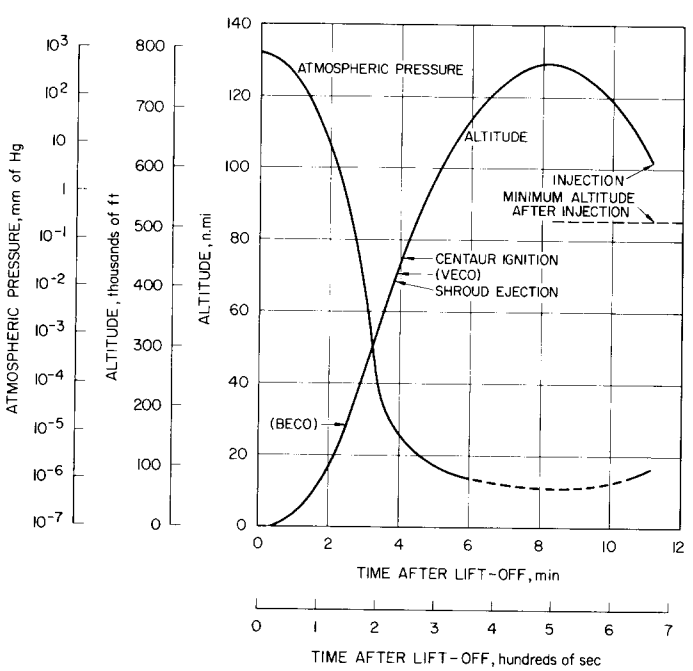

Fig. 12. Pressure versus altitude relationship for direct ascent trajectory

Table 3. Equipment installed in Compartment A and power dissipations during launch and DSIF acquisition

Item	Nominal power dissipation	
	Low power	High power
Transmitters (2)	7.4	52.4
Receivers (2)	3.3	3.3
RF switches (2)	—	—
Main battery	—	—
Battery charge regulator	3.2	3.2
Engineering mechanisms auxiliary	—	—
Television auxiliary	—	—
Thermal control and heater assembly	2.5	2.5
Auxiliary battery control	0.1	0.1
Total power dissipation	16.5	61.5

During the launch, injection, and DSIF acquisition phases of the mission, one transmitter, both receivers, the main battery, battery charge regulator, and auxiliary battery control are operating. During this time, the electrical power dissipations within the compartment are as given in Table 3. An analysis has been made of the predicted thermal history of the compartment during this phase of the mission. This analysis is based on the following assumptions and initial conditions:

(1) The spacecraft is launched with the transmitter on in its low power mode and with everything in Compartment A at thermal equilibrium at a temperature of 110° F.

(2) Sometime after launch, high power operation is initiated. At this time, Compartment A is in thermal equilibrium at a temperature of 110° F.

(3) During high power operation, there is a continuous power dissipation in the compartment of 72 w.

(4) The compartment radiating surface is either fully illuminated by the Sun or illuminated by the Sun with a 50% duty factor.

(5) The radiator solar absorptivity is 0.12 and its infrared emissivity is 0.75.

The results of this analysis are shown in Fig. 13. Here is plotted, as a function of time after initiation of high power operation: (1) the thermal tray average or bulk temperature, (2) the thermal tray temperature at the location of the transmitter electrical power conversion unit

(ECU), and (3) the thermal tray temperature at the location of the high power TWT for the cases of 100% and 50% solar illumination of the radiating surface.

As stated above, the equipment installed in this compartment is designed and qualification tested to a maximum local tray temperature of 125° F and thus operation at any temperature above this limit cannot be guaranteed by the suppliers. However, in many cases "unofficial" tests at above specification temperatures have been made and a survey of the predicted effects of above specification temperatures on these units is summarized below:

(1) *All nonoperating equipment.* The equipment that is not turned on at this time will be lagging behind the tray temperature and will have no "hot spots" at temperatures above the tray temperature. Thus it is felt that this equipment will not suffer any permanent damage at temperatures well above the specified 125° F and thus is not a limiting factor.

(2) *Main battery.* The main battery can withstand temperatures up to 140 or 145° F for relatively short periods of time (1 or 2 hr) without any significant degradation of battery life.

(3) *Transmitter.* The transmitter has two sensitive areas — the TWT and the ECU. As long as out-of-specification performance is permitted (e.g., reduced output voltage and increased frequency drift), the tray temperature at the TWT mounting can probably reach 160 to 170° F without causing any permanent damage to the TWT. In the case of the transmitter ECU, it is felt that it will probably withstand local tray temperatures as high as 150° F without permanent damage. However, the ECU may not respond to a turn-off command if its local tray temperature exceeds 130° F. In this event, power can be removed from the transmitter only by commanding all nonessential loads off. This removes all power from the 29-v nonessential bus including low power as well as the high power transmitter and all data processing. These other loads could then be turned back on by ground command. This is an undesirable mode of operation since with the nonessential bus off, there is no signal emanating from the spacecraft, i.e., no telemetry data, no doppler data, no angle position data, and the turn-on commands have to be sent blind.

(4) *Other operating equipment.* The other equipment in the compartment that is operating (receivers, battery charge regulator, and auxiliary battery control) can probably stand thermal tray temperatures of up to 140° F without any permanent damage, although performance will probably not meet specifications.

From this data and the curves in Fig. 13, the following conclusions are evident:

(1) All equipment will operate satisfactorily and within specification for high power transmitter on-times of up to 53 min for 100% solar illumination or up to 120 min for 50% solar illumination.

(2) If out-of-specification performance is permitted, but operational difficulties (transmitter ECU turn-off problems) are prohibited, high power transmitter on-times of between 55 min and 120 min can be tolerated for 100% and 50% solar illumination, respectively.

(3) If operating difficulties are permitted (transmitter ECU turn-off problems), but the possibility of permanent damage is to be avoided, high power operation times of up to 120 min can be tolerated.

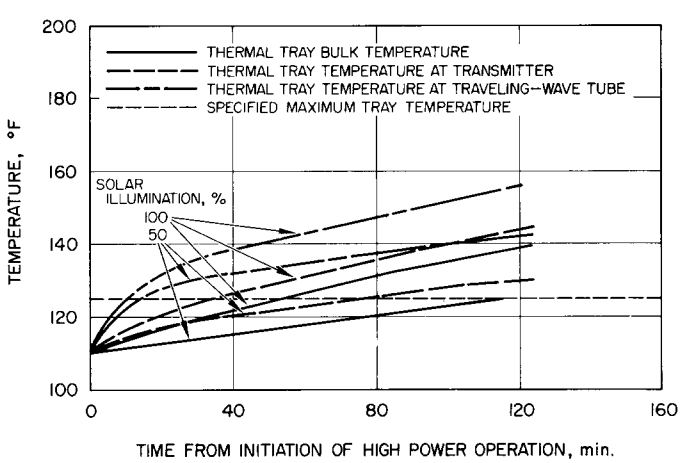

Fig. 13. Temperatures in Compartment A

3. Attitude Error Correction Subroutine

The following is a summary of the mechanization of a subroutine of the spacecraft performance analysis command (SPAC) attitude determination program. This subroutine is designed to optimize the use of available data to determine the spacecraft attitude after landing and to estimate the remaining error in the determination.

a. Discussion. Given two vectors (directions) which are known in both the spacecraft and selenographic coordinate systems, the spacecraft attitude with respect to the selenographic coordinate system may be established. In particular, consider these two directions to be those of the Earth and the Sun. The positions of the Earth and the Sun at a given time are well defined in the seleno-

graphic coordinate system and are computed in the attitude determination program. The location of the Earth and the Sun in the spacecraft coordinate system may be computed from the values of the spacecraft gimbal angles when the solar panel has been positioned on the Sun and the planar array has been positioned on the Earth separately. For use in describing the problem the gimbal angles will be defined as:

δ_s = the polar axis gimbal angle when the solar panel is pointed at the Sun.

β = the solar panel axis gimbal angle when the solar panel is pointed at the Sun.

θ_s = the roll axis gimbal angle when the solar panel is pointed at the Sun.

δ_e = the polar axis gimbal angle when the planar array is pointed at the Earth.

θ_e = the roll axis gimbal angle when the planar array has been pointed at the Earth.

ϕ = the elevation axis gimbal angle (assuming the same for both solar panel and planar array positioning), which is nominally zero.

These gimbal angles, which are obtained from spacecraft engineering data, are random variables. It is assumed that they are gaussian random variables with variances: σ_δ^2, σ_θ^2, σ_β^2 and σ_ϕ^2 about the polar, roll, solar panel, and elevation axes, respectively. The means of these random variables are unknown. If they were known, the spacecraft attitude could be computed exactly. The attitude computation subprogram forms unit vectors in the spacecraft system which point to the Sun and the Earth using the gimbal angles defined above. A constraint on the attitude computation is that the angle between the two unit vectors to the Sun and the Earth in the spacecraft system (computed from the gimbal angles) must be the same as the angle between unit vectors to the Earth and Sun in the selenographic system (parallax is neglected). Since the values of the gimbal angles are not, in general, equal to the mean (or true) gimbal angle values, the angle between the unit vectors computed in the spacecraft system, ξ_1, will differ from the true angle, ξ_2, between unit vectors to the Sun and the Earth in the selenographic coordinate system. The six gimbal angles should therefore be adjusted so that they describe vectors to the Sun and the Earth having an included angle equal to ξ_2, the true angle. This correction must be performed in such a way that the variances of the corrected gimbal angles are less than the variances of the uncorrected gimbal angles. The problem may be expressed mathematically after the following definitions:

$\bar{r}_s$ = unit vector pointing in the direction of the Sun in the spacecraft system.

$\bar{r}_e$ = unit vector pointing in the direction of the Earth in the spacecraft system.

$\bar{r}_s'$ = unit vector pointing in the direction of the Sun in the selenographic system.

$\bar{r}_e'$ = vector pointing in the direction of the Earth in the selenographic system.

$$\begin{aligned}\bar{r}_s = {} & \{\cos(\delta_s + \beta)\cos\theta_s - \sin(\delta_s + \beta)\sin\theta_s \sin\phi\}\,\bar{i} \\ & + \{\cos(\delta_s + \beta)\sin\theta_s + \sin(\delta_s + \beta)\cos\theta_s \sin\phi\}\,\bar{j} \\ & + \{\cos\phi \sin(\delta_s + \beta)\}\,\bar{k} \qquad (1)\end{aligned}$$

$$\begin{aligned}\bar{r}_e = {} & -\{\cos\delta_e \cos\theta_e - \sin\delta_e \sin\theta_e \sin\phi\}\,\bar{i} \\ & - \{\cos\delta_e \sin\theta_e + \sin\delta_e \cos\theta_e \sin\phi\}\,\bar{j} \qquad (2) \\ & - \{\cos\phi \sin\delta_e\}\,\bar{k}\end{aligned}$$

where $\bar{i}$, $\bar{j}$, and $\bar{k}$ are unit vectors along the spacecraft axes. The vectors $\bar{r}_e$ and $\bar{r}_s$ are generated by the program from the ephemeris and are assumed to be deterministic quantities.

$$\begin{aligned}\cos\xi_1 = \bar{r}_s \cdot \bar{r}_e \\ = {} & \sin(\theta_s - \theta_e)\sin\phi \sin(\delta_s - \delta_e + \beta) \\ & - \cos(\delta_s + \beta)\cos\delta_e \cos(\theta_s - \theta_e) \\ & - [\cos^2\phi + \cos(\theta_s - \theta_e)\sin^2\phi]\sin\delta_e \sin(\delta_s + \beta) \qquad (3) \\ = {} & F(\theta_s, \theta_e, \delta_s, \delta_e, \beta, \phi) = f(\theta_s - \theta_e, \delta_s + \beta, \delta_e, \phi)\end{aligned}$$

$F(\theta_s, \theta_e, \delta_s, \delta_e, \beta, \phi)$ can be simplified by defining:

$$\Delta\theta = \theta_s - \theta_e,\ \gamma_s = \delta_s + \beta$$

Then:

$$\begin{aligned}\cos\xi_1 = \bar{r}_s \cdot \bar{r}_e \\ = {} & \sin\Delta\theta \sin\phi \sin(\gamma_s - \delta_e) - \cos\gamma_s \cos\delta_e \cos\Delta\theta \\ & - [\cos^2\phi + \cos\Delta\theta \sin^2\phi]\sin\delta_e \sin\gamma_s \qquad (4) \\ = {} & f(\phi, \Delta\theta, \gamma_s, \delta_e)\end{aligned}$$

where

$\Delta\theta$ is a random variable with unknown mean and variance $2\sigma_\theta^2$.

γ_s is a random variable with unknown mean and variance $\sigma_\delta^2 + \sigma_\beta^2$.

ϕ is a random variable with unknown mean and variance σ_ϕ^2.

$\Delta\theta$, γ_s, δ_c, and ϕ are assumed to be normally distributed.

$\cos \xi_2 = \bar{r}_s' \cdot \bar{r}_c'$ and is precisely known from the post-landing attitude determination program.

The problem is to find a set of corrections, e_1, e_2, e_3, and e_4, to the angles ϕ, $\Delta\theta$, γ_s, and δ_e, respectively, such that:

$$f(\phi - e_1, \Delta\theta - e_2, \gamma_s - e_3, \delta_e - e_4) = \cos \xi_2.$$

The correction should also be such that the new variables, ϕ', $\Delta\theta'$, γ_s', and δ_e', have variances:

$$\sigma_{\phi'}^2 \leq \sigma_\phi^2$$

$$\sigma_{\Delta\theta'}^2 \leq 2\sigma_\theta^2$$

$$\sigma_{\delta e'}^2 \leq \sigma_\delta^2$$

$$\sigma_{\gamma s'}^2 \leq \sigma_\delta^2 + \sigma_\beta^2$$

The result is a set of adjusted gimbal angles ϕ', $\Delta\theta'$, γ_s', and δ_e' which are (on the average) closer to the true angles than were ϕ, $\Delta\theta$, γ_s, and δ_e.

The system under consideration has four angles to be corrected which can be represented as:

$$\phi_1 = \phi \quad \text{with} \quad \sigma_1^2 = \sigma_\phi^2$$

$$\phi_2 = \Delta\theta \quad \text{with} \quad \sigma_2^2 = \sigma_{\Delta\theta}^2$$

$$\phi_3 = \gamma_s \quad \text{with} \quad \sigma_3^2 = \sigma_{\gamma_s}^2$$

$$\phi_4 = \delta_e \quad \text{with} \quad \sigma_4^2 = \sigma_{\delta_e}^2$$

and

$$f(\phi, \Delta\theta, \gamma_s, \delta_e) = f(\phi_1, \phi_2, \phi_3, \phi_4) = f(\phi_i)$$

The angles ϕ_i are assumed normally distributed with unknown mean (or true value). The correction will consist of finding values of e_i that satisfy the following criteria:

(1) The correction for each angle is proportional to the standard deviation in that angle: $e_i = k_i\sigma_i$ where k_i is the correction coefficient.

(2) The total correction applied should be a minimum in the least squares sense since the most likely error is zero (the mean error in sample angle ϕ_i is zero). Thus, the following will be minimized:

$$\sum_{i=1}^{4} k_i^2 \text{ or } \sum_{i=1}^{4} \frac{e_i^2}{\sigma_i^2}$$

(3) $$|f(\phi_i - e_i) - \cos\xi_2| \leq \epsilon \qquad \epsilon \to 0$$

where ϵ is some arbitrary small number (which must be chosen).

Since the σ_i are assumed to be known, the problem reduces to that of determining the k_i ($i = 1, 2, 3$, and 4). This is done by applying iterative corrections to the angles ϕ_i such that the corrections satisfy all three criteria. The actual equations governing the corrections were derived using the method of Lagrange multipliers.

In addition, the error correction subroutine estimates the error remaining after the correction is performed. This is accomplished by adding a normal error to the corrected gimbal angles, correcting it out, computing the attitude, and comparing this attitude with the original attitude by some means that will evaluate the amount of error correction. This must be performed until convergence of the corrected errors is achieved. Fig. 14 illustrates the relationship between correction and evaluation routines and the attitude master program.

b. Results. Correction formulas derived from the above criteria were utilized to adjust angles that had been subjected to gaussian random errors with a known standard deviation. An epsilon of 5×10^{-5} was chosen to satisfy the inequality of condition 3. To date, over 15,000 corrections have been performed with the following results.

(1) The maximum number of iterations in over 15,000 calculations was four, while two and three iterations were prevalent.

(2) The corrected angles were distributed as shown in Fig. 15. The distributions are approximately gaussian. Out of 5000 samples, with a standard deviation of 0.57 deg for the inserted error, no error magnitude (the absolute difference between the injected error and the correction) exceeded 2.0 deg. The error magnitude exceeded 1.5 deg 0.88% of the time for the least accurate angle ($\Delta\theta$) and 0.02% of the time for the most accurate angle (δ_e).

(3) Table 4 shows the variance (σ^2) in each of the four angles (ϕ, $\Delta\theta$, γ_s, and δ_e) after 500 samples from different values of ϕ, $\Delta\theta$, γ_s, δ_e, and $\cos \xi_2$ (the Sun-Earth angle). The injected errors had a variance of 0.325 each. Fig. 16 shows the variance convergence of one of these cases as a function of n, the number of samples.

(4) The average variance for all angles over the entire range of possible values for ϕ, $\Delta\theta$, γ_s, and δ_e was 0.245 for an injected error with variance 0.325.

(5) The error correction subroutine is a feasible means of correcting the spacecraft gimbal angles to obtain the true Earth-Sun angle from the standpoint of time requirements. With a maximum of four iterations per correction set, 1000 correction sets may be run in 1 min.

(6) The error correction subroutine is a reasonable method for correcting the spacecraft gimbal angles from the standpoint of error improvement. In practically all cases to date, the gimbal angle variance after correction is less than that before correction. The improvement in mean square variance (all four gimbal angles) is about 25%. The results indicate that the corrected gimbal angles have normally distributed error (as they should, since the correction is a linear operation on a normal variate); thus, the corrected variance has the meaning of a normal variance and 95% confidence may be associated with 2.0 σ.

Table 4. Variance in corrected gimbal angles for different values of ξ_2

Case	Cos (ξ_2)	ξ_2 in degrees	σ_1^2 in degrees^2	σ_2^2 in degrees^2	σ_3^2 in degrees^2	σ_4^2 in degrees^2
1	0.9211	23.0	0.314	0.244	0.235	0.199
2	0.8321	33.7	0.302	0.328	0.188	0.163
3	0.6717	47.3	0.302	0.312	0.202	0.159
4	0.4805	61.3	0.319	0.295	0.198	0.175
5	0.3541	69.2	0.176	0.184	0.287	0.310
6	0.2686	75.3	0.270	0.318	0.204	0.177
7	0.1128	83.5	0.250	0.338	0.183	0.177
8	0.1056	84.0	0.233	0.194	0.306	0.300
9	−0.1338	97.7	0.221	0.207	0.262	0.250
10	−0.3407	109.9	0.218	0.267	0.235	0.230
11	−0.4948	119.6	0.280	0.310	0.200	0.180
12	−0.5810	124.5	0.320	0.298	0.170	0.180

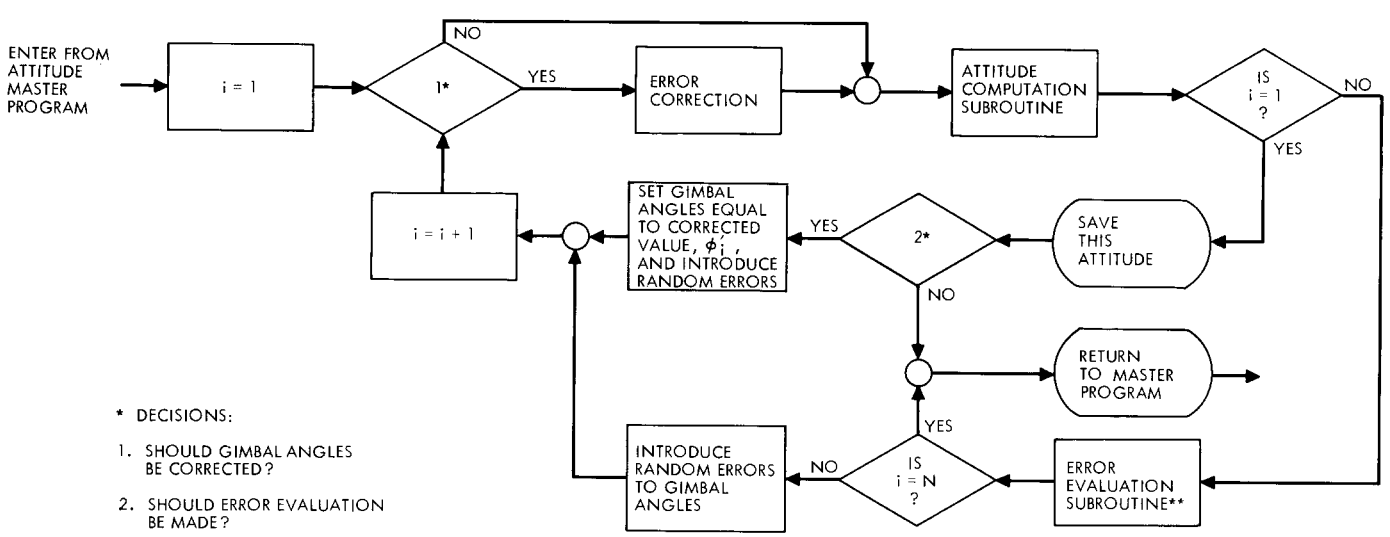

** THE ERROR EVALUATION SUBROUTINE COMPUTES THE ERRORS (MEAN AND VARIANCE) IN THE N SAMPLES USING THE VALUES ϕ_i' AS A REFERENCE. THE MEANS AND VARIANCES ARE CUMULATIVE.

Fig. 14. Attitude computation subroutine network

UNCLASSIFIED

(7) The error correction is performed with no apparent dependence on the gimbal angle magnitudes. Although it hasn't been demonstrated explicitly, the error correction is expected to be dependent on the gimbal angle geometry.

(8) The method presented here has not been shown to be the optimum manner with which to utilize the knowledge of the Earth-Sun angle to correct the spacecraft gimbal angles provided by engineering data. It is, however, a logical approach to improving the engineering data and has demonstrated acceptable results.

4. Computer Generation of Digital Data Tapes

In order to perform a successful checkout of the SPAC management computer programs, on an individual basis at Hughes and on an integrated basis at the Space Flight Operations Facility (SFOF), it is necessary to generate IBM-compatible digital magnetic data tapes of simulated *Surveyor* spacecraft telemetry. A computer routine has been designed which provides an extremely flexible method of simulating digital spacecraft data for program checkout and integration tests. The maximum length of time during the mission that can be simulated by one computer run is inversely proportional to the detailed variations desired in the simulated telemetry signals. The routine is based on representing the value of each signal

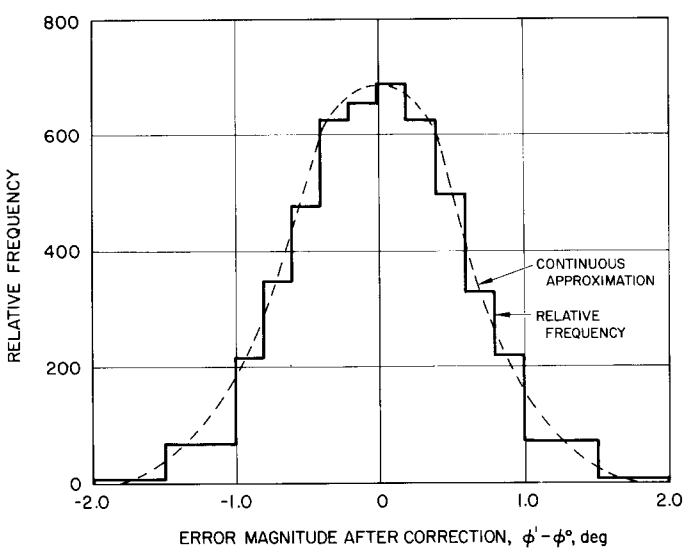

(a) Elevation angle, ϕ

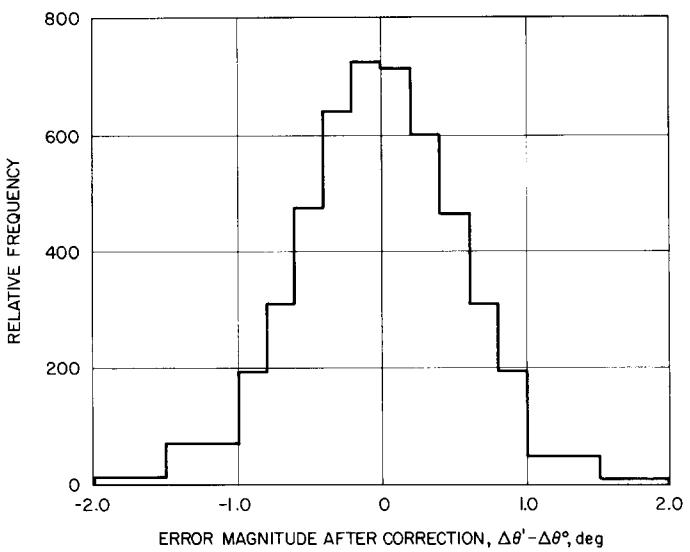

(b) Roll angle, $\Delta\theta$

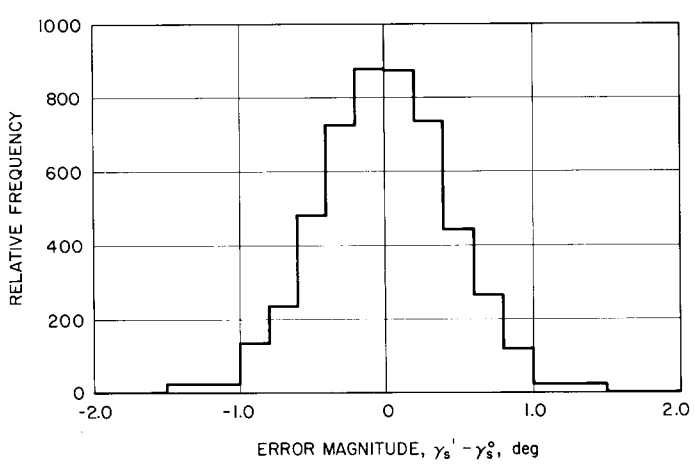

(c) Sun angle, γ_S (δ_S + β_S)

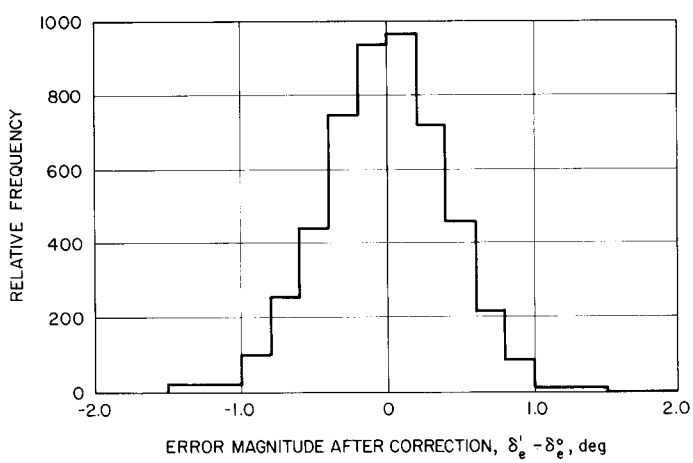

(d) Polar angle, δ_e

Fig. 15. Relative frequency of error magnitude in 5000 samples (0.3249 variance of injected error)

UNCLASSIFIED

that is telemetered by the spacecraft by a time-dependent polynomial or step function. The routine determines the nominal value of each parameter of the particular mode to be simulated for a given time during the mission and adds randomly distributed gaussian noise to each nominal value. The nominal values plus noise are assembled into frames and then output on magnetic tape. The routine has been successfully programmed and is being employed to generate simulated data tapes for the engineering data reduction routine (EDR).

a. Program inputs. All inputs to the program will be made using punched cards. The inputs can be divided into two classes, initialization inputs and run-data inputs. Initialization inputs which may be incorporated in the assembly consist of the time-dependent polynomial and step-function coefficients and the assignment of these equations to particular spacecraft data channels. The step functions are specified by the following constants: T_0, Y_1, T_1, Y_2, $T_2 \cdots Y_N$, T_N; where the symbols Y_N and T_N are defined by the diagrams in Fig. 17.

The polynomial equations are specified by the following constants: N, a_N, a_{N-1}, $\cdots a_1$, a_0, T_N, M, a_M, a_{M-1}, $\cdots$, T_M; where N and M are the orders of Equations N and M, respectively; a_N, a_{N-1}, $\cdots a_0$ are the coefficients of Equation N; a_M, a_{M-1}, $\cdots$ are the coefficients of Equation M; and T_N and T_M are the last times the Equations N and M are valid.

The order in which the equation reference numbers are listed will determine the assignment of a polynomial or step function equation to a particular parameter; i.e., the j^{th} entry will specify the function for the j^{th} signal. More than one parameter may be assigned to the same equation. The last class of initialization inputs consists of the assignment of σ values for noise-to-spacecraft parameters. This information will consist of the following data: σ_1, σ_2 $\cdots$ σ_{169}, where σ is the standard deviation of the additive gaussian noise and its position in the list determines the spacecraft parameter number to which it applies.

The run data inputs will consist of the following information: start and end times of the simulation period, spacecraft data mode (one of six possible modes), spacecraft data rate, system noise indicator and bad parity frequency, and simulation code number and flag. The data mode will be an integer between 1 and 6. The data rate will be in bits per second and will be one of the following numbers; 4400, 1100, 550, 137½, or 17¾₁₆. The system noise indicator and the bad parity frequency will be three-digit numbers between zero and one. The simulation code number will be a four-digit integer. The flag will be a four-digit integer controlling the optional printout.

b. Tape output. The output simulated data tapes will be in a format which is identical to the input tape format for the engineering data reduction routine. The output

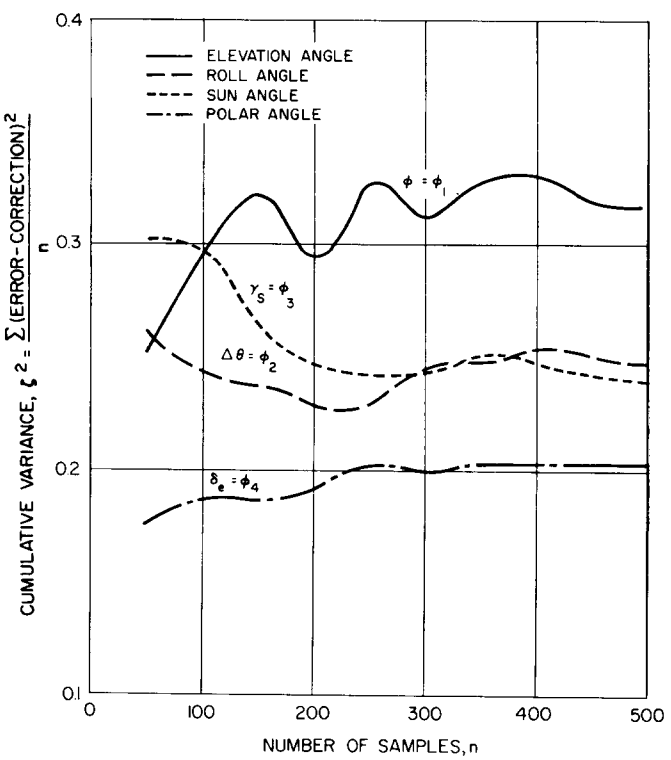

Fig. 16. Typical convergence plot for corrected variances (variance of corrected error = 0.3249, or $\sigma = 0.57$ deg)

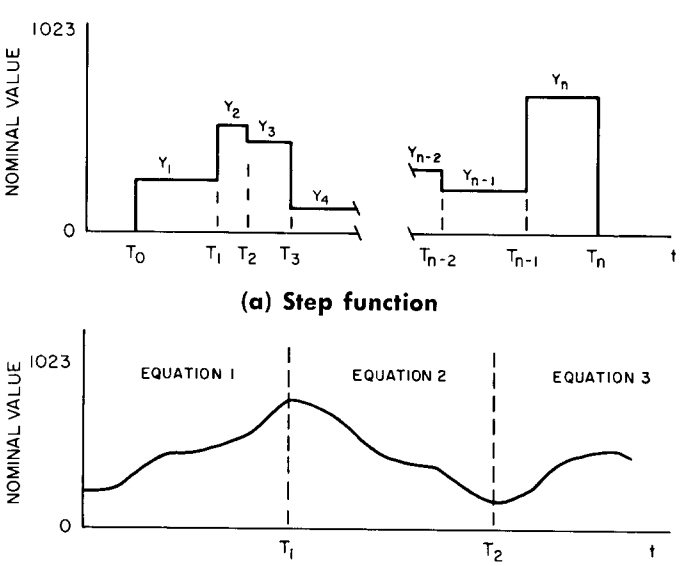

Fig. 17. Typical spacecraft data channels

tape will contain the data mode, bit rate indicator, and simulation code number for each frame of simulated data output.

c. Tabular outputs. The run data inputs are tabulated for each run of the program. In addition, provisions are included to tabulate the output data on an optional basis. The request for the optional data tab will contain, in addition to program control information, the tab frame repetition rate, i.e., tab every N^{th} frame starting with the first frame, where $N = 1, 2, 3, 4, \cdots$. The tabular format will contain the following information for each frame tabulated:

(1) Mode of the simulated data.

(2) Bit rate of the simulated data.

(3) Time tag of the simulated data frame.

(4) Simulation code number.

(5) Value (0 to 1023) of each word on the simulated data frame.

d. Determination of noise and bad parity. The noise value, N_j, to be algebraically added to the nominal parameter value, x_j, will be determined as follows:

$$N_j = (RV)\ (\sigma_j)\ (SNI)$$

where RV is a gaussian distributed random variable with zero mean and unit variance, σ_j is the initialization input standard deviation for the j^{th} parameter, and SNI is the input system noise indicator.

The value of the parity indicator which is attached to each output value will be determined by the following method:

$$\text{Parity indicator} = 0 \text{ if } RV_1 \leq \text{BPF}$$

$$= 1 \text{ if } RV_1 > \text{BPF}$$

where RV_1 is a uniformly distributed random variable, and BPF is the input bad parity indicator.

e. Program logic. A flow diagram of this routine is shown in Fig. 18. The run data is input and the required tab output is performed. The program running time, t, is set equal to the input start time and frame time increments, ΔT_F, are calculated. Using the input run data, a frame of simulated data is constructed employing t and the appropriate equations and constants. The magnitude of the nominal value plus noise must be between 0 and 1023. Each simulated value must be checked to ensure

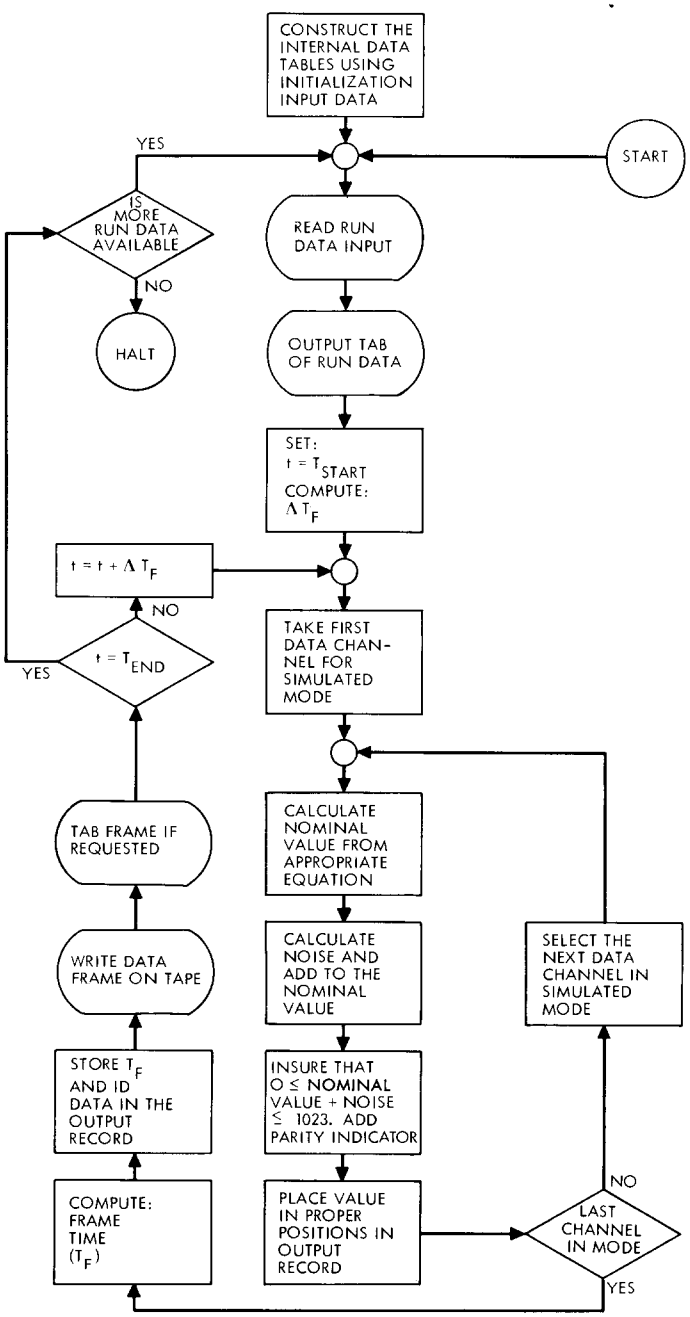
CONSTRUCT THE INTERNAL DATA TABLES USING INITIALIZATION INPUT DATA
START
YES
IS MORE RUN DATA AVAILABLE
NO
HALT
READ RUN DATA INPUT
OUTPUT TAB OF RUN DATA
SET: t = T START COMPUTE: ΔT F
t = t + ΔT F
NO
YES
t = T END
TAKE FIRST DATA CHANNEL FOR SIMULATED MODE
TAB FRAME IF REQUESTED
CALCULATE NOMINAL VALUE FROM APPROPRIATE EQUATION
WRITE DATA FRAME ON TAPE
CALCULATE NOISE AND ADD TO THE NOMINAL VALUE
SELECT THE NEXT DATA CHANNEL IN SIMULATED MODE
STORE T F AND ID DATA IN THE OUTPUT RECORD
INSURE THAT 0 ≤ NOMINAL VALUE + NOISE ≤ 1023. ADD PARITY INDICATOR
COMPUTE: FRAME TIME (T F)
PLACE VALUE IN PROPER POSITIONS IN OUTPUT RECORD
NO
LAST CHANNEL IN MODE
YES

Fig. 18. Flow diagram for computer simulation of spacecraft data

that this constraint is met. When all the calculations pertinent to the frame are completed, the frame is output on tape (tabulated also if requested) and t is increased by ΔT_F. This procedure continues until $t = T_{end}$.

D. Flight Control

1. Summary

The flight control subsystem consists of spacecraft units that provide velocity and attitude control during the transit and landing phase of the *Surveyor* mission. These units, which include optical sensors, inertial instruments, attitude controls, and flight control electronics, are discussed in this section. Although the lunar radar and propulsion are also functionally included, they are covered in other sections of this report.

Results of structural coupling tests on the S-2 vehicle indicated that no inertial control loop stability problems existed for simulated vernier engine vibration inputs. Acceptance tests were completed on the first flight models of the secondary Sun sensor, inertial reference unit, and electronics unit. In addition, type approval tests were completed on the gas jet valves and inertial reference unit.

2. Subsystem Tests

a. Flight control electronics unit. Type approval test performance was satisfactory during thermal–vacuum tests and all chassis temperatures monitored were in close agreement with predicted values (Table 5), except for Chassis 7 where temperatures were higher than predicted. This was caused by the insulating tape which isolates Chassis 7 from the electronics unit housing to eliminate a radio noise problem experienced earlier during T-2 system test. An investigation is being made into the feasibility of reducing the thermal impedance from Chassis 7 to the bottom radiator while still retaining acceptable noise characteristics.

Thrust axis vibration tests were successfully completed and the unit is undergoing vibration along the lateral axes.

b. SC-1 subsystem tests. Circuit balance and calibration tests on the ten chassis of the first flight model of the electronics unit were completed and the unit is undergoing acceptance tests as part of the flight control sensor group.

c. Inertial sensors structural coupling tests. Analytical investigations using a mathematical model to represent the spacecraft indicated that the inertial attitude and acceleration control loops were susceptible to structural coupling instability during vernier engine firing. To determine the extent of the coupling, the mechanical model of the flight control sensor group with an operational inertial reference unit (IRU) was vibrated on the spacecraft structural qualification vehicle (S-2). Transmissibility levels were measured from the vernier engine mounting brackets to the gyros and accelerometer in the IRU to determine whether spacecraft resonances added enough gain to the control system to cause an unstable condition. The

Table 5. Electronics unit temperatures

Thermocouple location	Coast phase temperatures, °F			Thrust phase temperatures, °F		
	Predicted	Measured		Predicted	Measured	
	Base = 93	Base = 70	Base = 105	10-min operation base = 93	10-min operation base = 105	15-min operation base = 105
Chassis 4 — CR29	72	66	95	146	105	110
Chassis 4 — Q46	72	61	86	146	123	129
Chassis 4 — Q49	72	61	89	146	151	156
Chassis 4 — Q50	72	64	94	146	129	133
Chassis 5 — Q10	86	86	111	172	155	160
Chassis 5 — Q19	86	72	98	172	135	138
Chassis 6 — Q28	135	131	148	150	160	164
Chassis 6 — Q18	160	189	205	169	208	210
Chassis 6 — Q5	160	137	160	169	175	177
Chassis 7 — Q4	136	190	213	145	225	230
Chassis 8	87	84	110	100	110	111
Chassis 9	78	71	97	91	98	99
Chassis 10	80	70	97	91	99	99

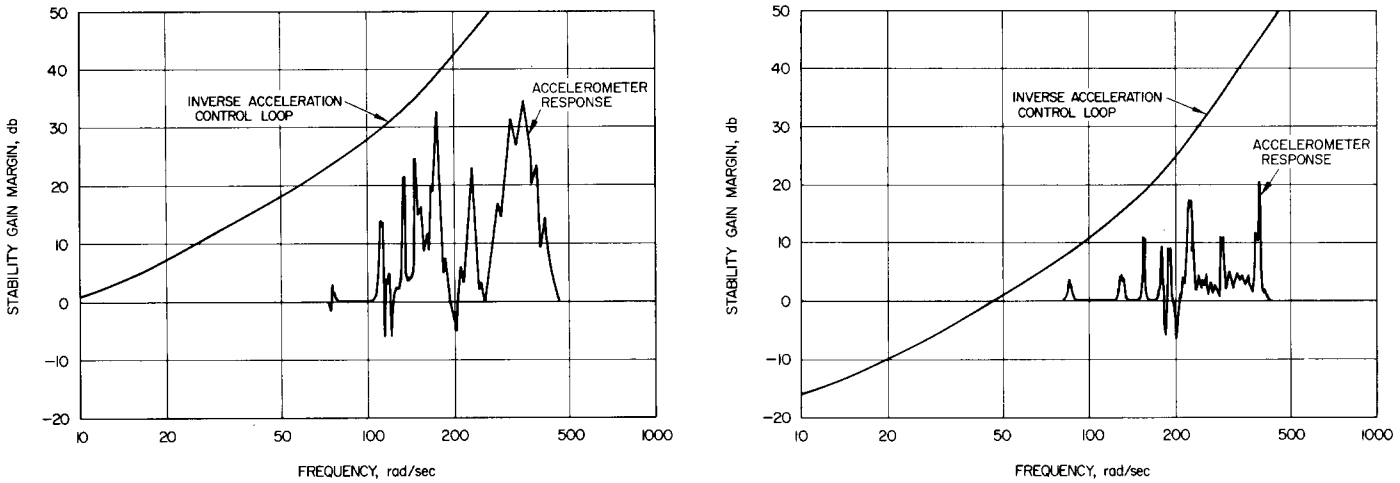

(a) Midcourse maneuver

(b) Terminal descent

Fig. 19. Transmissibility to accelerometer

measurements were accomplished by placing the S-2 vehicle on an elastic suspension system and applying input forces at the vernier engine mounting brackets with modal shakers. Frequency response measurements were made over a range from 7 to 100 cps for both a midcourse and terminal descent vehicle configuration using rotational inputs about the pitch and yaw axes as well as inputs along the thrust axis. Force inputs were from 7 to 15 lb at each of the three engine brackets. Data were taken from 30 accelerometers located such that the natural nodes could be verified and the amplification factors determined from the IRU gyro and accelerometer output signals. Typical results of the frequency response tests are shown in Fig. 19 and 20. The inverse of the open control loop transfer function is plotted to indicate the gain margin which exists since the product of control loop gain and elastic vehicle gain must be greater than one to produce an unstable condition. As shown in Fig. 19a, the smallest gain margin indicated was 6 db at approximately 175 rad/sec. Based on the results of these tests, it appears that there is no structural coupling instability over the range of force inputs used.

3. Optical Sensors

The spacecraft has a Canopus sensor, a primary Sun sensor, and a secondary Sun sensor. The Canopus sensor and primary Sun sensor are located in the flight control sensor group and provide the error signals for maintaining a fixed spacecraft attitude in the coast phases of flight. The secondary Sun sensor is located on the solar panel; it provides the signals for maneuvering the spacecraft until the Sun is within the field of view of the primary Sun sensor.

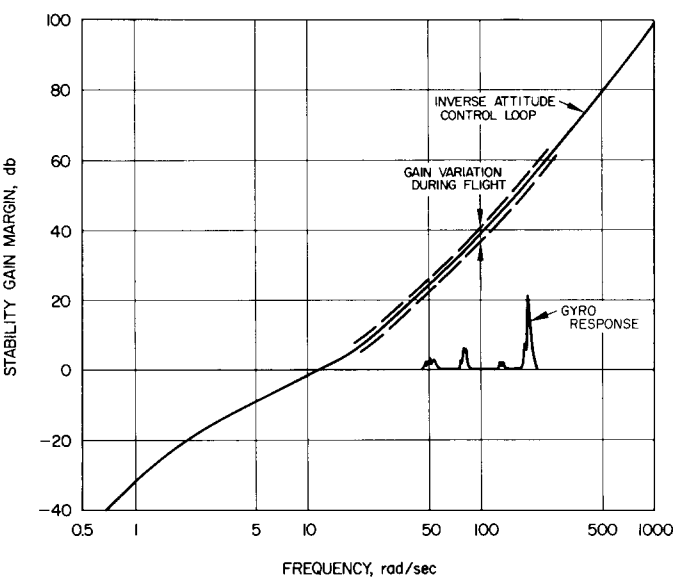

Fig. 20. Typical transmissibility to gyro for attitude loop (pitch-midcourse configuration)

a. Canopus sensor. Flight acceptance tests were completed on the fourth and fifth flight units (Serial Nos. 6 and 7), and testing of the six units remaining under the current contract is in progress. The reliability test program of two flight models was initiated. In this program each sensor will be subjected to a series of tests to simulate the prelaunch handling and test followed by 27 simulated mission cycles.

b. Sun sensors. Type approval tests on the secondary Sun sensor are continuing. Vibration, pressure shock, mechanical shock, and transit phase thermal–vacuum tests have been completed. Upon completion of the lunar

phase thermal–vacuum tests now in progress, a final sensor performance check will be made to complete the type approval program.

Flight acceptance tests were completed on the Set-1 secondary Sun sensor flight unit prior to installation on the SC-1 solar panel and the Set-2 primary Sun sensor which will be integrated into the SC-2 flight control sensor group wiring harness.

The Sun sensor test position was moved from the Chilao site to the Tucson, Arizona site in February. The relocation was made primarily because the clouds and high wind conditions at Chilao made testing difficult and time-consuming in recent months. Operation of the Tucson facility indicates a considerable improvement in utilization of testing time. The amount of test equipment movement necessary was greatly reduced because of the support available from the Hughes Tucson Engineering Laboratories. Sun intensities compare favorably with those encountered at Chilao with readings between 85 and 100 mw/cm^2 noted. Investigations also revealed that testing will be possible during at least 75% of the available hours.

4. Inertial Reference Unit

The inertial reference unit is mounted on the sensor group structure and includes three strapped-down integrating gyros and a linear accelerometer. The gyros provide a reference for maintaining spacecraft attitude and for executing precise attitude maneuvers before midcourse velocity correction and main retro firing. The linear accelerometer is aligned to the spacecraft thrust axis and supplies the acceleration measurements required during the midcourse velocity maneuver and terminal descent.

a. Gyros. Fifty-five gyros have been received to date. This total consists of 26 gyros from the initial order and 29 of 36 gyros from the follow-on order. Analysis of the results of acceptance tests on the first 25 of the follow-on gyros indicates considerable improvement in non-g sensitive drift performance. Reliability estimates based on this data predict that 99% of received gyros will meet the non-g sensitive drift requirement of 1 deg/hr with a confidence level of 90%.

Tumble tests were completed on the S/N-40 gyro in order to determine overall drift performance during a simulated mission. S/N-40 had previously been used in the gyro type approval program and had successfully survived exposure to vibration levels of 30 g. The simulated mission consisted of continuous gyro operation for approximately 120 hr during which the components of g-sensitive, non-g sensitive, and g^2-drift were monitored. The gyro was tumbled for 30 hr at ten times the Earth rate in the rate mode and for 90 hr in the inertial hold mode. During the test, all drift components remained constant within 0.2 deg/hr.

Gyro S/N-42 was disassembled at the gyro vendor's facility under the cognizance of Hughes engineering and quality assurance personnel to investigate the possibility of gyro flotation fluid contamination. The particle count, after flushing, exceeded what would normally be expected both in the number and the size of the particles. Although the vendor indicated that corrective action had already been initiated to reduce the potential sources of gyro contamination and to increase the effectiveness of inspection procedures used, there is some question as to the cleanliness of some of the gyros already delivered. Evidence of fluid contamination as indicated by gyro stiction or in the extreme case, a hangup of the gyro gimbal, has not been detected during approximately 17,000 hr of gyro running time logged to date. Although gyro acceptance tests do not include a specific stiction test, the elastic restraint tests measure gyro drift at and off null with low total drift rates. Peaks in monitored torque to balance current or average out-of-specification drift rates would have been noted if stiction were present. Generally, stiction in gyros is not an independent parameter but is a component of non-g sensitive drift. However, it is unlike other components of non-g sensitive drift such as flex lead and signal generator reaction torques in that its contribution might appear only if the gyros are used at low rates. Stiction tests were run on five gyros from the follow-on order, during which the output signals were observed for spikes as the gimbals were taken out to the stops at rates as low as 3 deg/hr. No unusual behavior was observed. In addition, it has been established that a dither of 0.2 to 0.3 deg/hr is imposed on the gimbal of the gyro by the on-off operation of the gyro heater. The dither appears on the gyro output signals and is synchronized with the heater switching. It is theorized that the heater cycling causes expansion and contraction of the flotation fluid which, in the presence of a bellows, causes oscillating fluid flow that drags the gimbal back and forth. The fact that the dither is seen continuously precludes stiction above the dither amplitude.

Consideration has been given to returning all the gyros suspected of having contaminated fluid to the vendor for replacement of the fluid. Each gyro to be refilled would have to be completely disassembled to the float level since draining, flushing, and refilling is not sufficient.

The potted electrical trim networks would also have to be replaced. Since it is felt that the reworked gyros would be less reliable, there are no plans for changing gyro flotation fluid at this time. However, gyro output signals will be closely watched for any evidence of stiction during all gyro and IRU flight acceptance testing. Special stiction tests will continue to be conducted. Any gyros returned to the vendor for repair for other reasons, requiring disassembly down to the fluid level, will be examined for contamination.

b. Unit. Type approval tests were successfully completed on the IRU following exposure of the unit to vibration levels of 18 g. Acceptance tests were completed on the first flight model of the IRU and the unit is undergoing subsystem tests as part of the flight control sensor group.

5. Attitude Controls

The attitude controls consist of six on-off cold gas jets that produce attitude control moments during coast phase and a roll actuator that supplies roll control moments during thrust phase by swiveling one of the vernier engines. The gas jet system also includes a nitrogen gas tank nominally charged to 4325 lb/in.^{2} at 70° F, a pressure regulator, pressure relief valve, squib-operated gas dump valve, and pressure transducer. The roll actuator consists of a two-phase induction motor, gear train, and position transducer.

a. Gas jet system. Type approval tests were initiated on the gas supply pressure regulator. During vibration tests excessive interface seal leakage was experienced. Investigation revealed that the silicone seals used were permeable to gas after extended periods of pressurization. The seal leakage was corrected by replacing the silicone O-rings with teflon spring expanded C-type "omniseals."

A "circle seal" pressure relief valve that successfully completed evaluation tests was also substituted into the pressure regulator because of marginal low temperature (—80° F) performance of the original design, and type approval tests were continued. The pressure regulator cover was modified as shown in Fig. 21 to accommodate the valve. The teflon seals and new relief valve will be incorporated into all flight units.

Type approval tests on the gas jet valve were completed and the unit operated satisfactorily after the 100,000-cycle life tests. Although the type approval gas jet used gold-plated valve seats, tests on a valve with an unplated seat indicate that it is feasible to use unplated valve seats on flight units. An engineering model of the jet valve with an unplated seat was cycled in different positions for a total of over 330,000 cycles at ambient temperature without leakage over specification limits.

Results of gas blowdown tests on the gas tank indicate that particulate matter discharged from the tank is within specification requirements and tank recleaning or the addition of a filter will not be necessary to ensure gas cleanliness.

b. Roll actuator. Type approval tests were delayed because of a failure that occurred when the unit was exposed to launch vibration levels with a simulated vernier engine load. The two tapered pins that couple the last stage gear to the output shaft sheared with no evidence of fatigue failure. At the time of failure, the actuator loading was in excess of expected values because of a resonance of the actuator-engine spring/mass system. A detailed dynamic loading analysis is in process to explore the various modes of loading that could occur during test and during the spacecraft mission. A severe resonant condition cannot be practically designed out of the system without added damping or a balanced engine, and therefore the engine must be restrained during launch if a rotary type actuator is to be used. Testing of the existing actuator design for the most adverse dynamic load conditions expected is in process. One such test has demonstrated that the mechanical stops which limit the output shaft range of travel will be deformed when the electrical power to both phases of the actuator motor is cut off and the bias spring is allowed to drive the actuator into the opposite stop from a position where the vernier engine is at the end of its travel range opposing the bias spring load. The speed attained is four to five times the actuator no-load speed when the mechanical stop is contacted and this load deforms the stop. Progressive deformation occurs at each impact. After

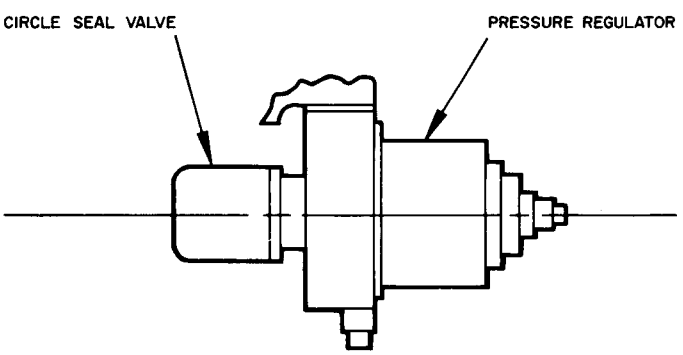

Fig. 21. Gas jet system pressure regulator

41 impacts with a 100% spring overload, the stop deformed enough to permit sector gear disengagement. A redesign of the mechanical stops is in process. Further testing will include exposure to spacecraft descent phase vibration levels.

A roll actuator of the current design will be delivered to the SC-1 spacecraft to permit system functional tests to be performed until a solution to the problem is obtained.

6. *Flight Control Electronics Unit*

Chassis for the first two flight units were delivered to the subsystem test area for circuit balance and calibration tests prior to unit assembly. Following acceptance tests on the flight control sensor group, the electronics unit will be reworked to incorporate several mandatory circuit changes, including the revised terminal descent command trajectory line segments. These changes will be incorporated into the chassis for the third flight unit prior to delivery.

E. Electronics

1. Introduction

The various systems of the spacecraft used for receiving and processing commands and transmitting data to Earth are discussed in this section and include the following: (1) the radio frequency components consisting of two sets of redundant receivers and transmitters, transponder interconnection circuits for operating the receivers and transmitters in the transponder mode, and the planar array (high-gain) and two omnidirectional antennas; (2) command decoding circuitry which receives Earth commands from the receiver and provides output signals to command all spacecraft functions; and (3) signal processing circuitry for processing data for individual scientific experiments and for processing basic spacecraft data through the engineering signal processor, as well as final processing and multiplexing of data which modulates the transmitter. Also included are radar systems associated with flight control functions of the spacecraft.

The television system, spacecraft flight control electronics, and power management are discussed in Sections B, D, and F, respectively.

2. Omnidirectional Antenna

The omnidirectional antenna is designed to provide essentially spherical coverage about the *Surveyor* spacecraft.

The *Surveyor* dynamic vehicles (SD-1, SD-2, and SD-4) have only one omnidirectional antenna, located approximately 15 in. above the planar array and solar panel. This position was chosen as probably giving the best coverage for a single antenna. In order to verify this coverage it was determined that complete spherical coverage patterns should be made on a model of the dynamic vehicle with one antenna. The most economical and quickest way of obtaining a model was to modify the MA-2 model used previously for flight-type antenna coverage tests. Fig. 22 shows the reworked model during pattern tests.

Patterns were measured with Antenna 10. An analysis of these patterns showing percentage of sphere below a certain gain as a function of that gain was made. Fig. 23 shows the results, which appear to provide adequate data on the coverage expected from all omnidirectional antennas.

Antennas 4, 8, and 10 have been assigned to the dynamic vehicle flight program. All tests on these units have been completed.

In previous reports, it has been indicated that pattern acceptance testing would probably be done on the omnidirectional antennas themselves (primary patterns) and not when mounted on the MA-2 model spacecraft (spacecraft patterns). The reasons for pursuing this change are that it is more economical and it appears to be a sufficient test. The economy is obvious since it takes only 1 day to measure primary patterns, whereas it takes 2 wk to measure spacecraft patterns.

The discussion in the following paragraphs indicates that pattern acceptance testing on the omnidirectional antennas themselves constitutes a sufficient test. Spacecraft patterns were originally decided upon for the development program in order to determine the effect of the spacecraft on the primary patterns. During the development program it was realized that these pattern perturbations could only be determined grossly, not to a fraction of a db, because of spurious reflections on the 3000-ft antenna range. By this means, good spacecraft coverage was shown for the developmental antennas.

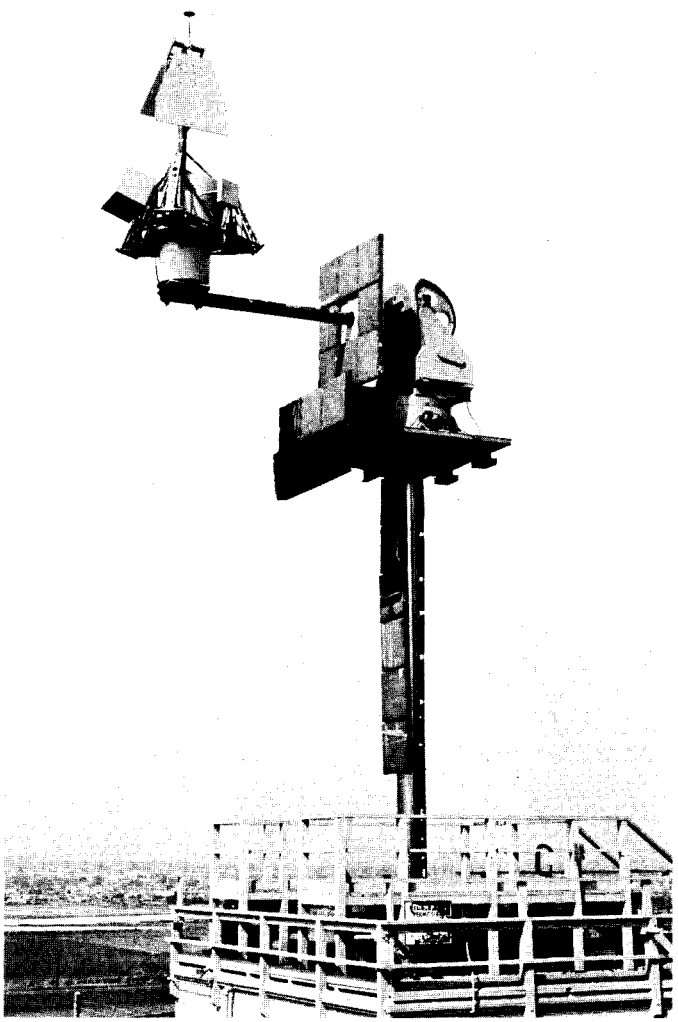

Fig. 22. Omnidirectional antenna coverage test for dynamic test vehicles

This good coverage has also been shown for the flight antennas by taking spacecraft patterns of five units. A typical flight unit pattern is shown in Fig. 24a. Some of the rapid fluctuations in this pattern are the spurious range reflections. It is difficult, if not impossible, to separate the true spacecraft pattern from this measured pattern. Hence, some of the nulls are questionable as to their true depth. Another problem on this range is the difficulty of obtaining a good axial ratio on the incident field in which the spacecraft is measured, which will tend to cause erroneous measurements for the lower gains. The best axial ratio achieved has been in the order of 1.5 to 2.0 db.

The range problems are considerably reduced by measuring the omnidirectional antenna primary patterns, because a much shorter range can be used (approximately 36 ft). This results in an antenna range that can be better isolated from the surrounding environment. This has also made it possible to obtain less than ½ db axial ratio on the incident field. A typical resultant primary pattern is shown in Fig. 24b. The measurement plane through the antenna is the same as for Fig. 24a.

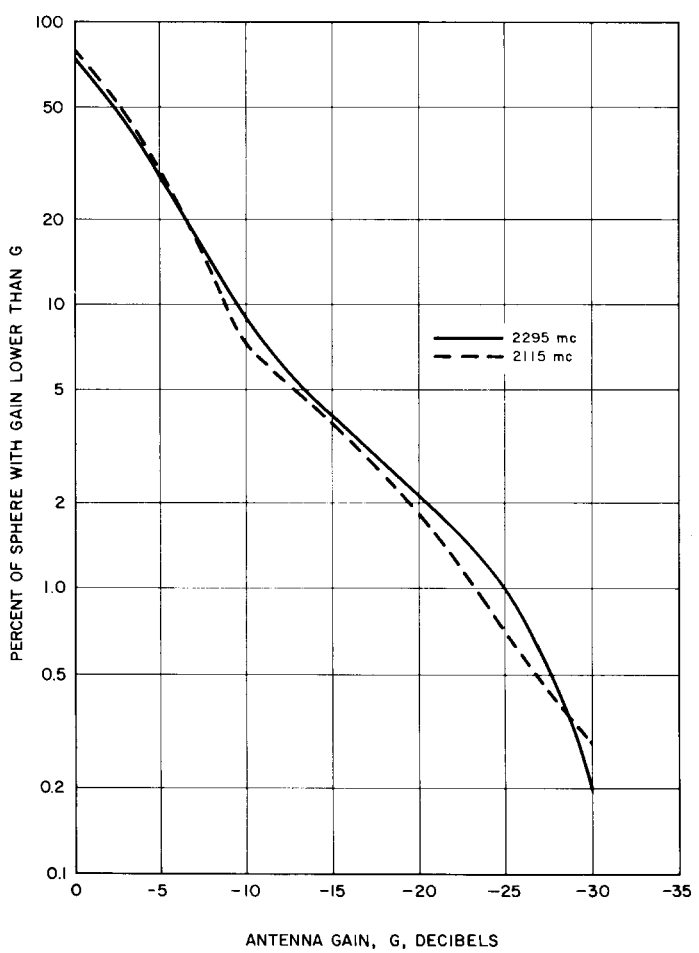

Fig. 23. Antenna gain coverage in dynamic test vehicle configuration

Since the omnidirectional antenna has a maximum dimension of approximately one wavelength and pattern fluctuations are consequently gradual, it should be possible to determine if a unit has acceptable patterns by taking a minimum number of cuts. By properly selecting some cuts, any pattern defect in any nonmeasured cut of the sphere should appear indirectly in the measured patterns. Three great circle cuts (designated principal plane) were decided upon; two cuts contain the antenna axis (axis of radiating conical surface), one passing through the long dipole and the other through the short dipole. The third cut is perpendicular to the antenna axis. Nine omnidirectional antennas have had primary patterns taken. All have shown acceptably similar patterns. Five of the nine units have also been used to take spacecraft patterns, resulting in four sets of complete spherical coverage patterns. A correlation study of the primary patterns and their associated spacecraft patterns is under way. From this study primary specification patterns having maximum and minimum gain limits will be generated for subsequent evaluation of individual omnidirectional antennas.

3. *Altitude Marking Radar*

The altitude marking radar (AMR) senses spacecraft-to-lunar slant range and initiates an altitude mark signal when a preselected range is reached.

a. AMR antenna. In *Space Programs Summary No. 37-26,* Vol. I, it was reported that the new antenna feed design was tested and found to meet all specifications; however, the voltage standing wave ratio was marginal. Additional tests of several flight feeds indicated that the matching technique of adjusting the short circuit position at the end of the feed was inadequate. A new matching technique was devised which inserts a probe into the broad wall of the half-height waveguide at a position approximately 1¼ in. toward the flange from the dipoles. Tests showed that this technique did not make the position of the short circuit at the end of the feed critical. The short circuit position can be fixed, but the exact location and depth of the probe for each feed will be determined during final fabrication, after each feed has been gold plated. During this reporting period, an investigation was made of the suspected heating effects on the polished antenna dish because of solar exposure. With a polished reflector, these solar loading tests indicated that hazardous temperatures (above 450°F) could exist at the antenna feed dipoles after only a 2-min exposure to the Sun. With the antenna parabola painted a

flat black, the maximum (5 min) temperature rise was 10° F. Subsequently, a flat black coating process suitable for application on the flight antennas has been prepared, and all AMR antennas are to be so treated.

The solar tests were performed with a production feed mounted in a standard test reflector that had been aluminized to simulate a production reflector. Three thermocouples were attached to the feed in the vicinity of the dipoles, and the Sun was tracked while the feed temperature was recorded as a function of time. The feed heated rapidly; for example, on the first run, the temperature increased from 64 to 450° F within 2 min.

Several possible solutions to this severe heating problem were explored, and some were checked electrically while the antenna was being prepared for the solar test. A 0.005-in. teflon sheet and a sheet of fiberglass cloth were stretched separately across the reflector, and the effect of each on the electrical characteristics of the antenna was recorded. Neither made any appreciable change in the antenna patterns or gain. As a third solution, black acrylic paint, HP 4-143, was sprayed over the surface of the reflector and the temperature as well as electrical characteristics checked. With the painted surface, there was no temperature change in the feed and no appreciable change in patterns or gain. Since spraying is the simplest solution, it will be employed in flight hardware.

Final details on the testing procedures of the type approval unit have been completed. Following TAT vibration, the antenna was removed and sent to the range for a boresight and pattern recheck; all values were within specification requirements. These results indicated that handling and mounting techniques are adequate for the antenna dish, feed, and coupler, and that the boresight measurements are reproducible.

Thermal–vacuum tests have shown that an excessive amount of heater power is required to attain and maintain the minimum 0° F operating temperature on the electronic units. Additionally the heating system was unable to maintain the temperature of the magnetron at or above the minimum acceptable temperature of −55° F. Because of the limited electrical energy available for heating purposes, additional heater power is not available.

A revised method of mounting and shielding the altitude marking radar units from the extreme radiative and conductive losses is under active investigation. Preliminary studies indicate that substantial reductions in losses are attainable with a minimum of redesign.

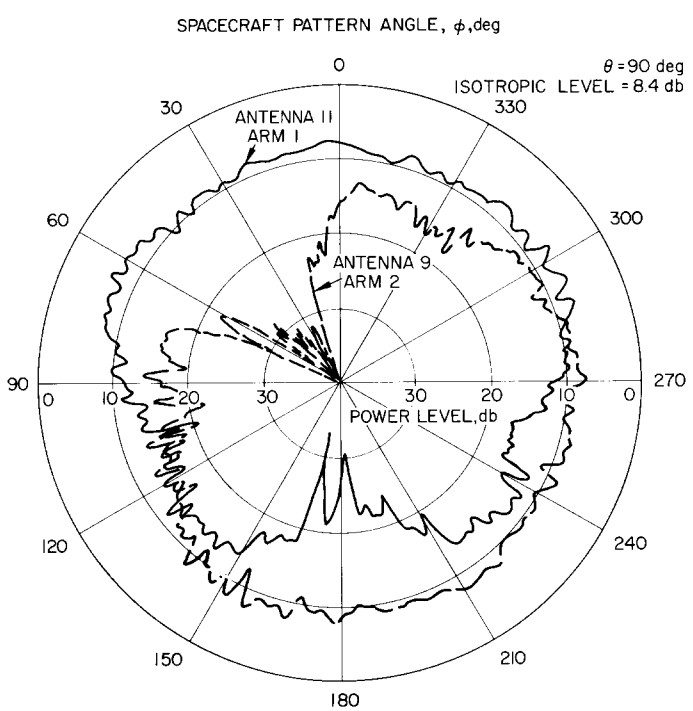

(a) Typical spacecraft pattern

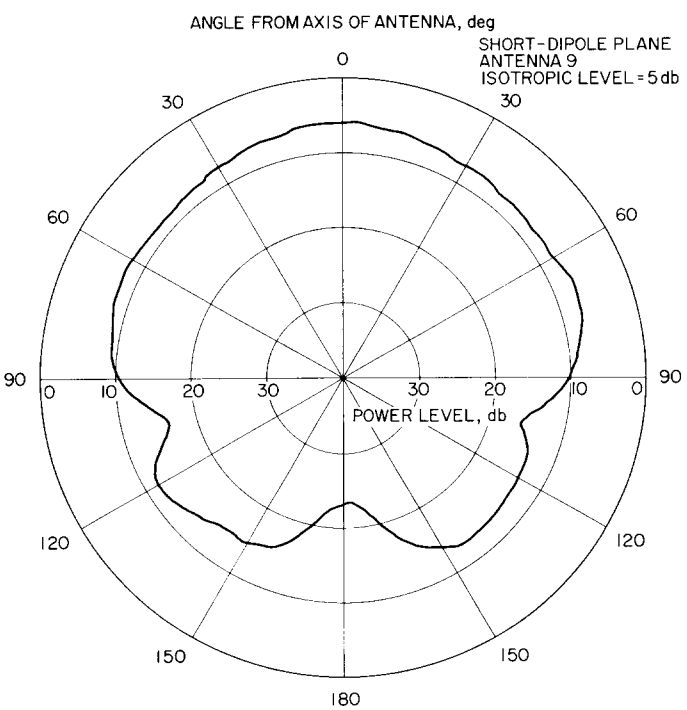

(b) Typical primary pattern

Fig. 24. Pattern acceptance testing on omnidirectional antennas (22.95 mc right-hand circular polarization)

4. *Traveling-Wave Tube*

The traveling-wave tube (Fig. 25a) developed by Hughes as the output power amplifier in the spacecraft transponder has met all requirements; the requirements are summarized below:

Frequency	2285 to 2310 mc
Duty	Continuous wave
Total dc power consumption (including heater power)	50 w (maximum)
Output power	10 w (minimum) for input power levels from 20 to 40 mw, and for rated power supply voltage ±2%
Stability	Short circuit stable at all frequencies and phases
Life	20,000 hr
Weight	16 oz (maximum)
Length	8 in. (maximum)
Cooling	Via conduction to a cold plate

Typical electrode voltages are as follows:

Element	*Voltage*	*Current*
Cathode (E_k)	−1250 v	54 ma
Anode (E_a)	+50 v	0.04 ma
Collector	−800 v	49 ma
Helix	Ground	5 ma
Heater	5.2 v	0.275 A

A stacked, self-aligning metal-ceramic gun assembly is used in which close tolerances can be held to assure good beam focusing and performance repeatability. An exploded view of the tube is shown in Fig. 25b. Platinum-cobalt permanent magnets in a periodic focusing stack provide low helix interception current under rf drive and collector depression to obtain specified operating efficiency. Fig. 25c shows the tube with the focusing stack in place.

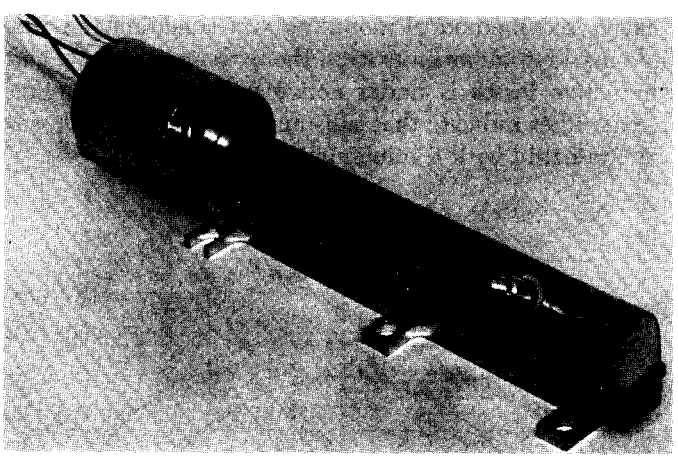

(a) Assembled view

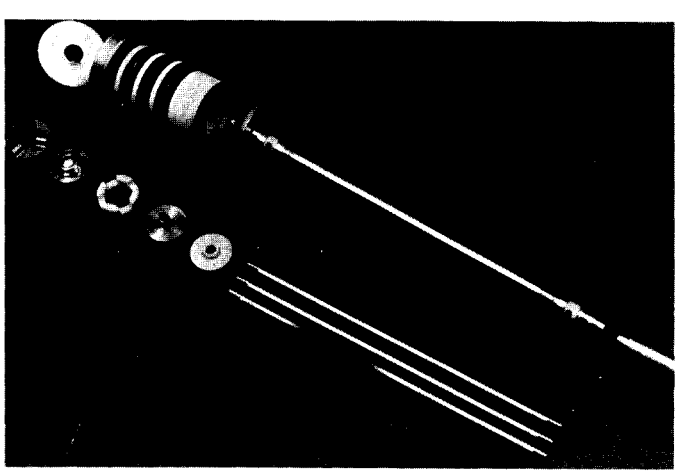

(b) Exploded view

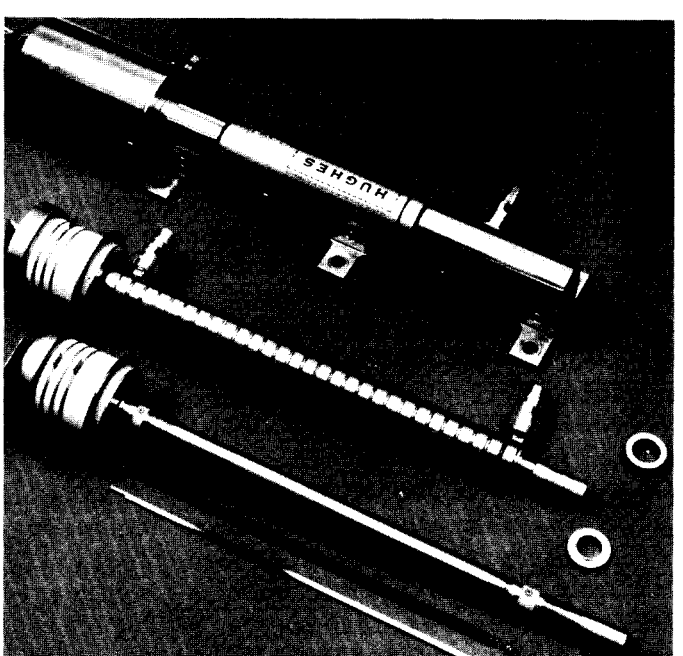

(c) View with focusing stack in place

Fig. 25. Traveling-wave tube

Table 6. Traveling-wave tube life test data

Operation	Serial number	ON hours	Total hours
Continuous	25	16,861	16,861
Continuous	51	14,048	14,048
Continuous	52	15,394	15,394
Continuous	56	15,437	15,437
Continuous	69	12,632	12,632
Continuous	101	7,428	7,428
Cycled (1 hr on, ½ hr off)	110	3980	5980

Note:
These calculations are based on number of failures, C = 0:
MTBF (95% confidence) = 27,200 hr.
MTBF (90% confidence) = 33,100 hr.

Table 6 shows life test data by tube serial number to date. Total accumulated hours indicate a current mean time before failure (MTBF) and confidence level of 3310 hr at 90% confidence, and 27,200 hr at 95% confidence level. The tube phase of the *Surveyor* program is currently on schedule.

5. Thermal Control and Heater Assembly

The compartment heater assembly provides a heater element, sensor element, and control circuitry for the purpose of maintaining and controlling the temperature of the thermal tray in Compartments A and B. The lunar night temperature of the thermal tray of Compartment A is maintained above 40° F and Compartment B is maintained above 0° F. The assembly can be commanded from the Earth to operate in either automatic or manual mode. In the automatic mode, operation of the heater element is controlled by the sensor element. In the manual mode, the sensor element is overridden by Earth command.

The functional, flight acceptance, type approval test specification and procedure for this unit was approved and released. The type approval tests were completed during March and complete acceptance given to the unit by the TAT review committee. The Compartment A unit and the Compartment B unit for SC-1 were delivered the first week of April.

a. Thermal–vacuum TAT results. A developmental test run prior to the thermal–vacuum portion of the type approval test indicated that regulation temperature at ambient pressure is 14° F below the regulation temperature in a vacuum. This difference in temperature was considered when the selective resistor was chosen. When the unit was again operated in a vacuum it regulated at the specified temperature.

After the selective resistor was chosen in this manner, the unit verified all performance characteristics listed in *Space Programs Summary No. 37-26*, Vol. I.

b. Flight acceptance test procedures. As a result of the developmental test discussed above, a thermal–vacuum test phase was added to the thermal test portion of the flight acceptance test procedure to verify the achievement of the specified regulation temperature in a vacuum. All units tested exhibited a 13 ±1° F difference in regulation temperature between high vacuum and ambient pressure.

6. Radar Altimeter and Doppler Velocity Sensor

The purpose of the radar altimeter and doppler velocity sensor (RADVS), being built by Ryan Electronics, is to provide altitude and velocity information to the flight control system during the final portion of the lunar landing phase of spacecraft flight.

Following delivery of the QA-1 prototype system, it was installed on the T-21 test vehicle. Problems of mechanical interference have been resolved as follows. The heat sink on the velocity sensor klystron was milled by Ryan on one edge to clear the mounting bracket. The spacecraft brackets supporting the interconnecting waveguide were lengthened to offset short shock mounts, thereby moving the waveguide from contact with the vernier engine fuel lines. Limited operating and vibrating tests were conducted to confirm integration suitability.

Type approval testing of the RADVS, in progress on system SN-1, has been delayed by problems encountered in vibration testing, several of which were discussed in the preceding report. The major problem at this time occurs in the antennas. In vibrating the antennas, both individually and as part of the RADVS system, large amplification factors at resonant frequencies cause the septum and shroud to vibrate excessively. This vibration during system operation causes undesirable rf energy to be introduced into the system at frequencies through which the trackers must search. An investigation of methods of reducing these amplification characteristics is in process. Possible solutions to the problem include fixing a radome to the front of the antenna, reinforcing the antenna with aluminum sheets and/or rods, and filling the antenna with rigid foam. Hughes personnel have been assigned to assist Ryan in solving this problem. Varian, the manufacturer of the klystrons used in the RADVS, is continuing an investigation of the problem in an effort to reduce velocity sensor klystron susceptibility to vibration. Varian has determined that the cathode structure is the element which resonates at the critical frequencies.

A second problem in the velocity sensor klystron has been solved. The rf outputs of several tubes have dropped below the required level with less than 30 hr of operation. The specification requires a minimum life of 250 hr. Inspection and test by Varian of one such tube has revealed that power loss results in the cathode structure from the characteristics of two dissimilar metals which are welded together. Varian has modified the cathode structure and has tested the resulting tube. These tests of life and cycling under laboratory conditions satisfy the requirements on this component.

7. Bit Error Rate Tests

A large amount of data from the *Surveyor* spacecraft will be processed and transmitted to Earth in a pulse code modulation (PCM) format. A measure of performance of this link is the number of bit errors that are introduced as a result of the signal transmission and detection in the presence of noise. A detailed examination of the bit error rates for *Surveyor* is currently in process. The first series of tests have investigated the performance of the 33-kc subcarrier oscillator (SCO) operating at a bit rate of 4400 bps.

The measurements of the bit error rate were made as a function of carrier-to-noise ratio (C/N) where the carrier is the unmodulated subcarrier oscillator power in the input bandpass filter of the SCO discriminator, and the noise is the total noise power in this same filter. Parameters used included PCM word format, input filter, and voltage to the SCO.

The test setup is indicated in Fig. 26. Here the SCO is modulated by the PCM word generator through a variable attenuator and variable low pass filter. The output of the SCO is added with white noise and supplies the input of the SCO discriminator. The output of the SCO discriminator feeds the PCM decommutator where the PCM code is detected and is available as a noise-free reconstructed PCM signal. This reconstructed signal is compared bit by bit in a comparator circuit with the original signal, thus detecting bit errors. The errors are counted, as are the total number of bits, to establish the bit error rate. The comparator circuit contains suitable delays to match exactly the delay through the signal path.

The bit error rates as first measured appear in Fig. 27a; the curves represent typical results of the presently implemented system. These results gave bit errors that were higher than expected and the cause of this was sought. Test results which show possible improvement are indicated in Fig. 27b. Here the bit error rate was improved by almost two orders of magnitude by a combination of filtering at the input of the SCO (4 kc equivalent) and reducing the amplitude of the signal modulating the SCO, thus reducing the peak deviation of the SCO.

The reason for the large improvement in the bit error rate which resulted from optimum input filtering to the SCO and reduced amplitude of the input modulation waveform was traced to the SCO discriminator. This phase-locked discriminator momentarily loses lock while demodulating the PCM signal. This was observed three ways:

(1) Counting the loss of lock indications[a] from the SCO discriminator.

[a]This indicates the number of times the error angle of the phase-locked loop exceeds a threshold, and always indicates a complete loss of lock.

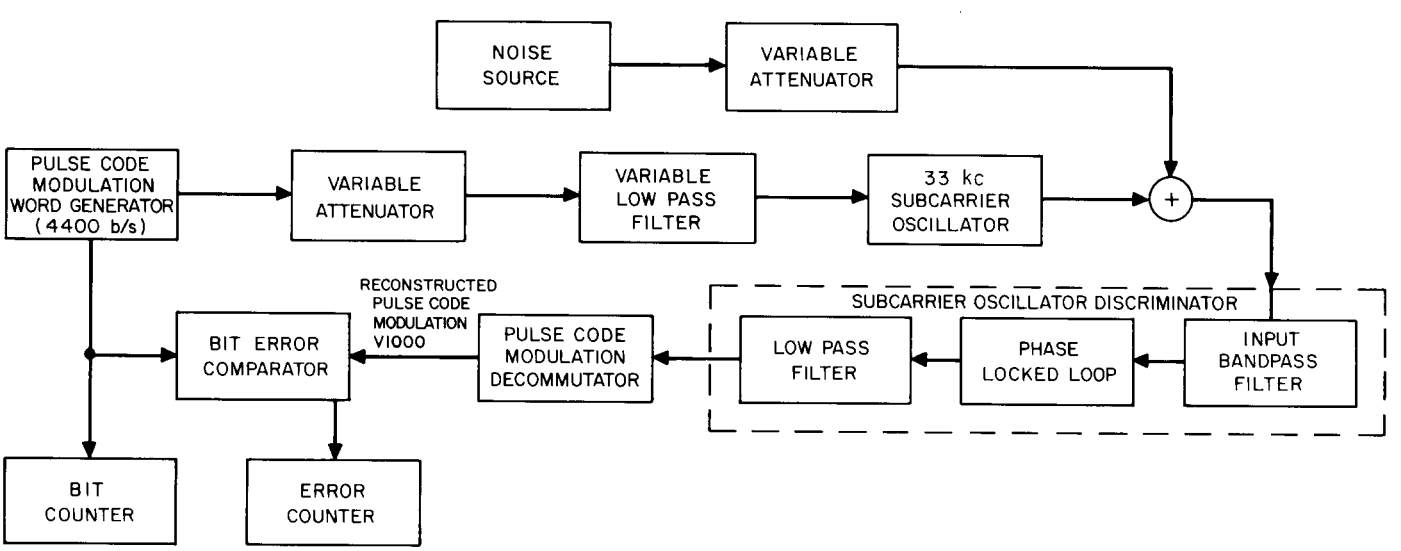

Fig. 26. Bit error rate test configuration

(2) Observing the spectrum of the output of the SCO discriminator and noting the noise spectrum due to thermal noise and the noise spectrum due to loss of lock as modulation and carrier-to-noise ratio were varied.

(3) Observing the detected PCM waveform and noting the normal thermal noise and the occasional sudden dropouts in the signal caused by loss of lock in the SCO discriminator.

The data of Fig. 27a indicates that the bit error rate of the present 33-kc SCO and SCO discriminator are excessive due to an unmatched modulation/demodulation implementation; the possible improvements are also indicated. A change is being made to correct this condition.

8. Command Decoding and Signal Processing

a. Command decoding. The command decoding system consists of two redundant central command decoders (CCD), a receiver-decoder selector (RDS), and up to 30 subsystem command decoders (SD) associated with the various engineering and scientific instrument subsystems of the spacecraft. The central decoder unit (CDU) contains the RDS, both CCDs, and four of the SDs. The SDs supply command pulses to the basic bus subsystems, except the flight control subsystem which has its own SD. Fig. 28 shows the functional relationship among these areas.

Two problems – ECU efficiency and inadvertent commands – have been encountered in the command decoding system and are described below:

(1) *Central command decoder/electrical converter unit (CCD/ECU).* The original design of the CCD/ECU module had very large voltage spikes on the base and collector waveforms of the switching transistors and also on the various outputs. These spikes could damage the switching transistors and

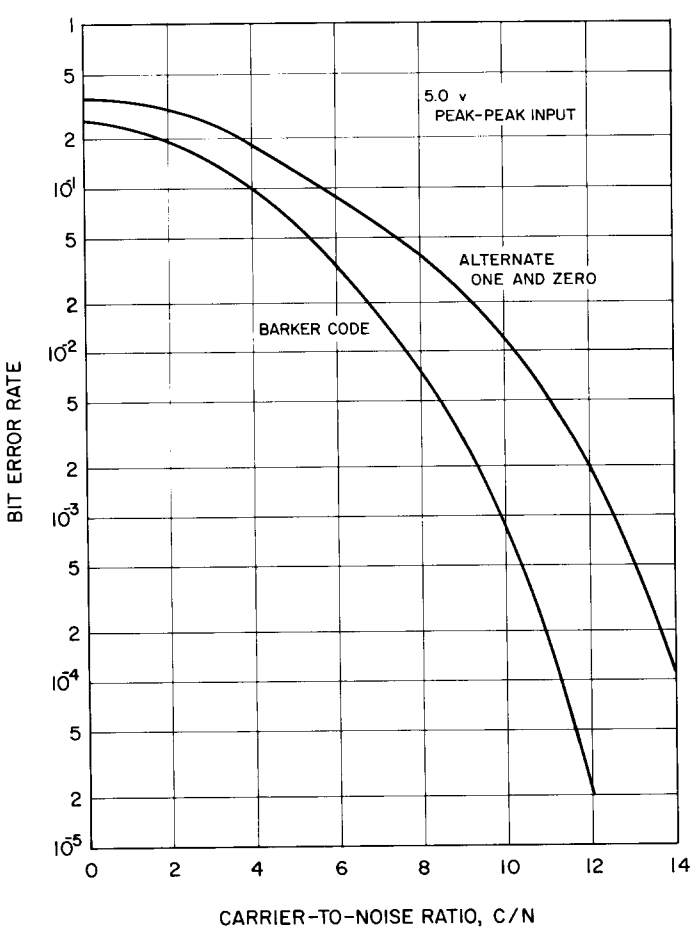

(a) Bit error rate versus carrier-to-noise ratio

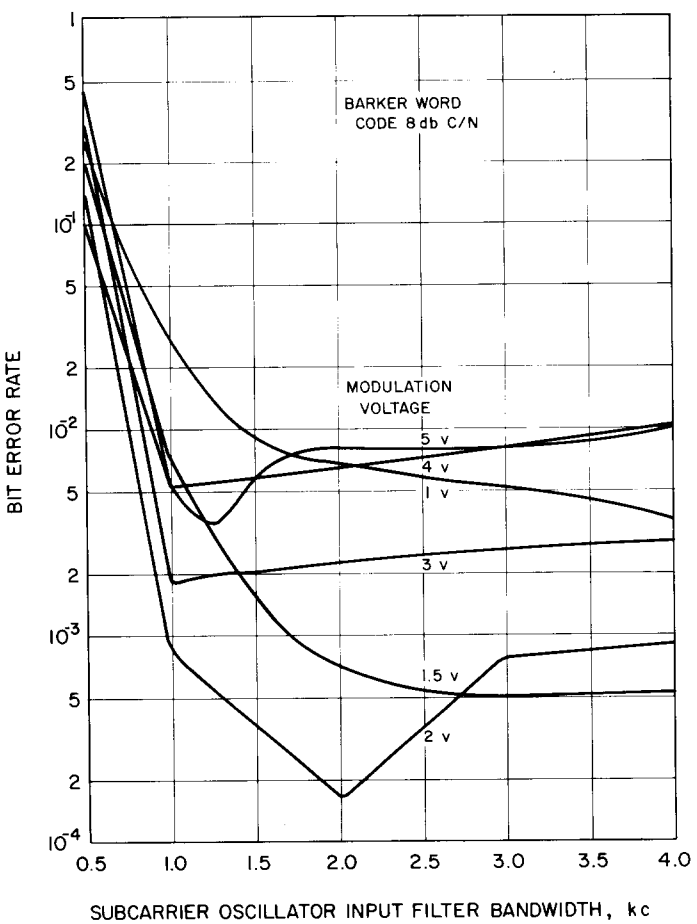

(b) Bit error rate versus subcarrier oscillator input filter bandwidths and modulation

Fig. 27. Bit error rates for *Surveyor*

also cause unreliable operation of circuits being fed by the outputs. Therefore, a means of eliminating or reducing these spikes without major circuit redesign was investigated. The basic ECU is shown in Fig. 29a.

It was previously found that the spikes could be substantially reduced by placing a 0.022-μf capacitor between the collectors. While the spikes were reduced, the efficiency of operation was only 34% under minimum load and 54% under maximum load. Because of the low efficiencies obtained under the above conditions, other schemes of despiking were investigated. A 300-μh choke between the junction of the two emitters and ground reduced the spikes without degrading the efficiency. See Fig. 29b. The efficiency with this circuit was found to be 63% under minimum load and 85% under maximum load. The low efficiency under minimum load is a result of the load power approaching no-load power. Measurement of transformer losses indicates that it is approximately 75% of no-load power. Therefore, the above efficiencies are about the best obtainable without complete transformer redesign.

It was also found that the spikes on the output could be further reduced by increasing the value of the filtering capacitor, but increasing capacitance is limited because of space allotment for the ECU. The capacitors were therefore increased to a maximum value for the allowable volume.

The addition of the choke and the increase in filtering capacitance has optimized the ECU circuit relative to spiking and efficiency.

(2) *Central decoder unit.* In system test, it was discovered that extraneous pulses were being generated by the subsystem decoders when power was turned off in a central command decoder as a result of receiver modulation being interrupted. Waveform analysis indicates that the relative decay times of the ECU output voltages differ greatly. The +12 and −8 voltages decayed rapidly under their heavy load. The +20 and −15 voltages decayed slowly under their light load. These relative decays cause an address enable signal to occur at power turnoff. Since the command enable signal loses control after power is turned off, a subsystem could then be selected and its amplifier turned on to drive its matrix which

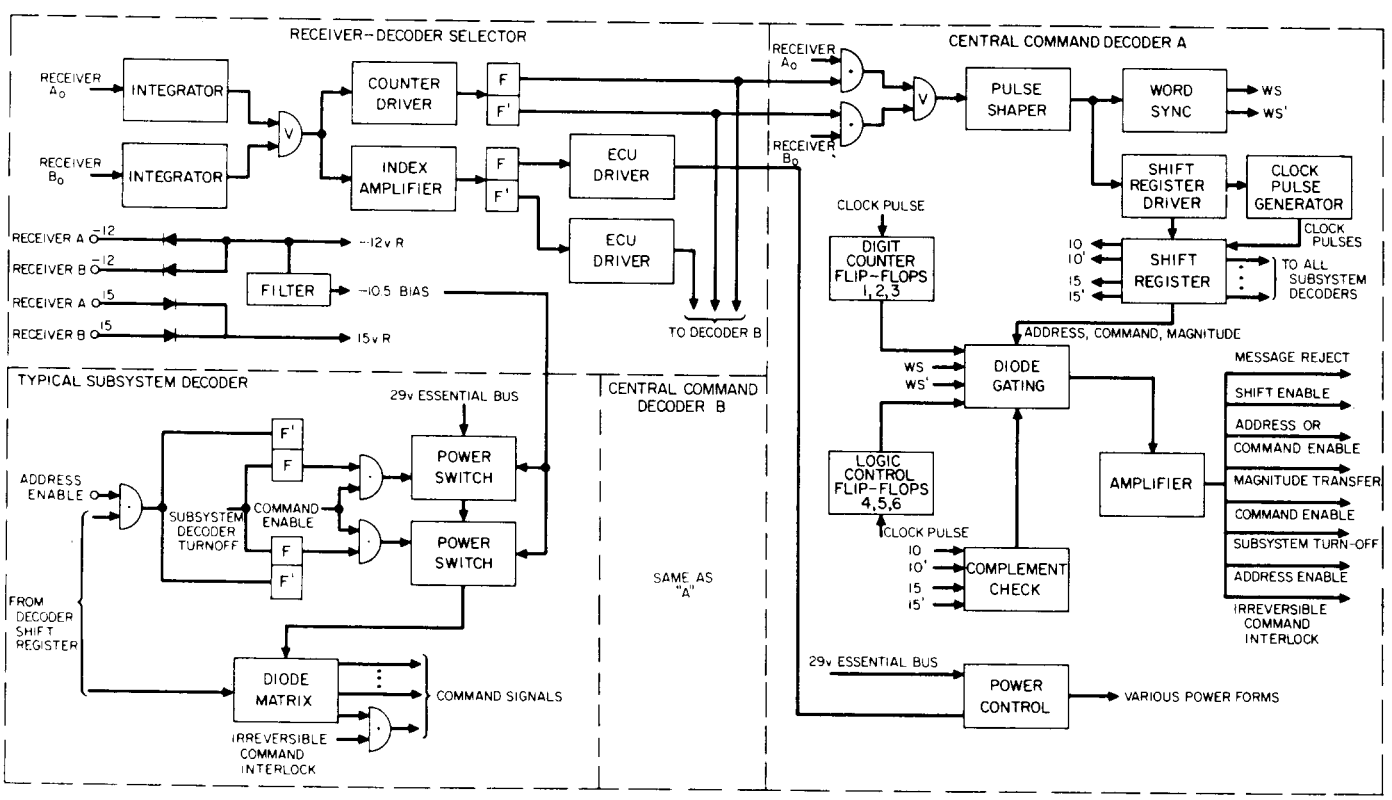

Fig. 28. Command decoding

provides the output command signals. The subsystem turnoff signal which normally occurs when power is turned off would prevent a subsystem from being or staying selected; however, the extremely slow decay (1 sec) of the −15 v supply delays the application of the subsystem turnoff signal until after the output command signals have occurred. The following investigations are in process in an effort to solve the problem:

(a) The subsystem turnoff amplifier is being investigated for possible modification to enable a faster response when power is turned off.

(b) The command enable amplifier is being investigated for redesign to inhibit a subsystem decoder amplifier from turning on without the application of a positive control current from the command enable amplifier.

(c) The address enable circuit is being examined.

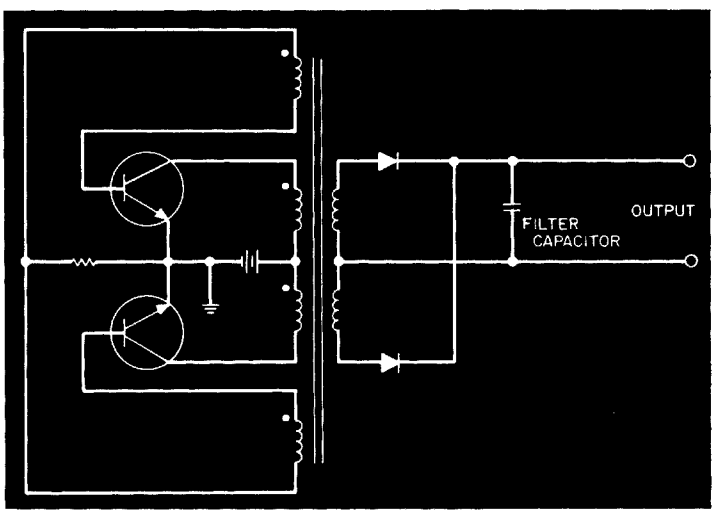

(a) Basic circuitry

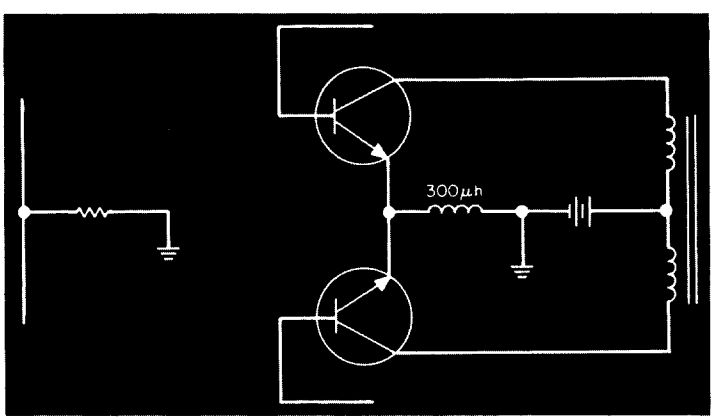

(b) Emitter circuitry

Fig. 29. Electrical converter unit circuitry

b. Signal processing. The signal processing system consists of a central signal processor (CSP), an engineering signal processor (ESP), an auxiliary engineering signal processor (AESP), signal processor auxiliary (SPA), and a low data rate auxiliary (LDRA). Fig. 30 illustrates the various functional relationships among these units.

An ECU problem has been uncovered in the central signal processor. Certain transformers cause electrical failures of the ECU circuit. The failure mode is caused by high frequency oscillations of the ECU switching transistors, which cause excessive currents to be drawn from the input 29-v supply. This excessive current burns out the switching transistors. The rejected transformers that caused the circuit failures were retested and passed electrical specifications.

Seven rejected transformers were obtained. These transformers had caused circuit failures when connected to an ECU module. In addition, they had subsequently been checked and were found to meet their electrical specifications. A breadboard of an ECU circuit, plus a circuit to provide ON-OFF control signals, was built. Each rejected transformer was used with the breadboard to form an ECU circuit. Six out of the seven transformers exhibited the failure mode. The switching transistors oscillated at approximately 1.0 mc. The 29-v power supply had been current-limited at 100 ma, and the circuit pulled all that the supply would deliver. Of these six transformers, three would exhibit high frequency oscillations only when the ON control signal amplitude was reduced to approximately 10 v. The circuit worked satisfactorily for the normal range of the ON control signal (between 22 and 29 v). The other three transformers exhibited high frequency oscillations for all ranges of the ON control signal.

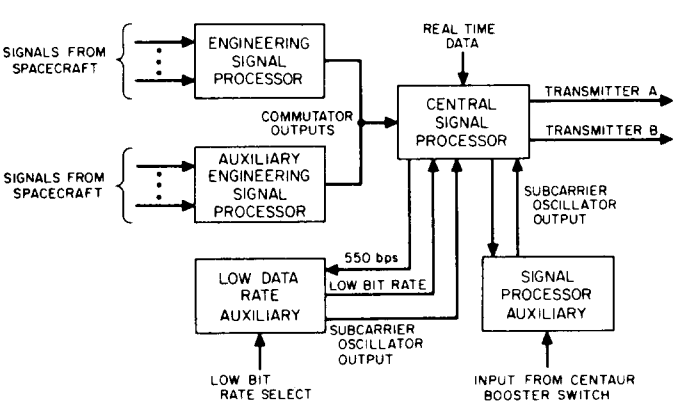

Fig. 30. Signal processing

Various modifications were made to the circuit to eliminate the high frequency oscillations. Only one method was found which eliminated the oscillations for all transformers and for all levels of the control signals. This consists of placing capacitors across the collector-to-base junctions of the switching transistors to reduce current gain at high frequencies. The minimum value of capacitance required is different for each transformer. The minimum was 50 pf, and 120 pf worked for all of them.

Since a small amount of capacitance is critical, an actual ECU module and an etched circuit board were obtained for investigation to determine if the component layout was contributing to the oscillations. This investigation is continuing.

F. Electrical Power Supply

1. Introduction

Electrical power for the *Surveyor* spacecraft is supplied by a Sun-tracking planar solar panel and a sealed, secondary silver-zinc main battery. On the first four spacecraft an auxiliary battery will be used to provide additional peak load capability and increased energy storage capacity during transit and lunar landing. The solar panel is the prime source of power during transit and lunar day, and the main battery provides the electrical energy for operation during lunar night and peak load periods.

The power management system is comprised of a central power control unit and a variety of voltage converters, regulators, and power switches located in other units to provide power management for the various instruments and subsystems. The central power control unit provides power conversion from the solar panel, main bus regulation, overload sensing, main battery charge control, and several switching functions.

The optimum-charge regulator circuit provides the most efficient conversion of solar panel power to battery charging current. The battery output voltage from the unregulated bus is converted to the main regulated bus voltage by a boost regulator. A main overload trip circuit using tunnel-diode sensing removes all nonessential spacecraft loads when an overload condition is detected. The main battery charge logic system controls the charging current to the spacecraft main battery. Normally, the system operates in the automatic mode, and the main battery is charged until its voltage reaches a predetermined level. A command mode is available whereby the battery may be commanded to be charged.

The auxiliary battery control unit provides battery voltage sensing circuitry, automatic control and selection of either one or both batteries, and command override of the automatic control mode.

2. Progress Summary

The solar panel type approval test program has been successfully completed. The fabrication of the first flight panel (SC-1) was completed and flight acceptance testing (FAT) has been initiated. Fabrication of the second flight panel is nearing completion. The new vibration levels for FAT have been established; these levels will allow confirmation of the structural integrity of the flight panels without causing panel fatigue.

A structural problem occurred in testing of solar cell module Lots 21 and 22 delivered by Heliotek and an investigation is under way. The problem appears to be isolated to these two lots and was probably caused by improper flux cleaning before soldering.

The solar panel performance analysis has been modified to include Table Mountain test results from the T-21 and type approval panel performance tests. A statistical determination of solar power was derived from solar module test data. The statistical determination compared favorably with actual panel test results.

Disassembly and analysis of the two prototype main batteries damaged in type approval vibration test showed that the positive plates were cracked. Several alternative designs were incorporated in test cell monoblocks and were successfully vibration tested. Batteries incorporating redesigned positive and negative plates are presently being fabricated. Shipment of the first two batteries is scheduled for the first week in May. Three auxiliary batteries successfully completed type approval testing. The first flight model auxiliary batteries are scheduled for delivery on May 1, 1964.

3. Solar Panel

a. Type approval solar panel. Type approval testing (TAT) was completed on January 20, 1964 with the post thermal – vacuum electrical performance test at Table Mountain. A summary of electrical performance for the TAT program is shown in Table 7. No significant degradation resulted from vibration; about 4½% degradation resulted from thermal – vacuum exposure, which was within predictions based on results of module type

Table 7. Type approval solar panel – summary of electrical performance tests at Table Mountain

Item	Power output, watts, at 100 mw/cm², 25° C			
	Specification requirement	After fabrication	After vibration	After thermal–vacuum
Total Panel	79.2	86.0	86.5	82.4
Subgroups				
V-1	8.8	9.41	9.42	9.28
V-2	8.8	9.39	9.39	9.00
V-3	8.8	9.31	9.33	9.14
V-4	8.8	9.38	9.36	9.12
V-5	8.8	9.40	9.46	9.11
V-6	8.8	9.39	9.51	9.01
V-7	8.8	9.54	9.52	9.01
V-8	8.8	9.31	9.64	9.07
V-9	8.8	9.29	9.24	8.91

approval tests. Panel performance still remained about 4% over the minimum requirement at the end of the type approval exposure.

On March 4, 1964 a type approval review committee reviewed results of the TAT program. Results were acceptable, although the program was not formally concluded since a separate shock test had not been run on the panel; shock equipment had not been available to conduct the shock test per specification requirements. Analysis of the type approval vibration test data indicated that panel shock requirements had been exceeded during the vibration test. Also, the panel will be subjected to the shock environment during the T-21 spacecraft drop tests. For these reasons the shock test has been deleted from the solar panel TAT specification. Formal TAT program completion will take place following release of the revised specification.

b. Flight hardware

SC-1 solar panel. Fabrication of the first flight solar panel (for SC-1) was completed on March 4, 1964 with the exception of secondary Sun sensor installation. Electrical performance testing is under way at Table Mountain and panel performance appears satisfactory. Fig. 31 shows the panel in the Sun-tracking test fixture at Table Mountain. Power output of each of the nine subgroups of modules was obtained with a test harness attached to feed-through terminals on the back of the panel. Previously, power of individual subgroups was obtained by attaching test leads to the front side of the terminals with a high probability of damage. The SC-1 panel is the first on which feed-through terminals have been incorporated. Addition of these backside feed-through terminals provides safety for the panel during test.

SC-2 solar panel. Fabrication of the second flight solar panel (for SC-2) was begun February 10, 1964. Brackets, sleeve inserts, and terminals have been installed; the panel has also been painted and the solar cell modules have been bonded to the panel substrate. The SC-2 panel in its present stage of completion is shown in Fig. 32. Wiring is presently under way and fabrication completion is scheduled for April 10, 1964.

c. Flight acceptance testing (FAT). Vibration levels for flight acceptance testing of flight panels have been established and incorporated in the FAT specification. These new vibration levels allow flight panels to be subjected to enough vibration to confirm construction quality without causing damaging stress or fatigue to the panel. A static loading of 13.7 g on the panel was calculated to be within safe limits of material stress and fatigue at an infinite number of cycles. Trial tests were run on a development solar panel on the FAT fixture to determine vibration inputs required at the fixture to produce 13.7 g on the panel. The development panel is shown in Fig. 33 mounted on the fixture during trial tests. The vibration inputs (see location of input accelerometer in Fig. 33) determined from these tests are shown in Fig. 34. Responses near the edge of the panel (see locations of response accelerometers in Fig. 33) to the vibration inputs are shown in Fig. 35. Accelerometer A, which was mounted near the unsupported edge of the panel, responded primarily at 5 to 50 cps. Accelerometer B, which was mounted on the center portion of the panel between the support brackets, responded primarily at frequencies from 100 to 1500 cps. Over the entire frequency range

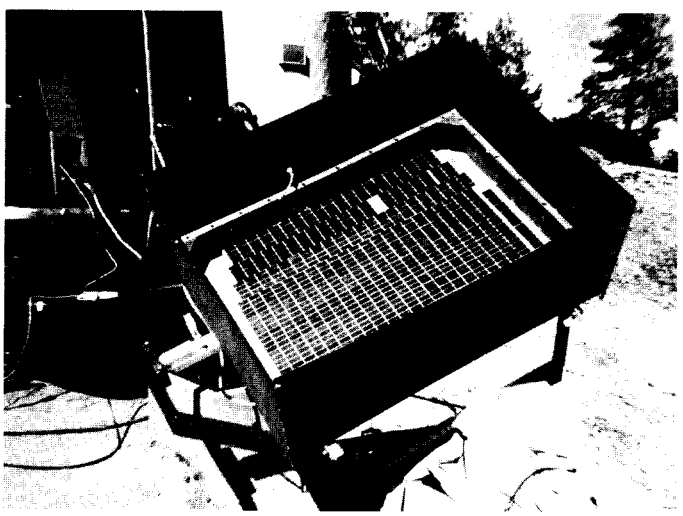

Fig. 31. Solar panel performance test at Table Mountain

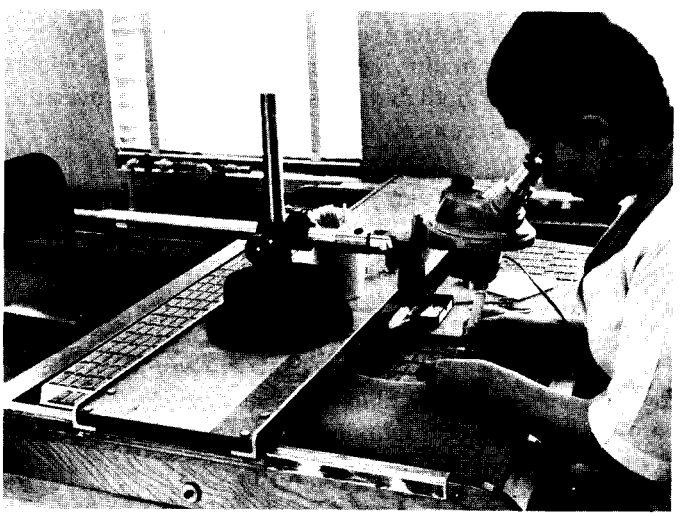

Fig. 32. SC-2 solar panel

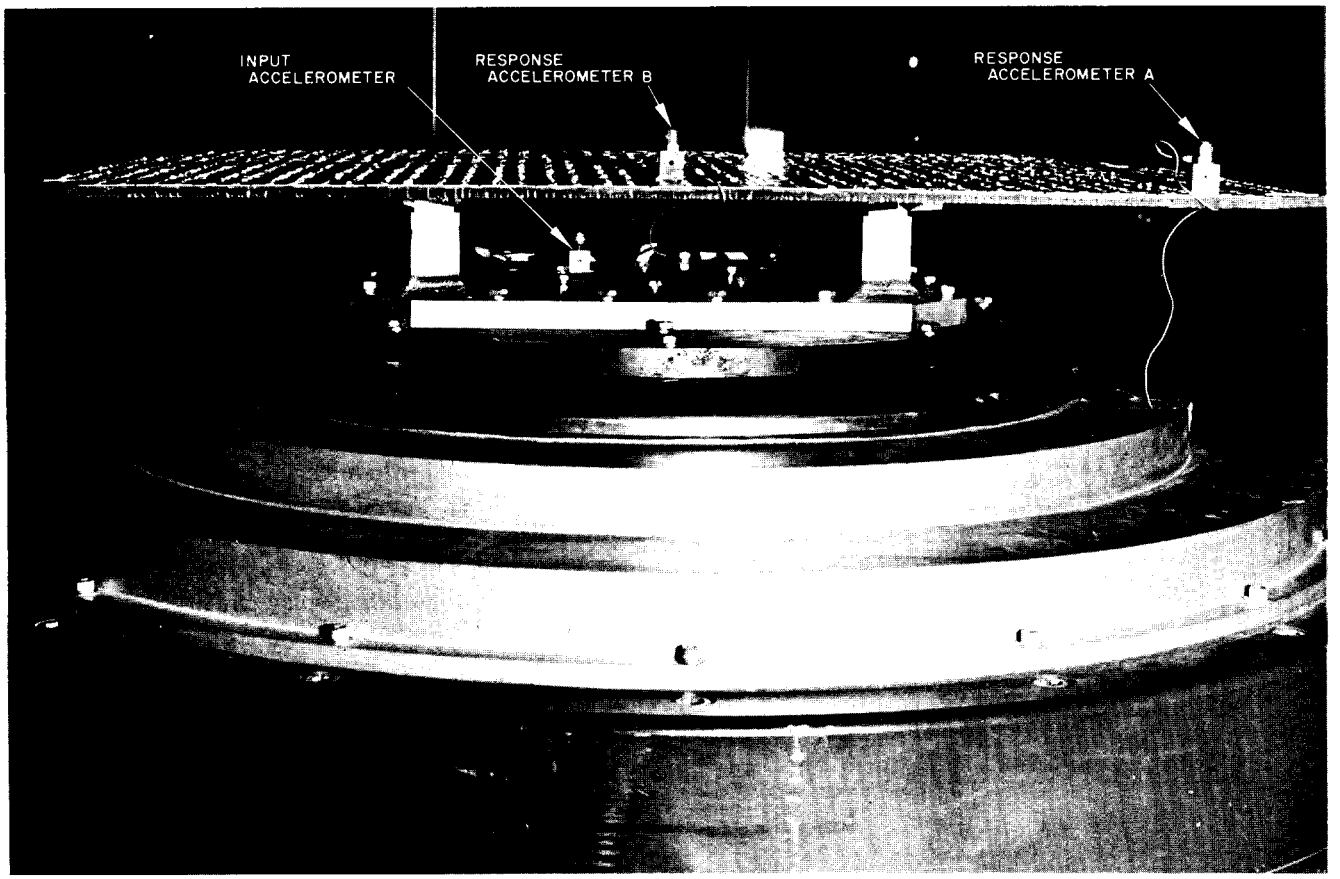

Fig. 33. FAT vibration test of solar panel

the combined responses produced g-loadings close to the 13.7-g level without exposing the panel to higher peaks.

d. Solar cell modules. Heliotek has delivered 22 lots of solar cell modules to date (400 modules/lot). However, Lot 21 has been returned to Heliotek for reinspection. Modules from Lots 21 and 22 tested at Table Mountain and at Heliotek were breaking at intercell solder joints. All the modules in Lot 22 were subjected to a beam test by Heliotek and a 5% breakage rate was reported. Lot 21 testing is under way. Investigation by Heliotek indicates that improper solder fluxing of the joints before shingling is the probable cause for cell breakage. It is expected this problem is associated only with Lots 21 and 22. However, Hughes will reinspect lots received prior to Lot 21. After receiving extensive testing, rework, and some module replacement, Lot 22 has been delivered to Hughes.

The third type approval test program (TA-3) on solar cell modules was started during this report period. Twenty-five modules from Lot 21 were used in the first sunlight electrical performance test. The intercell breakage described above, which occurred at the start of the TA-3 test, has temporarily delayed the test program. Twenty-five new modules will be selected from Lot 21 after rework and the test program will be reinitiated.

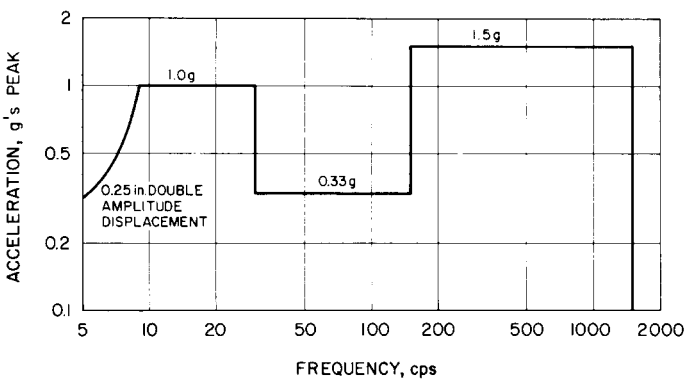

Fig. 34. FAT solar panel vibration inputs

e. Solar panel performance. The prediction of solar panel performance during transit and on the lunar surface mentioned in *Space Programs Summary No. 37-26*, Vol. I, was based on the minimum electrical performance requirements. To improve the accuracy of the prediction,

the performance analysis has been revised to incorporate T-21 and type approval solar panel data. The average maximum power output (at air mass one) of the two solar panels prior to environmental testing was 85.8 ±0.3 w. The average maximum power output after flight acceptance testing was 84.2 ±0.4 w.

Table 8 summarizes the performance of the *Surveyor* solar panel over the mission sequence. The mean power available during the transit phase of the mission will be 89 w at 46 v; the mean power available at lunar noon will be 63 w at 32 v. Fig. 36 presents the solar panel performance on the lunar surface assuming a noon landing at the lunar equator. The mean power output will vary from 63 w at lunar noon to 87 w just prior to sunset.

Table 8 and Figure 36 assume a mean solar intensity of 140 mw/cm². Seasonal variations can cause this value to vary by approximately ±3.5%. Since solar panel power is approximately linear with intensity, the band of power values given in the table and figure must be corrected in the same proportion that the intensity changes.

f. Solar cell module test data study. A statistical determination of solar panel power at 25, 50, and 110° C has been derived using test data from electrical performance measurements of 200 solar cell modules, 10 each from Lots 1 through 20. Modules selected were from the 25-module Heliotek samples measured at Table Mountain and the data used is that taken by Heliotek. The module data was corrected to 25° C and 100 mw/cm² and then extrapolated to determine solar panel outputs at 25, 50,

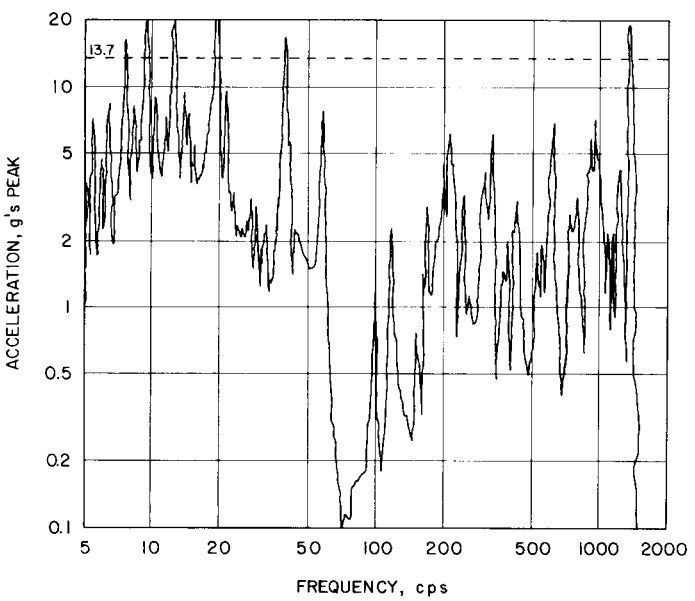

Accelerometer A

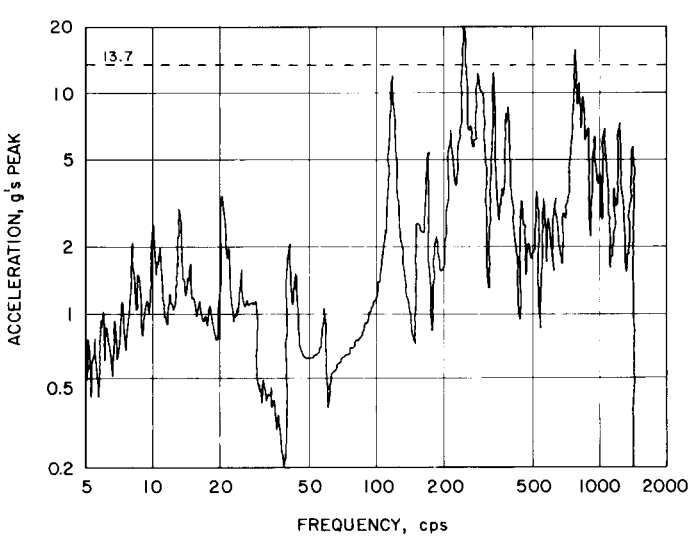

(b) Accelerometer B

Fig. 35. Solar panel response to FAT vibration inputs

Table 8. Summary of solar panel predicted performance (lunar equatorial landing at lunar noon)

Solar panel condition or mission event (air mass zero in all cases)	Temperature, ° C	Power, watts			Voltage at maximum power, volts
		Maximum	Mean	Minimum	
Prelaunch	25	103.2	101.9	100.6	51.8
Transit	47 to 53	93.3	88.5	83.6	45.4 to 46.8
Land at lunar noon	115	68.8	62.9	57.3	32.3
Begin first lunar day — sunrise	47	92.3	87.2	83.0	49.0

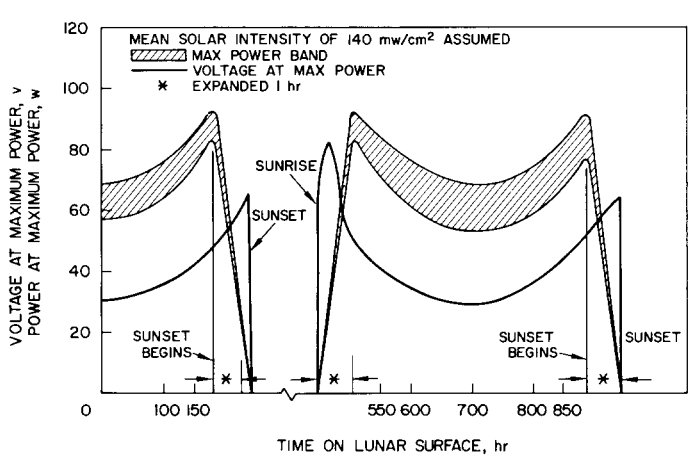

Fig. 36. Solar panel performance at noon on lunar equator

and 110° C; the extrapolated power values include correction for isolation diode resistance. The curves, shown in Fig. 37a, show 1σ limits from the means between the two curves.

Similar curves, based on Table Mountain test data for the T-21 and type approval solar panels before environmental testing, are shown in Fig. 37b for comparison. The mean power at 51.8 v and 25°C is nearly identical, indicating little loss in assembly; the statistical data indicate a mean power value of 86 ± 2 w under these conditions (Fig. 37a), while actual panel data indicate a mean power value of 85.8 w (Fig. 37b).

4. Batteries

a. Main battery. As reported previously, prototype Batteries S/N X-19 and X-21 failed the TAT vibration test and were disassembled for failure mode analysis. A typical positive plate fracture experienced in Cell 8 of Battery S/N X-19 is shown in Fig. 38. Cell damage occurred only in the outside row of seven cells. No damage was experienced in the inside row of seven cells adjacent to the mounting flange (see Fig. 39).

A parallel approach to the resolution of the vibration problem was undertaken — a more rugged cell design, and a more rigid canister design. On February 27, 1964, 12 four-cell monoblocks, each of a different mechanical configuration (see Table 9), were vibration tested at TAT vibration levels. The testing was conducted at the Associated Testing Laboratories, Inc. in Wayne, New Jersey. Subsequent to the vibration test, one cell from each monoblock was disassembled to explore the internal cell condition in detail. Results of vibration testing as observed after disassembly are shown in Table 10. Test monoblock Configurations 5, 7, 9, 10, and 14 were selected as the most promising and subjected to capacity tests to determine the second cycle charge acceptance. The second cycle charge acceptance was satisfactory and the data are presented in Table 11.

Table 9. Monoblocks mechanical configurations

Cell design number	Mechanical configuration
371	Present *Surveyor* battery cell design.
-1	371 design with 0.015 in. shim on internal cell case wall.
-2	371 design with concave shim 0.015 in. at center, 0.055 in. at sides on internal cell case wall.
-5	371 design with more flexible positive plate struts.
-7	371 design with 36 × 45 mesh screen for positive plate grid.
-8	371 design with full length strut on positive plate.
-9[a]	371 design with X-frame on negative plate.
-10[a]	371 design with full frame and X-frame on negative plate.
-11	Combination of -7, -8, and -1.
-13	Combination of -1 and -8.
-14[a]	Combination of -7 and -10.
-15	371 design with five 0.093 in. wide struts on face of positive plate.

[a]Cells constructed without one end negative plate as a result of assembly difficulty.

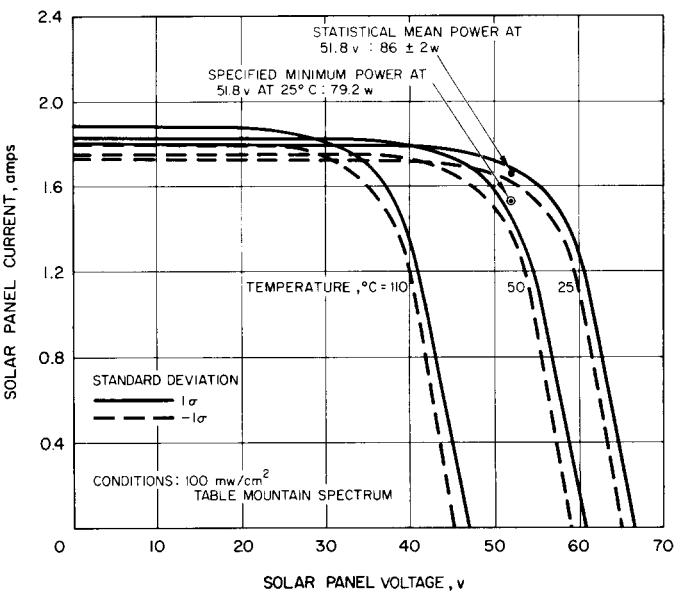

(a) Based on 200 solar cell modules

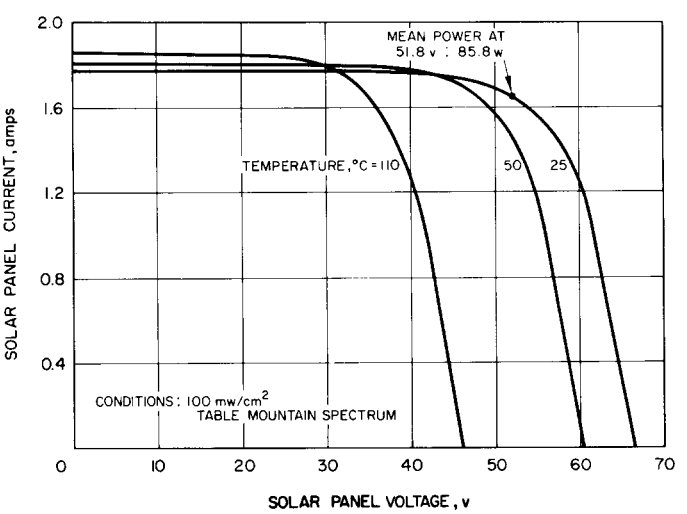

(b) Based on T-21 and type approval panel performance at Table Mountain

Fig. 37. Solar panel electrical characteristics

Table 10. Type approval vibration test results inside cell

Condition	Cell design number											
	-1	-2	-5	-7	-8	-9	-10	-11	-13	-14	-15	371
Positive plate leadwires broken	0	0	0	0	0	0	0	0	0	0	0	4
Positive plates fractured	4	3	0	0	6	4	3	2	5	0	0	6
Negative plates slipped	3	5	5	5	5	0	0	3	5	0	5	5
Negative material washout	yes	yes	yes	yes	yes	slight	slight	yes	yes	slight	yes	yes
End voltage under 85 amp load	1.286	1.255	1.259	1.329	1.247	1.260	1.265	1.300	1.269	1.339	1.281	1.156

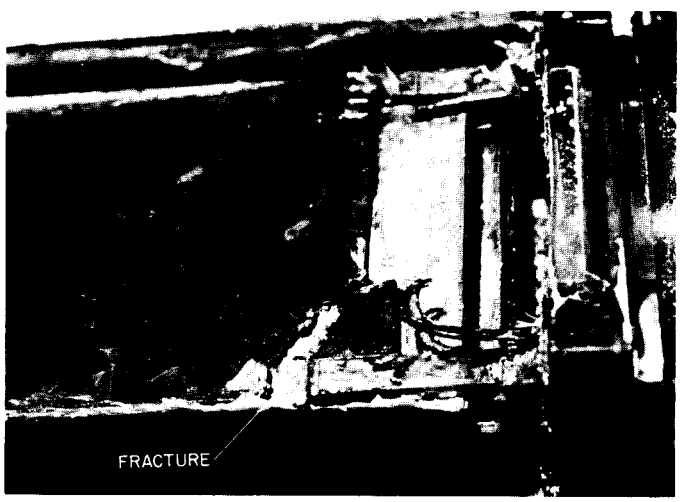

Fig. 38. Positive plate fracture

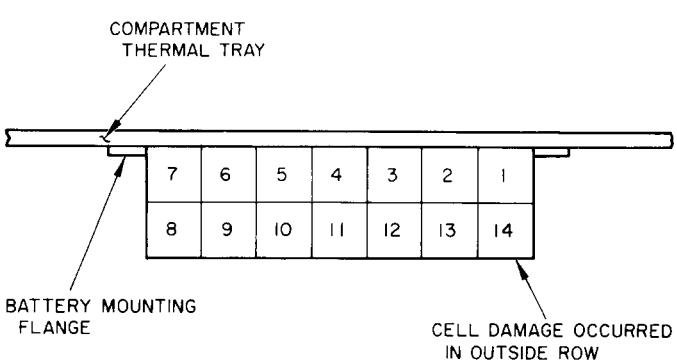

Fig. 39. Main battery cell arrangement in compartment

On the basis of these tests, Configuration 14 was selected for fabrication of eight prototype batteries. A minimum of two batteries will be subjected to TAT vibration levels to verify the results obtained with the test monoblocks. The scheduled date of TAT vibration test of the two batteries is May 15, 1964.

Table 11. Second cycle charge acceptance

Cell design number	Second cycle charge input, ampere-hour
-5	188.2
-7	186.5
-9[a]	175.3
-10[a]	173.5
-14[a]	163.2

[a]These cells were constructed without one of the end negative plates as a result of assembly difficulty.

The parallel program to reinforce the battery canister was implemented and two batteries with an improved canister design were received on March 22, 1964. These batteries are presently in vibration testing, and determination of the use of the strengthened canister will be made based on results of the test.

The new cell design results in a 5% battery capacity decrease and no weight change. Use of the reinforced canister could result in a weight increase of approximately 0.7 lb or a total battery weight of 47.1 lb.

Improved battery data handling techniques have been implemented. Previously much hand computation was required to establish watt-hour and ampere-hour capacities for battery charge-discharge tests. Battery parameters such as cell voltage, battery voltage, current, temperature, and manifold pressure were presented in tabular form and the summation and plotting were done manually. The computer program has been modified to plot all parameters and to sum watt-hours and ampere-hours. Data points during battery testing are recorded every 12 min and very good accuracy is therefore obtained.

The watt-hour and ampere-hour data are summations and include small variations in charge and discharge

current and voltage. The ampere-hour and watt-hour totals are computed as follows:

$$\text{A-H} = \sum_{j=o}^{n-1} \frac{i_j + i_j + 1}{2} \Delta t$$

where

n = the number of data points

t = time interval

and

$$\text{W-H} = \sum_{j=o}^{n-1} 1/4(i_j + i_{j+1})(V_j + V_{j+1})\ \Delta t$$

The tabular data are still obtained and are useful in determining cell balance at the end of discharge and during the float charge. The lunar load sequencer built for testing the main battery under simulated mission loads is undergoing tests. The unit is capable of testing six batteries simultaneously. Checkout testing to date has included simulation of transit, first lunar day, and first lunar night operations. The test is scheduled through completion of the second lunar day sequence. All functions are operating normally and a plot of the data obtained is presented in Fig. 40. The main battery used in this checkout testing has been maintained at laboratory ambient conditions.

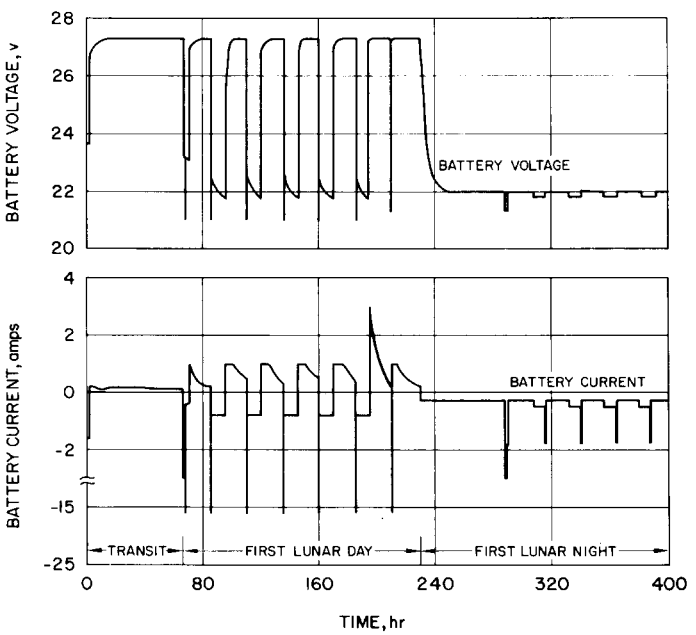

Fig. 40. Lunar load sequence test results

b. Auxiliary battery. As described in the previous report, the auxiliary battery electrical connector leakage condition has been resolved. Prototype battery testing indicated that the sealing compound proved effective and capable of withstanding battery environmental exposures. A detailed procedure on the formulation and application of the compound was forwarded to Eagle-Picher on February 18, 1964 for use in the fabrication of flight model batteries.

Prototype Batteries X-5, X-6, and X-7 were subjected to type approval tests. Tests included weight, center of gravity, insulation resistance, lead resistance, leak rate, vibration, shock, acceleration, thermal–vacuum, and battery capacity. Each battery successfully passed all phases of the test both mechanically and electrically. Battery X-7 was disassembled at the conclusion of the tests and detailed plate examination of two cells was performed to ensure that no mechanical degradation occurred. Fig. 41 shows Auxiliary Battery X-5 attached to its fixture on the vibration table in preparation for thrust axis vibration. During the thermal–vacuum test, each battery was discharged to a predetermined load profile to establish battery capacity. Fig. 42 is the discharge curve for Battery X-6 and is typical of the other two test batteries. Table 12 is a summary of the discharge capacities of each battery.

At the conclusion of the type approval tests, Batteries X-5 and X-6 were recharged to perform additional high current rate discharges. Battery X-5 was recharged to a capacity of 21.9 amp-hr and discharged at 70° F to the load profile shown in Fig. 43. Discharge was performed at three levels of battery capacity. The first discharge was at a battery capacity of 21.9 A-H with 3 min of a 50-amp

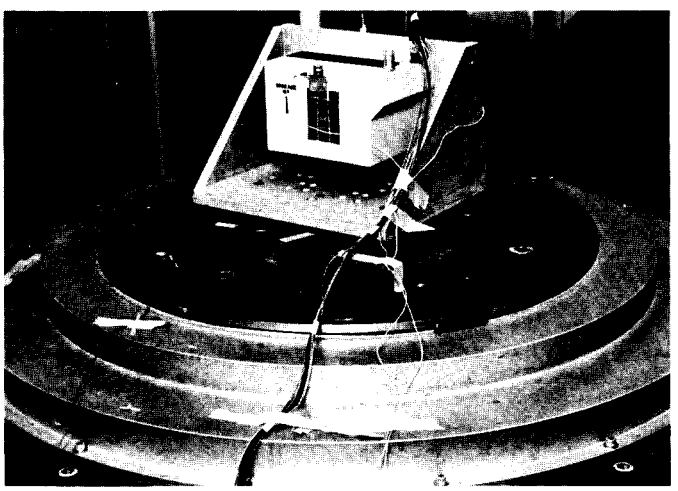

Fig. 41. Auxiliary battery in vibration test fixture

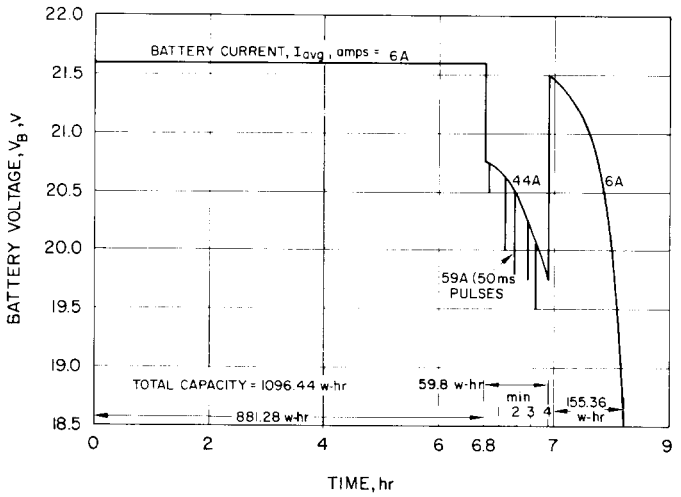

Fig. 42. Auxiliary battery discharge in vacuum

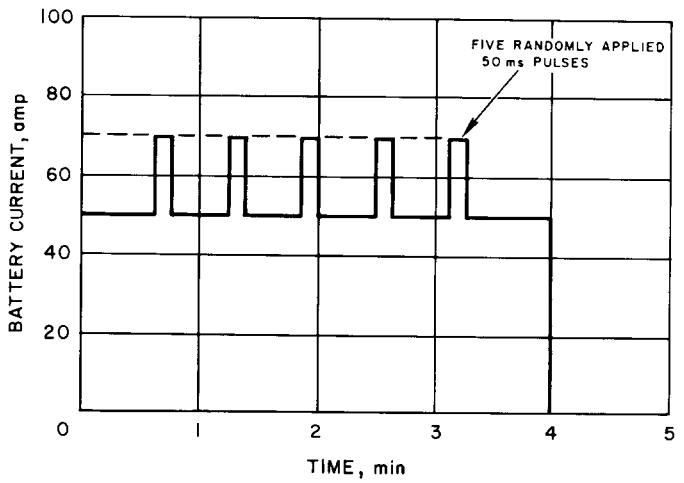

Fig. 43. High rate discharge profile for auxiliary battery

Table 12. Auxiliary battery discharge capacity

Battery S/N	Minimum capacity requirement, watt-hours	Actual capacity, watt-hours
X-5	1000	1050
X-6	1000	1096
X-7	1000	1049

load and with five 70-amp pulses. The second discharge was at a battery capacity of 18.9 A-H and the third was performed with a capacity of 14.7 A-H. The second and third discharges were identical – 4 min at 50 amp with five 70-amp pulses. Fig. 44 depicts the battery voltage versus discharge rate data obtained for the third discharge test. This curve is most representative of the characteristics of the auxiliary battery when discharged at high rates during the mission. Three of the five pulses were held for longer than a 50-msec duration to obtain a more accurate voltage reading. Battery X-6 was recharged to an 18.2 A-H capacity and also discharged in accordance with Fig. 43. Under all conditions of discharge for Batteries X-5 and X-6, the battery load voltage was above the minimum of 18.5 v.

Prototype Batteries X-8, X-9, and X-10 are to be flight acceptance tested and supplied for T-21 system testing. Battery X-9 has already passed the preliminary tests and is awaiting activation. Batteries X-8 and X-10 are to be

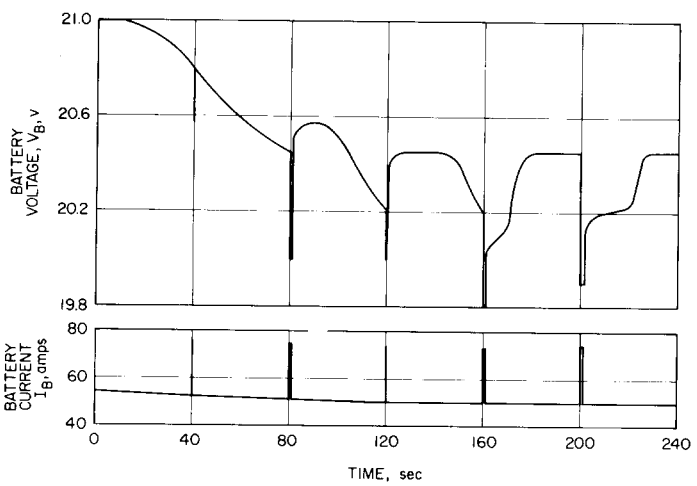

Fig. 44. Auxiliary battery high current discharge at 70°F

flight acceptance tested by mid-April 1964. The first flight model batteries are expected at Hughes on May 1, 1964.

5. Systems Integration Testing

Systems integration testing is proceeding as scheduled. A complete checkout of normal operating modes is scheduled for completion on April 30, 1964. Failure mode operational checkout is scheduled for completion on June 5, 1964.

G. Thermal Control

1. Introduction

The *Surveyor* thermal control system consists of the individual subsystems or unit thermal control systems integrated to provide acceptable thermal environments for all components during all phases of spacecraft operation. The passive and active methods employed include (1) special preparation of spacecraft external surfaces to achieve optimum thermal absorption and emission characteristics, (2) superinsulated compartments to house critical equipment, and (3) electrical heaters and thermal conduction paths controlled by bimetallically operated thermal switches to maintain compartment temperatures within acceptable limits.

System integration of spacecraft thermal control subsystems and thermal compatibility of proposed mission sequence operations are verified. Thermal switches and spacecraft coatings are developed; subsystem thermal–vacuum performance is evaluated by hardware tests with the MT-1 vehicle and other thermal models. Qualification of the spacecraft prototype thermal design is to be performed on the T-21 vehicle. Mission operation activities are supported by the development of Space Flight Operations Facility (SFOF) thermal management procedures.

2. Progress Summary

A formal design review of the entire spacecraft thermal control system was conducted on March 31, 1964. The review was at the prototype design point and was broad in scope. Several problem areas were identified and discussed such as vernier propulsion system thermal design modifications and radar altimeter and doppler velocity sensor (RADVS) thermal control capability.

Compartment thermal design changes as affected by S-2 structural testing are being evaluated for incorporation into the hardware design. A preliminary evaluation of the MT-1 Compartment A transit phase data gathered during the December 1963 thermal–vacuum test at JPL is complete. Test results correlated well with predictions.

Analytical investigations have been conducted on all portions of the vernier system in conjunction with studies of one of the proposed solutions to the Reaction Motor Division (RMD) thrust chamber assembly overheat problem. In addition, feasibility studies to establish preliminary thermal design requirements for other thrust chamber assemblies (TCA) are in progress. The reported results cover the capabilities of a thermal design with an optimized high-isolation propellant tank. The results are applicable to system requirements for the Rocketdyne and Space Technology Laboratories TCAs in addition to those of RMD. Studies have established the design feasibility of integrating the STL and Rocketdyne TCAs in the spacecraft thermal control system with no additional weight penalty.

Thermal control of the RADVS subsystem has focused on identifying problem areas uncovered recently when hardware design changes were found to be incompatible with the basic thermal design capabilities.

The shock absorber thermal design modifications are complete. The MT-1 landing gear assembly has been prepared for retest to evaluate the modifications.

A configuration of the T-21 vehicle has been defined for the transit phase portion of the system functional and thermal type approval tests (TAT) to be conducted in the Hughes 15-ft space simulation facility. A protection system for the T-21 attitude control system hardware has been defined to protect it from the severe thermal effects of simulated lunar day and night thermal testing.

Thermal management activities include a working computer program of the transit phase thermal model. The program will be upgraded to incorporate a number of input parameters that are being calculated. The status of spacecraft prelaunch temperature conditioning is being reviewed in light of the recent Lewis Research Center (LeRC) directive concerning the locations of the GD/A air conditioning unit control sensor.

Temperature drift problems in thermal switch actuation were encountered following type approval test postvibration performance testing. Of several solutions proposed, one was chosen for implementation into TAT hardware and rebuilt units will be retested. Delivery of T-21 units is delayed pending the results of the TAT retest.

3. Thermal Analysis and Design

a. Thermal control design review. A design review was held on March 31, 1964, at Hughes for personnel of Hughes and JPL to review the status of spacecraft thermal control. Analytical design of all spacecraft thermal control systems, verification of these designs in the MT-1 thermal development testing program, development of thermal coatings procurement of thermal sensors, preparation for the forthcoming T-21 systems functional and thermal type approval test program, and development and fabrication of thermal switches were reviewed. Problem areas and proposed solutions were identified; each of these topics is discussed in detail in subsequent sections of this report and in previous issues of the *Space Programs Summary*, Vol. I.

Briefly the problem areas were (1) difficulty in thermally controlling the RADVS components within the ±18°F temperature tolerances, and (2) drift in thermal switch closure temperature after repeated vibration.

Substantial progress in most thermal control systems was noted. Thermal design was confirmed and improved in the development testing phase. A transit configuration for the T-21 program which allows valid simultaneous systems functional and thermal testing in a solar/thermal-vacuum facility was presented.

b. Compartment system. The recent S-2 vibration tests revealed a need for redesign of the compartment system supports to satisfy structural requirements. The structural redesign of the Compartment A and B supports will affect the thermal performance of the compartments during lunar night. The low conductance fiberglass upper support tubes on Compartment A were increased in cross-sectional area with a corresponding lunar night heat loss increase of approximately 0.5 w. The redesign measures associated with Compartment B were more extensive. The number of upper support tubes has increased from three to six and the cross-sectional area of each tube is greater than in the previous design. The increase in lunar night heat losses from the redesign of the Compartment B supports is approximately 0.8 w. Therefore, the total increase in compartment system lunar night heat loss from the redesign of the supports is approximately 1.3 w.

The S-2 vibration tests also indicated the need for an increase in the clearance space between the bottom side of the radiators and the canister walls. This clearance will be increased to 0.40 in., and a teflon thermal radiation barrier will be inserted in the gap to reduce the probability of any thermal performance degradation during lunar operation. The relative motion of the compartment canister with respect to the thermal tray is being reduced by adding two small fiberglass standoffs between the outboard corners of the upper thermal tray and the outer canister wall on both Compartments A and B. The standoffs may cause an additional lunar night heat loss; the exact magnitude is not known, however, since the design of these standoffs has not been completed.

The thermal performance of Compartment A was evaluated during the MT-1 Sector I thermal–vacuum test in the JPL Space Simulator in December 1963. The test consisted of both cold shroud and fully illuminated phases, with each phase being run at various compartment power dissipations. Although a detailed analysis of the data is not yet completed, several conclusions appear warranted based on the evaluation conducted to date. At the completion of the detailed analysis, the MT-1 compartment thermal performance will be compared to that of actual flight hardware to verify the analytical techniques used to predict flight hardware performance.

From the data analyzed it appears that the thermal switch conductance was better than anticipated and exceeded the specification requirements of 0.5 Btu/hr °F per switch. This decreases the temperature difference between the thermal switch radiators and the thermal tray at a given power dissipation. The gradients within the thermal tray were as anticipated; therefore, the thermal tray design objectives were satisfied.

The thermal performance of the compartment in the 100% solar intensity, fully illuminated phase is shown in Fig. 45 along with the predicted performance for thermal properties of the Vycor radiator system ($\alpha = 0.14$ and $\epsilon = 0.75$). The thermal performance agrees well with the pre-test predictions at the lower dissipation levels; however, at the higher dissipation levels the thermal performance appears to be better than predicted. One reason for this behavior is that the thermal switch conductance was higher than assumed in the predictions at the higher power dissipation levels. Both the predictions and test results are based on the MT-1 hardware and the MT-1 vehicle test configuration. The results have not as yet been corrected to account for the differences

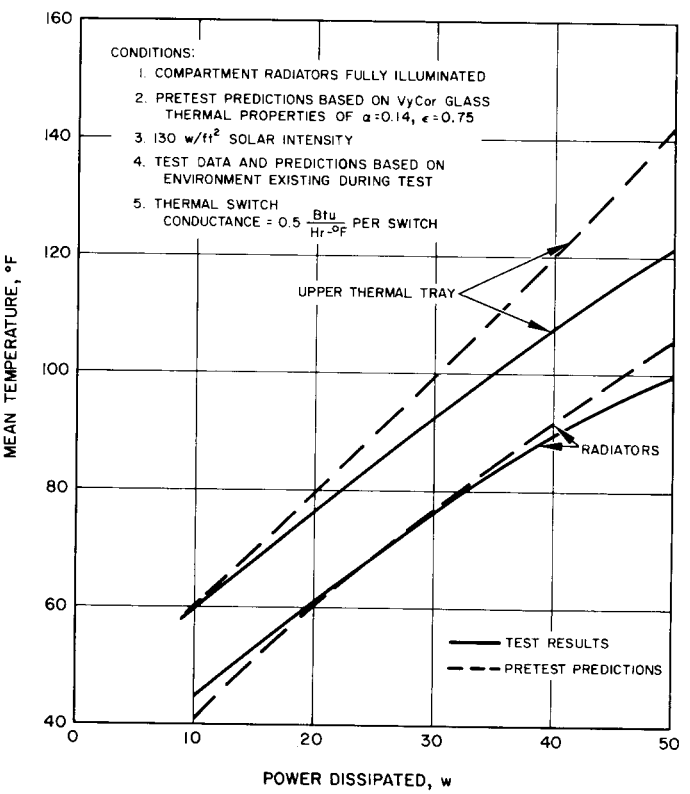

Fig. 45. Comparison of Compartment A test results and predictions

between the test configuration/thermal environment and the actual flight configuration/thermal environment.

c. Vernier propulsion system. A detailed analysis of the vernier feed system thermal control modifications caused by overheating of the RMD vernier engines during critical operating modes has been completed. Although the analysis was performed for an RMD system, the results can be applied to the thermal requirements for the STL and Rocketdyne thrust chamber assemblies under consideration.

In Tables 13 and 14 a description of the tank thermal design and the resulting temperature ranges of the propellant tanks are presented for the four systems considered in the study. The results show that all systems would impose a weight penalty compared to the original design because of the need for additional insulation or the use of a passive bias heat loss device.

Other valuable information that was learned from this study which could be applied to all future possible TCAs was that (1) no heater power is required for any tank, whether it is shaded or in the Sun; (2) predictability of the calculated temperatures existing at the completion of the terminal descent maneuver is within a 35°F range for insulated tanks and within a 65°F range for painted tanks.

These ranges allow for uncertainties in all the parameters that affect the nominal temperature such as the

Table 13. Vernier feed system thermal design description

Propellent tank	Original Reaction Motors Division (RMD)	RMD alternate	Rocketdyne alternate	Rocketdyne/RMD alternate[a]
	Temperature requirements during transit Fuel: 0 to 100° F Oxidizer: 0 to 100° F	Temperature requirements at terminal descent Fuel: 0 to 40° F Oxidizer: 0 to 60° F	Temperature requirements at terminal descent Fuel: 0 to 100° F Oxidizer: 20 to 80° F	Temperature requirements at terminal descent Fuel: 0 to 40° F Oxidizer: 20 to 80° F
Fuel Tank 1	Painted	Insulated bias heat loss[b]	Painted	Insulated bias heat loss[b]
Fuel Tank 2	Insulated	Insulated	Insulated	Insulated
Fuel Tank 3	Painted	Insulated bias heat loss[b]	Painted	Insulated bias heat loss[b]
Oxidizer Tank 1	Painted	Insulated	Insulated	Insulated
Oxidizer Tank 2	Insulated	Insulated	Insulated	Insulated
Oxidizer Tank 3	Insulated	Insulated	Insulated	Insulated

[a]Incorporates required temperature limits for the Rocketdyne and RMD alternate designs.
[b]Bias heat loss will be accomplished by use of a radiator.
Data here are based on aluminum tanks.

Table 14. Vernier feed system thermal control summary

Propellent tank	Original Reaction Motors Division	RMD alternate	Rocketdyne alternate	Rocketdyne/RMD alternate[a]
	Temperature requirements during transit Fuel: 0 to 100° F Oxidizer: 0 to 100° F	Temperature requirements at terminal descent Fuel: 0 to 40° F Oxidizer: 0 to 60° F	Temperature requirements at terminal descent Fuel: 0 to 100° F Oxidizer: 20 to 80° F	Temperature requirements at terminal descent Fuel: 0 to 40° F Oxidizer: 20 to 80° F
Fuel Tank 1	$40 \leq T \leq 100$	$3 \leq T \leq 37$	$40 \leq T \leq 100$	$3 \leq T \leq 37$
Fuel Tank 2	$33 \leq T \leq 62$	$13 \leq T \leq 42$	$33 \leq T \leq 62$	$13 \leq T \leq 42$
Fuel Tank 3	$40 \leq T \leq 100$	$3 \leq T \leq 37$	$40 \leq T \leq 100$	$3 \leq T \leq 37$
Oxidizer Tank 1	$35 \leq T \leq 100$	$22 \leq T \leq 58$	$22 \leq T \leq 58$	$22 \leq T \leq 58$
Oxidizer Tank 2	$26 \leq T \leq 54$	$26 \leq T \leq 54$	$26 \leq T \leq 54$	$26 \leq T \leq 54$
Oxidizer Tank 3	$37 \leq T \leq 73$	$7 \leq T \leq 43$	$37 \leq T \leq 73$	$37 \leq T \leq 73$

[a]Incorporates required temperature limits for the Rocketdyne and RMD alternate designs.
Notes and assumptions:
(1) 66-hr transit period.
(2) 170-lb propellant load at launch.
(3) Midcourse expenditure 0 lb $\leq W_{m\,c} \leq$ 60 lb and 34 lb is the 3σ nominal.
(4) Propellant temperature at launch = 85° F ±5° F.
(5) Aluminum tanks.

solar intensity, boundary temperatures, radiation properties of a painted surface, effective emittance of an insulated tank, propellant loading, and view factors to space. The ranges also include the effects of a ½-hr eclipse which is the maximum cooling condition that could occur during the terminal descent maneuver.

Additional studies concerning the thermal ramifications of an installation of any of several alternate thrust chamber assemblies (TCAs) into the spacecraft design have been conducted. A specific objective of the investigation was to determine if the passive thermal control techniques used with the RMD thrust chamber assembly during inactive modes could be employed successfully on the Rocketdyne or Marquardt TCA designs. Furthermore, the adequacy of the existing provisions to protect affected spacecraft surfaces from the effects of vernier exhaust convective and radiative heating was examined.

Results of the study are summarized in Tables 15 and 16 and include the STL study results for comparative purposes. Temperature control of the STL and Rocketdyne TCAs in the range of 0 to 100°F can be achieved during inactive periods utilizing passive techniques including the use of a solar collector to heat the shaded TCA at Leg 2. The Marquardt design did not possess sufficient projected area for complete solar heating; consequently, an additional weight or power penalty allocation was needed. The existing thermal control provisions would be marginally satisfactory with the Marquardt TCA, and satisfactory for the other TCAs considered, in preventing spacecraft overheating from vernier operation.

d. Radar altimeter and doppler velocity sensor (RADVS). RADVS thermal design performance has been established for a passive temperature control system and major design problem areas have been defined. The performance has been evaluated for the configuration existing prior to the recent electrical design modifications discussed in a subsequent paragraph.

The performance analysis, which is given in *Space Programs Summary No. 37-26*, Vol. I, indicates that the ±18°F electrical activation temperature range requirement will be difficult to attain on any of the units. However, nominal design point temperatures for the klystron power supply and modulator (KPSM), signal data converter (SDC), and antenna preamplifiers are attainable based on bulk average temperatures. The nominal antenna temperatures are also attainable, although the specified temperature distribution and temperature tolerance cannot be satisfied.

In general, the major problems occur because (1) there is a difference in temperature requirements for two similar units, the velocity sensor preamplifier and the altimeter/velocity preamplifier (the required nominal temperature is 30°F for the former and −30°F for the

Table 15. Thermal control of alternate engines

Item	Marquardt engine	Rocketdyne engine	STL engine
Type of engine	Radiation cooled. Thrust chamber and expansion nozzle are molybdenum, coated with molybdenum disilicide.	Ablation cooled thrust chamber and expansion nozzle.	Ablation cooled thrust chamber and radiation cooled titanium expansion nozzle.
Propellants	90% N_2O_4, 10% NO, and mono-methylhydrazine	N_2O_4 and mono-methylhydrazine	90% N_2O_4, 10% NO, and mono-methylhydrazine
Required temperatures (nonoperating conditions) for valves and injector	0° to 100°F	20° to 120°F	0° to 125°F
Nonoperational mode thermal control			
Thermal energy source	Solar energy directly on TCA augmented with either 1.5 lb solar collector per spacecraft or electrical heating	Solar energy directly on TCA augmented with approximately 0.7 lb solar collector per spacecraft	Solar energy directly on TCA augmented with approximately 0.7 lb solar collector per spacecraft
Passive design	• Thrust chamber assemblies insulated from spacecraft • Valves coated with vacuum aluminizing and black paint	• TCA insulated from spacecraft • Valves coated with vacuum aluminizing and black paint • Combustion chamber outer shell polished steel	• TCA insulated from spacecraft • Valves coated with vacuum aluminizing and black paint • Combustion chamber untreated titanium
Predicted temperatures (nonoperating) for valves and injector			
Transit coast phase	70° ± 30°F	80° ± 30°F	70° ± 30°F
Maneuvers (½-hr eclipse)	≧ 10°F	≧ 30°F	≧ 10°F

latter); (2) the thermal performance using passive techniques does not provide the required predictability and the required RADVS antenna temperature distribution; and (3) recent electrical design modifications initiated by the subcontractor will have additional adverse effects on thermal performance.

It is important to emphasize two of the major changes: (1) the use of a microwave absorber lowers the antenna bulk average temperature by approximately 90°F such that the minimum temperature limits may be exceeded, and (2) vibration isolation of the velocity sensor klystron divides the KPSM package into two thermally isolated sections. The latter change negates the validity of the single homogeneous thermal mass system assumption which is a prerequisite to successful use of the passive thermal control technique.

e. Landing gear assembly. The thermal design of the shock absorber was modified to assure that a nominal temperature range of 80 to 90°F will occur at the beginning of the terminal descent maneuver to allow for either cooling or heating conditions during the lunar descent phase. The expected temperature distribution including prediction uncertainties throughout transit is summarized in Table 17 (see also Fig. 46). The modified surface treatment employs aluminized teflon on approximately 40% of the area and leafing Kemacryl aluminum paint on the remainder. The expected circumferential and longitudinal temperature gradients of up to 10°F for 30 min during the coast and eclipse phases are acceptable. A test program to determine the ultraviolet stability of aluminized teflon bonded with epoxy adhesive has been conducted. The test confirmed the compatibility of the aluminized teflon with the thermal design requirement.

A solar/thermal–vacuum test of a prototype shock absorber installed in an MT-1 leg assembly will be conducted in the near future to verify the ability of this design to maintain the shock absorber within the required temperature limits as specified in Table 17.

4. System Development and Support

a. T-21 system test support. A system of shrouds has been devised for use on the T-21 spacecraft during thermal–vacuum–solar testing. The shrouds are used to produce discrete shadows on parts of the spacecraft normally shadowed in transit by the upper portions of the spacecraft, particularly the solar panel. The solar panel cannot be employed in solar simulation tests because interception of the divergent rays from the simulator does not produce sharp shadow boundaries as in sunlight; the semishadowed area at the base of the spacecraft could be as wide as 25 in.

The arrangement of the shrouds, which are cooled by liquid nitrogen, is shown in Fig. 47. The shroud con-

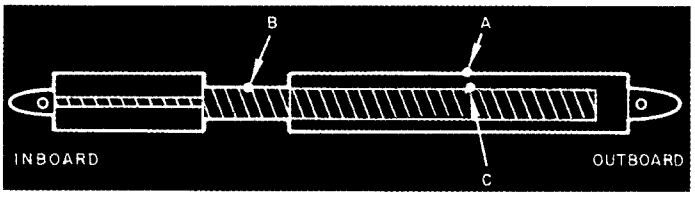

Fig. 46. Shock absorber thermocouple locations

Table 16. Vernier engine heating effects and spacecraft thermal protection systems

Vernier thrust chamber assemblies	Thermal environment created during vernier engine operation			Spacecraft thermal protective provisions		
	Convective flux (Btu/sec ft²) at		TCA maximum temperature, °F	Convective heating[a]		Radiative heating at affected local surfaces
	Altitude marking radar dish, tip	Crushable blocks		At altitude marking radar dish, tip	At crushable blocks	
Reaction Motors Division	7.0	4.0	2600	¼-in. thick refrasil insulation enclosed in 1.5 mil stainless steel foil[b]	Half-cylinder ablative fiberglass shield[c]	Low emittance surface treatments[d]
Space Technology Laboratories Mira 180	3.0	< 3.0	1900	Present protective designs compatible with alternate TCA installations		
Rocketdyne	< 5.0	< 5.0	700			
Marquardt	< 5.0	< 5.0	2800			

[a]Convective heating protection design as recommended by Hughes Aircraft Company.
[b]Heat transfer through insulation results in negligible temperature rise of AMR dish after 200 sec firing.
[c]Controls maximum temperature of aluminum honeycomb crushable block to < 100° F after 200 sec descent firing.
[d]Low emittance treatment controls spaceframe temperature to < 200° F after 200 sec firing.

figuration consists of six sections. Section 1 follows, in general, the projection of the solar panel and is in a horizontal plane just above the compartment radiators. Extensions of the shroud boundaries beyond those of the solar panel prevent decollimated rays from striking the spacecraft in some plane below that of the cold shrouds. Shroud 2 is designed to shadow TV Camera 3. Shrouds 3 and 4 are designed to cast a discrete shadow line on the vernier engine. The recess in Shroud 1 over the engine is located so that the shroud will not intercept the decollimated light directed at the vernier engine solar collector. Shroud 4 prevents light from entering the gap between Shrouds 1 and 3. Shroud 5 shadows the mast support tube. Shroud 6 is not part of the transit configuration and would not be used ordinarily. It provides the option to completely shadow Compartment A to reduce the temperature of the interior enough to test thermal switch opening and regulation of the thermal control and heater assembly.

The functional and thermal design of the jet attitude control system is based on transit flight conditions. During the T-21 type approval tests, special lunar day and night protective systems are required for components which cannot be removed and could be damaged if left unprotected. Table 18 describes the jet attitude control protective system, resulting component temperatures, and temperature limits for an unpressurized jet attitude system. It is assumed that the Hughes 15-ft vacuum chamber would be used with a lunar surface simulator.

During the transit tests of the T-21 vehicle, the legs of the spacecraft will extend beyond the edges of the

Table 17. Shock absorber transit temperature

Shock absorber locations[a]	Operational temperature limits, °F	Performance predictions, °F			
		Prelaunch and acquisition	Coast	Touchdown	
				Lunar night	Lunar day
No. 1 and 3					
Case (A)	— 20 to 125	15 to 90	65 to 95	5 to 35	90 to 120
Fluid (B)	20 to 125	40 to 90	75 to 105	30 to 55	80 to 115
Fluid (C)	20 to 125	50 to 90	65 to 95	25 to 55	70 to 105
No. 2					
Case (A)	— 20 to 125	15 to 90	65 to 95	5 to 35	90 to 120
Fluid (B)	20 to 125	40 to 90	70 to 100	25 to 50	75 to 110
Fluid (C)	20 to 125	50 to 90	65 to 95	25 to 55	70 to 105

[a]Letters in parentheses refer to locations indicated in Fig. 46.

Table 18. Jet attitude control protective system

Unit	Thermal environment	Special protective system	Design temperature, °F	Maximum allowance temperature, °F[a]
Nitrogen tank	Lunar day	Top of tank and valve assembly covered with one sheet of 2-mil aluminized teflon ($\alpha = 0.17$, $\epsilon = 0.58$)	190	250
Three attitude jets	Lunar day	None (Solar intensity decays to 15% of one solar constant at 6 ft. radius)	190	250
Hard mounted nitrogen tank	Lunar night	Install 10-w capacity heater on outside of tank. Cover tank and valve completely with a single sheet of aluminum foil.	—200	—250
Three attitude jets	Lunar night	Install molded 3-w heater on outside of each jet and cover each one completely with a single sheet of aluminum foil.	0	—30

[a]Nonoperational and unpressurized system.

solar beam; the nitrogen jets will require heating to maintain normal transit temperatures during the system flow checks. The protective system designed for the jets for lunar night tests will provide the necessary heating and temperature control for the transit test.

b. Thermal management program. The preliminary version of the transit analog model mentioned in *Space Programs Summary No. 37-26*, Vol. I, has been completed and is being used to check the thermal management computer program. The portions of the transit model input parameters which remain to be completed are electrical power dissipations, reflected solar energy, and radiation between components. In the present form, the transit model requires approximately 5 min on the 7090 computer to analyze the transit portion of the mission (assuming a normal transit attitude for approximately 65 hr). The parameters defining the electrical power dissipations, reflected solar energy, and radiation between components are being calculated. These parameters will be incorporated into the program during April. Following this, the program and model representation will be checked using the data available from the MT-1 sector tests.

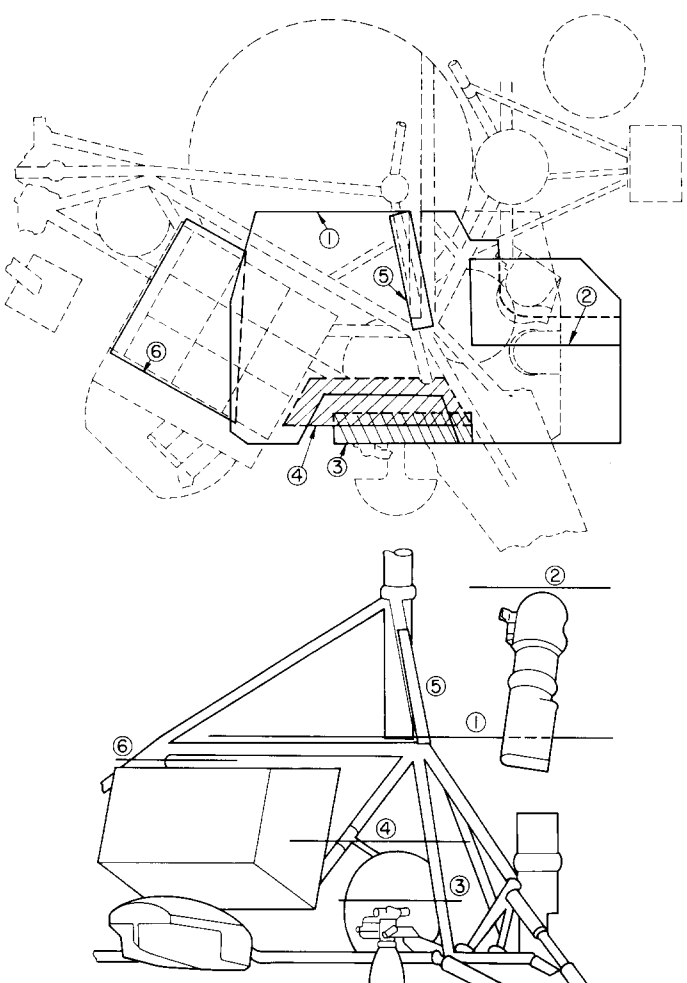

SHROUD	LOCATION
1	OVER TOP SPACEFRAME AND COMPARTMENT RADIATORS
2	OVER TV 3
3	OVER VERNIER ENGINE 2
4	OVER FUEL TANK 2
5	OVER MAST SUPPORT TUBE
6	OVER COMPARTMENT RADIATORS FOR COMPLETE SHADOWING

Fig. 47. Shadow simulation for T-21 transit tests

The basic concept of developing three separate analog models for each mission phase, transit, lunar day, and lunar night, has been revised. The new concept is to provide two models – a transit phase model and a lunar model. These models will have the same basic nodal breakdown. The main retro-engine and altitude marking radar nodes will be omitted from the lunar model. This change will also affect the radiation parameters among the components for the lunar model. The new concept was chosen to simplify the number of parametric calculations required for the different models and also to establish one basic nodal breakdown for both models. The use of the new concept was made possible by revising the thermal management computer program logic. The logic revision allows any number of nodes within the model to be set as boundary conditions with either fixed or forced temperature profiles. The temperatures of the remaining model nodes are then calculated and are influenced only by adjacent boundary nodes. This method shortens the computer run time, decreases the required number of analog models, and permits the operator to analyze either a subsystem, a group of subsystems, or the entire spacecraft.

Other tasks accomplished include definition of the required input and output formats to be used with the thermal management computer program at the Space Flight Operations Facility and more detailed investigation of requirements for the spacecraft performance/analysis/command (SPAC) scale model system. This system is used to generate on a real-time basis parameters needed by the thermal management computer program.

c. Air conditioning test evaluation. The *Surveyor/Centaur* air conditioning test data presented in *Space Programs Summary No. 37-25*, Vol. I, was a result of a preliminary review of the test data. Since then the data have been analyzed and evaluated in detail, and minor corrections have been incorporated and retabulated (Table 19). The conclusions stated previously for the air conditioning system performance remain unchanged.

The location for the control sensor, according to a Lewis Research Center directive, will be in the lower distribution duct on the payload adapter. Based on available test data, this choice of control sensor location reduces

the temperature controllability of temperature critical spacecraft units to a degree that may be incompatible with the established spacecraft prelaunch temperature requirements.

5. Thermal Switch

An upward drift in closure temperature was experienced as a result of the type approval test (TAT) vibration program. The closure temperature increased from 65 to 71°F and from 50 to 60°F for the Compartment A and Compartment B units, respectively. Several potential sources of the problem have been examined including yielding of the bimetal element, stress relief from insufficient heat treatment, and bimetal wear. Insufficient heat treatment, which could result in areas of stress concentrations, appears to be the most likely source of the problem. The TAT units have been rebuilt with stress relieved bimetals and are presently being flight acceptance tested in preparation for repeating the TAT vibration program. Delivery of the T-21 units is being delayed pending the results of the TAT retest.

6. MT-1 Thermal Development Test Program

Plans are being formulated for repeating the thermal tests of the landing gear with the lightweight configuration in the new Hughes Aircraft Company 15-ft simulation facility. The exact scheduling of this test is yet to be determined and is dependent on the completion of the solar simulator evaluation program which is in progress. The Hughes Aircraft Company/Jet Propulsion Laboratory solar simulator comparison test using MT-1 Sector 1 will be performed following the landing gear test. The Sector 1 data report for the testing done at JPL in December 1963 has been completed during this report period.

Table 19. *Surveyor/Centaur* air conditioning test results

Spacecraft thermally critical components	Specified temperature range, °F	Stabilized temperatures, °F[a], Atlantic Missile Range environments				Unit power dissipation, watts
		Test 1 85°F, day	Test 2 105 to 140°F, hot day	Test 3 40°F, cold night	Test 4 day/night cycle	
Compartment A radiator	0 to 95	85	91	84	83 to 85[d] 85 to 86[e]	13[h]
Compartment B radiator	0 to 95	—[g]	93	86	84 to 86[d] 82 to 89[e]	25
Inertial reference unit gyros	180 ± 2	180[c]	180[c]	180[c]	180[c]	10 to 39
Gyro cases	—	147	149	147	84 to 87[d] 141 to 155[e]	—
Radiator[b]	130 to 155	122	123	122	84 to 85[d] 121 to 123[e]	—
Flight control electronics radiator[b]	0 to 95	101	105	100	84 to 85[d] 108 to 110[e]	20[i]
Propellant tanks[f]	80 to 100	81 to 85	85 to 90	82 to 83	82 to 85	—
Retro-rocket engine	80 minimum	83	87	83	84 to 87	—
Environmental air temperature—						
plenum	—	89	86	86	82 to 90	
Upper distribution ring	—	85	86	84	82 to 88	
Lower distribution ring	—	82	87	80	82 to 84	
Environmental air temperature out[f]	—	85	88	81	81 to 85	

[a]Instrument accuracy ±2° F for all thermocouples, except those on retro-rocket motor which were ±1° F. Temperatures presented are the time average of thermocouples per unit.
[b]Post-test data evaluation indicated that these slight deviations from the specified temperature range were acceptable.
[c]Verified by a power cycling of temperature controller.
[d]Equilibrium temperature range with no power applied during day/night cycle.
[e]Equilibrium temperature range with power applied.
[f]Temperatures indicated are a time average of four thermocouples.
[g]Erroneous data point due to faulty temperature recorder.
[h]Power dissipation for this unit has increased to 22 w.
[i]Power dissipation for this unit will change as a result of redesign study.

H. Engineering Mechanics

1. Introduction

The activities reported in this section include touchdown dynamics, static and dynamic structural analyses, and structural tests. Touchdown dynamics includes the specification, analysis, and testing of the soft-landing system. A significant portion of this work pertains to procurement of the landing gear shock absorbers. A similar activity is the specification of design and test parameters for spacecraft retro-engine separation. The section also covers stress and dynamic analyses on major spacecraft structures, the specification of loads and other design criteria, and the determination of structural test requirements. The results of the static and dynamic testing of structural models, including full-scale simulated spacecraft, are reported. This task includes procurement of flight engineering instrumentation such as accelerometers, amplifiers, deflection potentiometers, and strain gages.

2. Progress Summary

The mathematical model for the rigid-body touchdown dynamics program is being modified with the aid of S-2 drop test data. This will permit more accurate computation of force inputs for the elastic vehicle response computer program.

A developmental shock absorber failed during drop testing at a maximum landing load condition of 8000 lb. The failure started in the aluminum housing which has since been redesigned and thickened. The changes resulted in a weight increase of 0.04 lb per shock absorber. The failed unit was not a type approval test article; it had been subjected to several hundred test cycles and was probably worn and fatigued. After the required design modifications were made, two type approval test (TAT) units were drop-tested successfully at loads in excess of the required 8000 lb. The strength of the National Water Lift (NWL) shock absorber is adequate and exceeds design requirements.

Dynamic model SD-4 completed type approval vibration testing successfully in two lateral directions on February 18 and was shipped to NASA's Lewis Research Center.

The drop test portion of the S-2 vehicle TAT has been completed. Three drop configurations were used to establish dynamic loads on the spacecraft under various surface conditions. The maximum recorded inertia loads were as follows: 1) Compartment A, 15 g; 2) Compartment B, 21 g; 3) planar array, 23 g; and 4) solar panel, 38 g.

After several structural modifications are made to S-2, a new series of type approval vibration and drop tests will begin in May.

Data from the S-2 drop tests have been compared with computations of component inertia loads and stresses by using a forced response elastic vehicle computer program developed for *Surveyor*. Good correlation between the measured and computed data indicated that the computed vehicle response during other lunar landing conditions is probably quite close to the actual responses.

As a result of the high bending stresses measured in the mast, its wall thickness will be increased. This is in addition to the redesign efforts on the mast and antenna/solar panel positioner discussed in *Space Programs Summary No. 37-26*, Vol. I.

Twenty-four Endevco accelerometers, amplifiers, and associated coaxial cables (Set 1 and Set 2 for T-21) have been received. One amplifier failed in a shock test during flight acceptance test (FAT) and is being corrected at the vendor. Only painting and identification of the amplifier assembly remains to be completed before installation on T-21.

Qualification of the Semi-Conductor Magnetics strain gage amplifier continued during the report period. Leakage and radio frequency interference (RFI) problems are under study. T-21 units have been manufactured and will undergo FAT as soon as the TAT cycle has been completed.

Eight aluminum-to-fiberglass bonded specimens representative of thermal-insulating substructure joints have been tested at room temperature to evaluate fatigue strength. One control specimen was loaded in compression and failed at 40,100 psi, which is well above the required 25,000 psi. The remaining seven specimens were fatigue tested. All but one test article failed in the bond. Data from these recent tests correlate well with the results from 15 previous fatigue tests using two similar types of specimens. The metal-to-fiberglass joints used to isolate Compartments A and B, the TV cameras, and the nitrogen and helium tanks exhibit adequate fatigue resistance.

3. Touchdown Dynamics

The mathematical model for the rigid-body touchdown dynamics program is being re-examined in conjunction with the S-2 drop test results reported later in this section. The stability characteristics of the vehicle as predicted analytically have been demonstrated successfully by the T-1 vehicle drop tests. However, during drop tests with maximum landing gear load employing the A-25

version of T-1, the A-21 version of T-1, and now S-2, the shock absorber force has not reached the levels analytically predicted. Since the shock absorber maximum force is primarily caused by damping, which is a function of the square of the velocity at touchdown, the single downhill leg is not impacting at the predicted velocity. This reduction implies that vehicle pitch rates are not as high as predicted. Modification of the mathematical model for the rigid-body vehicle touchdown dynamics program to provide a better comparison with the S-2 landing gear loads will result in better force inputs for the elastic vehicle response program.

4. Shock Absorber Development

Type approval testing of the shock absorber began early in February. A 3-wk delay was incurred from failure of the engineering development unit under design loading conditions. The TAT units were modified, and two units have since been tested successfully at load levels in excess of those experienced under maximum landing conditions.

The type approval test specification requires that each unit be subjected to drop tests in which the loads will be 4000 lb for the nominal condition and 8000 lb for the maximum landing-load condition. The drop test involves the dropping of a weight onto the footpad of an inverted leg assembly. The falling weight is approximately 185 lb; the height of the drop governs the load levels to which the shock absorber is subjected. Suitable snubbing procedures are used to duplicate load versus stroke profiles during simulated drops of the *Surveyor* vehicle as predicted by the computer analysis.

Drop conditions were established experimentally by using the engineering development shock absorber. At the 8000-lb load level, the shock absorber failed as shown by Fig. 48. The sequence of events indicated by high-speed motion pictures showed that failure started in the aluminum housing. This caused failure of the piston rod and disintegration of the pressurized (1700 psi) helium gas cylinder. The load versus stroke data obtained from these drops are shown in Fig. 49. The failure occurred under an axial compression load of approximately 8000 lb at a 1.5-in. stroke with a lateral inertia load of between 60 and 80 g.

An investigation to establish the cause of failure was initiated since this unit was designed to withstand a compression buckling load of 8600 lb. When an end load of 8000 lb is applied to the unit, it should have a 25% margin of safety on ultimate stress. This engineering development unit had been subjected to approximately 700 test cycles prior to failure; about 30 of these cycles were at loads between 4000 and 8000 lb with a large number of cycles at loads near 4000 lb. This large number of test cycles may have been a contributing factor in the failure since fatigue, permanent set, or distortion may have occurred in the aluminum housing. However,

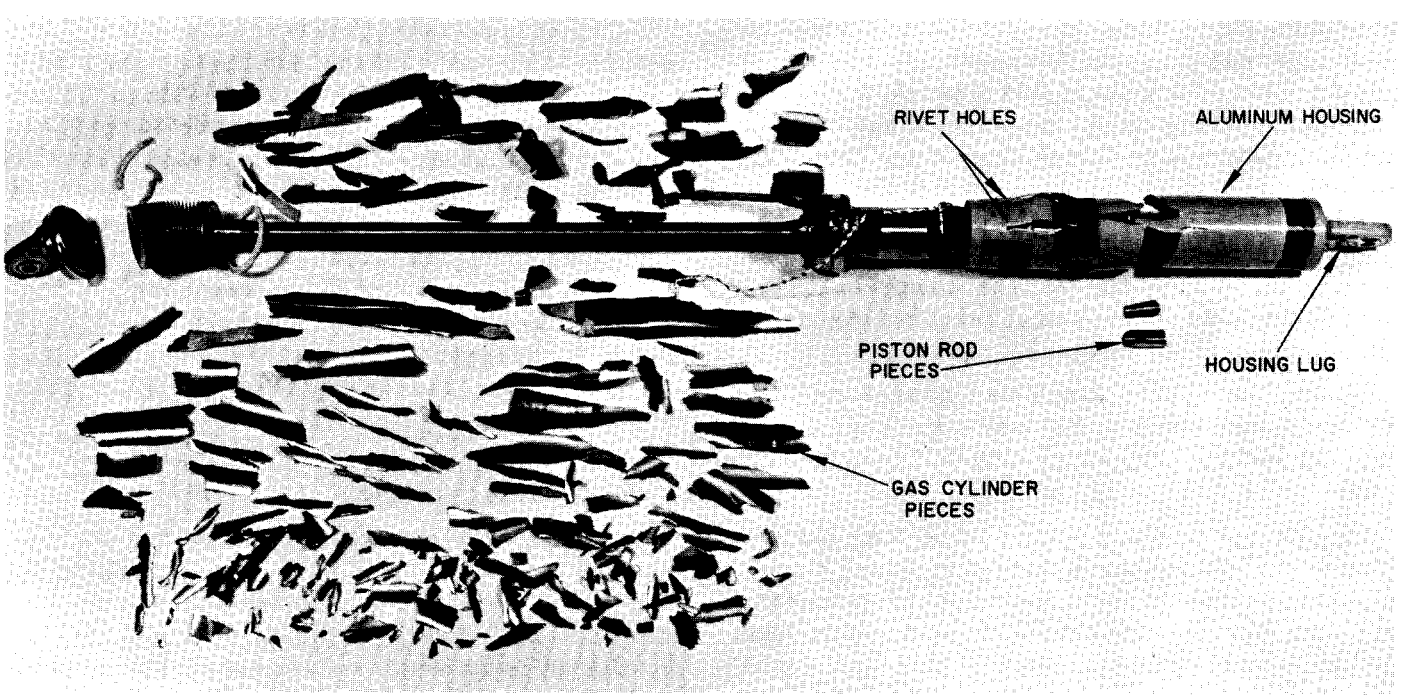

Fig. 48. Development shock absorber after drop test

the housing design allowed the possibility of prohibitive stress concentrations at rivet holes used for attachment of the squib lock housing. (Splits emanating from two of the four holes can be seen in Fig. 48.) The lateral g loading to which the shock absorber had been subjected was in excess of the 50 g design value because of inadequate representation of the footpad on the drop test rig. This additional g load reduced the safety margin of the unit. Type approval testing was halted until modifications could be made to the shock absorber and to the drop test rig.

Shock absorber modification included an increase in the aluminum housing thickness to improve the buckling load capability and to reduce the effect of stress concentrations. This change, together with some modifications to the lightening holes in the housing lug end, resulted in a net weight increase of 0.04 lb per shock absorber. The alteration in external dimensions required no corresponding alterations in the cam detent lock fingers or squib lock assembly. On the drop test rig, the beaded styrofoam representing the footpad was increased in thickness from 2 to 5 in. The revised load-stroke profile is a better representation of the profile for the actual footpad and reduced the lateral g loading to which the shock absorber is subjected in a drop test.

Two revised units were successfully tested in maximum landing-load drops. A load versus stroke profile for one of the units is shown in Fig. 49. The load level is considerably in excess of the desired 8000-lb value; the strength of the shock absorber is, therefore, adequate and exceeds design requirements.

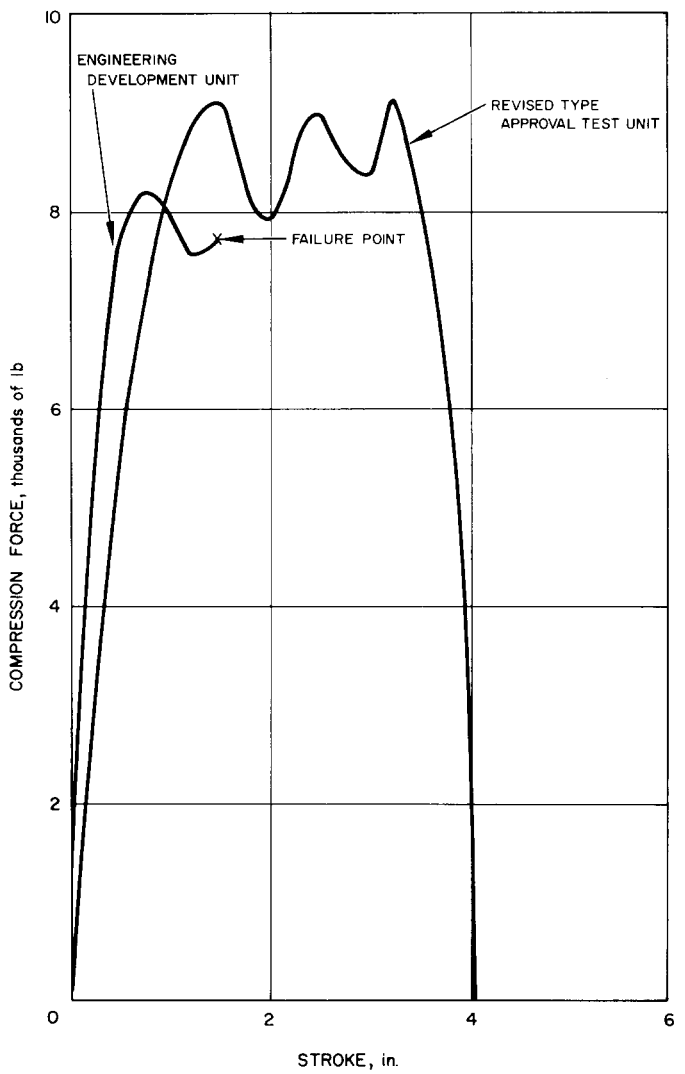

Fig. 49. Shock absorber load versus stroke at maximum landing-load conditions

5. Dynamic Tests

The SD-4 dynamic test vehicle with an improved antenna/solar panel positioner was subjected to type approval vibration in two lateral directions on February 18. No structural failures resulted from these tests. The longitudinal test had been completed, as reported in *Space Programs Summary No. 37-26*, Vol. I. A summary of the significant accelerations and stresses for frequencies below 100 cps during the lateral vibration test appears in Table 20. Locations of the various accelerometer and strain gage sensors are shown in Fig. 50.

A series of type approval drop tests was conducted on the S-2 vehicle during the period of February 20, 1964 to February 26, 1964. Three drop configurations were used to establish dynamic loads on the spacecraft occurring during touchdown under various surface conditions. Because of interference with the solar panel and the planar array, the restraining device used to simulate lunar gravity in the T-1 drop tests could not be used. Therefore, the S-2 drop tests employed free fall of the vehicle under Earth gravity. The drop test under Earth gravity cannot provide an exact simulation of a lunar landing, since the action of the landing gear and the crushable blocks is governed by both velocity and displacement; i.e., the energy to be dissipated is both kinetic energy and potential energy. Instead of attempting simulation of specific lunar landing conditions, the standard selected for the drop tests was a vertical velocity of 20 fps at first touchdown. The conditions for the three drop tests are shown in Table 21. The drop tests may be best compared with a lunar landing on the basis of total energy dissipated in the landing gear and the crushable blocks. The touchdown velocity for a lunar landing which provides the same energy dissipation as the drop tests is also shown in the table.

Some significant inertia loads encountered by various components of the spacecraft are given in Table 22.

In Drop 1 an upper support member on Compartment B fractured through the fiberglass section. This failure was not considered significant, since these supports were already in the process of redesign from a failure which occurred during vibration tests. The support member was repaired for the next drop.

In Drop 3 the solar panel support structure failed at a welded joint. High-speed motion pictures of the drop showed that the failure was caused by a support cable that snagged one corner of the solar panel during the

Table 20. Summary of maximum loads at frequencies under 100 cps for SD-4 vibration tests

Type of transducer	Location	Axis of sensitivity	X-axis shake		Y-axis shake	
			Load	Frequency, cps	Load	Frequency, cps
Accelerometer (load units, ±g)	Mast	X	[a]		[a]	
	Mast	Y	4.6	13.3	16 15	10.5 13
	Omnidirectional antenna boom	X	35 17 37	11.8 53 77	7.6 24 38	10.5 56 77
	Omnidirectional antenna boom	Y	6.4 5.6 7.4	11 11.5 74	30 13.5 15 19	10.5 12.3 66 73
	Ballast	XYZ (skewed)	5.2 5.4 11	25 36.5 38	5	50
	Ballast	Z	4.6 4.8 22 3.9	22.3 25.3 49 65.5	8 9 9.8	24.5 49 51.5
Strain gage (load units, ±1000 psi)	Mast	X	16	12.2	2.2 1.3	10.9 13.3
	Mast	Y	2.9	13.5	11.9 8 3.3	10.8 13.3 25
	Upper assembly	XZ (on antenna support tube)	14 13	13.5 24.5	5.4 1.8	14.7 25

[a]No data

drop. (The support cable was one of three attached to the upper spaceframe to permit lifting S-2 off the ground immediately after the drop, since the shock absorbers cannot support the vehicle under Earth gravity.) This incident induced a large bending moment on the structure which caused stresses at the weld joint to exceed the ultimate strength.

Another series of drop tests will be conducted on an improved S-2 vehicle during May 1964. S-2 will be updated for the tests with several design changes. Compartments A and B will be changed from the present ballast units to developmental units. The antenna/solar panel positioner and mast will be relocated to the new location near the Y-axis of the spacecraft. The omnidirectional antenna booms will be replaced with more representative developmental hardware. A battery pack will be installed in Compartment B. The helium tank will be relocated at its present position on A-21. A vernier engine roll actuator will be installed on one of the simulated engines. The auxiliary battery and its support structure will be installed on the spacecraft. A representative radar altimeter and doppler velocity sensor and wave guides will also be installed.

Table 21. S-2 drop test conditions

Condition	Drops		
	1	2	3
Vertical velocity at touchdown, fps	20	20	20
Vehicle incidence, deg	0	0	5
Site slope, deg	0	15	15
Single leg direction	Not applicable	Uphill	Downhill
Surface	Smooth	Rough	Rough
Touchdown velocity for equivalent lunar landing, fps	21.3	23.2	22.7

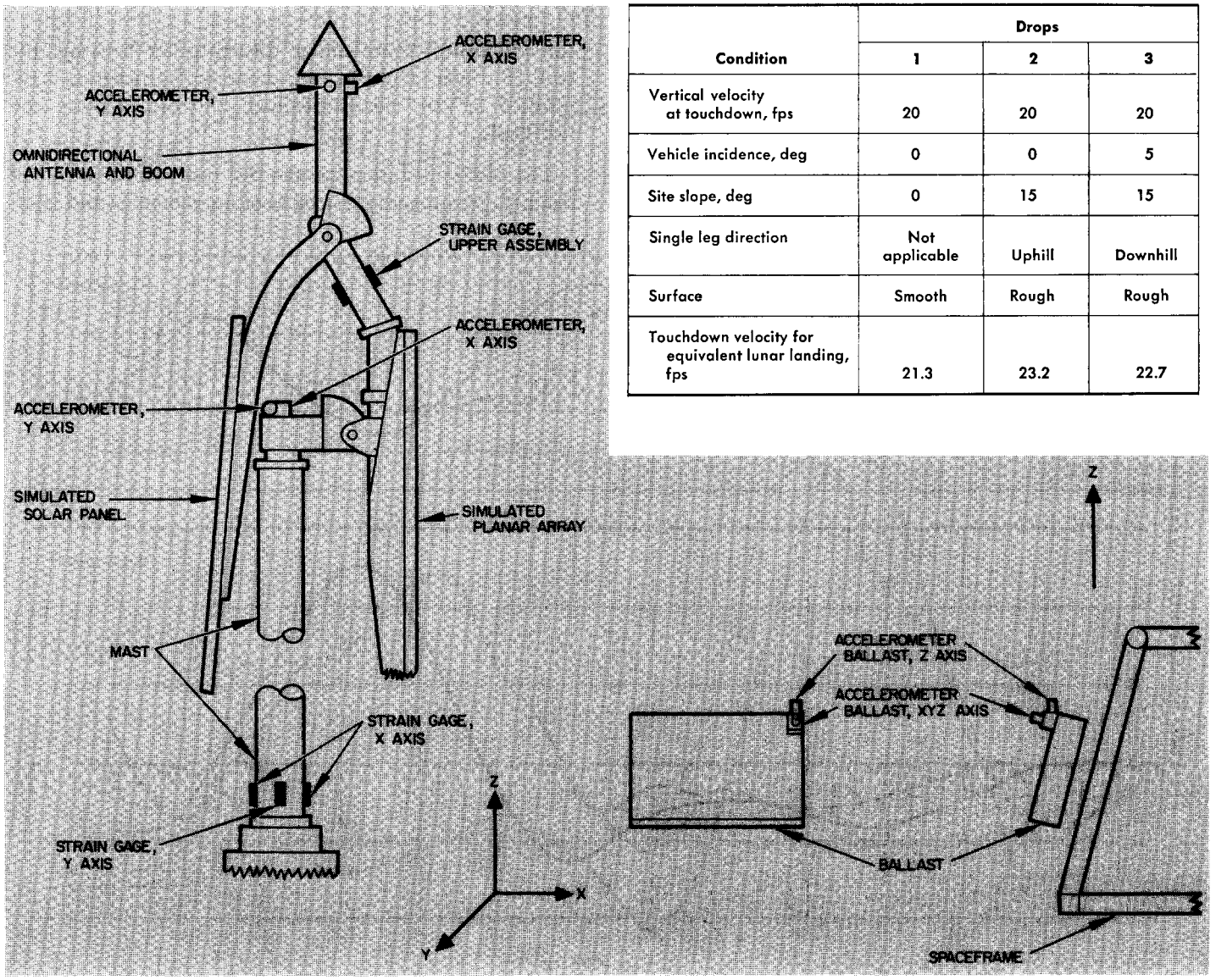

(a) Antenna/solar panel positioner (b) Ballast block

Fig. 50. Dynamic model instrumentation locations

Table 22. Component inertia loads at fundamental natural frequencies from S-2 drop tests

Component	Inertia load, g								
	Drop 1			Drop 2			Drop 3		
	Vertical[a]	Normal[a]	Lateral[a]	Vertical[a]	Normal[a]	Lateral[a]	Vertical[a]	Normal[a]	Lateral[a]
Compartment A	12	11	3	15	9	3.5	[b]	[b]	[b]
Compartment B	21	7	2	15	0	12	[b]	[b]	[b]
Planar array antenna	15	20	5	21	17	6	23	16.5	15
Solar panel	13	16	2	20	14	6	30	38	[b]

[a]Axis system is defined relative to primary plane of component which is tilted inboard at the top.
[b]No data available.

6. *Dynamic Analyses*

Completion of the S-2 drop test series has provided experimental data on spacecraft component inertia loads and support structure stresses for comparison with the prediction of the forced response elastic vehicle analytical program. Initial comparison of the analytic and test results indicated some minor discrepancies between the two. However, slight modifications to the program have resulted in very close agreement between analytic and test loads.

The instrumentation on the S-2 test vehicle included strain gages to measure mast bending moments and land-

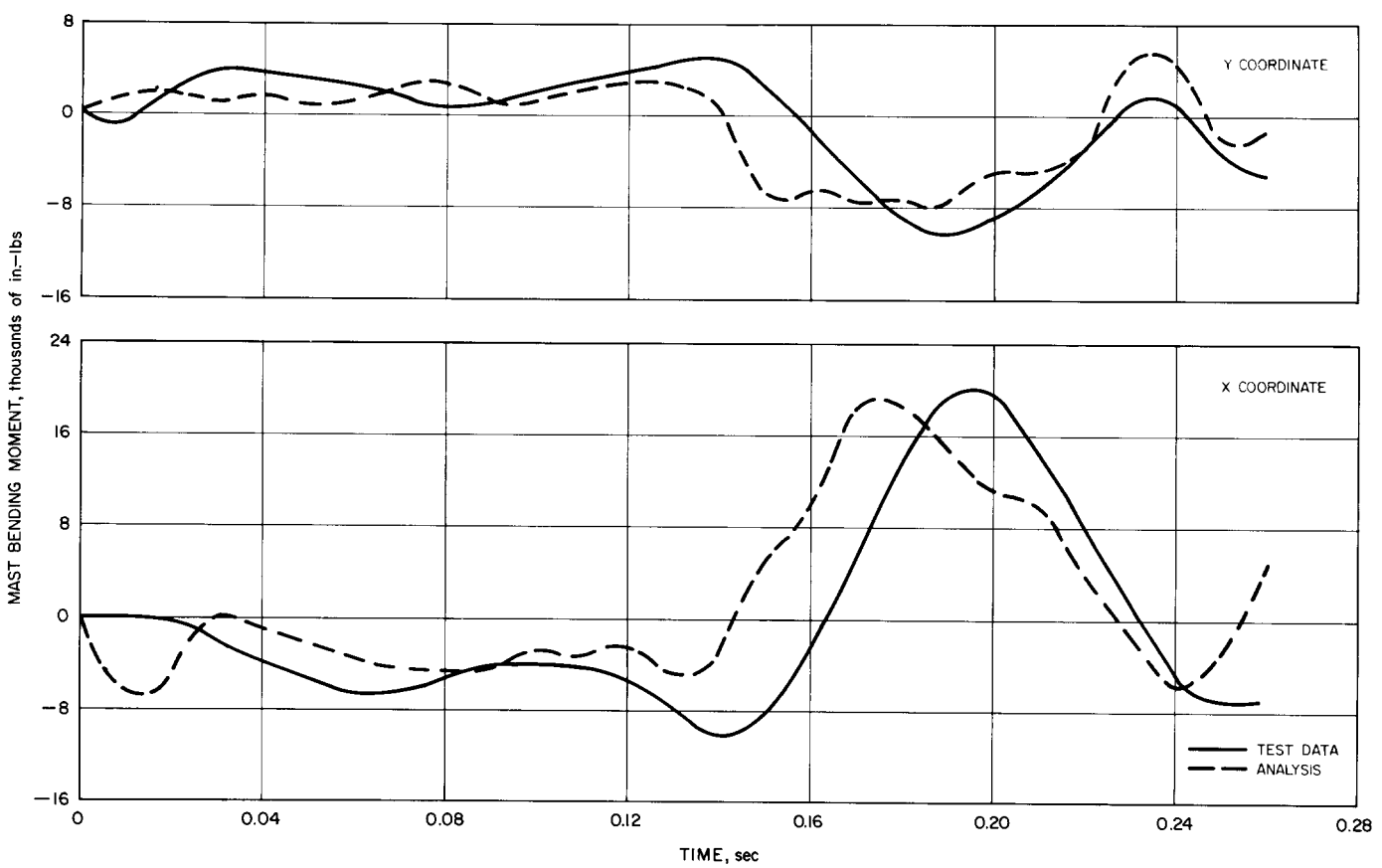

(a) Upper mast

Fig. 51. S-2 bending moments due to inertial loads in spaceframe

ing gear forces. In Drop Test 3 the mast bending moments approached the design limit although the forces in the landing gear were about 65% of the forces predicted for other lunar landing conditions. A redesign of the mast to withstand the more critical landing conditions has been started. The present design loads are based on measurements from Drop Test 3. These loads will be modified on the basis of analyses of lunar landings of the elastic flight vehicle.

The three drop tests have provided experimental data for correlation with the analytical results obtained from the modal model of the elastic vehicle. The landing gear forces and crushable block forces acting on the vehicle during the drop test were measured and used as forcing functions for the analytical model. The responses obtained from the analyses were in good agreement with the responses measured in the drop tests. Fig. 51 shows the comparison of mast bending moments measured in Drop Test 3 with mast bending moments obtained by analysis. With this quality of agreement, the analyses of lunar landing conditions may be made with a high degree of confidence.

7. Flight Vehicle Instrumentation

a. Accelerometer amplifiers. The application of thermal paint and identification markings on the T-21 amplifier assembly has been postponed until mid-April to concur with the *Surveyor* retrofit dates. This is the only remaining effort on the units for T-21.

Units for SC-1 were flight acceptance tested at Endevco Corporation starting March 2, 1964. Unit 16 failed during the shock sensitivity test. Endevco has prepared a failure analysis, now under review at Hughes.

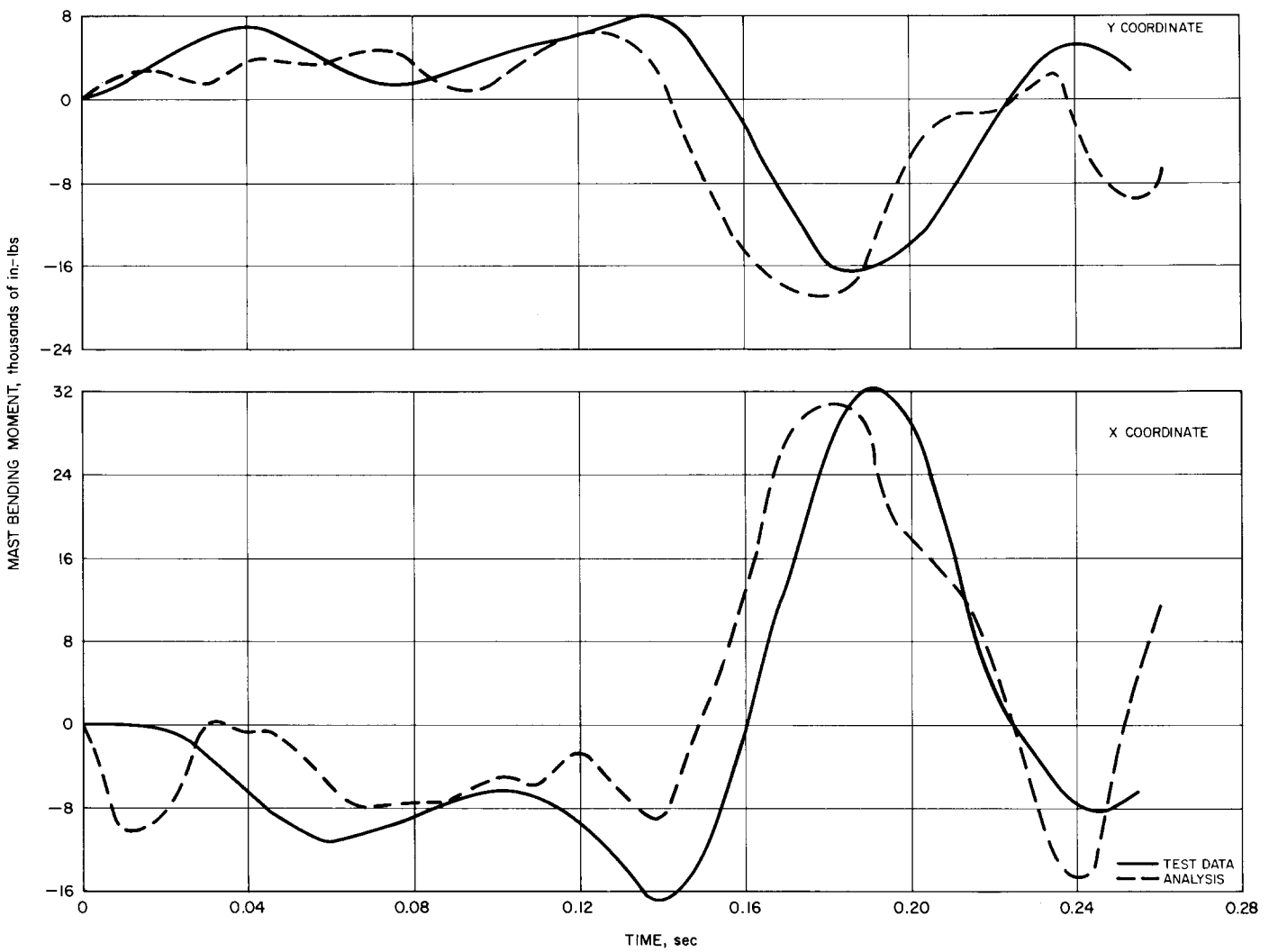

(b) Lower mast

Fig. 51 (continued). S-2 bending moments due to inertial loads in spaceframe

Units received at present are: T-21 units S/N 1 to 8; SC-1 units S/N 1 to 15, and SC-2 units S/N 17 to 24.

b. Strain gage amplifier system. Qualification of the strain gage amplifier from Semi-Conductor Magnetics Incorporated (SMI) continued during the report period. A leakage was observed around the cover of the amplifier during the qualification test. The unit was returned to the vendor for inspection and analysis. Leakage was caused by improper soldering. To save time, the leakage portion of the TAT will be done on a flight model unit assigned to T-21. A leakage test is performed on all flight units.

The RFI portion of the TAT has been completed on the T-21 unit S/N 4. The unit was not within specification requirements, but none of the RFI deviations is believed to be a significant problem. Units for T-21 are ready for flight acceptance tests pending completion of the TAT and the return of unit S/N 4 to SMI. The T-21 units incorporate the filtering found necessary during the RFI evaluation of the qualification unit.

Nytron, Inc. submitted a second strain gage amplifier qualification unit on March 13, 1964; it is being evaluated.

8. Fatigue Evaluation of Bonded Fiberglass Joints

Eight bonded specimens were tested to failure to obtain additional design information for bonded fiberglass-to-aluminum joints. These specimens (see Fig. 52) are representative of the bonded structural joints used in *Surveyor* substructure wherever fiberglass thermal insulators are required, e.g., Compartments A and B, TV cameras, nitrogen tank, and helium tank. However, a solid aluminum rod was used instead of tubing to eliminate the aluminum failure mode; the bond length was increased in an attempt to obtain some fiberglass failures.

The control specimen, No. 1, was loaded to failure in compression; failure occurred in the fiberglass tube at a stress of 40,100 lb/in.^{2}; the minimum guaranteed compressive strength is 25,000 lb/in.^{2}. Strain in the free length of fiberglass tube was linear throughout the loading range (0.0067 in./in.). The modulus of elasticity in compression for the fiberglass is calculated as:

$$E_c = \frac{\sigma_c}{\epsilon} = \frac{40100}{0.0067} = 6.00 \times 10^6 \text{ lb/in.}^2$$

The remaining seven specimens were cycled to failure under a completely reversing axial load. The results of these tests are shown in Table 23. The fiberglass stress levels are also presented in terms of percent of compression ultimate strength, since the compressive strength of this group of tubes is approximately 60% greater than the minimum guaranteed value. The primary failure mode was shearing of the bond with only one fiberglass tube failure. The fact that there were not more tube failures is attributed to unusually high axial strength of this group of tubes.

Fig. 53 is an S-N curve showing average bond shear stress versus cycles to failure. The curve represents the failure points of Table 23 plus 15 additional points obtained from early tests presented in previous *Space Pro-*

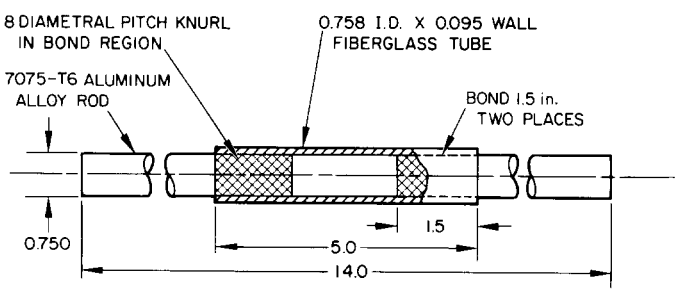

(a) Group A

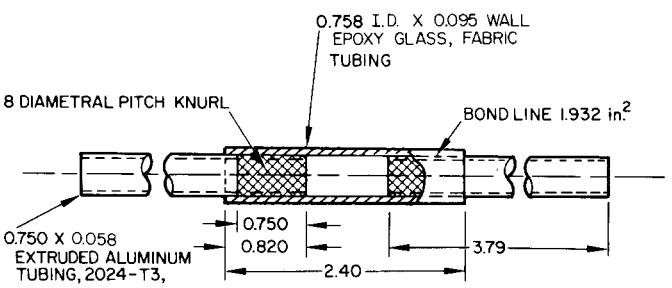

(b) Group B

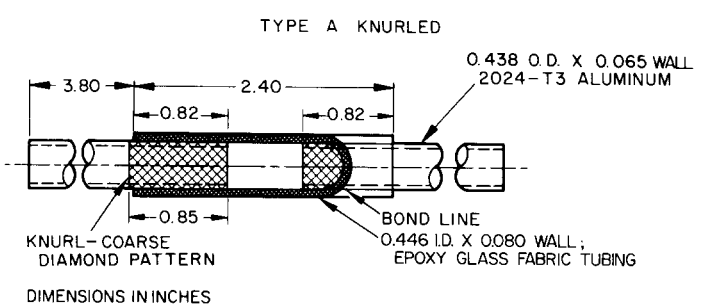

(c) Group C

Fig. 52. Bond test specimens

Table 23. Fatigue test results (room temperature)

Specimen number	Alternating axial load, lb	Alternating stress		Cycles to failure	Failure mode	Fiberglass stress load,[b] %
		Fiberglass tube, lb/in.^{2}	Bond,[a] lb/in.^{2}			
2	± 3920	± 15,400	± 1100	11,000	Bond shear	38.4
3	± 3920	± 15,400	± 1100	13,000	Bond shear	38.4
4	± 3520	± 13,900	± 990	17,000	Bond shear	34.7
5	± 3520	± 13,900	± 990	25,000	Fiberglass tube	34.7
6	± 3140	± 12,400	± 883	35,000	Bond shear	30.9
7	± 3140	± 12,400	± 883	52,000	Bond shear	30.9
8	± 2940	± 11,600	± 827	85,000	Bond shear	28.9

[a]Minimum guaranteed static bond strength = 2200 lb/in.^{2}
[b]Ratio of fatigue stress to compression stress at failure in the control specimen (No. 1).

grams Summaries, Vol. I. Dimensions of the three types of specimens are shown in Fig. 52. The same materials were used in all specimens with the exception that 7075-T6 aluminum rod was substituted for 2024-T3 aluminum tubing in Group A. Groups B and C represent the maximum extremes of D/t (outside tube diameter-to-wall thickness ratio) used in actual *Surveyor* substructure members. Although four specimens failed in components other than the bond, these failure points fall very close to the mean curve of bond failures. The curve also shows that increasing the bond length from 0.82 to 1.5 in. (Group A) does not have a noticeable effect on the fatigue strength of the bond. It may be concluded that the S-N curve is representative of the allowable fatigue strength which can be obtained for all bonded assemblies having the dimensions of Groups A, B, and C.

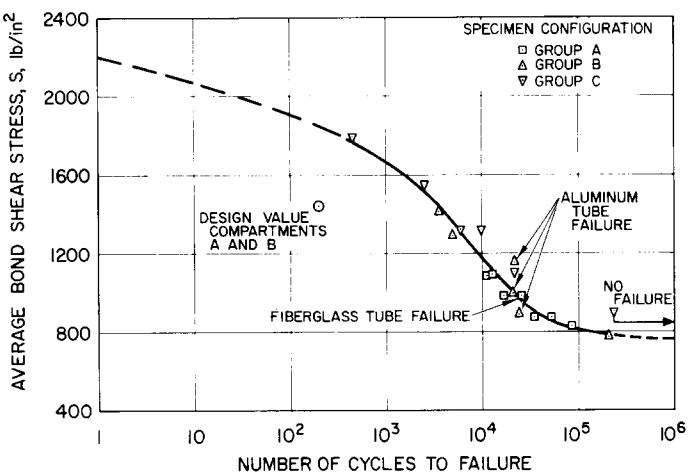

Fig. 53. Fatigue test results

I. Propulsion

1. Introduction

The spacecraft propulsion system comprises a spherical solid-propellant retro-rocket engine and a liquid-propellant vernier propulsion system. The retro-rocket engine, developed by the Elkton Division of Thiokol Chemical Corporation under a subcontract, performs the major portion of the deceleration of the spacecraft on approach to the lunar surface. The vernier propulsion system is used for the midcourse maneuver, attitude control during retro-rocket engine burning, and terminal descent.

2. Progress Summary

a. Main retro-rocket engine. Two flight-weight retro-rocket engines, A-21-14 and A-21-8, were tested successfully under simulated altitude conditions after exposure to temperature conditioning to simulate the expected thermal gradient resulting from the 66-hr transit period. The remaining two developmental engines, A-21-11 and A-21-12, were delivered to Arnold Engineering Development Center (AEDC) on March 2, 1964 and are scheduled for simulated altitude testing in June 1964. A case assembly was subjected to hydrostatic burst testing on March 11, 1964 and ruptured at 995 psia. The type of failure and rupture pressure confirmed the satisfactory design margins demonstrated on previous tests.

The engine and component designs have been frozen and fabrication has been initiated for the quality assurance test program. The qualification tests are to be conducted in July. Prior to the design freeze, the aft case insulation was modified to accommodate a maximum propellant weight of 1250 lb. All quality assurance units will be cast to a 1230-lb nominal propellant weight.

b. Vernier propulsion system. The vernier propulsion system subcontract with the Reaction Motors Division (RMD) of Thiokol Chemical Corporation was partially terminated on March 18 at the direction of JPL. Items of work remaining with RMD include field service and certain other support functions necessary for systems testing at AFMDC. Termination inventories are being generated and items of development hardware are being transferred to Hughes for use in the upstream systems development programs and T-2 system support. An evaluation of alternate thrust chamber assemblies was completed.

The flight-type helium regulator being manufactured by the Carleton Controls Corporation has completed the series of approval tests at RMD. Analysis of all the test results indicates that the regulator, as designed, is suitable for flight use. Additional tests of the regulator will be conducted at Hughes in conjunction with the helium pressurization system tests.

Hughes has initiated a development program to produce propellant tanks for flight use. Machined tank halves of the 7178 aluminum alloy are being procured and welding is being performed by a local tungsten-inert gas welding vendor. This weld test program is scheduled for completion in the near future. An alternate tank program is in the planning stages to manufacture tanks of 6Al-4Va titanium alloy.

Vibration testing of the S-7 vehicle has been completed. The final vibration envelope for random and sinusoidal outputs has been established and will be used as the basis for component vibration testing. The S-7 vehicle has been rebuilt and has been shipped to the Hughes AFMDC test facility for the initial phase of upstream (from the thrust chamber assembly) system development testing. The first tests of the series, the loading and unloading tests, will be conducted in the near future.

3. Main Retro-Rocket Engine

a. Developmental engine tests. Two flight-weight engines, A-21-14 and A-21-8, were successfully tested at Elkton on February 20 and 27, 1964. Prior to testing in the altitude test chamber, both engines were subjected to temperature conditioning to duplicate the predicted thermal gradient resulting from the 66-hr spacecraft transit period. The nozzle of Engine A-21-14 was subjected to temperature conditioning to duplicate the conditioning of Engine A-21-7 as previously reported. The nominal temperature at the exit plane prior to firing was —260° F. Fig. 54 shows Engines A-21-14 and A-21-8 prior to firing. The test results for Engines A-21-7, A-21-14, and A-21-8 are presented in Table 24 and Fig. 55.

The time between removal of temperature gradient conditioning and firing was decreased from 9 hr on Engine A-21-7 to less than 5 hr on Engines A-21-14 and A-21-8.

The primary influence of the thermal gradient condition on performance is shown in Fig. 55 which compares the pressure versus time records of Engine A-21-7 and Engine A-21-10 at a 50° F constant temperature. The performance of the engine subjected to thermal gradient conditioning duplicates the performance of an engine at a constant 40° F temperature condition.

The second hydrostatic burst test of a flight-weight case assembly was conducted successfully on March 11, 1964. The case LSU-R1, which was previously rejected

from the firing program because of a local thin spot in the case membrane, ruptured at a pressure of 995 psia. The failure mode, shown in Fig. 56, was identical to that of the previous burst-test case which ruptured at 976 psia. The failure did not propagate from the local thin spot. The rupture of both cases demonstrates a satisfactory safety margin over the 683-psia case-proof pressure. The minimum design yield pressure was 770 psia. During pressurization, a thrust force of 12,500 lb was applied to the attachment fittings. Dial indicator readings obtained during the hydrostatic burst test will be evaluated with respect to relative motion of the case produced by case dilation.

Table 24. Performance comparison of Engines A-21-7, A-21-14, and A-21-8

Parameters	Engine number/test date		
	A-21-7 January 24, 1964	A-21-14 February 20, 1964	A-21-8 February 27, 1964
Throat area reduction, A_{TO}/A_{TF}, in.^{2}	8.509/9.237	8.511/9.197	8.512/9.149
Throat erosion, %	8.56	8.06	7.48
Burning time, t_{burn}, sec	39.278	38.375	38.068
Action time, t_{action}, sec	42.025	41.575	40.770
Chamber pressure, P_{avg}, psia	509	509	524
Burning rate (500 psia/60°F), in./sec	0.242	0.242	0.247
K_N (500 psia/60°F), in./sec	207	208	200
Propellant weight, lb	1194.00	1191.35	1197.76
Hold time after gradient conditioning, hr	9	>5	>5

The last two retro-rocket engines in the development program, A-21-11 and A-21-12, were delivered to AEDC on March 2, 1964 for testing in the altitude facility. The engine tests, originally scheduled for March 15 and 22, 1964, have been delayed until June 1964 because of altitude cell operational problems and schedule conflicts with three *Minuteman* tests. The tests will be conducted in the J-5 horizontal stand equipped with side load cells to evaluate thrust vector shift during engine burning.

b. Quality assurance test program. The design of all engine components has been frozen and fabrication of engines has been initiated for the ten-engine quality assurance test program. The aft case insulation was extended to provide a loaded propellant capability of 1250 lb. The ten engines for the quality assurance test program will be loaded to a nominal propellant weight of 1230 lb. The first engine was loaded on April 1, 1964. Completion of the quality assurance test program is currently scheduled for August 1, 1964.

c. Flight-weight nozzle. Nine successful tests have been conducted utilizing the flight-weight nozzle. Fabrication of ten nozzles for the quality assurance program was initiated at H. I. Thompson Co. on March 16, 1964. The evaluation of improved nozzle liner materials has been terminated.

d. Safe and arm assembly. Fabrication of safe and arm assemblies has been started by the Bristol Division of Thiokol for units for the quality assurance test program. Testing of the safe and arm units is scheduled to start in mid-April 1964.

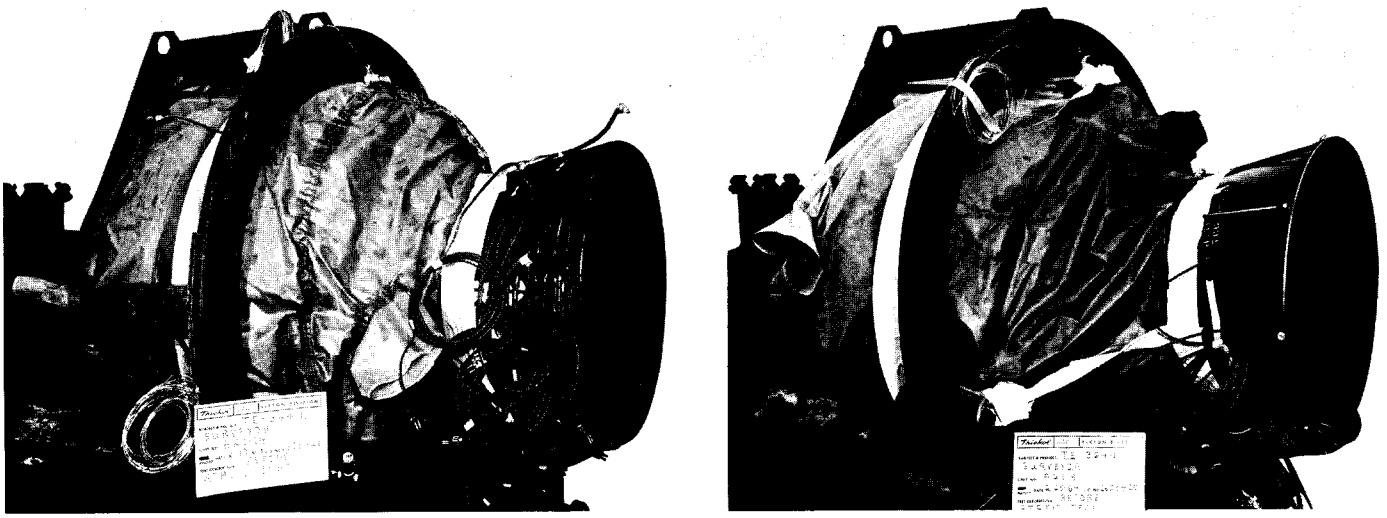

(a) A-21-14 (b) A-21-8

Fig. 54. Engines preparatory to thermal gradient firings

Approval has been received from the cognizant audit agencies to permit transfer of the remainder of the Hi-Shear squib qualification program from *Dyna-Soar* to *Surveyor*. Although termination of the *Dyna-Soar* program resulted in a 3-mo schedule delay for completion of squib qualification, *Surveyor* schedules have not been jeopardized. Qualification of the Hi-Shear PC-37 squib and the safe and arm assembly will be conducted concurrently.

e. Thermal control. Additional propellant specimens have been prepared from the propellant batch cast on April 1, 1964. The specimens will be subjected to thermal conductivity and heat capacity determination testing at four independent laboratories. By closely monitoring the tests, it is believed that the present uncertainty in propellant thermal properties will be eliminated, thus minimizing the uncertainty in the predicted thermal gradient resulting from the 66-hr transit period.

The Hughes computer program for prediction of ballistic performance at the thermal gradient condition is being revised and improved. The program revision was necessitated by the requirement for propellant cutback on flight engines and the difficulties in calculating the burning surface area at the forward end. The program will be revised to accommodate the cut-back configuration shown in Fig. 57.

Fabrication of thermal control blankets has begun for the upgrade of T-21A and S-2 inert engines and for Engines A-21-19 and A-21-22 which will be subjected to vibration testing in the quality assurance test program.

4. Vernier Propulsion System

a. System development. The S-7 vibration test data has been reduced and the test report issued. The final vibration envelope for random and sinusoidal outputs can be used as a basis for component vibration testing. The report groups the test results in three sections according to the three subsystems – helium tank and valves assembly, propellant tanks, and vernier engine. Load

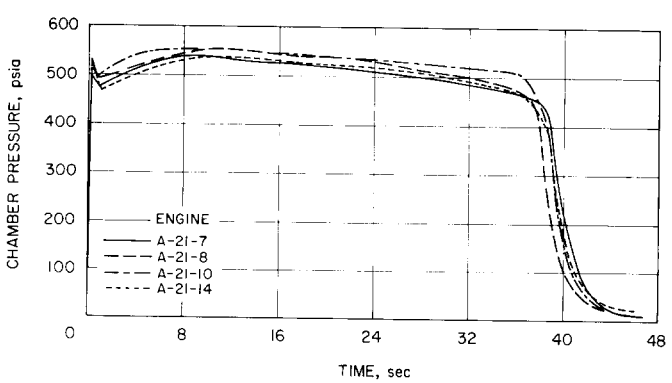

(a) Pressure versus time

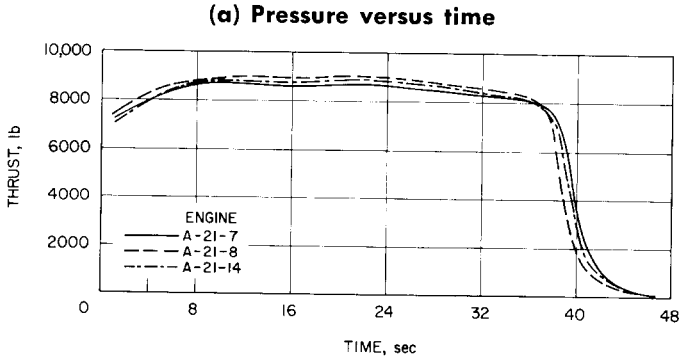

(b) Thrust versus time

Fig. 55. Main retro-rocket engines performance comparison

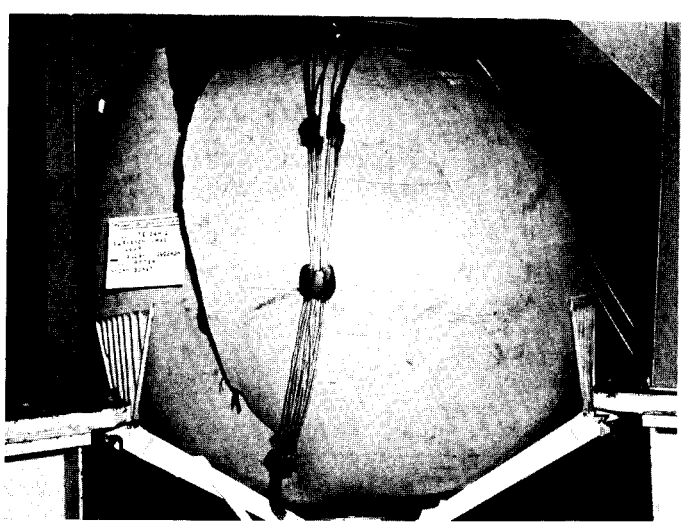

Fig. 56. Engine case after burst test

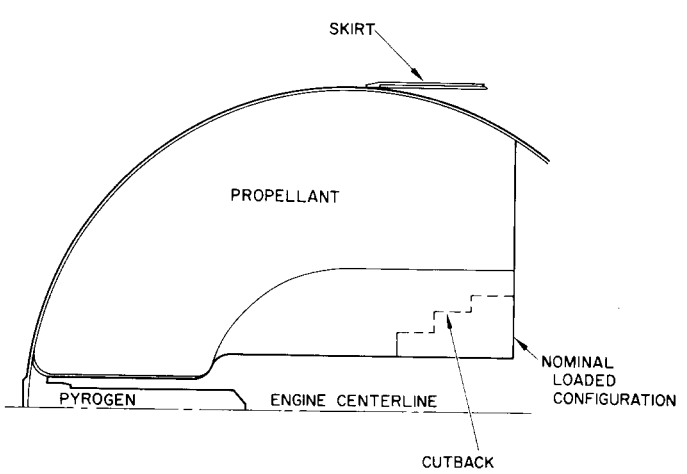

Fig. 57. Retro-engine propellant cutback configuration

attenuation of the different component groups is also included in the report. The report concludes that:

(1) The dynamic dissimilarity of the S-7 spaceframe without the retro-engine, compared to the T-21 spaceframe with the engine, caused a negligible increase in the output levels of the components.

(2) The mast and equipment compartments imparted large deflections to the vernier system at frequencies up to 50 cps.

(3) The components of the propulsion system were less affected in the legs-down (landing) configuration than in the stowed configuration.

T-2 operations at AFMDC were limited to additional horizontal firing tests to investigate further the acoustical effect of the engines on the radar system.

Fourteen horizontal test firings were made during the past report period. Difficulty was encountered with clogged oxidizer filters and thrust chamber injectors. Corrective action consisted of vacuum flushing of the thrust chamber assembly between each firing; however, two thrust chambers had to be removed from the T-2 vehicle and sent to Thiokol RMD for inspection and more thorough flushing. One throttle valve failed to pass a solvent flow check and was returned to RMD for repair. Two throttle valves were returned to Hughes for repair because of excessive seal leakage. Balloon suspension and drop tests will be started early in the next report period.

The vernier system developmental test plan was released. The test program, which uses the S-6 and S-7 spaceframes, was started at AFMDC near the end of this report period. The cold flow tests for the upstream system are designed to be conducted without the use of a thrust chamber. However, throttle valves will be utilized for flow control and special adapters will simulate the injectors. A special piston valve has been designed to demonstrate the efficiency of the vehicle filling technique. This valve will be fabricated at Hughes and will be available for the initial system loading test program. Plans are also being made to conduct a series of bladder elasticity tests to determine if there is a propellant center-of-gravity shift from variations in bladder elasticity under various operating conditions. The overall system test program includes propellant loading, unloading and flush procedures, expulsion efficiency, expulsion unbalance, environmental temperature tests, dynamic flow tests, preflight checkout procedure tests, and engine system firings.

b. Component development. Hughes effort on three-way valve and fluid regulator components designed for the RMD engine has been terminated. No further development or evaluation is contemplated.

During the report period engine testing was initiated to demonstrate the adequacy of reduced oxidizer-to-fuel (O/F) ratio at minimum thrust and 40° F fuel inlet temperature as solutions to the fuel boiling problem. As a preliminary effort to this program, extensive throttle valve testing at RMD and Hughes led to the use of a slotted first stage nozzle to prevent a fuel flow rate below that corresponding to 1.0 O/F ratio when the oxidizer flow is for minimum thrust. Using this design, a 1.5 O/F ratio was maintained down to approximately 43 lb thrust below which the O/F ratio decreased linearly to 1.0 at minimum thrust.

An improved throttle valve incorporating all teflon seals with a configuration more amenable to calibration and service was developed at Hughes. Prototype valves are on order. They will be evaluated with propellants at the Hughes Propulsion System Field Laboratory for possible incorporation in the alternate thrust chamber assembly and in support of system testing.

Uncompensated mixture ratio excursions caused by propellant temperature variations from nominal will result in unusable residual propellant at mission completion. A quantitative analysis of these excursions has been completed during the report period. The resultant data on the amount of additional propellant required to produce a simultaneous depletion is shown in Fig. 58.

Approval testing of the Carleton flight-type regulator was completed successfully at RMD during the report period.

An evaluation of the current helium relief valve design was made to determine the feasibility of modifying the design to meet specification requirements. It was concluded that modification was not possible and that a

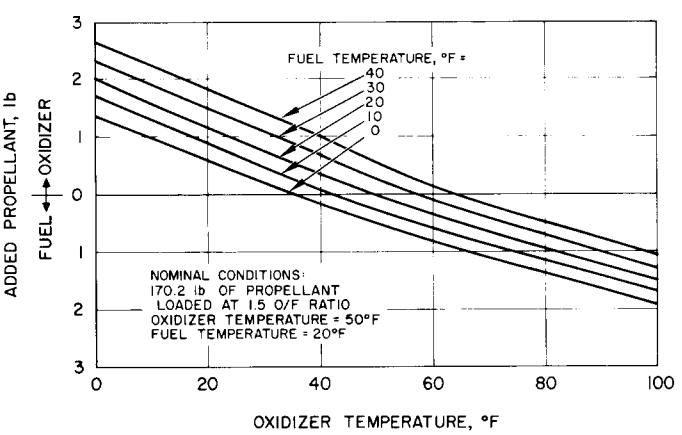

Fig. 58. Additional propellant for simultaneous depletion

complete redesign was required. As a result a specification has been prepared by Hughes and proposals have been solicited for this item.

A test program is in progress to attempt to establish the degree of confidence that can be placed in the 7A1-4Mo titanium alloy helium and nitrogen pressurization tanks from the standpoint of man-safety rating. The vibration testing phase of this program has been completed without incident. Vibration was conducted in three axes with the tank pressurized to 110% of maximum working pressure (see Fig. 59).

c. Propellant tank development. The second S-5 failure at RMD, which was traced directly to the propellant tank weld area, made it necessary to establish a test criterion for existing tanks so that they might be used on T-2. Existing tanks from RMD were subjected to a pressure proof test and then to a pressure cycle test of 150 cycles minimum and 300 cycles maximum. The tests were completed successfully, allowing existing propellant tanks to be used in the T-2 program.

A weld development program involving electron beam welding and tungsten inert gas (TIG) welding was completed during the period. TIG welded samples of 7178-T6 Alclad and electron beam welded samples of bare 7075-T6 were made. The feasibility of electron beam welding was demonstrated. Two contracts were let for electron beam and automatic tungsten inert gas welding in three phases – first, flat specimens; second, rolled hoops; and finally, pressure bottles. The electron beam contract was terminated due to the inability of the Air-rite electron beam machine to achieve proper vacuum. The automatic TIG Phase 1 samples made from bare 7178-T6 were tested in the as-welded condition and provided an average allowable stress of 52,900 psi for five different weld settings on a total of 46 test samples. The design stress level is 24,800 psi. Rolled hoops and pressure bottles were TIG-welded, and results are being analyzed.

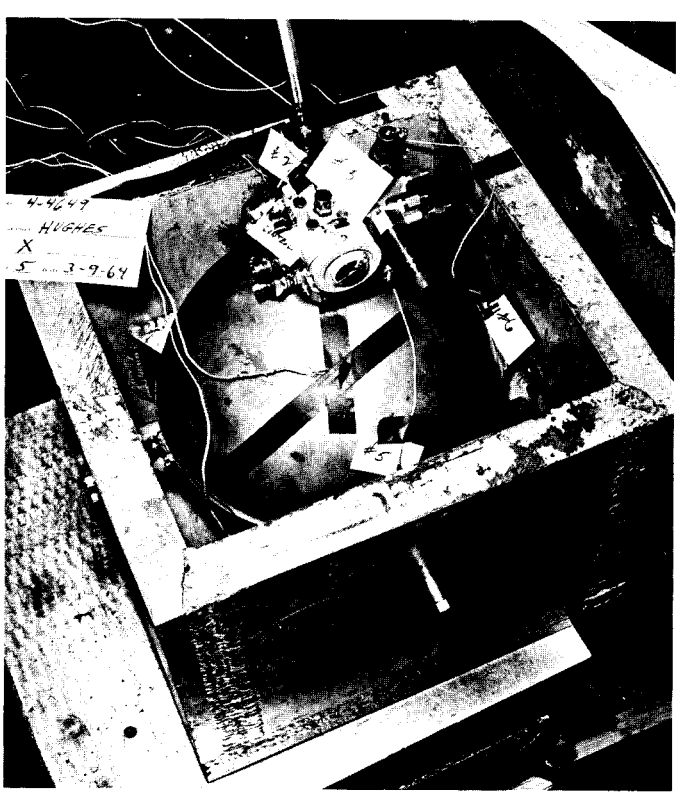

Fig. 59. Vibration testing of helium tank

d. Feed system assembly. Following the S-7 vibration test program, the feed system was removed from the vehicle to facilitate cleaning prior to the propellant loading and unloading tests. The simulated masses were also removed from the vehicle. Upon completion of the cleaning process, the feed system was reinstalled on the S-7 vehicle and the vehicle was shipped to AFMDC (Fig. 60).

e. Alternate thrust chamber. Bids on an alternate thrust chamber assembly (TCA) were received from Rocketdyne, Marquardt, and Bell. Rocketdyne proposed a modification of the *Gemini* 100-lb thrust, hard throat engine. During a demonstration firing of this engine coupled to a Hughes throttle valve, the engine performed satisfactorily in all respects, throttling over the 30- to 104-lb thrust range. Instrumentation difficulties prevented the acquisition of reliable transient data.

Marquardt proposed a modification of the 100-lb thrust radiation cooled *Apollo* engine. The results of a firing using a modified injector were promising. Light weight, coupled with chamber durability, make the Marquardt proposal extremely promising. Mounting problems and several other TCA difficulties are being resolved. The Bell proposal was unattractive because of (1) an injector design using two-phase flow, (2) lack of a prequality assurance program, and (3) lack of proven hardware. The Marquardt, Rocketdyne, RMD, and STL chambers were then evaluated to determine which offered the greatest likelihood of success for the time constraint imposed by the presently scheduled *Surveyor* launch date. Based on this evaluation the following recommendations were made to JPL:

(1) Continue with the RMD TCA at least until June.

(2) Begin a back-up program with Rocketdyne and in June drop either the Rocketdyne or RMD program depending on an evaluation at that time.

(3) Continue the STL program with the intent of integrating their TCA into a system beyond SC-1, since their design does not appear to be developed sufficiently to meet present SC-1 schedules.

JPL directed Hughes to terminate the RMD TCA program March 18, 1964. A Hughes-STL-JPL team has since assembled to generate a Hughes-controlled interface document to define the spacecraft feed system/engine constraints. The document includes specifications, outline and mounting drawings, and system interaction parameters.

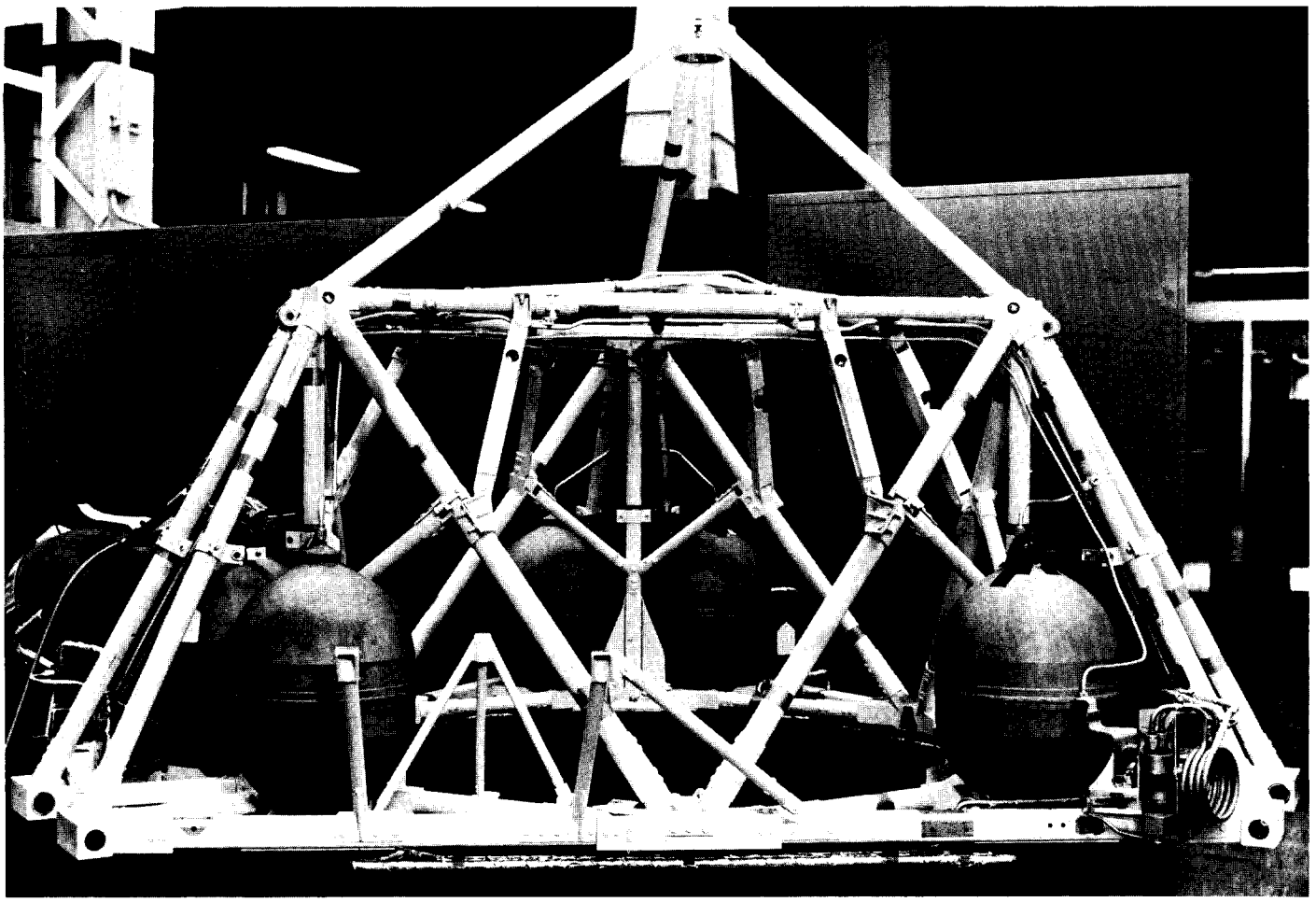

Fig. 60. S-7 test vehicle

J. Spacecraft Vehicle and Mechanisms for Basic Bus

1. Spacecraft Vehicle

Vehicle activities reported in this section include design and fabrication of spaceframes and substructures and the assembly of complete vehicles for flight and test spacecraft. Fabrication, assembly, and tests of the thermally controlled equipment compartments, wiring harness, landing gear, and ground handling equipment are also the responsibility of this activity. Overall spacecraft configuration studies, weight reports, etc., are reported in Section A.

a. Vehicle status

T-21 — system type approval test vehicle. This vehicle continues to be utilized in the system functional test program. It will then undergo a retrofit upgrade for approximately 4 wk. A series of mission simulation tests will be conducted after which another upgrade will occur to include several structural assemblies that could not be redesigned and installed in time for the first upgrade. These changes include reinforced radar altimeter and doppler velocity sensor (RADVS) antenna supports, stronger antenna/solar panel positioner mast support structure, and new thermal compartments. These changes resulted from previously reported test data obtained from S-2 structural tests.

T-21A — system type approval test spacecraft. Scientific payload substructure design was begun in March. Detail design to the new payload interfaces will begin immediately and continue through the next reporting period. Fabrication of the new T-21A spacecraft has begun; the new vehicle is scheduled to be delivered for system tests in February 1965.

T-1 — separation type approval test model. This vehicle will be returned from General Dynamics, Astronautics Division on June 1, 1964, for use in a series of retro-rocket separation tests. The necessary test specifications and procedures are being prepared.

S-2 — structural test vehicle. Drop tests conducted on this vehicle are reported in Section H. At the conclusion of these tests, a structural upgrade was started.

S-6 — vernier propulsion system qualification vehicle. A new special test manifold, fitted with additional instrumentation, is being fabricated for this vehicle.

S-7 — vernier propulsion system qualification vehicle. At the conclusion of a modal vibration survey in early March, this vehicle was stripped of ballast and shipped to the Air Force Missile Development Center (AFMDC).

S-8 — tether test vehicle. This vehicle will be used to study the interaction between the flight control sensor group and the vernier engines during actual engine firings while suspended from an Aerobee Tower at AFMDC.

Design of the substructure was released during this reporting period and fabrication has begun. Bids have been received for the modification of the Aerobee Tower. The modifications included reinforcing the structure and adding a 35-ft boom at its top; the subcontractor is expected to begin modification in April. The suspension system for this vehicle has undergone a series of tests at Hughes. A simulated vehicle weighing approximately the same as the *Surveyor* at launch was suspended from the elastic system to check the spring rates (Fig. 78).

SC-1 — first flight spacecraft. Fabrication and installation of substructure has continued during this period. Some delays in completion of portions of the substructure have occurred from redesign arising out of S-2 structural test results.

SC-2 — second flight spacecraft. Fabrication of key spaceframe subassemblies is continuing. These subassemblies will be mounted into the assembly jig for basic frame buildup during the next reporting period.

b. Wiring harness. Major engineering effort has been expended in upgrading drawings for retrofitting the T-21 and SC-1 harness to incorporate changes determined on T-21 during systems test. Except for these changes, fabrication of SC-1 harness assemblies is nearly complete.

c. Testing. The lightweight landing gear leg (L-5) was subjected to the dynamic portion of its type approval test and met the requirements. The nitrogen flexible line that was attached to the landing gear leg ruptured during this test and could not maintain pressure when tested for leakage. This item was not part of the landing gear type approval test program, but did point out a potential problem. Tests of the flexible nitrogen line will be conducted to assure adequacy of the attitude jet plumbing system.

During the boost vibration testing of the L-5 leg, the assembly was enclosed in a plastic bag, which was inflated with dry nitrogen. The dry nitrogen was maintained under pressure during the entire vibration test to eliminate the possibility that the vibration table oils might penetrate and damage the thermal finish of the leg (Fig. 61).

L-5 is currently undergoing a series of structural static deflection tests for further investigation of lightweight structure (Fig. 62).

2. Mechanisms for Basic Bus

a. Omnidirectional antenna mechanisms. The two omnidirectional antenna mechanisms use tapered, fiberglass cloth tubes bonded to aluminum hinge bracket assemblies. They deploy and lock the two omnidirectional antennas into operating position prior to *Surveyor/Centaur* separation.

Both Antenna A and B mechanism type approval units previously had completed flight acceptance tests during the preceding report period.

The Antenna A mechanism completed the type approval vibration levels in the Y-axis (lateral) and in the Z-axis (thrust) direction. Failures were experienced during the X-axis (lateral) test. A fracture (Fig. 63a) at the mounting tab of the clevis support and a fatigue failure of three of the four metal straps that restrain the antenna coaxial cable within the fiberglass tube (Fig. 63b) occurred during this test.

The clevis support has been strengthened by a change in material and by the addition of a generous fillet in the area of fracture. A U-shaped saddle has been added to the coaxial cable retaining mechanism to eliminate the possibility of excessive bending thereby fatiguing the metal strap. The retest of this mechanism is scheduled for completion during April.

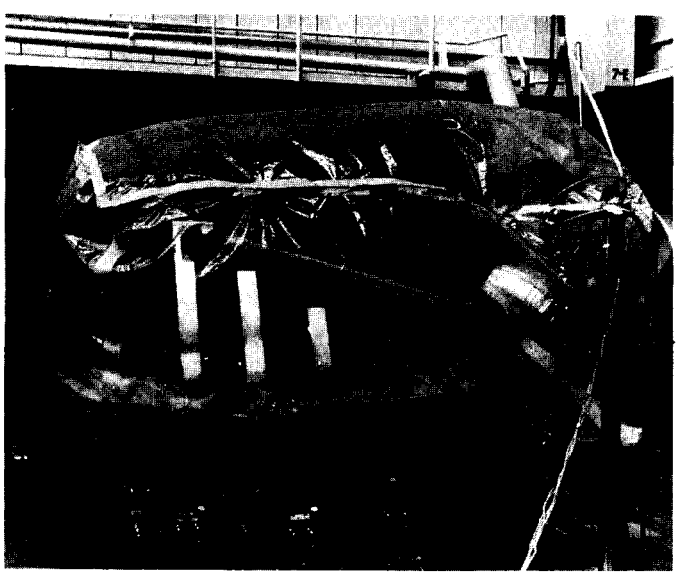

Fig. 61. Vibration test of landing gear (with thermal finish protective tent)

The Antenna B mechanism successfully completed the type approval vibration levels in the X- and Y-axes (lateral) and the Z-axis (thrust). Descent vibration tests in the two lateral and thrust directions were completed successfully with the mechanism deployed. Landing shock tests with the mechanism deployed were also completed. The final environmental test is the thermal–vacuum exposure to be conducted during April 1964.

The assembly of the Antenna A mechanism for SC-1 has been delayed pending the outcome of retesting the type approval unit. The Antenna B mechanism for SC-1 has been flight acceptance tested and delivered to bonded stores.

The Antenna A and B mechanisms for the SP-1 flight spare have been thermally coated; assembly will be completed after receipt of the antennas.

b. Antenna/solar panel positioner. The positioner provides mounting, positioning, position indicators, and launch and landing locks for the planar array antenna and solar panel. The antenna support structure has three controllable axes; the solar panel is mounted to the an-

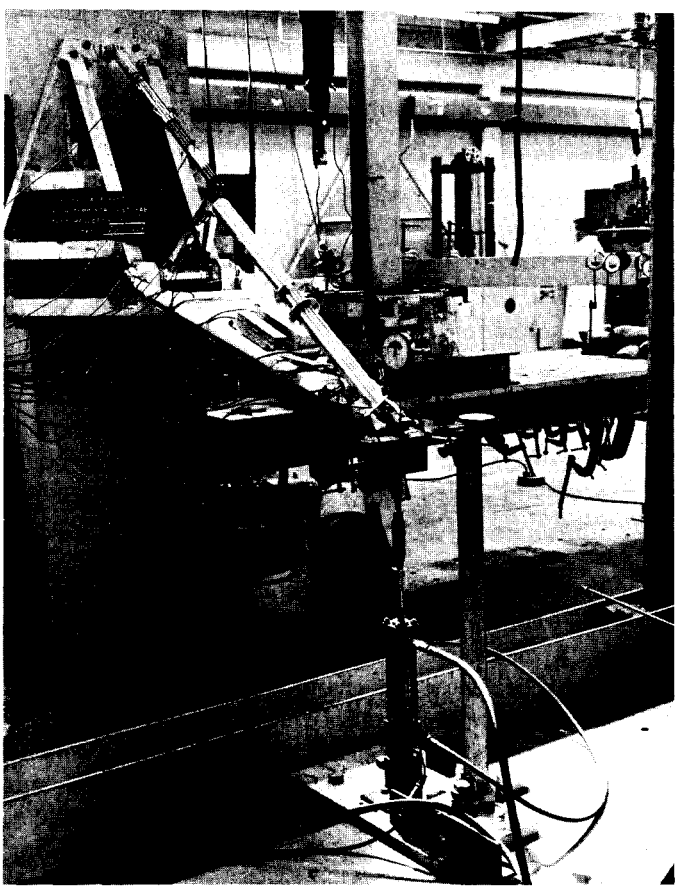

Fig. 62. Landing gear static deflection test

tenna support structure by a single controllable axis. The roll, elevation, and solar axis drives utilize three-stage planetary gear reductions. The polar axis drive uses a single-stage planetary and a double enveloping worm gear drive. All axes use solenoid stepping motors for drive and wire-wound potentiometers for position indication.

The E-1 engineering unit, which experienced a failure during the third and last axis of type approval level vibration testing on the S-2 spacecraft, was rewelded, heat treated, and reinstalled on S-2. During the fourth S-2 drop test, the positioner failed again at the same rewelded joint. Accelerometers and strain gages on the S-2 spacecraft indicate that the present input loads on the positioner are considerably in excess of the current design levels.

All effort on the current hardware was halted, and an accelerated redesign program was initiated. The redesigned unit will use existing drive mechanisms and will retain the same gimbal system geometry. All structure will be redesigned for 7075 aluminum alloy instead of 6061 aluminum alloy. All welding will be eliminated except on the solar panel mounting arms. Provisions for a transit phase roll maneuver, roll relock, and roll relock indication will be incorporated.

A development breadboard unit (X-1) of the new design is being fabricated for early delivery to the S-2 spacecraft. This unit will be followed immediately by a new T-21 positioner.

c. Motors and mechanisms drive units. The Ledex stepper motors used in the antenna/solar panel positioner have successfully completed the thermal–vacuum life cycling tests. These tests conclude the qualification program for these motors. As noted in *Space Programs Summary No. 37-26*, Vol. I, all flight motors are being lubricated and sealed in accordance with the procedure developed during the qualification program.

Detenting accuracy tests have continued on the Curtiss-Wright motors using the inertia simulation fixture described in the above *SPS*. With the spring loaded ball and star wheel detent mechanism, the motor positioned the maximum inertia load accurately over the operating voltage range, with friction loads varying from zero to values twice as great as those measured on the unit assembly. This detent mechanism has been redesigned to mount directly to the face of the motor in the existing design space with minimum rework.

d. Separation sensing and arming device. These devices (three per spacecraft) provide redundant interruption for the postseparation squib firing circuits and the vernier engine solenoid circuit until after the spacecraft separates from the *Centaur*.

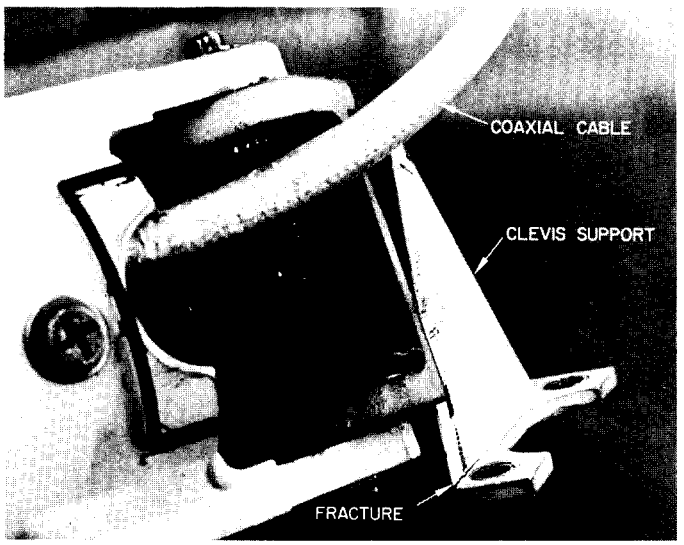

(a) Clevis support

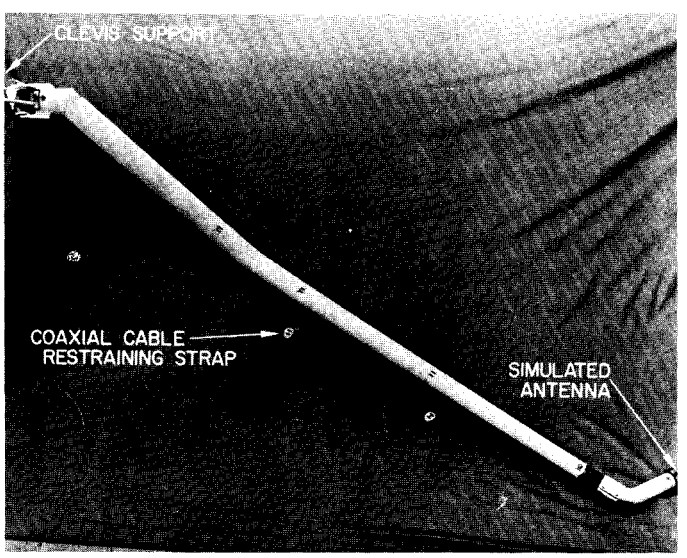

(b) Cable restraining straps

Fig. 63. Antenna A mechanism type approval vibration failures

With the type approval program successfully completed (as previously reported), three sets (three devices per set) of flight hardware have been flight acceptance tested and delivered to bonded stores. These sets are for the SC-1, SC-2, and SP-1 (flight spare) vehicles.

K. Reliability, Quality Assurance and System Test

1. Reliability

a. A priori reliability estimates (system and subsystems). For the flight and landing phases, the estimated *a priori* reliability of the A-21 spacecraft is 0.805; this estimate did not change during this reporting period. For the first 80-hr lunar phase, the system *a priori* reliability estimate decreased from 0.945 to 0.913. The system *a priori* reliability for the first lunar month decreased from 0.662 to 0.521. The decrease in both lunar phases results primarily from a re-evaluation and subsequent decrease in the reliability estimate of the electrical power subsystem during lunar operation.

b. Reliability estimates and growth based on test data. Reliability estimates of subsystems based on current test data show an increase for the telecommunications subsystem (0.183 to 0.800) and the electrical power subsystem (0.512 to 0.619). The increase in telecommunications reliability is primarily a result of the addition of 200 hr of transmitter operation and 700 hr of receiver operation without failure. The electrical power reliability increase is attributed to 125 hr of failure-free central power control test time.

A decrease in reliability was experienced by the flight controls subsystem (0.330 to 0.045). This was caused by a failure during a recent RADVS test.

Additional test data generated no substantial change in the reliability estimate of the data processing subsystem (0.976), command data subsystem (0.990), structures subsystem (0.976), mechanisms subsystem (0.281), and propulsion subsystem (0.113). The primary cause for the low propulsion subsystem reliability is the poor vernier engine test performance. This point is illustrated by noting that if the vernier engine performed at the level estimated at design *(a priori)* the propulsion subsystem reliability would be approximately 0.91, whereas test data on the vernier engine generate a reliability of 0.113 for the propulsion subsystem.

In computing the preceding estimates, *a priori* reliability is used when test data for a particular unit are not available.

c. Equivalent mission cycle program. Test data from various sources are continually collected, examined, and converted into equivalent mission cycles (EMC) for the purpose of spacecraft reliability demonstration. Table 25 summarizes the current status of EMCs and failures. As of this date, the EMCs and failures primarily reflect type approval and flight acceptance test data.

Table 25. Current status of equivalent mission cycle program based on test data

Units	Equivalent mission cycles	Mission failures[a]
Central decoder	0.1	0.1
Signal processing auxiliary	0.2	0
Central signal processor	0.2	0
Thermal control and heater assembly (Compartment A)	1.3	0
Transmitter	1.0	0
Planar array antenna	0.8	0
Roll actuator	0.2	0
Solar panel	0.7	0
Central power control	2.1	0
Separation, sensing, and arming devices 1, 2, 3 (Total of three)	1.0	0

[a]Weighted failures per Hughes Aircraft Company *Surveyor* Quality Assurance Plan, Volume 2, Reliability, Part II, Section G, 4c.

d. Electropyrotechnics. Hi-Shear Corporation is proceeding with the developmental testing of the main retrorocket separation device. It has been found necessary to use higher strength material for the more highly stressed parts with some compromise to nonmagnetic properties.

The production lot of pyrotechnic switches from Atlas Chemical Industries is being remade following a failure in the reliability test program. An initiator was expelled from one switch body when it was fired. Dudding of another initiator caused by improper test implementation also occurred. Strengthening of the bond between the initiator and switch and a requirement of 100% Hughes Aircraft Company source inspection of the bonding process are being imposed for the new lot.

Reliability margins testing as a means of reliability verification is being applied to four programs:

(1) Atlas – pyrotechnic switches (140 were fired in margins test with one failure; lot rejected).

(2) Hi-Shear – separation device.

(3) Holex – helium valve squib.

(4) Ordnance Associates – nitrogen valve detonator (70 fired in margins test with 6 failures; lot rejected). Pinpuller squib, shock absorber positive lock squib, and pressurized gas power supply release valve squib (130 fired in margins test with no failures).

Margins testing, sometimes called narrow limit testing, is a combination of attributes and variables testing in that it is a test for an acceptable failure percentage, as well as a test for acceptable parameters of the population distribution consistent with the specified reliability and confidence level. It takes advantage of the immediate decision process used in attributes testing plans and, at the same time, uses the smaller sample sizes required for variables testing. Test limits are placed on individual characteristics by considering required reliability, confidence, amount and number of stresses applied, sample size for each test condition, and the worst acceptable frequency distributions for individual measurements.

Two unresolved problems of the last report – increased bridgewire resistance of one squib and reduced insulation resistance of another – remain under investigation. These parameters are being closely monitored on two units as they continue through type approval testing. The final step in TAT is to fire these units, at which time it will be verified if performance or safety is degraded.

A summary of pyrotechnic tests is given in Table 26. Although there have been failures and discrepancies serious enough to report and cause lot rejection and/or indicate marginal reliability, none of these conditions in flight would positively cause mission failure.

The following is a summary of output tests conducted by Ordnance Associates.

(1) *Ball travel tests on detonators* (Fig. 64)

Sample size	10
Failures	0
Specified range (desired but not required)	0.5 to 0.75 in.
Observed range	0.514 to 0.7535 in.
Estimated test error (cumulative)	0.05 in.
Mean	0.65 in.
Standard deviation	0.067 in.

(2) *Brissance (dent test) on detonators*

Sample size	101
Failure of fired units	0

Table 26. Pyrotechnics test summary

Type	Vendor	Quantity fired				Results
		Lot size	Previous report	To date	Future	
Pinpuller/shock absorber squibs	Ordnance Associates	1000	199	250	251	No change except additional firings.
Mast extension gas release squibs	Ordnance Associates	250	54	57	135	No change except additional firings.
Attitude jet gas dump squibs	Ordnance Associates	245	116	135	110	No change.
Helium valve squibs	Holex	389	0	0	131	No change.
Separation device squibs	Hi-Shear	845	0	0	755	New contract.
Pyrotechnic switch squibs	Atlas	541	0	200	~500	One failure in margins tests; lot being remade.
Retro-rocket igniter squibs	Hi-Shear	Common lot with *Dyna-Soar* squibs; results based on *Dyna-Soar* tests				No change.
Pinpullers	Houston Fearless	363	0	0	51	No change.
Mast extension gas power supply	Conax	40	0	3	20	Three failures in type approval testing; failure analysis in process
Nitrogen valve	Conax	58	12	12	~25	Minor failures that do not affect mission success.
Separation devices	Hi-Shear	307	0	0	244	New contract.
Helium valve	Holex					These valves are reworkable after firing (squib and nipple replacement). Many have been and will continue to be tested as part of the vernier engine program. Eight valves will be tested as a part of the squib type approval testing program.

Observed range	0.032 to 0.068 in.
Mean	0.049 in.
Standard deviation	0.0081 in.

There are no specified test limits for this test. It is performed merely to detect possible low-order firings. The histogram (Fig. 65) is smooth, unimodal, and appears to be quite normal.

(3) *Peak output pressure in 1 in.³ bomb of power supply release valve squib*

Sample size	54
Failures	0
Specified range (desired but not required)	200 to 500 psi
Observed range	226 to 404 psi
Estimated test error	20 psi
Mean	323 psi
Standard deviation	40 psi

The histogram (Fig. 66) indicates a smooth, normal, unimodal distribution.

(4) *Peak output pressure in 1 in.³ bomb of pinpuller squibs*

Sample size	121
Failures	0
Specified range (desired but not required)	200 to 500 psi
Observed range	204 to 488 psi
Estimated test error	30 psi
Mean	347 psi
Standard deviation	44 psi

The histogram (Fig. 67) indicates a smooth, normal, unimodal distribution.

e. Additional reliability activities. A current summary of reliability test data generated by unit, subsystem, and system tests is provided by Table 27.

To facilitate immediate and accurate systems test data collection and reduction, the following computer program has been developed. System test commands and real time data are recorded on magnetic tape at the test facility. The magnetic tape is subsequently converted to a punched paper tape compatible to the Monrobot XI computer. Data on the modified tape is reduced by the

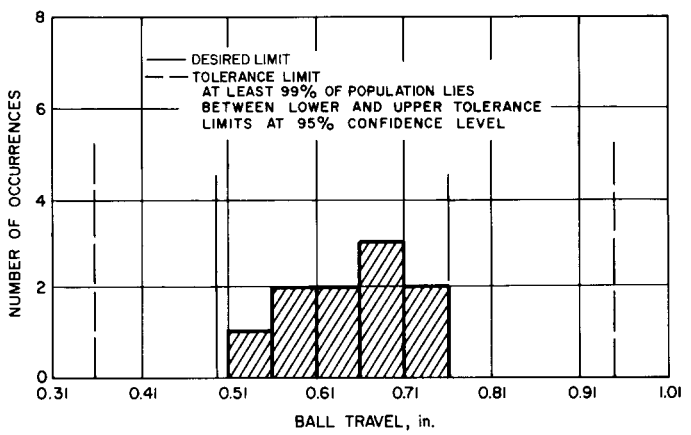

Fig. 64. Distribution of detonator ball travel

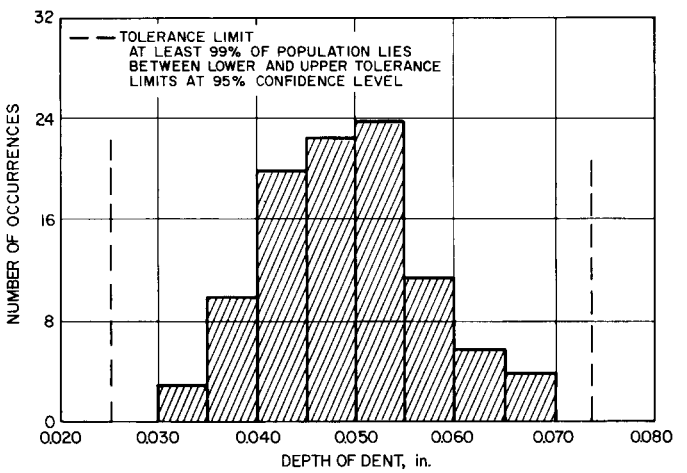

Fig. 65. Distribution of detonator dent depth

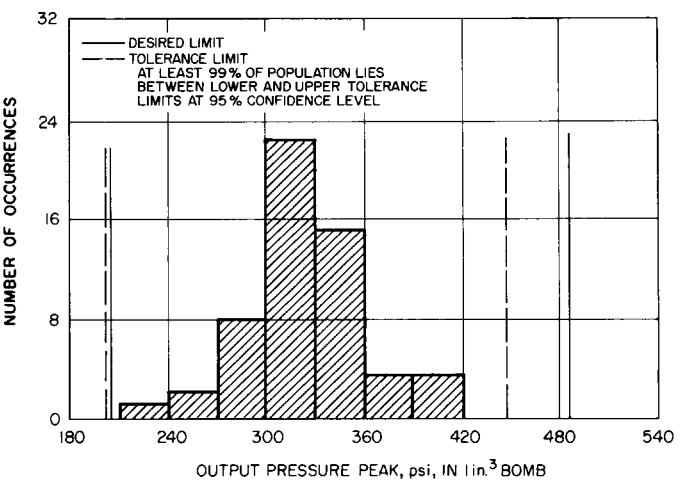

Fig. 66. Distribution of release valve squib pressure peak

computer, and a report accumulating time and cycles by unit is generated. Reliability representatives provide a list of failures, unit serial numbers, and environmental conditions pertinent to the test data.

Table 27. Reliability test data summary

Unit	Time, hr	Cycles	Failures
Central command decoder	691	607	1
Engineering signal processor	527	2347	0
Auxiliary engineering signal processor	101	96	0
Central signal processor	621	559	1
Transmitter	465	1027	2
Receiver	1130	987	2
Flight control sensor group	660	2688	2
Altitude marking radar	48	183	0
Radar altimeter and doppler velocity sensor	28	57	1
Roll actuator	40	90	0
Central power control	487	942	3
Separation, sensing and arming devices		7	0
TV Camera 4 and auxiliary	51	146	1
Main retro-engine		15	0
Solar panel	201		0
Planar array antenna	80		0
Signal processing auxiliary	25		0
Thermal control and heater assembly	81		0

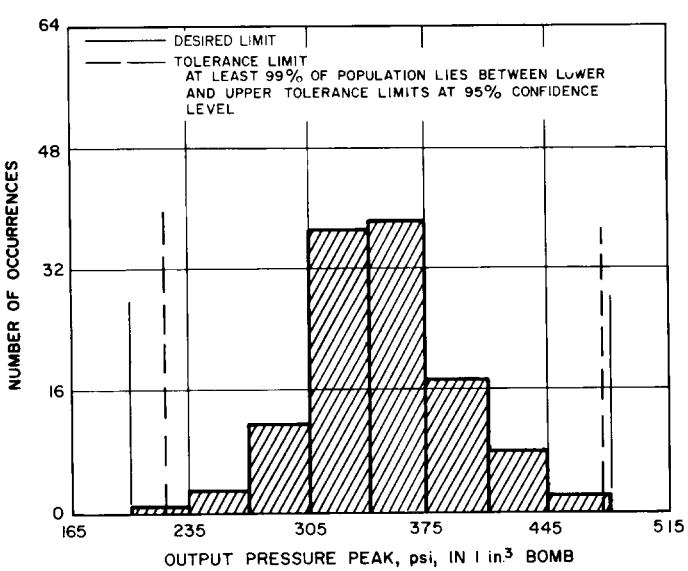

Fig. 67. Distribution of pinpuller squib pressure peak

Gyro non-g sensitive drift rate analyses of the first-buy gyros have indicated that the variability of non-g sensitive drift rate was excessive with respect to the 1 deg/hr requirement. A recent analysis, based on 25 gyros of the second delivery, indicates that the expected percentage of gyros that will be within specification with respect to non-g sensitive drift rate is greater than 99%. This percentage increases to almost 100% for the last seven gyros (S/N 45 to 51). These estimates were based on normal curves with mean and variance equal to that obtained from the sample (0.041 and 0.336 deg/hr for the group of all gyros and —0.027 and 0.215 for the last seven gyros). The normality assumption was preceded by a goodness-of-fit test; the equating of sample and population parameters appears justified because of the large sample size. Frequency histograms and fitted normal curves are shown in Fig. 68.

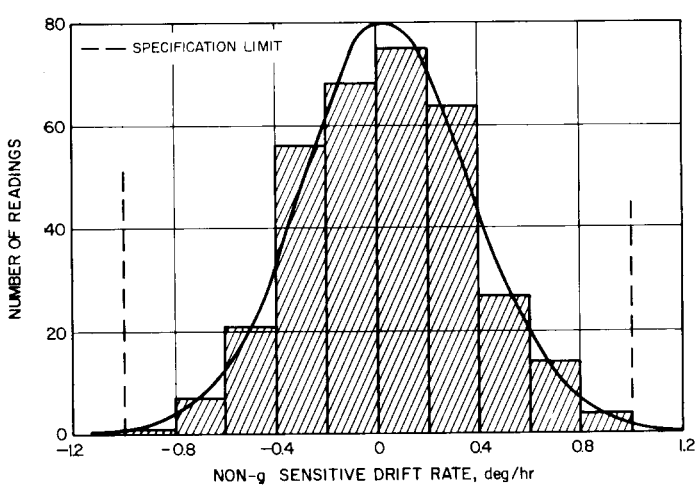

(a) Gyros 27 to 51

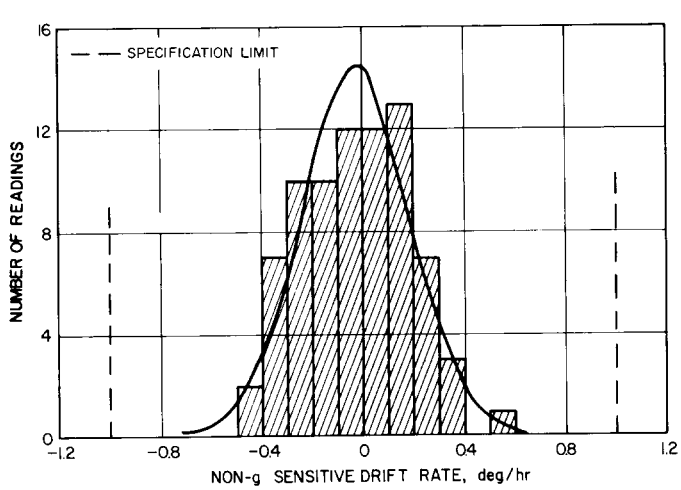

(b) Gyros 45 to 51

Fig. 68. Gyro non-g sensitive drift rate

f. Subcontractor status

(1) *Systron-Donner Company (linear force balance accelerometer).* The complete order of 13 fluid-damped accelerometers was delivered to Hughes. Three were rejected during acceptance testing. Two units, S/N 9250F and 9251F, failed the tests; analysis revealed melted solder inside the accelerometer case and oil leakage caused by excessive heat, estimated to be approximately 450°F. The diaphragm, which allows for oil expansion and contraction due to temperature changes, was permanently distorted as shown in Fig 69a. The normal position of the diaphragm is flat at ambient temperature (78°F) as shown in Fig. 69b.

The units are subjected to heating to 180° F both in the assembly process at Systron-Donner and in the incoming acceptance test at Hughes. A survey of both processes indicated that overheating to the extent that produced the failures is most improbable. How the two units received the overheating has not yet been determined.

When a unit fails because of excessive temperature, oil leakage occurs and air bubbles form in the oil reservoir. The presence of air bubbles in the vicinity of the accelerometer mechanism will cause highly erratic performance or catastrophic failure which is readily detected during testing prior to assembly in a spacecraft. This eliminates the possibility of a unit defective in this manner being put on a spacecraft.

Nineteen accelerometers (9 air damped and 10 fluid damped) have accumulated a total operating time of 2245 hr and 5671 on-off cycles at Hughes without a relevant failure.

(2) *Kearfott* (gyro). Twenty-nine gyros (second buy) have been delivered to Hughes. A summary of the units tested at Hughes is as follows:

Accepted	18
Rejected	11
Acceptance yield at Hughes	62%

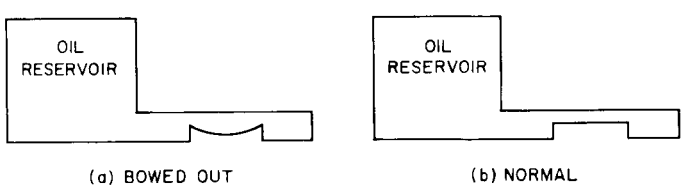

Fig. 69. Accelerometer diaphragm position

Four of the last six gyros delivered to Hughes were rejected for failure to meet specifications during acceptance test — two for vector mass unbalance, one for non-g sensitive drift, and one for torquer scale factor. These failures are awaiting verification by the vendor.

(3) *Santa Barbara Research Center* (Canopus sensor). The RCA photo-multiplier tube passed the qualification tests and the liens were removed from the equipment.

The reliability demonstration test procedure is almost completed and should be submitted to Hughes for approval in April. The proposed plan is to subject two units, S/N 3 and S/N 7, to a total of 27 mission profiles each of 66 hr.

(4) *Thiokol/Elkton and Bristol Divisions (retro-engine and safe and arm device).* Recent engine successes have increased the reliability estimate for the engine, less safe and arm device, to 0.878 from 0.869 at 80% confidence. The reliability goal, including the safe and arm device is 0.97 with 80% confidence. Evaluation of the safe and arm device, including 100,000 failure-free operational cycles, has been concluded by Thiokol/Bristol, the vendor. At the present time qualification test hardware is being fabricated by both subcontractors.

During a reliability audit of Thiokol/Elkton on February 11 and 12, it was mutually agreed that probabilities associated with normal engine tolerance limit variations would be calculated by Thiokol/Elkton using qualification test firing results. These values will be used as the basis for compliance with Hughes performance requirements expressed in terms of allowable sigma variation, and will also satisfy the requirement for variables data analysis. Thiokol/Elkton is currently investigating the methodology and parameters to be investigated for these analyses.

Documents reviewed by Hughes during the current reporting period include those for the safe and arm acceptance test and qualification test programs, the engine qualification test program, and the safe and arm reliability prediction and failure modes analysis. Comments on each of the above documents have been submitted to the two subcontractors.

The method of reliability calculation of the retro-engine system has been simplified to the extent that the 20% confidence value determination has been deleted from the reliability growth curves.

Reliability growth curves have been updated to show four values for each point estimate. These include required reliability, *a priori* predicted value, and nominal and lower 80% confidence estimates based on test data. The failure tabulation, used as the basis for reliability growth assessment, has been revised at Hughes' request to include both the date and the reason for configuration changes resulting from test firings.

(5) *Thiokol/RMD (vernier propulsion system).* At the termination of this subcontract, the duty mission reliability of the vernier engine subsystem (0.005) was unchanged from the value given in the last report period. The flight reliability estimate, 0.121, was also unchanged. A detailed study of failure types reported by RMD during its testing program between October 1963 and February 1964 was performed by Hughes to determine significant areas of unreliability remaining in the vernier engine program. During the 4-mo period, 95 development tests were performed. The results of the investigation are shown in Table 28. It should be noted that the data does not discriminate between firing-test, pre-test, or post-test failures.

From the data, the following critical valve performance probabilities are calculated.

(a) Probability of valve leakage during a test $= \frac{63}{83}(100) = 0.76.$

Leakage reliability $= 1 - 0.76 = 0.24.$

(b) Probability of valve mechanical defect (such as an incorrect part installation or wrong part installed) which would cause a

$$\text{malfunction} = \frac{25}{44} = 0.57.$$

Valve functional reliability $= 1 - 0.57 = 0.43.$

(c) Probability of successful valve performance (reliability) during any given test $= (0.24)(0.43) = 0.103.$

(6) *Ryan radar altimeter and doppler velocity sensor (RADVS).* Results of a Class C (packaging,mechanical and product design stage) reliability analysis of the RADVS on March 2, 1964, indicate a probability of success of 0.9995 for the terminal phase of the *Surveyor* mission and an overall reliability of 0.9982 for the total mission. This represents a decrease from the last Class B (developmental stage) reliability analysis report of April 26, 1963 which indicated 0.9998 and 0.9985 for the terminal phase and total mission probabilities, respectively. The small decrease in reliability is due in part to more accurate stress and parts data utilized in the Class C analysis.

Recommendations for reliability improvement through component reduction and derating resulting from a Hughes failure mode audit are under

Table 28. Vernier system failure data

Type of failure reported	Number of times failure reported on valves				Valve failure total	Other component failure total[e]	Grand total reported
	TV[a]	SOV[b]	TWV[c]	SV[d]			
Leakage	48	10	5	0	63	20	83
Mechanical defect (e.g., torn or deformed O-rings, cracked nozzle, etc.)	12	9	0	1	22	19	41
Wrong part installed	3	0	0	0	3	0	3
Broken part	0	0	0	0	0	7	7
Parameter out of tolerance	3	0	0	0	3	2	5
Electrical	1	0	0	0	1	0	1
Totals	67	19	5	1	92	48	140[f]

[a]Throttle valve (pintle) — three used in system.
[b]Shutoff valve — three used in system.
[c]Three-way valve — three used in system.
[d]Squib valve — one used in system.
[e]Includes thrust chamber, fluid regulator, and quick disconnects.
[f]Value reported is based on 95 tests performed during this period.

evaluation by Ryan to determine which recommendations should be incorporated in the RADVS.

With regard to thermal–vacuum outgassing of Hysol 12007A and B (*Space Programs Summary No. 37-26*, Vol. I), Ryan has been granted approval to use the material because it is difficult to obtain an acceptable substitute and the material is acceptable for the transit phase of the *Surveyor* mission. Hughes is presently developing a substitute epoxy freeze coating to be incorporated in the RADVS effective on S/N AM-5. The isoelastic material, Viton A, used on the antenna septum and mounting pads, was found to be incapable of withstanding temperatures below −50°C because of hardening which resulted in loss of vibration damping properties. With no substitute material available, investigation is in progress at Hughes to determine a solution via active thermal control, structural modifications to alter the vibration spectrum, or an alternate damping method.

A list of apparent discrepancies between the RADVS bill of materials and Hughes list of approved parts and materials is currently undergoing investigation to determine necessary action. The only outstanding RADVS failure occurred at Hughes on the klystron power supply modulator QA-1 and is presently undergoing failure analysis at Ryan. The power supply voltages were out of regulation and the output power on all beams was an average of 25% below specification during test in the Space Environmental Simulation Laboratory. Two failure reports are under analysis.

(7) *Vector (subcarrier oscillator).* An *a priori* reliability prediction of 0.9992 on the new procurement was reviewed by Hughes and compared favorably with the previous estimate of 0.9983 on the old procurement. An estimate based on test data was rejected because the two failures accounted for were not realistic in terms of the actual number of failures experienced. The vendor was requested to furnish an updated reliability estimate based on the agreed total of five failures to date.

Failure analysis by Vector of the 14 subcarrier oscillators (SCO) returned on the previous procurement resulted in the following changes to the new units to correct the basic problems of frequency drift and output voltage variations caused by shelf life.

(a) Seven deposited-carbon resistors were replaced with metal film because of their greater stability under temperature cycling and resistance to moisture.

(b) All components were subjected to 250 hr of aging at 200°C; only semiconductors had been aged previously.

(c) Semiconductor aging time and temperature were increased from 100 hr at 100°C to the requirement in (b) above.

(d) Finished SCOs were subjected to aging under power for 120 hr at 80°C; no aging was performed on the original procurement.

(e) A zener diode regulator was incorporated in the output amplifier.

To date 69 units tested at Hughes after an average in-house time of 3 mo have not experienced any shelf-life problems.

Thirty-seven SCOs failed to meet the low-pass filter requirements when measured at the 3-db points using a sinewave input. Failure analysis performed by Vector resulted in modification of these units to incorporate a temperature cycled tantalum capacitor in the input filter circuit to ensure stability.

A total of five SCO failures on the new procurement, other than low-pass filter problems, have been experienced during subsystem tests at Hughes. Two of these failures were catastrophic with no output from the SCOs and three were center frequency shifts beyond the specification requirements. Complete technical diagnosis is in progress through a joint effort between Hughes and Vector and a failure review is to be conducted at the vendor's facility.

(8) *Magnetic Research (magnetron modulator).* The magnetron modulator performed satisfactorily during Hughes evaluation tests of a breadboard model and during type approval tests. Production has begun in the new procurement. The vendor has been requested to submit an updated reliability prediction based on the new design.

g. Materials and process studies

(1) *Thermal–vacuum testing.* Six additional samples of copper clad laminates submitted by Ryan Electronics are in the process of being tested in the thermal–vacuum environment at 260 ± 5°F. The materials represented by the samples are intended for use on the radar altimeter and doppler velocity sensor, provided the characteristics are determined to be suitable.

(2) *Thermal control coatings.* Thermal–vacuum and ultraviolet exposure test results obtained for three white organic thermal control paints are given in Table 29.

Several other paints were investigated to determine their suitability for the lower alpha characteristic which is required for the thermal switch radiators. Aluminum oxide paint was found to be unsatisfactory. However, test results using a paint with a composition of sintered aluminum oxide resulted in an initial alpha equal to 0.1, and after 500 solar hr equivalent the alpha was equal to 0.31. Test results using Lethafrax as a pigment are also under investigation.

(3) *Inorganic paint application.* Extensive test results indicate that 0.012 in. is the maximum surface thickness that should be specified for a coat of inorganic paint. If the surface coat is greater than 0.012 in. peeling will result. This thickness results in an absorptance of 0.13.

(4) *Procedures for touch-up and cleaning of white inorganic painted surfaces.* For touch-up of small areas no larger than 0.3 in.^{2} use of the following procedure is recommended:

(a) Blow away loose powder with a jet of dry nitrogen gas at a gage pressure of 10 psi.

(b) Apply a fresh coating of inorganic white paint using a camel hair brush.

(c) Cover painted area loosely with lintless tissue so that it does not touch the wet coating. (The tissue protects the wet surface from dust.)

(d) Allow the coating to dry.

(e) After drying, and with the tissue still in place, heat the localized area to approximately 260°F for 10 min with a hot air blower. Monitor the temperature with a thermometer placed under the tissue close to the repaired area.

The resulting thermal–physical characteristics of the touch-up using this procedure are shown by the test results presented in Table 30.

The following procedure was developed to remove blemishes such as fingerprints, grease, and metal markings from white inorganic paint:

(a) Prepare a paste consisting of alumina powder (100 grit) and de-ionized water. Rub the paste into the blemished area with a cotton swab for 1 min using a circular motion. Repeat this procedure two more times using fresh paste each time.

(b) Rinse the surface with a jet of de-ionized water for at least 1 full min.

(c) Cover surface with lintless tissue and allow to dry.

(d) With the tissue in place, heat the cleaned area with a hot air blower to 260°F, as described in the touch-up procedure.

The thermo–physical properties before and after cleaning are shown in Table 31.

(5) *Removal of white inorganic paint.* The process for removing inorganic white paint has been improved and is now as follows: Immerse the surface to be cleaned into a 1% solution of sulfuric acid at 195°F and hold for 1 min. Light brushing will remove the paint. Rinse thoroughly in warm tap water and three times in hot distilled water. This procedure

Table 29. Properties of three white organic paints

Material	48 hr at 10^{-6} Torr at 260°F		Thermal radiative properties			
			Initial		After 350 solar hr equivalent of ultraviolet	
	De-posits	Weight loss, %	α	ϵ	α	ϵ
Acrylic tripolymer — TiO_2 (American Cyanamid Co.) 4.0 mils, cured 1½ hr at 250°F	None	1.0	0.22	0.84	0.28	0.85
No. 202-A10 white velvet coating acrylic lacquer (3M Co.) 3.5 mils, cured 1½ hr at 250°F	None	5.6	0.22	0.90	0.31	0.88
No. 302-A10 white velvet coating acrylic enamel (3M Co.) 4.1 mils, cured 1½ hr at 250°F	None	6.7	0.23	0.91	0.43	0.90

Table 30. Thermal physical properties of touched-up white inorganic paint

Sample	Absorptance, α		Emittance, ϵ	
	Before chipping	After touch-up	Before chipping	After touch-up
1	0.16	0.14	0.91	0.93
2	0.16	0.15	0.92	0.93
3	0.16	0.15	0.91	0.93

is intended only for use when the painted surface has no assemblies attached.

h. Specification status. The following specifications will require modification as a result of the activities discussed.

(1) *Specifications 988807, 988809, 988835, and 988837 (transistors).* Before complete qualification of the two new vendors can be completed, two parameter problems involving gain-bandwidth characteristics and a measurement correlation problem in matching pairs must be clarified.

(2) *Specifications 988352 and 988353 (stepper motors).* Qualification of the stepper motor has been achieved by a design modification. Previous difficulties in meeting qualification requirements involved problems of lubrication in the space environment. Properly sealing the motors, using fine molybdenum disulfide powder as a lubricant and a slight modification of the clutch provided the solutions to previous deficiencies for qualification.

Table 31. Thermal physical properties of cleaned white inorganic paint

Sample	Absorptance, α		Emittance, ϵ	
	Before soiling	After cleaning	Before soiling	After cleaning
1	0.15	0.16	0.91	0.91
2	0.16	0.16	0.92	0.92
3	0.17	0.15	0.92	0.92

i. Failure analysis and review. During the reporting period, five failure review board (FRB) meetings involving four different control items were held. Action was completed on three of the items – the central power control, roll actuator, and antenna solar panel positioner. The battery, which failed during type approval vibration (see Section F), will require special testing to determine the best redesign to prevent future failure.

A summary of failures reported is shown in Tables 32 and 33. FRB actions resulting from analysis of this summary are presented below:

Table 32. Unit level failure summary

Unit	Number	Total failures to date	This period	Repetitive	Primary failure	Action completed	Action pending	Delinquent
Flight control sensor group	235000	51	6	3	35	34	17	0
Antenna/solar panel positioner	236400	17	2	0	2	17	0	0
Engineering signal processor	233350	15	2	1	4	11	4	0
Control command decoder	232000	8	0	0	1	7	1	0
Central signal processor	232200	8	1	0	3	4	4	0
Central power control	263600	6	1	0	6	5	1	0
Command receiver	231900	3	0	0	3	3	0	0
Roll actuator	235900	4	1	0	0	4	0	0
Altitude marking radar	232600	3	3	0	3	1	2	0
Wiring harness Compartment A	264030	3	1	0	2	2	1	0
Wiring harness Compartment B	264032	4	3	2	4	0	4	0
Gas supply attitude jet	235600	2	2	0	0	2	0	0
Antenna mechanism omnidirectional Antenna A	236900	6	3	0	0	3	3	0
Signal data converter	232908	3	3	0	3	0	3	0
Klystron power supply modulator	232909	3	3	0	3	0	3	0
Miscellaneous		48	3	0	24	44	4	0
Total		184	34	6	94	137	47	0

(1) *Central power control*

Problem: The boost regulator had catastrophic failure of several parts.

Analysis: Q4 in the series regulator shorted which caused several other parts to fail. Q4 failed because it is overloaded when power is applied to the unit. During normal operating conditions, once power is applied, this over-stress would not occur.

Solution: The transistor was changed to increase the V_{CEO} rating from 40 to 80 v and a 10-ohm resistor was placed in the collector circuit to reduce current surges.

(2) *Roll actuator*

Problem: The feedback potentiometer was 180 deg out of phase, causing two failures in system tests.

Analysis: Failure was attributed to the testing procedure at unit level. The built-up test position at unit level does not provide a closed-loop test, resulting in the possibility of reversing polarity when connecting the jacked-in cable, which has no indicated polarity.

Solution: Corrective action was to revise the unit level test procedure to prevent recurrence.

(3) *Weld failures of antenna solar panel positioner*

Problem: During vibration testing of the SD-4 type approval test, the fillet-weld of the support arm failed.

Analysis: The failure was attributed to corrosion from entrapped processing fluids, inappropriate joining methods, and poor welding technique.

Solution: Corrective action was to use only butt-type welds for critical load joints with 100% penetration and radiographic inspection and use of fillet type welds for shear-only application at low stress level with root penetration mandatory. Test samples are required for all critical weld joints. The test samples will be subjected to radiographic inspection with both static and fatigue tests to verify structural reliability.

Table 33. System level failure summary

Unit	Number	Total	Human error	Engineering	STEA induced	Parts	Workmanship	Pending	Not a failure
Flight control sensor group	235000	19	3	4	0	2	1	9	0
Engineering signal processor	233350	8	1	3	0	0	2	2	0
Central signal processor	232200	5	2	1	0	0	1	1	0
Central power control	263600	5	1	1	2	0	0	1	0
Engineering mechanisms auxiliary	263500	5	2	1	1	0	0	0	1
Wiring harness Compartment B	264032	4	0	0	0	2	2	0	0
Central command decoder	232000	3	0	1	1	0	1	0	0
Approach television camera	233102	3	0	1	0	1	1	0	0
Altitude marking radar	232600	3	0	0	0	0	1	2	0
Wiring harness Compartment A	264030	3	1	0	0	2	0	0	0
Signal data converter	232908	3	1	0	0	1	0	1	0
Klystron power supply modulator	232909	3	0	0	0	2	1	0	0
Auxiliary engineering signal processor	264900	3	0	2	0	0	0	1	0
Receiver	231900	2	0	2	0	0	0	0	0
Miscellaneous		9	1	4	0	1	1	2	0
Total		78	12	20	4	11	11	19	1

(4) *Battery*

Problem: After vibration testing, the output voltage was low. Disassembly of the battery revealed broken plates in four cells.

Analysis: The probable cause of failure of the plates was vibration normal to the plane of the plates.

Solution: The corrective action is to redesign the battery structurally to increase the strength of the plates. In addition, improved test methods and instrumentation to detect plate breakage during vibration were recommended.

j. Reliability assurance test program

(1) *Accumulation of equivalent mission cycle (EMC) data.* During this period, the formulation and establishment of the method of collecting EMC data were implemented. The reliability assurance test director acted as an advisor to the EMC committee and established the relationship between conditions during testing (considered for EMC) and actual mission environmental profiles. Although the present rate of accumulation of EMC data indicates that the predicted accumulation of data from developmental test (one EMC) will not be met, it is apparent that the predicted one-half EMC from flight acceptance testing will be exceeded (probably greater than two EMC from this source) and will make up for the loss of developmental test EMC. Present predictions are that the necessary seven EMC will be accumulated from various test sources.

(2) *Program implementation.* Cable interconnection lists were completed for the signal processing auxiliary, low rate data auxiliary, engineering signal processor, central command decoder, central signal processor, altitude marking radar, and the flight control sensor group. Design of cables for these units has started. Completion of design and procurement of necessary connectors and wire for these and the remainder of the units will be accomplished during the next reporting period.

Definition of the fixtures for testing the transmitter, command receiver, thermal switches, central command decoder, central signal processor, engineering signal processor, engineering mechanism auxiliary, central power control, low rate data auxiliary, flight control sensor group, and the altitude marking radar started during this period and is 75% complete. Completion of design definition for these and the balance of the reliability assurance test units will be accomplished during the next reporting period.

(3) *Detailed test procedures.* Preparation of detailed test procedures is continuing and is presently 20% complete. Procedures will be completed by September 15, 1964.

2. Quality Assurance

a. Documentation. The documents that specify standard practices for *Surveyor* fabrication have received a major upgrade. A system for standard disposition of components in various categories has also been documented and has facilitated material review and disposition actions.

b. Quality of product. Some of the more significant activities in controlling and improving quality are discussed in the paragraphs which follow. Certain technical problem areas mentioned here are discussed in more detail elsewhere in Section IV.

(1) *Quality audit.* A system whereby *Surveyor* quality assurance personnel regularly audit all project work areas has been implemented.

(2) *CDC shipment to Goldstone.* A substantial effort was exerted to achieve the quality verification necessary prior to shipment of the command and data handling console to the Goldstone DSIF station.

(3) *Handling of thermal control surfaces.* Two training sessions were conducted in March to acquaint laboratory and shop personnel with the protection and handling required in connection with these critical surface finishes.

(4) *System test screen room.* Steps were taken to improve air cleanliness, including filter and inlet relocation and increasing the air pressure, in the rf screen room employed in system testing.

(5) *Cannon D connectors.* Failure prevention is being studied utilizing JPL experience with the failure modes of these connectors.

(6) *Atlas connectors.* Excessive pin retention failures have been encountered with these connectors and special efforts, including rework, have been required to obtain them on an adequate schedule.

c. Review board actions. Material review board actions totaled 149, and preliminary review board actions 454, during the report period. An increasing proportion

of preliminary board actions results from improved procedures facilitating more material dispositions at inspection rather than at higher project levels.

d. Quality audits of **Surveyor** *subcontractors.* The subcontractor audits utilize the checklists shown below.

Number	*Description of checklist*
1	Administration inspection control
2	Measuring and testing equipment
3	Control of subcontractual supplies
4	Inspection during manufacture
5	Special processes
6	Inspection of completed supplies
7	Sampling inspection
8	Indication of inspection status
9	Nonconforming supplies
10	Government property
11	Evidence of approvals
12	Storage
13	Transportation
14	Quality control records
15	Corrective action
16	Drawing and change control
17	Product inspection and test

Santa Barbara Research Center. The audit covered checklists 1, 3, 6, 7, 8, 10, 11, and 12; all elements within these lists were found to be satisfactory.

Ryan Electronics. Acceptable elements were noted for all checklists except lists 10 and 13 which were not audited at this time and list 15, which was found to be marginal in that no corrective action records or written feedback system (other than verbal) were being maintained as specified in the Ryan quality control manual. This problem has since been corrected. Type approval testing is at a standstill until resolution of vibration problems.

Systron-Donner. All fabrication has been completed. Systron-Donner is currently reworking two returned units. A complete audit of their quality system was conducted and two areas were found to be marginal (checklists 8 and 15). Company management was notified of deficiencies.

Vector. A quality audit of all check list items was performed. The results show good controls over the manufacturing and testing areas. Eighteen units were tested during this audit and accepted.

Thiokol, Elkton Division. An audit of the Elkton facility, covering checklists 1 through 7, shows a good quality control system. A program is now under way to update their inspection plan. This plan is due at Hughes in April 1964.

Hi-Shear. A draft of the *Surveyor* inspection plan was submitted to Hughes for approval. A review of this submittal was performed and the plan was found inadequate. The plan was returned to Hi-Shear with comments.

Kearfott. Results of a recent audit covering checklists 1 through 9 show an adequate quality control system. Corrective action has been taken to avoid contamination of the gyro fluid, which was a former problem.

Bell and Howell. A quality audit shows that this subcontractor had not submitted an inspection plan as required. An inspection plan is being written and should be delivered in April. Checklists 1 through 5 were reviewed and found adequate.

Ordnance Associates. Government source inspection has been requested on squibs from this subcontractor.

Atlas Chemical. A failure was experienced by this subcontractor as a result of the squib blowing out of the switch body. An audit shows that the cause of the failure was determined and corrective action taken. Corrective action consists of a redesign of the crimp area to employ a straight, rather than tapered, shoulder for additional strength. Hughes source inspection will witness the crimping operation on future manufacturing lots. The failed lot was not accepted. Checklists 1 through 9 were reviewed and the subcontractor's quality system for these elements was found adequate.

Electric Storage Battery. The vendor is updating flow charts and operation sheets to reflect design changes as a result of structural failures in type approval vibration tests. Checklists 1 through 10 were reviewed and all but list 8 were found adequate. Corrective action is being taken on list 8.

National Water Lift. An audit shows that National Water Lift quality control is functioning well and that all requirements for *Surveyor* Project are being met.

Heliotek. This subcontractor is adequately performing on *Surveyor* quality requirements, and no problems have been encountered in the delivery of solar cells.

Hughes – Tucson, Arizona. Present and past quality directions given to Tucson were reviewed and resulted in the issuance of a directive that defines work flow at Tucson. Particular emphasis has been placed on proper use of corrective action and feedback reports.

e. Type approval test reviews. The following TAT reviews were conducted and accepted by the TAT review committee during this reporting period:

Thermal control and heater assembly

Landing gear assembly, L-3 and L-4

Separation sensing and arming device

Auxiliary battery control

Central power control

Transmitter

Solar panel

Canopus sensor

f. T-21 Committee. Quality Assurance representation to the T-21 task force committee has been continued to assure quality support and coordination of the T-21 functional and environmental testing.

3. System test

a. T-2 descent dynamics test program. The descent dynamics test program employs a simplified test spacecraft, T-2, on which the vernier propulsion and flight control systems will be tested in vehicle descents from a tethered balloon at Air Force Missile Development Center (AFMDC). The drop test phase of the program will start in the next report period.

The Series 12 tests in which static vernier firings were made with T-2 mounted in a horizontal position were summarized in *Space Programs Summary No. 37-26,* Vol. I; these tests demonstrated: (1) that acoustic coupling contributed substantially to erratic radar performance in the presence of vernier engine noise, and (2) the feasibility of eliminating the problem by use of foamed material as acoustic insulation on the radar antennas. Two additional series of T-2 horizontal tests and preparations for a further series of tests of the flight control system, including the RADVS, in a helicopter installation designated T-2H are summarized here.

Horizontal test firings. With the improvement in radar altimeter and doppler velocity sensor (RADVS) operation as a result of on-site addition of acoustic foam material during the Series 12 tests on T-2, a more complete investigation of acoustic protection was pursued and evaluated during test Series 13 and 14. Polyurethane foam was formed over the antenna backs, including the preamplifiers. Across the front (transmit and receive side) of the antennas, a set of rf-transparent stafoam radomes was installed, with milled cross sections of 1 or 1.5 wavelengths. Since the X-1 and X-2 RADVS antenna did not have skirts completely extending around the antennas, the foam material was formed to provide full skirts to enhance the acoustic attenuation. Fig. 70 shows the doppler velocity sensor (DVS) antenna before and after foam application.

(1) Test Series 13. A RADVS/vernier engine acoustic check was attempted on February 14. The objectives of the tests were to (1) evaluate the polyurethane foam covering on the antennas in reducing acoustic noise during engine firing, (2) determine the amount of polyurethane foam that could be removed from the back of the antennas without degrading the acoustic shielding, and (3) check the reaction of the RADVS to flight-type honeycomb footpads in approximate landing position.

Three firings were planned to accomplish the above objectives. However, in the first of the planned firings, the No. 1 and 3 engines malfunctioned causing damage to the propulsion and instrumentation system. A bulge and rupture in the helium pilot manifold to Leg 3 engine was found. A ¾ × ¼ in. piece was missing from this ¼ in. aluminum tubing about 6 in. away from the propellant inlet. Review of the telemetry data showed a pressure spike of approximately 600 psi

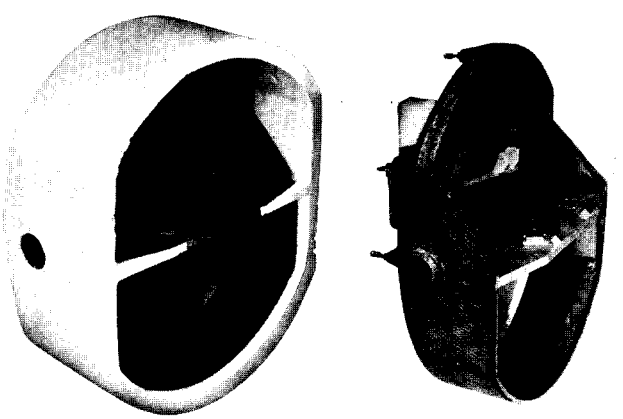

Fig. 70. Stafoam application

at the fuel manifold transducer; however, it is believed that this spike actually was of greater magnitude but had been attenuated by the plumbing before arriving at the transducer. This spike probably reflected a detonation in the helium manifold. Following a 40-hr vacuum flush, a flow check was performed. The pressure reading indicated that the filter at Leg 1 was partially clogged, accounting for the erratic engine performance. At Leg 3 the filter was almost completely clogged. The possible flow was calculated to correspond to only 0.05% of maximum thrust. This small amount of oxidizer flow would be insufficient to ignite the fuel in the concentration present at the nozzle.

When the vernier engines were disassembled and inspected, traces of iron nitrates were found in the injector area. Accordingly, it was decided to return the thrust chamber and injector assembly to Reaction Motors Division of Thiokol for water flow check to assure that the injectors were not clogged.

The repair of damage at Leg 3 was effected by replacing the leads to the propellant and throttle valves, pressure transducer, and air bag inflation terminal board.

(2) Test Series 14. The objectives of this series of tests were the same as those of the previous test series, but also included three-engine operation with instrumentation including preamplifier outputs, propulsion output data, 13 microphones, and five accelerometers. This instrumentation was installed around the RADVS antenna at positions similar to those required during the Series 12 tests reported in the previous issue. For each test the configuration of the system, the RADVS results, and the engine performance are shown in Table 34.

For Test 14-A, the T-2S vehicle (spare for T-2) was positioned in the horizontal firing test stand through bungee cord attachments. The resonant modes of the suspension system were all below 2 cps. The antennas incorporated the 1-wavelength radome (0.89 in.) and were covered with polyurethane on the back. The test firing indicated that all trackers locked up. Upon close examination, it was noted that high rises were experienced in two preamplifier crystal holders. Upon tightening the crystal, the response lowered to an acceptable level. At this time an attempt was made to foam the crystals in place using the same polyurethane as was used on the antennas. Significantly better results were obtained. Using a spare preamplifier, the P2 (90 deg) output was measured, showing a 40 to 45 mv peak rise when excited by a 138-db air horn. After foaming, the rise was 12 to 15 mv. Additional tests provided equally good results; hence it was decided that in future tests the crystals would be foamed in place.

In Test 14-B another firing was attempted during which the klystron power supply modulator (KPSM) and preamplifiers were protected by stafoam boxes and a 1.5-wavelength stafoam radome was used. The firing time was 6.2 sec. and D_1 was the only signal which locked up (for 0.3 sec.). Generally D_2 and D_3 were more sensitive and no problem was observed.

Although Tests 14-C, 14-D, and 14-E were run, all were aborted because of engine malfunction as described in Table 34. Only on Test 14-E were all trackers locked up at engines-off, indicating a KPSM problem with the 2150-v postregulation. This was verified and repaired prior to Test 14-F.

In Test 14-F a landing leg, footpad, and crushable block were installed on the three legs of T-2S. Fig. 71 shows the installation. Engine operation was normal during this firing; however, the D_2

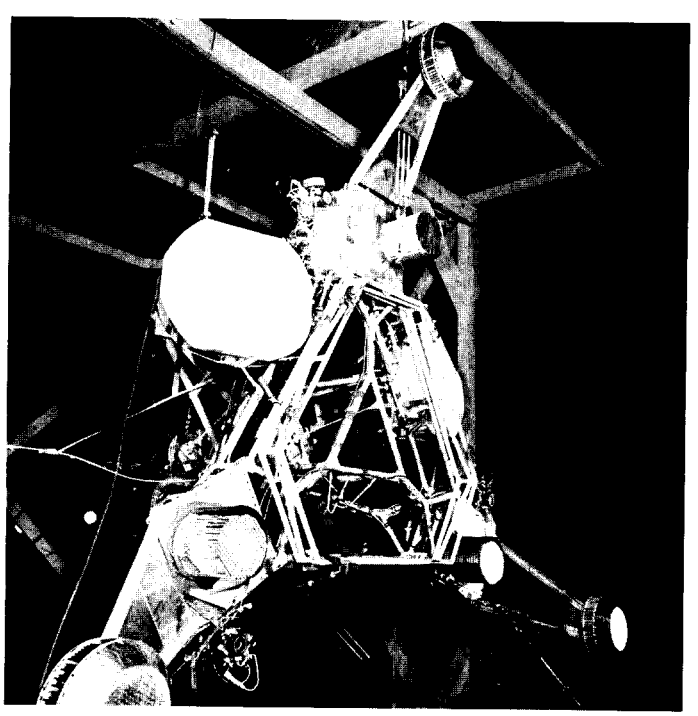

Fig. 71. Test 14-F setup

tracker locked up during the entire engine run, indicating a strong coupling with the simulated landing gear.

To verify satisfactory radar operation during Test 14-F, Test 14-G was rerun without landing gear and crushable blocks. The test results indicated that all trackers continued to search during the engine run.

To accomplish the third objective of determining the amount of polyurethane foam that could be removed from the back of the antenna without degrading the acoustic shielding, Test 14-H was conducted by removing the rubberized coating and drilling ½ in. diameter holes in the foam at the back of the antennas. About 0.3 lb per antenna was removed. The firing results indicated that D_2 went in and out of lock five times.

To establish the level of excitation that a landing gear might provide as disturbance to the radar, Leg 1 was reinstalled with an accelerometer attached to the footpad. Test 14-I showed that during engine operation, D_1 and D_2 again locked up on the landing gear. The acceleration at the footpad was 33 g (rms). Results from the T-21/QA-1 vibration evaluation tests indicate excitation of 1 g (0 to peak) or less from 100 to 5000 cps with an accelerometer attached to the hinge point of the footpad attachment.

In Tests 14-J and 14-K, another ½ in. of foam material was removed from the antenna for a further weight saving per antenna of 0.8 lb. The radomes were reshaped to fit directly into the cavities of the receive and transmit areas of the antennas. Although the thickness of the radomes was still 1.5 wavelengths (1.34 in.), D_2 locked up on both tests. Hence, in Test 14-L the radome thickness was increased to 2 wavelengths (1.75 in.) in the DVS antenna. The receive side of the radar altimeter (RA) antenna was left unprotected to show a comparison. During this test, D_2 operated well without lockup, while D_1, which was unprotected, did lock up. Fig. 72 shows preamplifier outputs before and after the optimum configuration of antenna protection. Based on these results the RADVS antennas are considered ready for a balloon drop test.

In accomplishing the objectives of the Series 14 test firings of T-2 in the horizontal firing stand, the antenna acoustic protection evolved to the configurations shown in Fig. 73. These configurations were derived through several Series 14 firings where the original foam covering was sanded and bored with ½-in. diameter holes to give the lightest weight consistent with the best possible acoustic protection. The final weights for the antenna configurations are shown in Table 35.

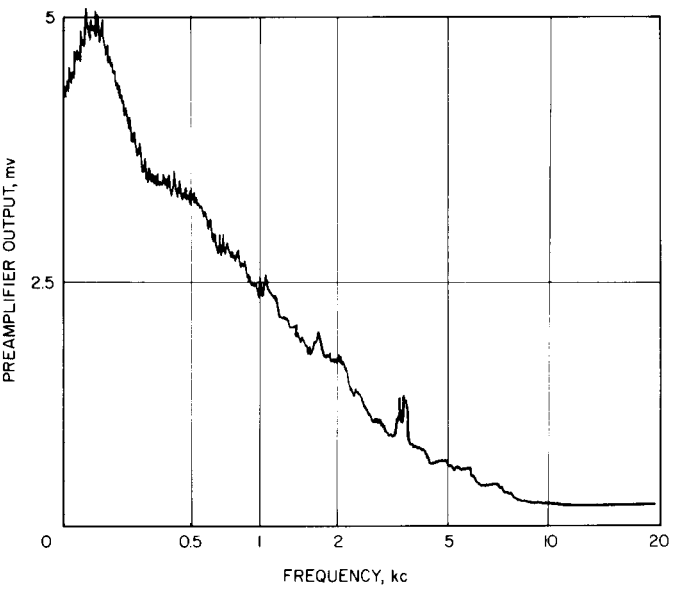

(a) With non-optimum antenna protection (22.3 mv overall output)

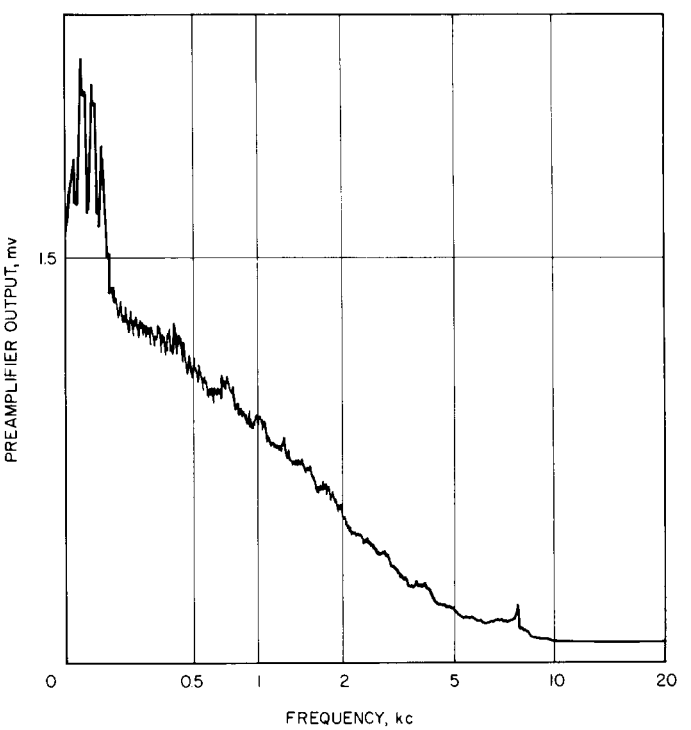

(b) With optimum antenna protection (8.9 mv overall output)

Fig. 72. Output of P-2 preamplifier (90-deg, 1000-cps bandwidth)

Table 34. Summary of Series 14 acoustic tests

Test number and date	System configuration	Radar altimeter and doppler velocity sensor performance	Engine performance
14-A (3-7-64)	(1) Used one wavelength radome. (2) Antennas covered with polyurethane. (3) Preamplifiers covered with polyurethane.	(1) All trackers locked up. (2) The known power frequencies which the trackers were locked on were computed to be: $P_1 = 6$ kc $P_3 = 6$ kc $P_2 = 8$ kc	All engines performed normally.
14-B (3-8-64)	(1) Klystron power supply and modulator covered with stafoam box. (2) Preamplifiers covered with stafoam boxes. (3) Used one and one-half wavelength radomes. (4) Antennas covered with polyurethane.	(1) D_1 trackers locked up for 0.3 sec between T + 2.67 and T+ 2.97. Firing time was 6.2 sec.	All engines performed normally.
14-C (3-11-64)	(1) Klystron power supply and modulator covered with a stafoam box. (2) Preamplifiers covered with stafoam boxes. (3) Used one and one-half wavelength radomes. (4) Antennas covered with polyurethane. (5) Crystal holders filled with polystyrene.	(1) All trackers continued to search; however, D_2 tracker was "chipping" but did not exceed the delay time constant of 0.2 sec required for lockup.	(1) Engine 1 did not develop thrust. (2) Engine 2 followed thrust commands; however, a 1-sec lag was noted before reaching high thrust after the command. (3) Engine 3 reached midthrust only.
14-D (3-11-64)	(1) Klystron power supply and modulator covered with a stafoam box. (2) Preamplifiers covered with stafoam boxes. (3) Used one and one-half wavelength radomes. (4) Antennas covered with polyurethane. (5) Crystal holders filled with polystyrene.	(1) D_2 tracker locked up 0.3 sec after high thrust and dropped out at engines off. Engines were shut down at T + 3 sec due to improper Engine 1 operation.	(1) Engine 1, very low thrust only. (2) Engine 2, normal. (3) Engine 3, midthrust level only.
14-E (3-11-64)	(1) Klystron power supply and modulator covered with a stafoam box. (2) Preamplifiers covered with stafoam boxes. (3) Used one and one-half wavelength radomes. (4) Antennas covered with polyurethane. (5) Crystal holders filled with polystyrene.	(1) All trackers searched during the engine run; however, all trackers locked up at engines off, indicating a klystron power supply and modulator problem with the 2150-v postregulation. This was verified and repaired prior to Test 14-F.	(1) Engine 1, normal. (2) Engine 2, normal. (3) Engine 3, low thrust only.
14-F (3-12-64)	(1) Klystron power supply and modulator covered with stafoam box. (2) Preamplifiers covered with stafoam boxes. (3) Radomes for both antennas were one and one-half wavelengths thick. (4) Antennas were covered with polyurethane. (5) Crystal holders were filled with polystyrene. (6) A landing leg, pad, and crushable block were installed on the three legs of T-2S.	(1) The D_2 tracker locked during the entire engine run (landing pads were installed on all three legs).	Engine operation was normal on all three legs. Engine 3 was replaced prior to this firing.
14-G (3-12-64)	(1) Klystron power supply and modulator covered with stafoam box. (2) Used one and one-half wavelength radomes. (3) Preamplifiers covered with stafoam boxes. (4) Antennas covered with polyurethane foam. Material was not removed until Test 14-H. (5) Crystal holders were filled with polystyrene.	(1) All trackers continued to search during the engine run.	All engines performed normally.

Table 34 (continued). Summary of Series 14 acoustic tests

Test number and date	System configuration	Radar altimeter and doppler velocity sensor performance	Engine performance
14-H (3-12-64)	(1) Used one and one-half wavelength radomes. (2) Klystron power supply and modulator protected by a stafoam box. (3) Removed portion of antenna foam by (a) removing the rubberized coating and drilling ½-in. diameter holes on the back of the antennas; (b) trimming the preamplifier stafoam boxes. (4) Antenna weight reduction at this time was 0.3 lb/antenna. (5) Crystal holders were filled with polystyrene.	(1) D_2 chipped in and out of lock five times (four 0.25-sec intervals and one 1.0-sec interval).	All engines performed normally.
14-I (3-13-64)	(1) The klystron power supply and modulator was covered with a stafoam box. (2) Used one and one-half wavelength radomes. (3) Crystal holders filled with polystyrene. (4) Reduced antenna weight by (a) removing the rubberized coating and drilling ½-in. diameter holes on the back; (b) trimming preamplifier stafoam boxes. (5) A landing leg and pad were installed on T-2S Leg 1. (6) Accelerometer 6 was installed in the center of the footpad.	(1) D_2 and D_1 locked up.	All engines performed normally.
14-J (3-13-64)	(1) Radomes were one and one-half wavelengths thick. (2) Crystal holders were filled with polystyrene. (3) Antenna weight was reduced by approximately 0.8 lb/antenna. (a) Prior to Test 14-H the rubberized coatings were removed and ½-in. diameter holes drilled in the back of the antennas. (b) Approximately ½-in. of foam was shaved off the back and sides of the antennas. (4) The klystron power supply and modulator were covered with a stafoam box. (5) Landing Leg 1 was removed. (6) Accelerometer 6 was returned to the radar altimeter antenna attach bracket.	(1) D_2 locked up throughout engine run. (2) D_1 locked up during last 2.2 sec.	All engines performed normally.
14-K (3-13-64)	Same as Test 14-J except: (1) Removed the klystron power supply and modulator stafoam box. (2) Cut off outside portion of radomes and fitted them inside the antenna shrouds. Approximately 0.2 lb/antenna was removed.	(1) D_2 locked up during the entire run at high thrust.	Some indication of rough starting; however, high thrust levels were reached during the terminal 4 sec of the run.
14-L (3-14-64)	(1) Fabricated new "cork fit" two wavelength radomes. Two halves were fabricated for the doppler velocity sensor antenna and one half was made for the radar altimeter antenna. The pretest installation consisted of: Doppler velocity sensor antenna Transmitter portion was 1.75 in. thick Receiver portion was 2.00 in. thick Radar altimeter antenna Transmitter portion was 2.00 in. thick Receiver portion was unprotected (2) Removed stafoam box from klystron power supply and modulator. (3) Crystal holders filled with polystyrene. (4) Antenna weight reduced by 1 lb per antenna.	(1) D_1 locked up during engine operation.	Slightly erratic start, but all engines reached high thrust level during the terminal 5 sec creating a normal acoustic environment. Fuel vaporization was suspected as the cause of the erratic starts.

(3) Test 15: Vertical drop test from balloon with radar attitude control. The objectives of this next test in the T-2 program are as follows:

(a) Evaluate radar reliable switching logic.

(b) Evaluate fuel utilization.

(c) Evaluate radar attitude control.

(d) Verify radar tracking capacity through a low velocity region.

(e) Evaluate roll loop operation under varying disturbing torques.

(f) Evaluate operation of radar "lockon" and reliable indication.

(g) Verify separation techniques.

(h) Verify engine/radar noise compatibility.

(i) Verify resistance of systems to landing shock.

The descent profile for Test 15 is shown in Fig. 74. In this test the vehicle will be suspended from a balloon at an altitude of 1200 ft above the terrain. Radar lockon logic switching will be actuated to allow lockon when the velocity requirement is satisfied. A preset, high, constant-thrust command will be switched in by the radar reliable signal plus the event programmer 5-sec output. This will ensure a vehicle velocity greater than 40 fps before high thrust is commanded. The radars will control the lateral velocity, but the radar thrust loop will remain open. Pre-drop switching will be completed and the vernier engines will be ignited before release. After ignition, T-2 separation will be delayed for 5 sec to evaluate radar operation. All pre-drop switching will be accomplished by rf link. The on-board switching during the drop, including engine shutdown and recovery, will be accomplished by the on-board event programmer; however, the radar power will remain on and will be turned off by the generation of the 13-ft mark. A backup radar shutoff and telemetry shutoff will be provided by the airbag foil switches in case a 13-ft mark is not generated. An emergency recovery override is provided by both rf and hardline link.

Table 35. Comparison of RADVS antenna weights

Configuration	Doppler velocity sensor, lb	Radar altimeter, lb
Bare antenna	4.2	5.3
Antenna with original foam covering	7.7	7.5
Antenna with final foam covering	6.8	6.9
Weight of final foam covering	2.6	1.6

T-2H buildup and test plan. The developmental RADVS flight control equipment and wiring harness were removed from the T-2H test vehicle during this period, and the QA-1 RADVS was installed in late March. Following completion of the QA-1 RADVS checkout, the T-2H system was transferred to AFMDC for reinstallation on the Bell 47-G helicopter. In designing this helicopter installation, special emphasis has been placed on minimizing ambient electrical noise, which was a problem in the previous helicopter tests. In this installation,

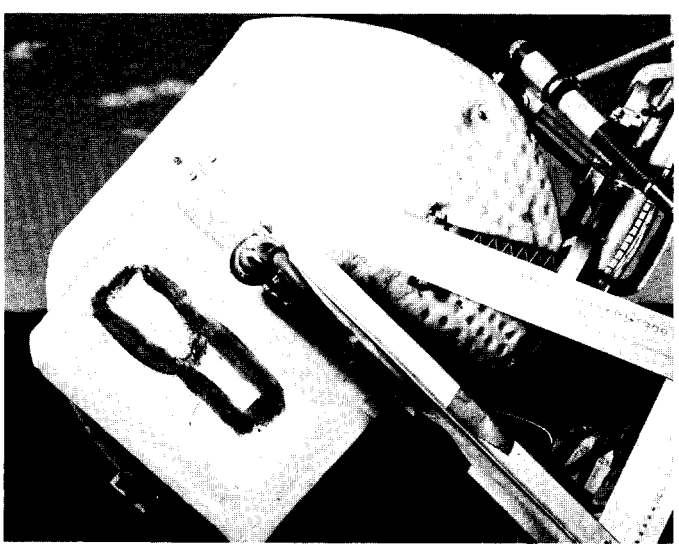

(a) Radar altimeter antenna

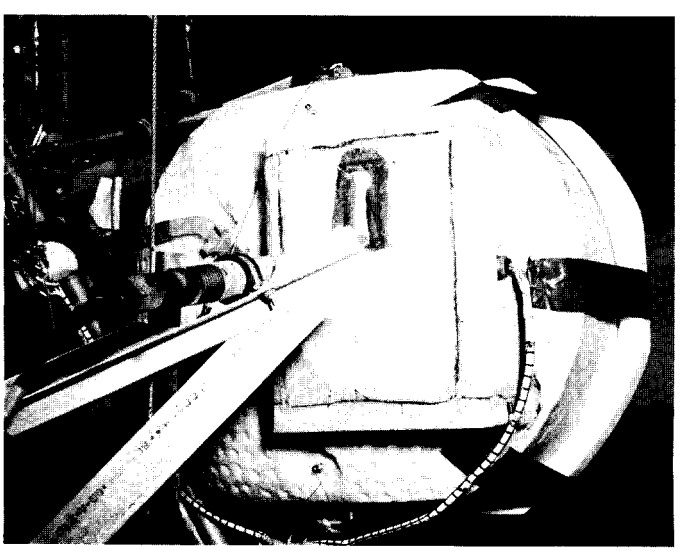

(b) Doppler velocity sensor antenna

Fig. 73. Antenna acoustic foam protection

the RADVS preamplifier and analog outputs first are amplified locally on the T-2H vehicle, then are routed to the tape recorder at an amplified signal level. This scheme improves the signal-to-noise ratio of the overall recording system. The RADVS wiring techniques reflect the noise-reduction experience gained on the developmental RADVS installation and during the T-21 tests. Fig. 75 shows the T-2H/QA-1 RADVS test system ready for installation on the helicopter.

The T-2H/QA-1 tests will be conducted at AFMDC in April and May 1964. Certain flight parameters tested previously will be repeated in this testing to obtain comparison data. In addition, the flight regime will be expanded to test functional requirements that were not yet operational during the previous testing. This testing will include additional gain states and automatic switching logic required in a mission.

All testing will be conducted utilizing the presently available cinetheodolite tracking stations at AFMDC. Velocity parameters to be derived from the optical instrumentation are predicted to be accurate within 5 fps at the longer ranges and are expected to improve to an accuracy of 1 fps as the vehicle approaches the five-station tracking complex now installed at the *Surveyor* impact point test site.

b. T-21 test status. The system functional test phase of T-21 type approval testing (TAT) has progressed to a point where group and integration tests (with the exceptions of vernier propulsion, television, and telecommunications tests) have essentially been completed on a one-time-through basis. The test requirement status summary is shown in Fig. 76, both in terms of total number of requirements and percentage of test phase completion. As seen in the lower half of the figure, some requirements, though tested, are awaiting acceptance. In general, data items in suspense are a result of a component failure, a requirement for a test technique change and consequent retest, or a change of tolerances.

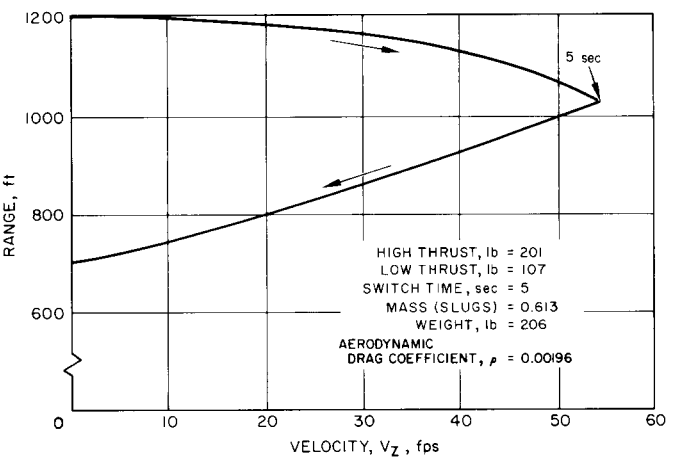

Fig. 74. T-2 descent

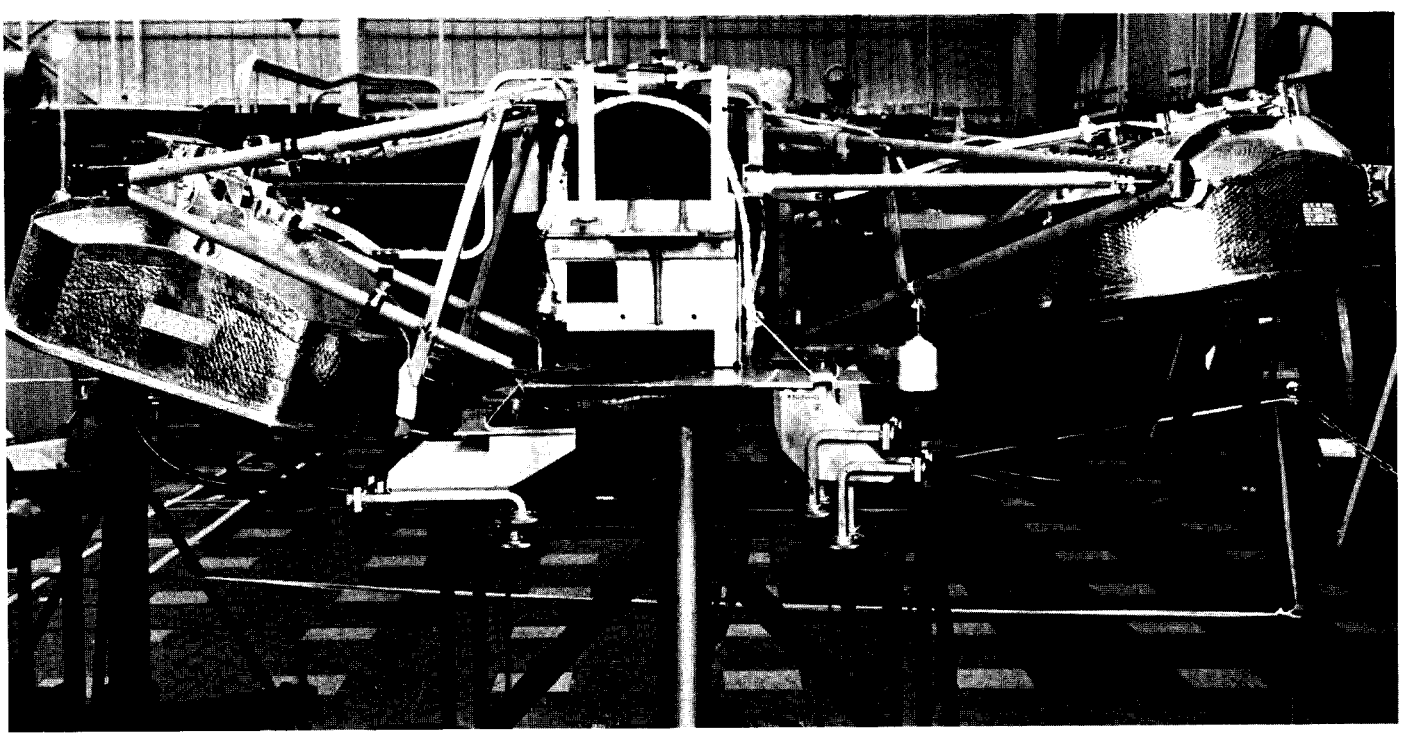

Fig. 75. T-2H/QA-1 RADVS system

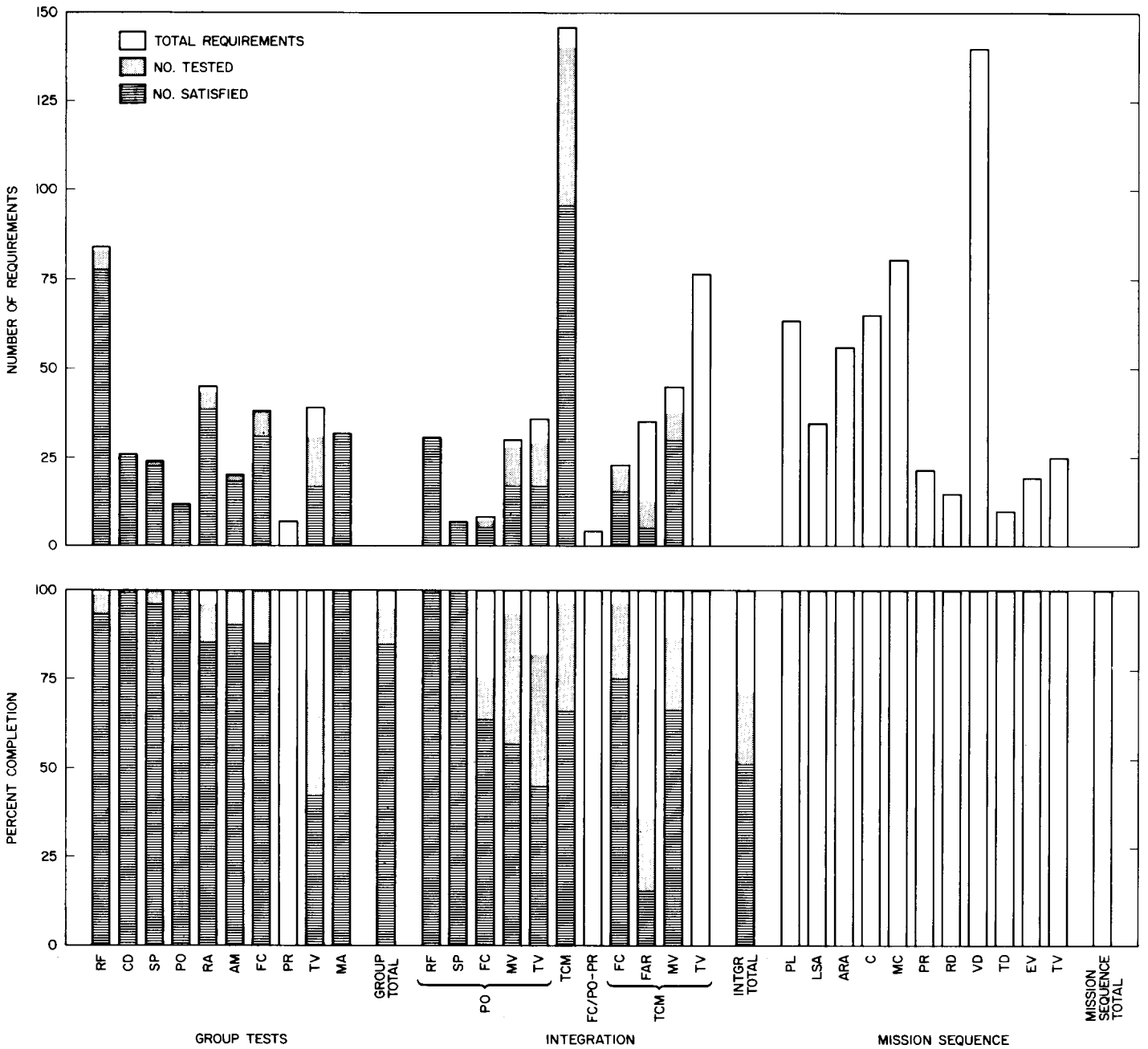

GROUP TESTS

- RF = RADIO FREQUENCY
- CD = COMMAND DECODING
- SP = SIGNAL PROCESSING
- PO = POWER
- RA = RADVS
- AM = ALTITUDE-MARKING RADAR
- FC = FLIGHT CONTROL
- PR = PROPULSION
- TV = TELEVISION
- MA = MECHANISMS AUXILIARY

INTEGRATION

- PO { RF = RADIO FREQUENCY; SP = SIGNAL PROCESSING; FC = FLIGHT CONTROL; MV = MECHANISMS AND VEHICLE; TV = TELEVISION }
- TCM = TELECOMMUNICATIONS
- FC/PO-PR = FC/POWER-PROPULSION
- TCM { FC = FLIGHT CONTROL; FAR = FC-AMR-RADVS; MV = MECHANISMS AND VEHICLE; TV = TELEVISION }

MISSION SEQUENCE

- PL = PRELAUNCH
- LSA = LAUNCH, SEPARATION AND RF ACQUISITION
- ARA = ATTITUDE REFERENCE ACQUISITION
- C = COAST MODE
- MC = MIDCOURSE CORRECTION
- PR = PRE-RETRO MANEUVER
- RD = MAIN RETRO DESCENT
- VD = VERNIER DESCENT
- TD = TOUCHDOWN
- EV = ENGINEERING VERIFICATION AND PRE-EXPERIMENT PREPARATION
- TV = TELEVISION EXPERIMENTS

Fig. 76. T-21 system functional test requirements

UNCLASSIFIED

Special tests were run to determine the interaction between the QA-1 RADVS and other subsystems on the spacecraft. Secondary objectives of these tests included monitoring all squib lines for inadvertent firing, verification of proper operation of the engineering mechanism auxiliary (EMA) in firing a live RADVS pyro switch, and proper generation of flight control programmer commands (both manual and automatic). The operational procedure employed was a much abbreviated mission sequence. Significant test results were:

(1) No inadvertent squib firings occurred.

(2) EMA/pyro switch operation is apparently satisfactory, although the expended switches are being scrutinized to determine if one of them had any effect in one instance where the klystron power supply modulator (KPSM) failed to time in.

(3) No effect on receiver automatic gain control (AGC) or transmitter spectrum was discernible with RADVS turn-on.

(4) Some increase in noise on the 22- and 29-v lines was observed, but was not of sufficient magnitude to degrade other subsystems except television.

(5) Television video is nearly masked by noise when the RADVS is on.

Further investigation of the susceptibility of the television to noise will be conducted, using a source other than the RADVS for noise generation.

Prior to cessation of T-21 system functional testing to allow upgrading of the vehicle, a period is being devoted exclusively to intensive system problem investigation and retest of suspense items. The more significant problems being looked at during this period are:

(1) It has been observed frequently that when the spacecraft receiver was being phase-locked to the ground transmitter (transponder mode), indexing of receiver-decoder selector (RDS) in the central command decoder (CCD) would occur. This resulted in several command lines being erroneously activated and causing spacecraft functions to occur inadvertently. Investigation has revealed that the shift in voltage controlled crystal oscillator (VCXO) frequency momentarily results in loss of modulation, causing the CCD to index which, in turn, presents a varying load to its electrical conversion unit (ECU). Two internal supply voltages have different fall times, depending on their load, and result in address-enable and command-enable being randomly generated. It has been possible to duplicate this action in the developmental laboratory and a circuit redesign is currently under way.

(2) Flight control gyros intermittently will not null in the rate mode, unless digital word gate No. 4 is opened. Investigation revealed that as the 1000-ft mark signal is sampled, sufficient feedback on the signal line occurs to cause the flight control electronic switches to close and change pitch and yaw amplifier gain. As a result, feedback is amplified and the gyros torqued. A circuit modification is being studied and is expected to be incorporated during the spacecraft upgrade.

(3) Central power control (CPC) telemetry signals are not correct at present in either system or group configuration. Investigation and analysis revealed a fourfold problem: some shunts were reversed, an open switch existed in the auxiliary engineering signal processor (AESP), an incorrect scale factor was defined for one shunt, and a ground loop developed in the system test equipment assembly (STEA). Harnessing is being changed to correct the shunt reversal; the AESP switch will be replaced during the spacecraft upgrade; the incorrect scale factor has been changed, and the STEA ground loop eliminated.

(4) Command-reject and command-enable signals are apparently modulating the spacecraft transmitter in the transponder mode. As a result, momentary loss of lock occurs and spacecraft telemetry is also momentarily lost. This problem is currently under investigation.

(5) Some signals are missing on the AESP and engineering signal processor (ESP) commutators. This problem is now under investigation.

(6) Television cameras appear to be very susceptible to noise on the power supply. This was noted particularly during special RADVS tests and is being investigated further.

(7) Stray-energy monitors and squib simulators were activated randomly during the T-21/QA-1 vibration test. Analysis of the problem shows it is not linked to the actual vibration test and that very little correlation with other electrical events is possible. It does appear, however, that there may be a strong correlation with problem (1) above. All squib lines are being monitored and the problem will be intensively investigated prior to the spacecraft upgrade.

T-21/QA-1 high-frequency vibration test. During the second week of March a vibration evaluation was undertaken involving the T-21 test vehicle incorporating the QA-1 RADVS system. The purpose of the vibration tests

UNCLASSIFIED

was to establish realistic test parameters for the QA-1 RADVS antennas by vibrating the vehicle at each vernier engine bracket and scaling the results according to power spectral densities obtained from AFMDC firing test data. This was accomplished by installing monitoring accelerometers at the engine brackets similar to the installation of the accelerometer on the engine bracket of T-2, plus additional accelerometers at ten points on each of the doppler velocity sensor (DVS) and radar altimeter (RA) antennas as shown in Fig. 77. By alternating accelerometer points additional data were collected at the transmitter-receiver, flight control sensor group (FCSG), accelerometer, KPSM, and at the footpad.

In addition, an operating test was conducted primarily to evaluate RADVS operation with dummy loads and to check the telecommunications link under the same

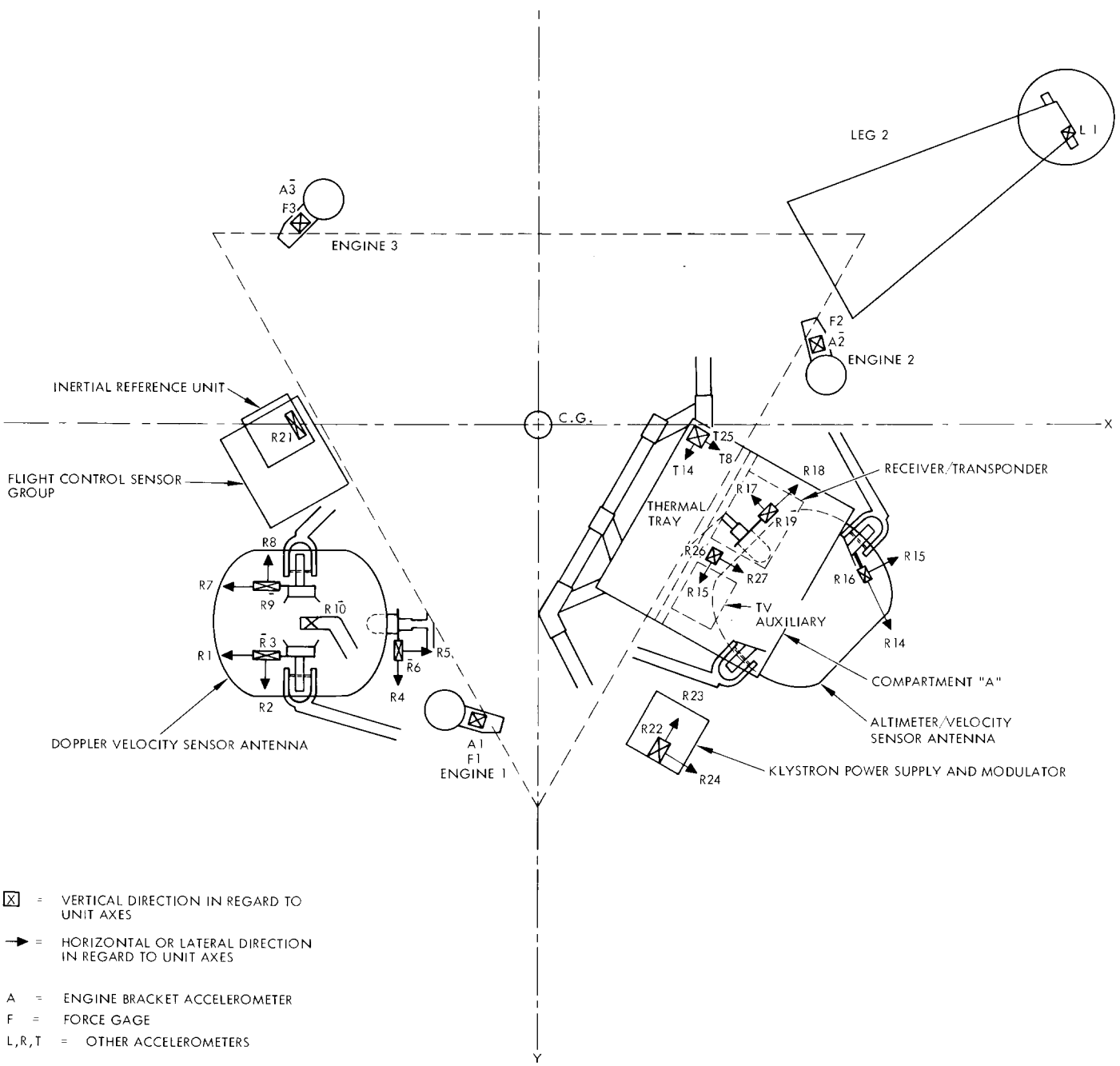

Fig. 77. T-21 accelerometer installations

vibration conditions. To meet the objectives of the test, T-21 was suspended on the S-8 soft suspension system as shown in Fig. 78. Two Stevens modal shakers in "piggyback" fashion were used at levels up to 10 lb (force) rms from 100 to 5000 cps. Fig. 79 shows the shaker installation with an Endevco force gage attached to the shaker drive rod and engine trunnion. The T-21 vehicle configuration represented the space vehicle during lunar descent after retro-rocket ejection and weighed 567 lb.

Sinusoidal vibration testing at force inputs of 2, 6, and 10 lb peak was conducted from 100 to 5000 cps at each engine. Random vibration testing at 3 and 10 lb (force) rms was also conducted at each engine (Table 36).

From more than 75 plots of acceleration versus frequency in the sinusoidal tests several resonant modes were observed for each antenna as well as for other spacecraft equipment. A primary spacecraft resonant mode appeared at about 150 cps. The several DVS antenna modes appeared at 240, 310, 420, and 900 cps. The predominant modes for the RA antenna appeared at 220, 390, 450, and 1100 cps. The 900 to 1100 cps range seems to be the resonant frequency of the engine bracket and corroborates the results obtained from the T-2 firing test results. Table 37 illustrates some of the peak g levels experienced during 10 force-pound input tests and represents the maximum values over the 100 to 5000 cps frequency range.

For random excitation, white noise excitation levels of 3 and 10 lb rms between 100 and 2000 cps were applied and the acceleration responses at the input engine bracket and 26 spacecraft locations were measured. A typical test input spectral density is shown in Fig. 80 for 10 lb rms.

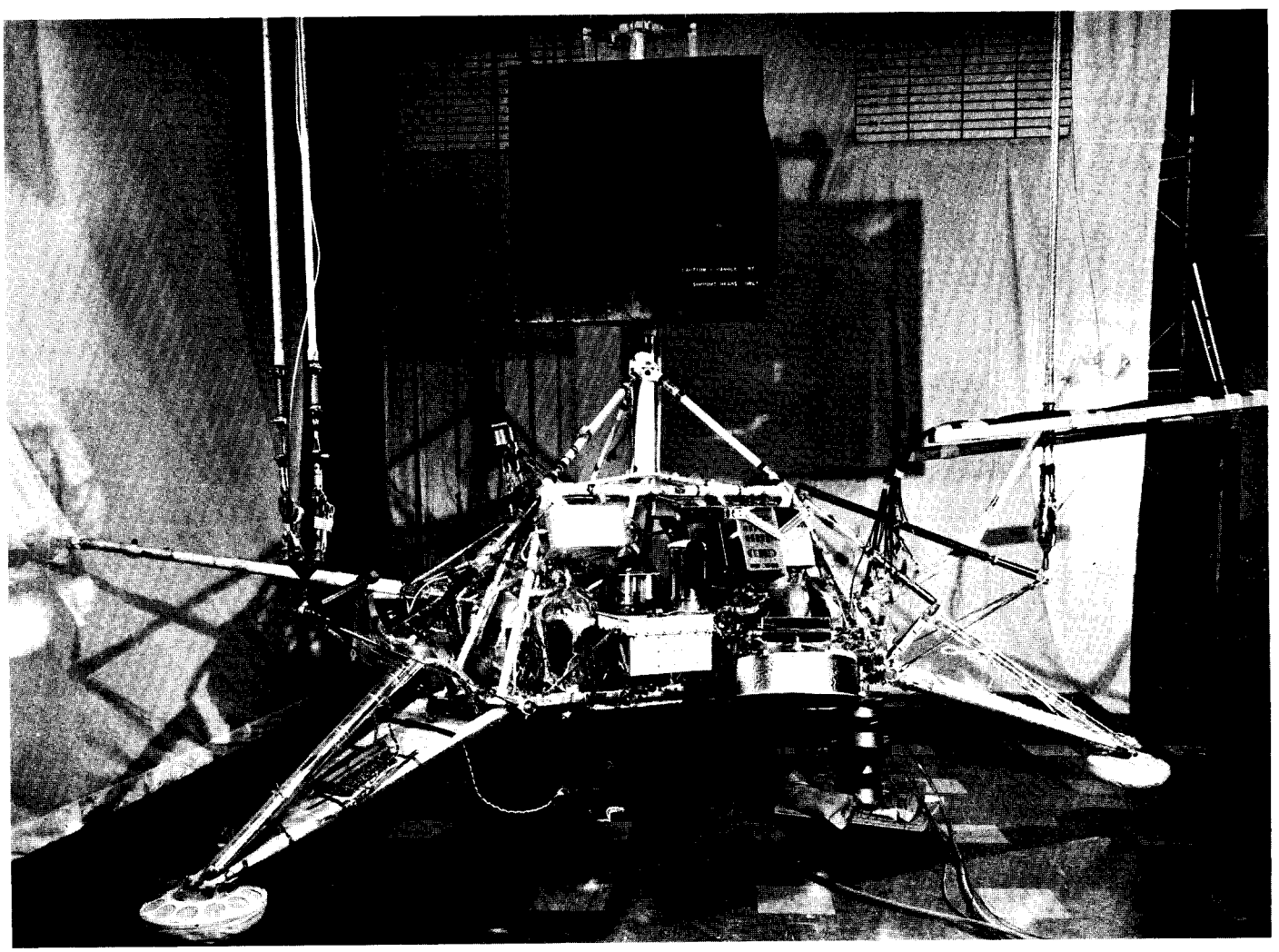

Fig. 78. T-21/QA-1 vibration test setup

Table 36. Summary of T-21/QA-1 vibration tests

Engine	Condition	Number of runs				
		Peak sinusoidal input, lb (force)			RMS random input, lb(force)	
		2	6	10	3	10
1	Sinusoidal testing (100 to 5000 cps)					
	Engine trunnion bar input	2	2	2		
	Engine dummy weight input			2		
	Three tape track summing		1	5		
	Random testing (100 to 2000 cps)				1	2
2	Sinusoidal testing (100 to 500 cps)					
	Engine trunnion bar input		2	2		
	Engine dummy weight input			2		
	Three tape track summing			5		
	Random testing (100 to 2000 cps)				1	2
3	Sinusoidal testing (100 to 500 cps)					
	Engine trunnion bar input	2	2	2		
	Engine dummy weight input			2		
	Three tape track summing			5		
	Random testing				1	2

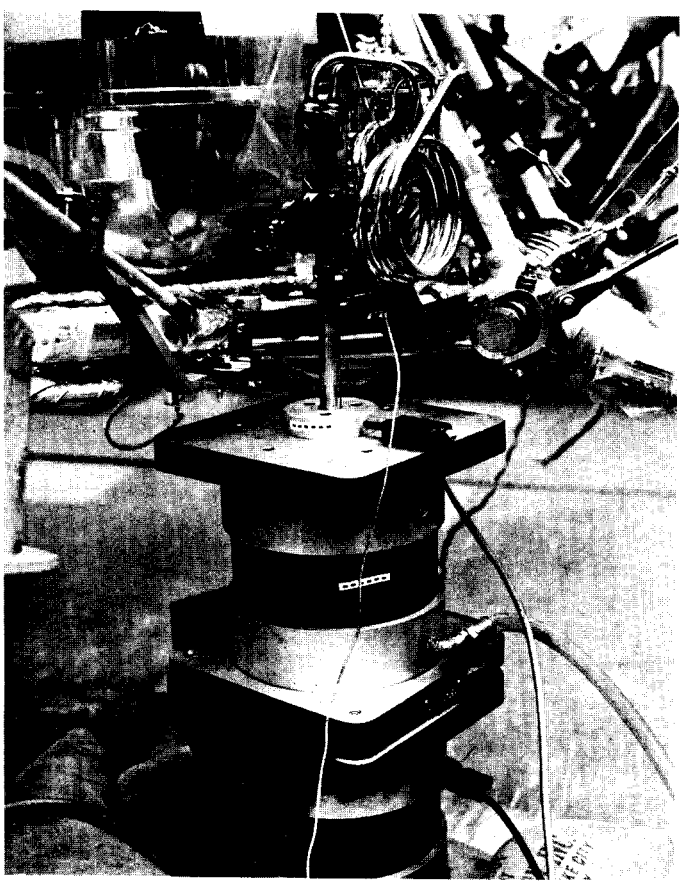

Fig. 79. Shaker installation

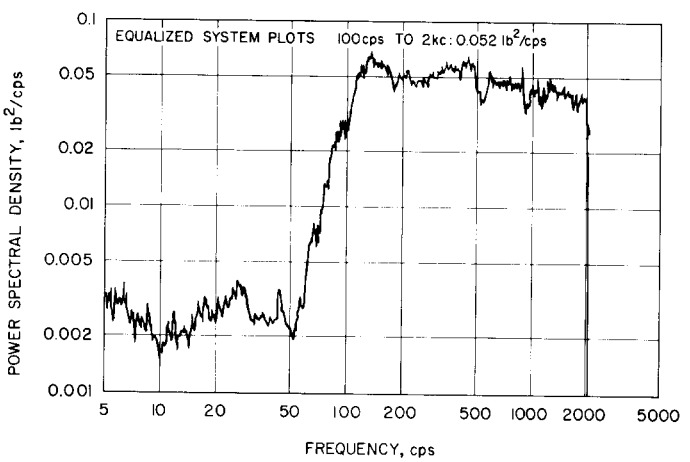

Fig. 80. Typical input spectral density

The response spectral density in three orthogonal directions at the three attachment brackets of the DVS antenna during 3 lb rms excitation at Engine 1 was calculated. These values were then scaled at each frequency by the ratio of the T-2 engine firing data to the spectral density observed at Engine 1 bracket on T-21 during the random vibration testing. A typical firing such as Test 12-B at AFMDC was utilized to obtain the spectral density of Fig. 81 at Engine 1 which was operating at 70 lb thrust. The overall vibration level observed during the AFMDC firing at Engine 1 bracket based on the

Table 37. Summary of vibration levels sine testing

Description	Accelerometer location	Maximum peak level, ±g	Resonant frequencies, kc
Transmitter	T8	1.8	0.6 and 1.0
	T14	3.5	1.0
	T25	6.0	1.0
Receiver	R25	4.0	1.3
	R26	2.3	1.0
	R27	3.6	1.0 and 2.2
DVS[a] antenna (vertical)	R3, R6, or R9	9.2	0.24, 0.31, 0.42, and 0.9
DVS[a] antenna waveguide above septum and cg	R10	4.0	0.24 and 2.5
RA[b] antenna	R13, R16, or R10	4.1	0.22, 0.39, 0.45, and 1.1
RA[b] antenna waveguide above septum and cg	R20	1.0	0.2 and 1.2
Leg hinge at footpad	L1	1.6 (95% under 1 g)	
KPSM[c]	R22	1.42	0.2
	R23	2.4	0.3, 0.7, and 1.2
FCSG[d]	R21	1.0	0.2 and 1.2

[a]Doppler velocity sensor.
[b]Radar altimeter.
[c]Klystron power supply and modulator.
[d]Flight control sensor group.

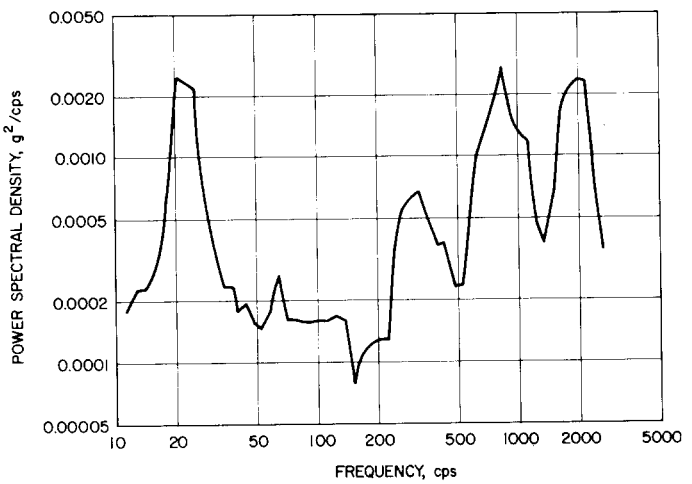

Fig. 81. Typical spectral density of engine bracket acceleration

latter spectral density is 1.8 g rms. The overall mean square acceleration responses observed at the DVS antenna are given in Table 38. Further data review and analysis are yet to be conducted on other equipment.

Because of the high g levels observed at the inboard DVS attachment bracket during sine testing (Table 37), a test was conducted during random excitation with this bracket disconnected. The g levels in a vertical direction before and after disconnection indicated 1.16 g rms versus 0.17 g rms at the DVS antenna inboard bracket and 0.54 g rms versus 0.26 g rms on the DVS antenna waveguide. Such a reduction warrants a consideration of incorporating a vibration isolator at this antenna attachment point.

The RADVS system was operated with dummy loads attached to all feed horns during the three-tape track summary sinusoidal tests as well as during random testing. Since the vibration sensitivity of the dummy loads is an unknown factor the data obtained are considered qualitative, but some conclusions have been drawn.

In general, radar operation appears better than anticipated. The preamplifiers did not switch lower than the 65-db gain state and only intermittently into the 65-db state during all of the vibration tests. Some individual tracker lockons were observed, but the trackers did not lock on all at the same time. The RA antenna did not exhibit lockon or gain state changes.

During sinusoidal vibration testing, peaks at 200, 400, and 800 cps of sufficient magnitude to cause gain state changes and lockon in some DVS channels were observed. These frequencies agree with some of the antenna resonant frequencies observed from the vibration data.

During the random vibration with 10 lb rms inputs, the preamplifier outputs were lower and gain state changes

Table 38. DVS antenna overall mean square acceleration response, 3 lb rms random vibration test

Excitation location		Engine 1	Engine 2	Engine 3	Total of three engines (Σ)	Σ / Engine 1
Channel	Direction	g^2	g^2	g^2	g^2	
R1	Normal to septum	0.1354	0.0041	0.0071	0.1466	1.083
R5		0.2052	0.0028	0.0088	0.2168	1.057
R7		0.0552	0.0040	0.0095	0.0687	1.245
R3	Vertical	0.0686	0.0014	0.0025	0.0725	1.06
R6		0.0767	0.0025	0.0067	0.0859	1.12
R9		0.0299	0.0008	0.0029	0.0336	1.12
R2	Parallel to septum	0.0529	0.0014	0.0023	0.0566	1.05
R4		0.0955	0.0088	0.0266	0.1309	1.375
R8		0.0076	0.0010	0.0024	0.0110	1.445
R10	Vertical on waveguide	0.0172	0.0006	0.0026	0.0204	1.185

and lockons were fewer than on previous sinusoidal tests. The DVS transmitter spectrum was monitored and no vibration-induced noise was visible on the analyzer.

A substantial reduction in preamplifier output noise was obtained when the inboard attachment bracket of the DVS antenna was disconnected from the space-frame. Noise level rises of 220 mv with the inboard attachment connected dropped to only 15 mv rises after the attachment was disconnected.

In checking telecommunication links under the various vibration excitations, a phase jitter test in the phase modulation (PM) mode was conducted with the RADVS off. From the data, it appears that phase lock could not be maintained below about 1400 cps of vibration input. Additional tests with the RADVS on indicated the same difficulties. Engineering changes in both the transmitter and receiver are already in process to remedy this difficulty.

During the vibration test series, no RADVS components failed. However, several stray energy monitors were activated and the problem is under investigation.

c. Test planning and analysis. Planning effort for the T-21 environmental test phases has continued with emphasis placed on the test specifications, instrumentation, and long lead-time hardware items. Tables 39, 40, and 41 summarize the status of pre-test implementation for the T-21 environmental test phases. A brief discussion of the principal items of the implementation follows.

Solar thermal–vacuum pre-test implementation.

(1) Test specification. Comments received on the preliminary release of the solar thermal–vacuum phase specification have been reviewed for incorporation into the final release copy.

(2) Instrumentation plan. An instrumentation plan describing special thermocouple installations for the T-21 vehicle has been released and will become part of the overall T-21 solar thermal–vacuum test plan.

(3) T-21 solar thermal–vacuum test plan. A detailed test plan covering all aspects of the solar thermal–vacuum test is being prepared. This will include establishment of test responsibilities, task assignments, and time sequencing of all test operations.

(4) Test procedures. Procedures will be developed for vehicle operation, facility control operation of special instrumentation recording equipment, and environmental fixture control. Vehicle operating procedures will be based on those developed during T-21 system functional testing.

(5) Functional test access. All test cabling from the system test equipment assembly (STEA)—external and internal to the vacuum chamber—blocking heaters, special compartment test covers, etc., are included in this category. A photograph of the completed chamber penetration plates that provide vacuum-tight connections between internal and external cabling is shown in Fig. 82.

Table 39. Solar thermal–vacuum test implementation

Item	Complete, %
Documentation	
Test specification	95
Instrumentation plan	90
Test plan	10
Test procedures	0
Hardware and equipment[a]	
Functional test access	40
Test stimuli	65
Mounting fixtures	30
Thermal instrumentation	15
Environmental fixtures	10
Special facilities preparation	90

[a]Includes design, drafting, procurement, fabrication, assembly, and checkout.

Table 40. Vibration test implementation

Item	Complete, %
Documentation	
Test specification	100
Instrumentation plan	100
Test plan	0
Procedures	0
Hardware and equipment[a]	
Test fixtures	95
Vehicle instrumentation	80
Special facility preparation	20
Vehicle special equipment	20

[a]Includes design, drafting, procurement, fabrication, assembly, and checkout.

Table 41. Shock test implementation

Item	Complete, %
Documentation	
Test specification	80
Instrumentation plan	100
Test plan	0
Procedures	0
Hardware and equipment[a]	
Test fixtures	30
Vehicle instrumentation	80
Special facility preparation	20
Vehicle special equipment	20

[a]Includes design, drafting, procurement, fabrication, assembly, and checkout.

(6) Test stimuli. Test equipment is provided to present controlled stimuli to the television cameras and to the Canopus sensor. Fig. 83 shows the approach camera target system, and Fig. 84 shows the Canopus hood which shields the Canopus sensor from undesirable stray light.

(7) Mounting fixtures. Design is complete on the spacecraft-to-chamber mounting fixture and is continuing on the various support and mounting brackets for equipment, lines, and cables.

(8) Thermal instrumentation. Thermal instrumentation includes not only the actual installation of thermocouples onto the vehicle and test fixtures, but also the preparation and checkout of data recording and monitoring equipment. Part of the thermocouple installation will be performed during the T-21 upgrade periods; the remainder will be accomplished immediately before the solar thermal-vacuum testing.

(9) Environmental fixtures. Environmental fixtures are those items of equipment needed to assist in the functional checkout of the spacecraft in an Earth-gravity environment and those items required for better simulation of the true solar/thermal conditions. Included are landing gear and omnidirectional antenna extension fixtures, shadow shrouds, blocking heaters and their controls, and thermal mockups. All items have been defined and detail design is under way.

(10) Special facilities preparation. Certain additions or minor modifications were necessary to the thermal-vacuum chamber resulting from specific *Surveyor* requirements. These included special view ports,

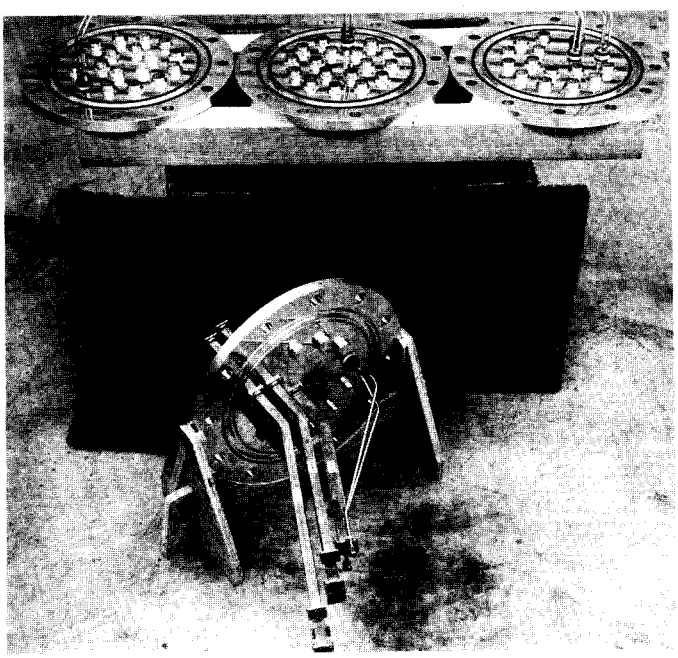

Fig. 82. Chamber penetration plates

new penetrations, and special liquid nitrogen supplies to environmental fixtures. This effort is essentially complete.

Vibration pre-test implementation

(1) Documentation. The vibration test specification has been released and the instrumentation plan issued. Work is scheduled to begin on the detailed test plan during the next reporting period and will make full use of experience gained during S-2 testing. Vehicle operating procedures will be based on those developed during T-21 system functional tests.

(2) Hardware and equipment. The test fixtures required for T-21 testing were developed for joint use between S-2 and T-21. The main support fixtures are shown in Fig. 85. Essentially all strain gage instrumentation has been installed on T-21. Accelerometer installation will occur immediately

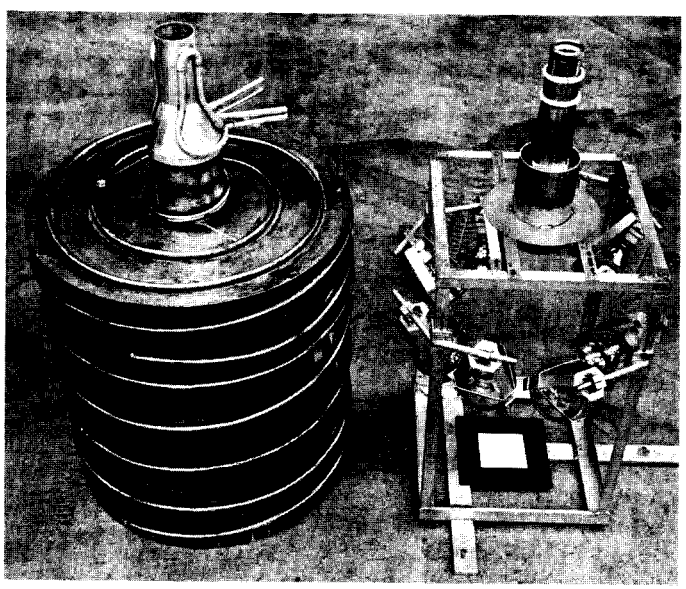

Fig. 83. Approach camera target system

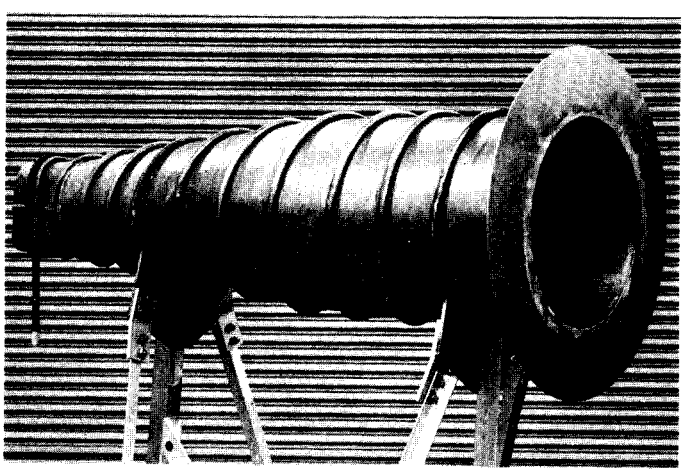

Fig. 84. Canopus sensor hood

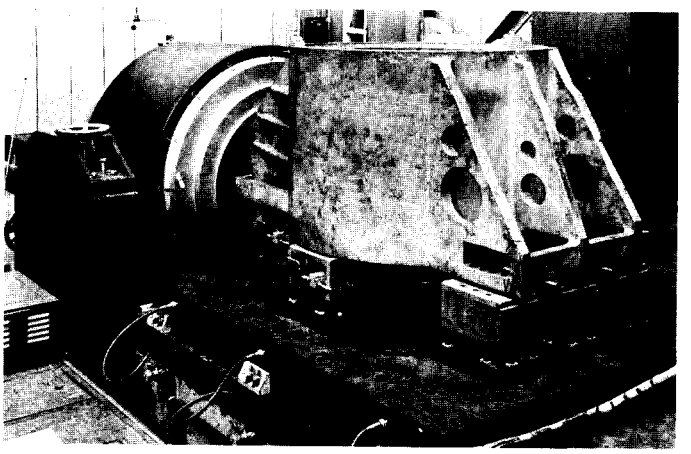

(a) Lowered

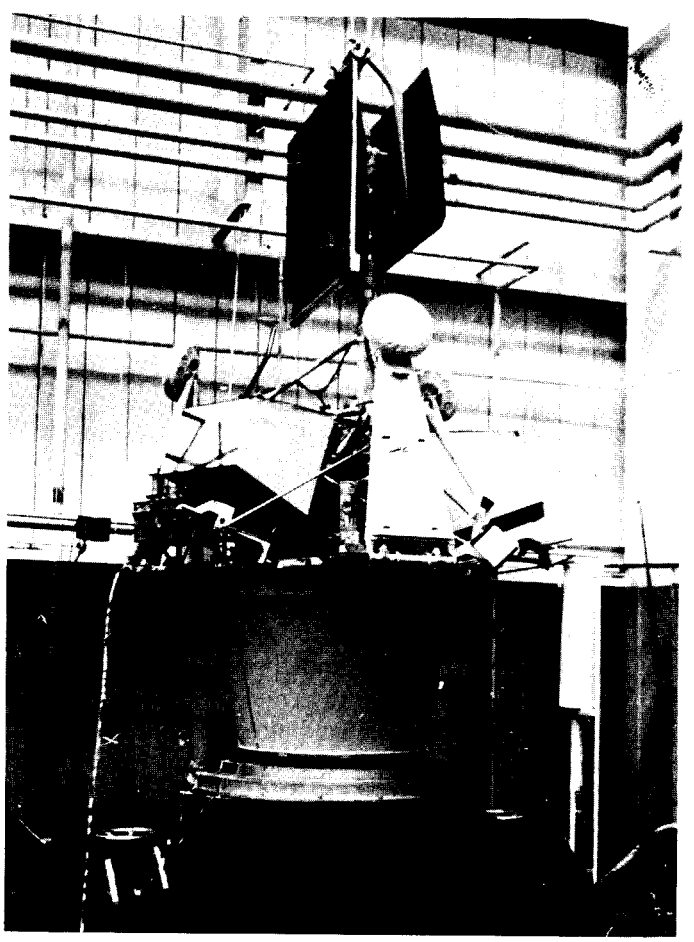

(b) Upright

Fig. 85. Vibration support fixture

prior to the vibration test. The same special compartment test covers will be used for vibration as for solar thermal–vacuum. Minor modification to adapt the shaker for use with T-21 and provision of fixtures to enhance vehicle and personnel safety are in the design stage.

Shock pre-test implementation

(1) Documentation. A preliminary issue of the T-21 shock test phase specification has been distributed. The instrumentation plan is complete and issued. Experience gained in S-2 and T-1 drop tests will be used in preparing the detailed test plan scheduled to be started during the next reporting period. Vehicle operating procedures will be based on procedures developed during T-21 system functional tests.

(2) Hardware and equipment. All fixtures and equipment are in design process. Vehicle instrumentation required for the shock tests is the same as that required for vibration tests.

d. Surveyor *test equipment*

Scientific instrument system test equipment assembly (STEA) status. Design of the scientific instrument STEA is now approximately 85% complete. With the recent approval of the payload engineering change proposals the remaining design work can now be completed. Following are descriptions of the two STEA subassemblies completed during this report period.

(1) Common function panel. The common function panel was designed to assemble in one panel most of those features of the various experiment test panels that are common to two or more experiments. A significant saving in equipment costs is thereby gained through elimination of duplications. Only a slight loss in versatility is sustained, since sufficient capacity has been provided in the shared functions to handle two or more experiments simultaneously. A considerable saving in rack front panel space is also realized by the adoption of the common function panel.

The common function panel incorporates the following equipment.

(a) Power supplies necessary to power STEA electronic circuitry located in the STEA racks and spacecraft function box.

(b) Management of all power sources originating in the STEA, except for the 22- and 29-v spacecraft power simulators.

(c) Precision voltage calibrating source, variable from 0- to 30-v, with ±0.01% accuracy for use with various instrument panels and STEA-mounted commercial test equipment.

(d) Local monitoring of all STEA power supply voltages and total currents.

(e) Local visual monitoring of selected instrument or STEA dc signals, using a Triolab Model 310-2 transistorized voltmeter.

(f) Constant current excitation source for instrument temperature sensors. The sensor excitation switches for each experiment will be located in the appropriate experiment panel.

(g) A command pulse generator having a suitable number of degrees of freedom of adjustment to allow for its use in failure-mode analysis of command circuitry. The command excitation switches for each experiment will be located in the appropriate experimental panel.

(h) Simulated spacecraft clock rates, locally variable in frequency of suitable amplitude and rise time to allow for use in failure-mode analysis of clock-dependent circuitry.

(i) Provision for absolute or differential precision voltage measurement of all power supply voltages and currents and of various instrument or STEA dc signals.

The front panel layout of the common function panel is presented in Fig. 86. Power control pushswitches and indicators are located at the upper left. The meter is mounted at the top center. Meter management is accomplished by the controls at the upper right. The constant-current trim control and the 4.85-v trim controls are included with this grouping for convenience. Clock adjustments and output jacks are located at the lower right. Command pulse generator functions are located at the lower center. The precision reference controls are located at the lower left. The three-terminal connectors shown are Deutsch model DM-9611 quick-disconnect types which allow for management of signals carried on guarded twisted pairs. These connectors have been adopted as standard for three-terminal panel outlets in all experiment panels and associated equipment throughout the scientific instrument STEA.

(2) Alpha scattering experiment. System test planning has disclosed a need for a generator to insert height-to-time-converted (HTC) pulses into the

electronics unit of the alpha scattering instrument in place of the pulses from the sensor head unit. For trouble-shooting purposes, the HTC pulses transmitted by the sensor head on either the alpha or proton signal channels are inadequate because of randomness in both duration and time of occurrence. A portable test unit called the HTC pulse generator has been designed to fulfill the need. All variables of the simulated HTC pulses from the generator may be controlled.

The front panel of the HTC pulse generator is shown in Fig. 87; its specifications are as follows:

(a) Input characteristics:

Power – 120 v ac.

Triggering – internal or external.

Internal trigger – single pulses or repeated pulses at 1, 5, 20, or 50 pps.

External trigger – any pulse between 2 and 20 v will cause triggering.

(b) Output characteristics:

Waveform – duration or width-modulated, positive pulses of from 1 to 10 (adjustable).

Pulse duration – from channel 1 to channel 255.

Channel n duration, t_n, is given by $t_n = (n - \frac{1}{2})\, T_{osc}$, μsec and T_{osc}, which is the period of the driving oscillator, may be varied by adjustment from 1.05 to 1.18 μsec.

Output lines – HTC pulses: two for alpha and two for proton; also a sync output is available for oscilloscope triggering.

Pulse rates – (see internal trigger).

Pulse modes – HTC pulses:

(a) Alternating between alpha and proton channels.

(b) On alpha channel only.

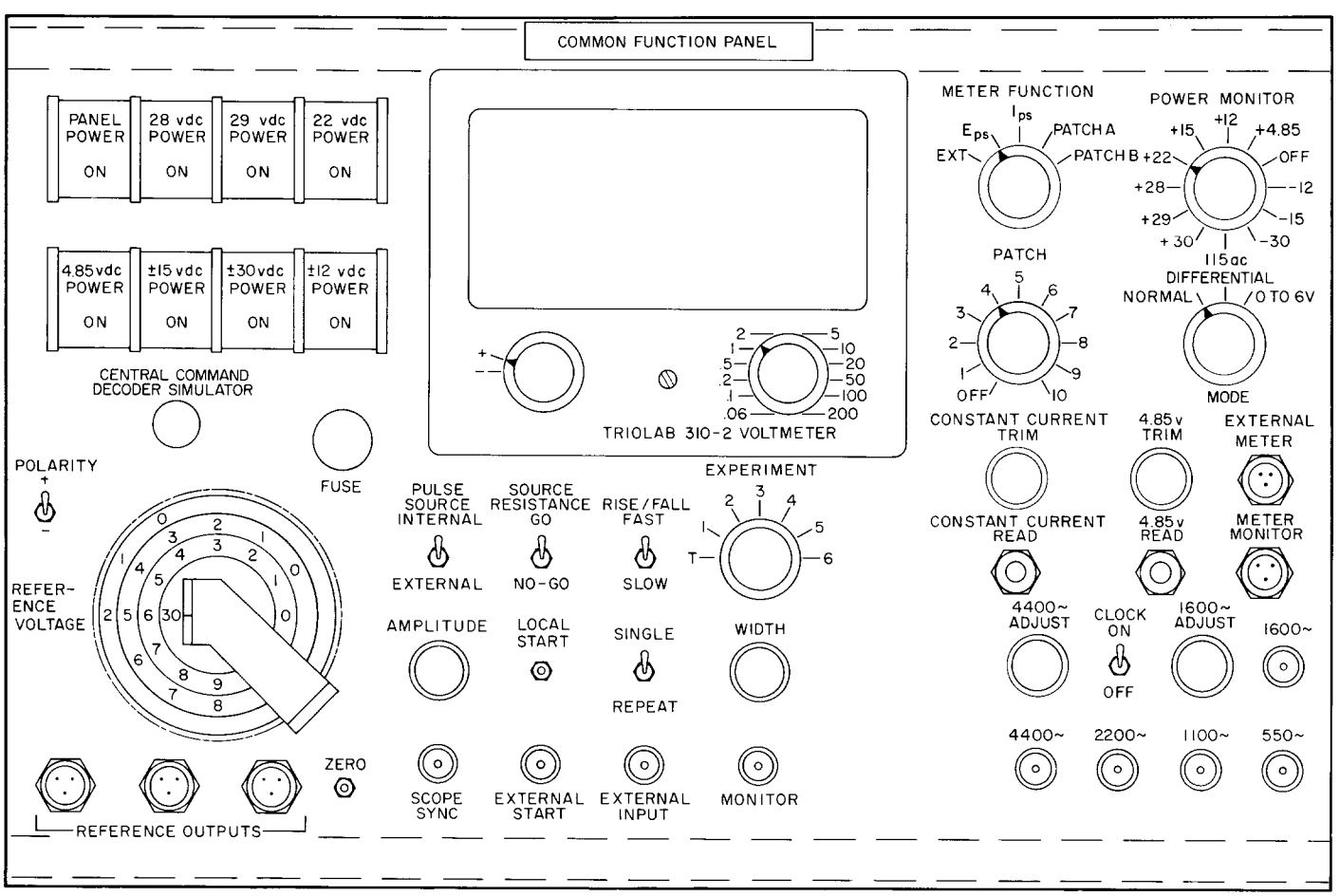

Fig. 86. Common function panel

(c) On proton channel only.

(d) On both channels.

The versatility provided in the various "pulse modes" of operation will enable the HTC pulse generator not only to isolate errors in the signal channels of the alpha scattering electronics unit but also to ascertain errors in the telemetered transmission of the alpha scattering instrument signals. In addition it will help locate errors in the data translator if used in conjunction with a data translator self-test unit.

(3) Portable anechoic chamber. The first anechoic test chamber for omnidirectional antenna test was delivered on March 19, 1964. After some preliminary test analysis, the unit was used to evaluate the omnidirectional antenna assemblies and system performance, producing a high degree of reliability and repeatable results. It is anticipated that use of the test chamber during system test will greatly reduce the length of rf test procedures with attendant reductions in the amount of test time required. It will also provide a quick indication of rf system degradation.

(4) System test instrumentation trailer. Fabrication of the instrumentation trailer is nearly completed. All cabling with the exception of a few small remote control cables has been installed. All test equipment except for the tape recorders and noise analyzer are on hand and are being installed. A check with both vendors indicated these remaining items will be received shortly. Complete checkout of the trailer is scheduled to be completed in early May.

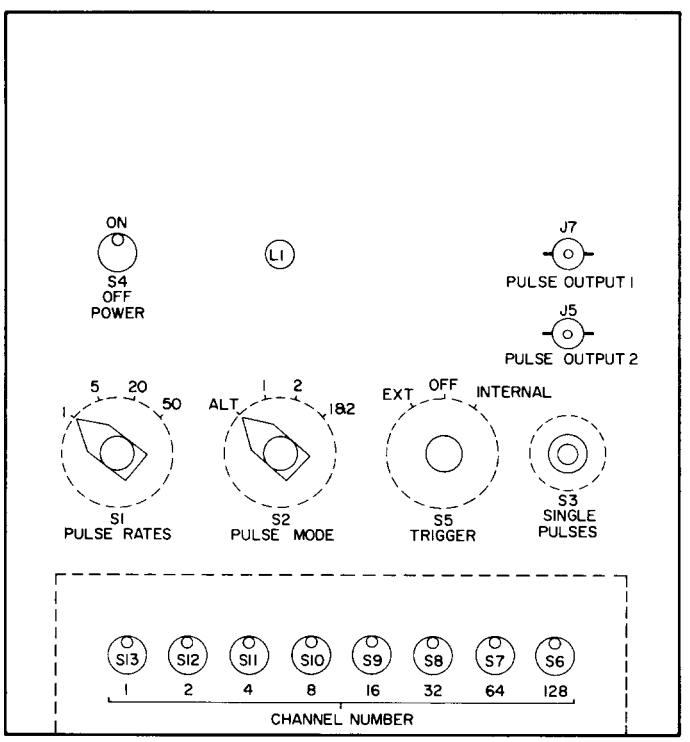

Fig. 87. HTC pulse generator front panel

e. S-8 suspension system tests. Testing of the elastic suspension system to be used at AFMDC during the S-8 buzz test was completed in the Space Environment Simulation Laboratory at El Segundo. The hardware tested is identical in all respects to the AFMDC configuration except for cord length. The AFMDC system will be 2.55 times longer, which will reduce natural frequencies to the desired values. Items observed and tested include the following:

(1) Natural frequency about the three rotational axes and in vertical translation.

(2) Damping ratio for all modes of motion.

(3) Verification of theoretical frequency data.

(4) Winch system operation.

(5) Ability to establish initial attitude and acceleration test conditions.

(6) Release device operation including live squibs.

(7) Instrumentation system.

(8) Coupled motion between pitch and yaw.

(9) Shock cord force, elongation, and creep.

The theoretical natural frequencies in pitch (about the X-axis) and in yaw (about the Y-axis) are shown in Fig. 88 as a function of the attach point for three different cases. Also shown are the data points taken during testing in the environmental facility for the ¾-in. cord system. The points taken at attach points of 0, 4.0, 6.5, and 7.5 in. compare favorably with the theoretical curve. The damping ratio determined from test data is also shown; this ratio increases quite rapidly as the natural frequency approaches zero. The vertical natural frequencies obtained from the environmental facility testing, as well as those extrapolated for AFMDC, are given in Table 42. The spring constant, K, is the value measured at the load point during testing in the environmental facility.

Winch system operation was quite satisfactory throughout the testing; however, a cable inspection after completion of testing revealed that the cables were being kinked because the first layer was not laying in properly. To correct the problem, the spools will be grooved.

The desired attitude control was achieved allowing initial attitudes to be set in within ¼ deg. using individual winch controls and reading out the inclinometers directly on digital voltmeters. Initial acceleration test conditions can be set up within ±5 lb by using the direct meter readouts from the elastic cord load cells. Accelerometers used to describe angular and translatory motion were found to be unsatisfactory because of the difficulty of separating the various modes of motion. It is recommended that optical means be used for describing vehicle motion.

Table 42. Suspension system characteristics

Parameter	Space environmental research facility	AFMDC (estimated)
Four ¾-in. cords per leg, 2100-lb system		
K per leg, (average)	44 lb/ft	28 lb/ft
Natural frequency, (vertical)	1.53 rad/sec	0.96 rad/sec
Damping ratio, (vertical)	0.019	
Natural frequency, (roll)	2.06 rad/sec	1.29 rad/sec
Four ½-in. cords per leg, 700-lb system		
K per leg	12 lb/ft	7.5 lb/ft
Natural frequency, (vertical)	1.3 rad/sec	0.8 rad/sec
Damping ratio, (vertical)	0.018	

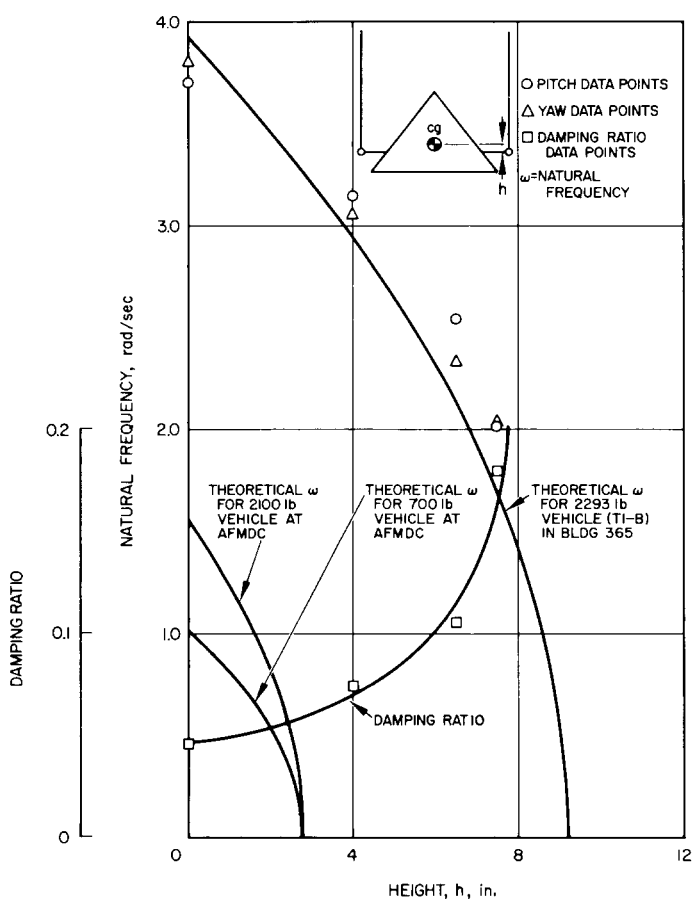

Fig. 88. Natural frequencies and damping ratios for suspension system

The squib-pinpuller release devices were operated a total of 27 times under various load conditions and operation was quite satisfactory. The most extreme case was the acceleration-with-snubbing test in which the vehicle was pulled down by the lower snubbing cable with a force of 700 lb and then released. The elastic cord in the lower snubbing cable started absorbing energy just above the static suspension point. This condition was established to simulate a possible failure case at AFMDC in which the vernier engines would be at full throttle for the entire upward vertical travel. One minor problem was encountered in the upper release devices when the black paint caused the device to hang up. Removing the paint corrected the problem.

Considerable coupling exists between pitch and yaw motion particularly when initial pitch or yaw conditions are established with a vertical displacement. The primary cause is unequal spring constants in each of the legs. For the system tested an 18% difference existed. However, this can be equalized by switching individual elastic cords.

At the conclusion of the tests using the ¾-in. cord 2100-lb system, a test was set up to determine vertical natural frequency and damping for one leg of the ½-in. 700-lb system. This consisted of a 231-lb mass suspended by four ½-in. cords. The mass was instrumented with a Statham accelerometer and a load cell in series with the cord attachment yoke. The mass was excited manually and the load cell and accelerometer outputs were recorded as shown in Fig. 89.

Samples taken from the shock cord used in the suspension development tests have been tested using the shock cord tester. Fig. 90 shows a typical force/percent elongation curve for the shock cord used in the suspension system tests with a 2293-lb simulated spacecraft. The predicted natural frequency (1.36 rad/sec) was computed using the slope of the curve at the operating point as the spring constant. The predicted frequency was 11% lower than the actual vertical frequency.

It is concluded from the test results that the vertical natural frequency requirement of less than 1 rad/sec can be achieved in the AFMDC configuration for both the ¾-in. cord/2100-lb and ½-in. cord/700-lb systems. The natural frequency in roll (about the Z-axis)

UNCLASSIFIED

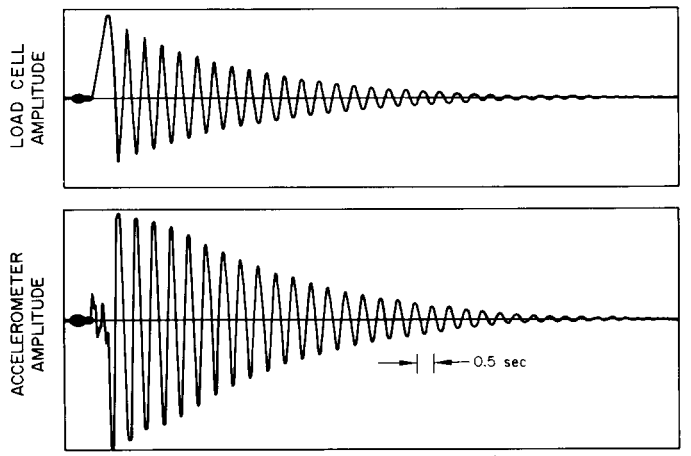

Fig. 89. Load and acceleration traces for the ½-in., 200-lb, 4-cord system

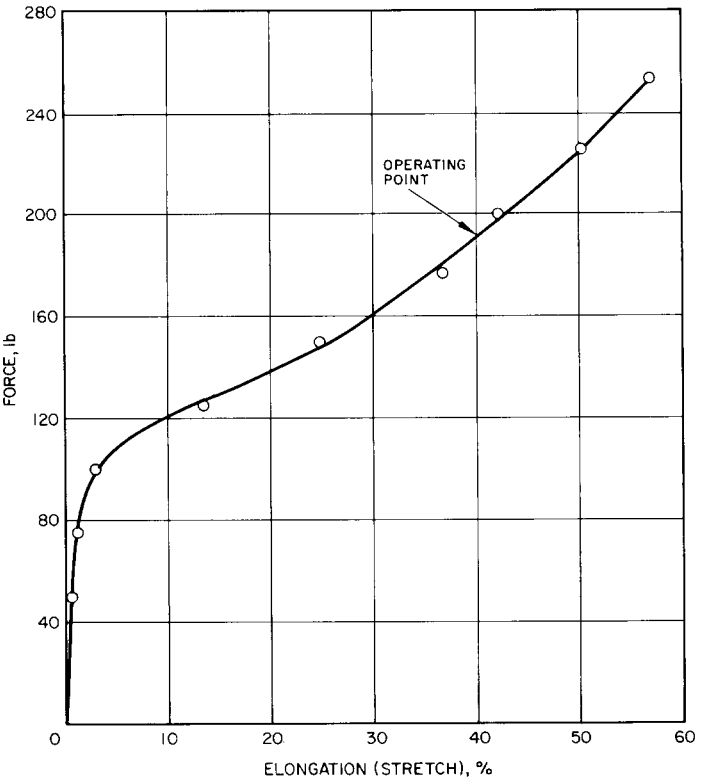

Fig. 90. Typical force/percent elongation of suspension system with ¾-in. shock cord

extrapolated to the AFMDC case also meets the requirement of less than 1.5 rad/sec. It was demonstrated that the attitude natural frequencies (pitch and yaw) could be controlled within limitations by the adjustment of the attachment point with respect to the center of gravity (h distance), and the actual pitch and yaw data points compared favorably with the theoretical frequencies. Assuming the same relationships hold when extrapolating to the longer AFMDC case, the required natural frequency of less than 1.5 rad/sec in pitch and yaw can be achieved with the attachment point set very close to the center of gravity. For the AMFDC case it is desirable from a stability standpoint to have the distance h as small as possible, since zero frequency occurs at an h of only 2.8 in.

UNCLASSIFIED

L. Mission Operations

1. Spacecraft Readiness Test Procedure

During this reporting period, the method of producing and maintaining spacecraft readiness test procedures (SRTP) and the countdown procedure was formulated. All the information to produce a test procedure and to punch the corresponding punched paper command tape is combined in a single deck of cards. A computer program that prints out the test procedure from this card deck has been written. A computer program is currently being formulated to permit the punching of the command tape directly from the test procedure card deck. This command tape contains both spacecraft commands and programmed automatic telemetry evaluator (PATE) programming information.

A workbook, which is a printout of all the information on a test procedure card deck, is utilized for change control. All changes are entered in this workbook allowing simultaneous changing of both procedure and command tape. The changes in the workbook are entered into the test procedure card deck; then a multilith master of the revised procedure, a corresponding command tape, and a current workbook are produced.

Revision A of the Spacecraft Readiness Test Procedure was published using the computer program mentioned above. A general description of the procedure follows:

Spacecraft readiness tests (SRT) will be performed before gantry removal. The test will be oriented toward efficient data return through minimized mode switching. Spacecraft power will be provided from two prelaunch power supplies, a solar panel simulator which supplies power through the optimum charge regulator (OCR), and a battery simulator which parallels the battery. Tested systems will be exercised within the practical limitations dictated by the encapsulated and mated condition of the spacecraft. Test control and safety aspects will be maintained and spacecraft performance monitored by the test conductor at the Spacecraft Checkout Facility (SCF). Maximum usage will be made of the programmed automatic telemetry evaluator (PATE).

The test configuration will be as follows:

(1) Spacecraft encapsulated and mated to the *Centaur* launch vehicle on the launch pad.

(2) Remote countdown test equipment (RCTE) in the SCF.

(3) Passive repeater (an antenna relay system to allow the establishment of an rf link before the gantry is removed) in the gantry.

(4) Solar panel simulator and battery simulator power supplies in the Launch and Service Building.

(5) Propellant sniffers on the umbilical tower.

(6) Blockhouse console in the blockhouse.

The RCTE consists of a command and data handling console (CDC), receiver, transmitter, antenna, and PATE. All required commands will be initiated on the CDC by either manual keyboard or tape entry. Primary data will be displayed by the CDC and evaluations of incoming telemetry data will be made by PATE. Certain functions, such as turn-on of the ground power supplies, voltage and current monitoring of these supplies, retro-rocket temperature monitoring, TV target illumination, and propellant sniffer monitoring will be accomplished at the blockhouse console.

During the operation of the CDC in conjunction with PATE, the indicators on the display console (CDC Bay 3) are no longer the primary means of evaluating spacecraft engineering data. Analog meter 16 is used to display the telemetry data word being routed to PATE. This leaves 15 analog meters, 5 BCD Nixie indicators, and 16 binary indicator lamps, which are available for monitoring any desired telemetered data. The data displayed on these indicators is controlled by a switching panel located in the PATE rack. It is planned that these indicators will be used to monitor critical data (such as power parameters) at all times when this data is available.

In developing this procedure, an attempt was made to verify the reception and subsequent performance of all spacecraft commands that could be sent under the limitations of the test configuration. Every possible telemetry return was monitored, and all systems that could give significant test results were exercised.

It is currently planned that this test (with necessary modifications as a result of changed environment and spacecraft configuration) will be run several times before the final readiness test on the launch pad. A spacecraft readiness test will be performed at the conclusion of system testing during combined systems tests, during Spacecraft Checkout Facility operations, and at the conclusion of Explosive Safe Area operations, as well as during Launch Complex operations. In this manner, confidence in the test and in the spacecraft can be obtained and maintained until launch.

The Spacecraft Readiness Test Procedure contains the following information:

(1) The estimated countdown time for each major check.

(2) The communications channel over which the listed step will be coordinated.

(3) A sequential step and substep number. Change control is accomplished by a decimal system.

(4) A code to refer the listed step back to the test requirements identification system where applicable.

(5) The operator performing the listed step.

(6) An English language description of the listed step. For steps involving commands, the step is written out (e.g., CMD SUMMING AMPS OFF). For steps involving data channels, the data word is written out and the CDC decommutator frame word number is listed for reference (e.g., VERIFY XMTR B TEMP W30). For digital data words, each bit is listed as a substep with the bit number for reference (e.g., MANUAL DELAY MODE Z10 B9).

(7) The octal command number for steps involving commands.

(8) The mode by which the step is executed. The modes are coded as follows:

Command entry

K – Keyboard

A – Automatic

X – Automatic (magnitude command)

I – Automatic (interlocked command)

PATE operation modes

M – Magnitude comparison

B – Bit comparison

O – Single word printout

S – Sequential printout

In the magnitude comparison mode, PATE compares the incoming telemetry data with preprogrammed upper and lower limits. In the bit comparison mode, PATE compares selected bits of digital words with preprogrammed desired bits. The single word printout provides a continuous printout of a selected incoming data word. The sequential printout provides a record of each word in the telemetry frame with recycling.

(9) The octal sequence number of each taped step. This allows searching the tape to find any desired point in the procedure. Change control is accomplished by leaving spares.

(10) The data channel designation of the parameter being observed.

Prior to the start of the spacecraft readiness test (SRT), the remote countdown test equipment will be prepared by an F-1 day procedure. This procedure will include preparation of the PATE, system test equipment assembly, receiver/transmitter, blockhouse console, ground power supplies, passive repeater, propellant sniffers, communication links, and other related equipment. Immediately following the SRT is a period of rf silence during critical *Atlas/Centaur* operations. The countdown, beginning at T-80M, follows the rf silence period and culminates in the launch.

2. Real Time Data Handling and Transmission

A system for the handling and transmission of real time telemetry during the final countdown and during the period from launch until Deep Space Instrumentation Facility (DSIF) acquisition has been agreed upon by Atlantic Missile Range, Hughes, and Jet Propulsion Laboratory. Fig. 91 depicts the overall system while Fig. 92 shows the Hughes operational interfaces with Atlantic Missile Range and JPL.

The following tenets of operational philosophy during the postlaunch period have been agreed upon:

The 3 × 3 data switch matrix, the clock select switch, and the data quality strip chart recorder will be in close proximity to the Hughes CDC for ease of operational control. These items of equipment, which control the CDC input, will be operated by a member of the Hughes launch operations team.

The data path through the CDC is the primary data path. The path through the polar to neutral converter is the backup data path. All real time *Surveyor* engineering data transmitted to the Space Flight Operations Facility (SFOF) will either be routed through the CDC or the CDC will be receiving a parallel input.

Down-range received data will be selected for transmission to the SFOF and for display and evaluation on the CDC by scanning down-range data on the data quality strip chart recorder and selecting the most distant station with usable data.

The CDC at AMR will serve as backup to the SFOF in obtaining acquisition data if the AMR-SFOF data link should fail. Strip chart recorders displaying selected spacecraft data at the down-range stations and ships will serve as backup to the SFOF in obtaining acquisition data should the up-range data link fail.

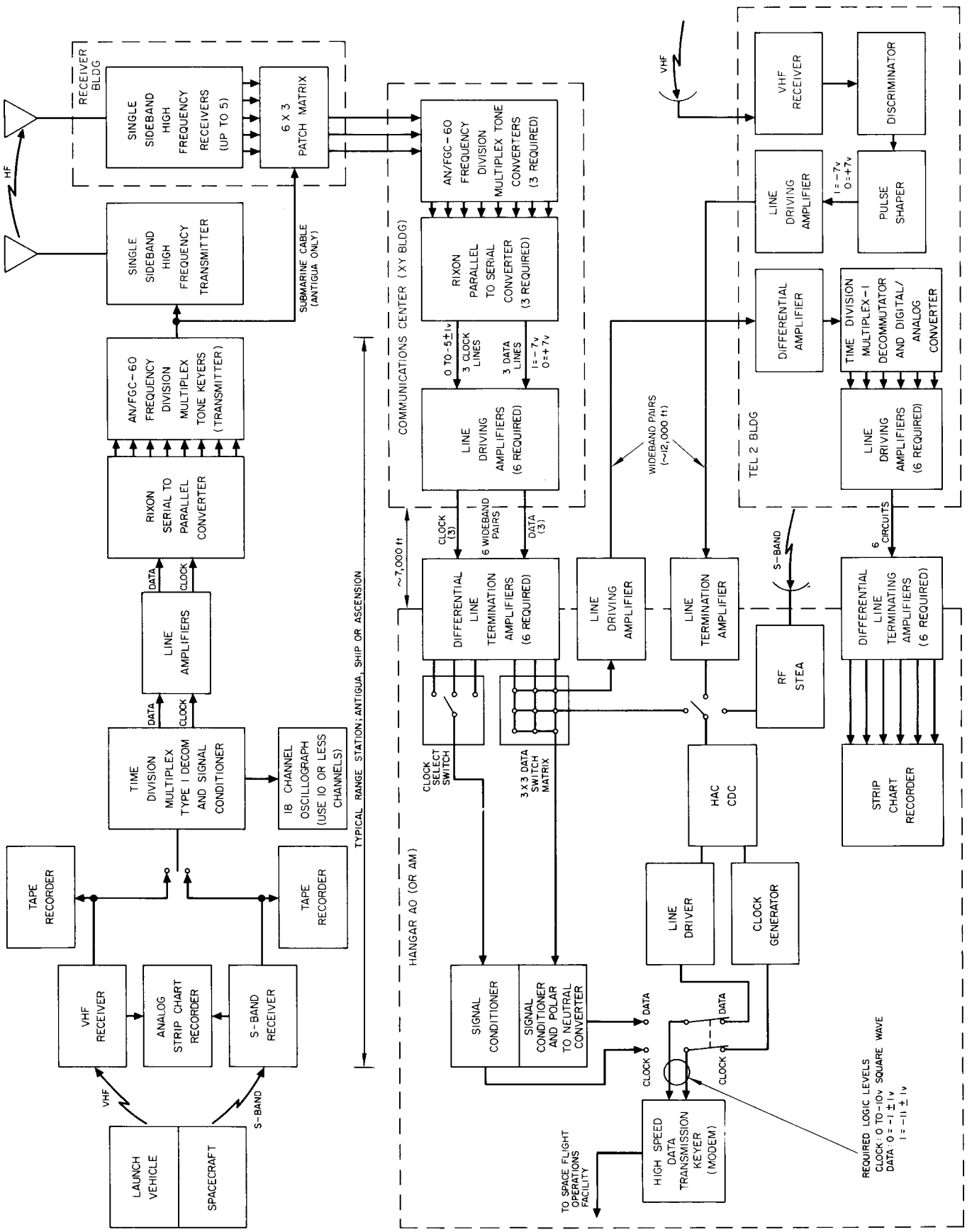

Fig. 91. Real time telemetry data system

Voice and teletype links between the Hughes launch operations team and the SFOF will be established. The SFOF will be informed of changing spacecraft configuration or operation during the countdown via these links. This procedure will be extended into the postlaunch period so that the SFOF can be kept informed of the down-range data quality and, in case of failure of the AMR-SFOF high speed data link, of the spacecraft status.

3. AMR Pad Safety Report

A revision of the AMR Pad Safety Report, a document required by Atlantic Missile Range, was issued in February 1964. Copies have been sent to JPL and GD/A for review. This report contains descriptions and instructions on storage and handling for hazardous items, including ordnance and pyrotechnic devices, propellants, and high-pressure gas systems on the spacecraft as well as ground equipment.

4. Launch Complex Operations

The Launch Complex Operations Directive, providing direction for the accomplishment of *Surveyor* operations at Launch Complex 36, has been released. This document includes the tasks in direct support of launch complex operations and the tasks directly involving the spacecraft itself.

Tasks to be performed at the launch complex are summarized as follows (Fig. 93):

a. AMR-SFOF net checks

(1) *AMR-SFOF compatibility test.* A one-time test to assure compatibility of the AMR-SFOF communication and data processing interface.

(2) *AMR-SFOF tracking and telemetry data test.* Performed as required to verify the operational readiness of the AMR-SFOF interface.

(3) *Space Flight Operations Complex and AMR operational readiness test.* Performed twice during the 7-day period preceding each launch to verify the readiness of the Space Flight Operations Complex and the AMR.

b. RF link checks. These checks verify the capability of the rf link to maintain a usable signal level.

c. Remote countdown test equipment verification. This verification will check the operational status of the CDC, the rf STEA, and the PATE.

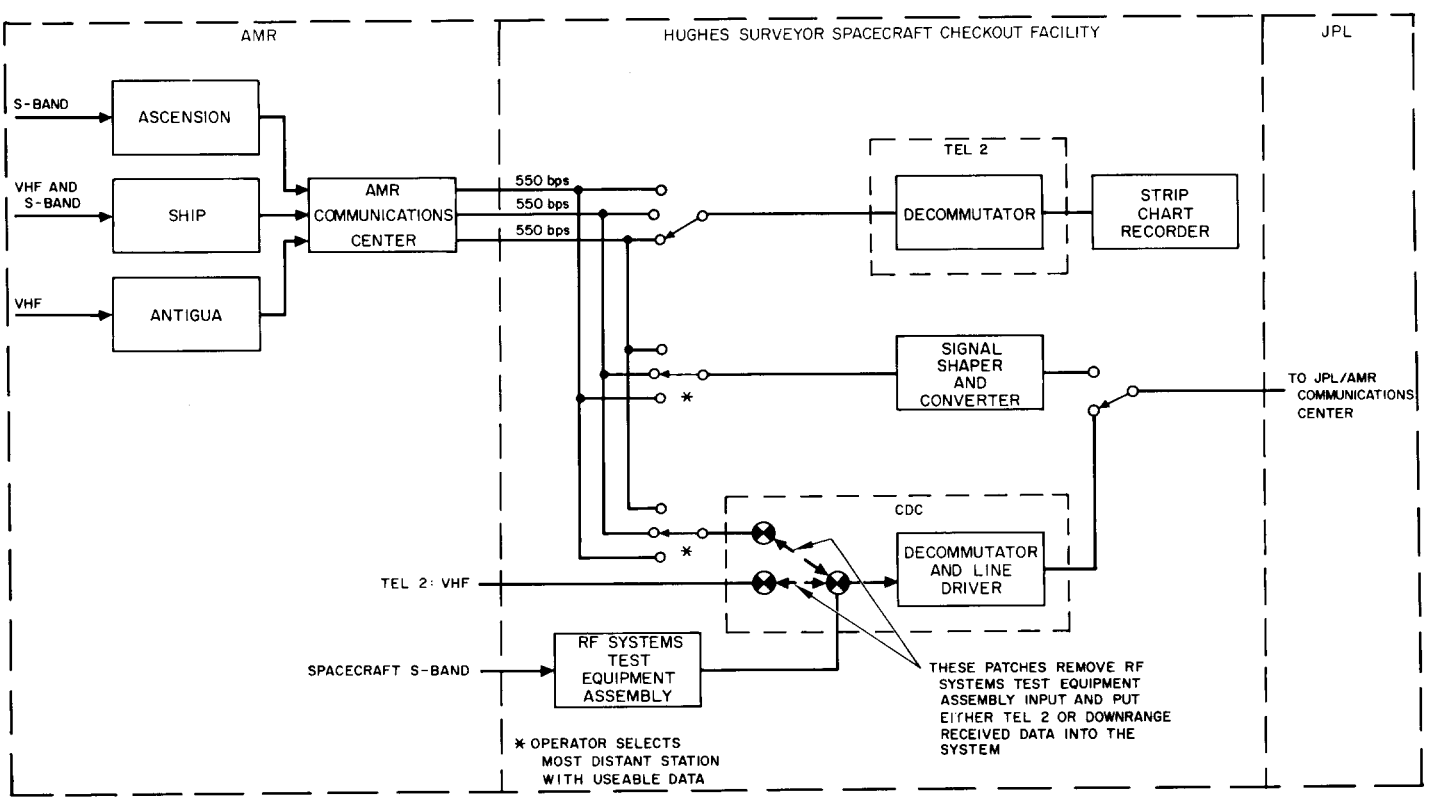

Fig. 92. Hughes real time data handling operational interfaces

d. Blockhouse console verification. The operational status of the blockhouse console, launch control rack, and toxic vapor detectors will be verified.

e. Missile operations intercommunication system verification. A check of communication circuits and procedures used during launch complex operations will be made.

f. Transport spacecraft to the launch pad. Transportation of the spacecraft from the Explosive Safe Area to the launch pad and the positioning of the spacecraft in the hoist area will be accomplished.

g. Mating operations. This task consists of electrical and mechanical mating of the spacecraft to the *Centaur* and the connection of pad air conditioning and toxic vapor detectors.

h. Spacecraft readiness test. An on-stand checkout of the spacecraft will be made to assure that all systems are operating within their design specification, and to determine that the spacecraft is ready to progress into its final phase of flight preparation.

i. Spacecraft countdown. A final check of critical subsystems will be made and the spacecraft placed in a flight configuration.

j. Postlaunch operations. These operations consist of monitoring telemetry data after launch and prior to spacecraft acquisition by the Johannesburg Deep Space Instrumentation Facility.

5. PATE/CDC Integration

The prototype programmed automatic telemetry evaluator (PATE) was integrated with the command and data handling console (CDC) during this report period. All modes of operation were successfully demonstrated, including operation utilizing the pulse code modulated (PCM) bursts used with TV transmission. Several demonstrations of PATE were given for NASA, JPL, and Hughes personnel. An operational description of PATE follows:

a. PATE function. The PATE system has been designed to expedite the handling of *Surveyor* spacecraft telemetered data. The system will supplement the telemetry processing function of the CDC. The time allotted for spacecraft testing on the launch pad is well defined and the boundaries governing the initiation and subsequent conclusion of the testing period are generally inflexible. Consequently, rapid and precise checks of the *Surveyor* operating parameters that are telemetered from the spacecraft are required.

b. Programmed automatic telemetry evaluator. The PATE system is integrated functionally with the CDC (Fig. 94) and provides a means for making frequent and

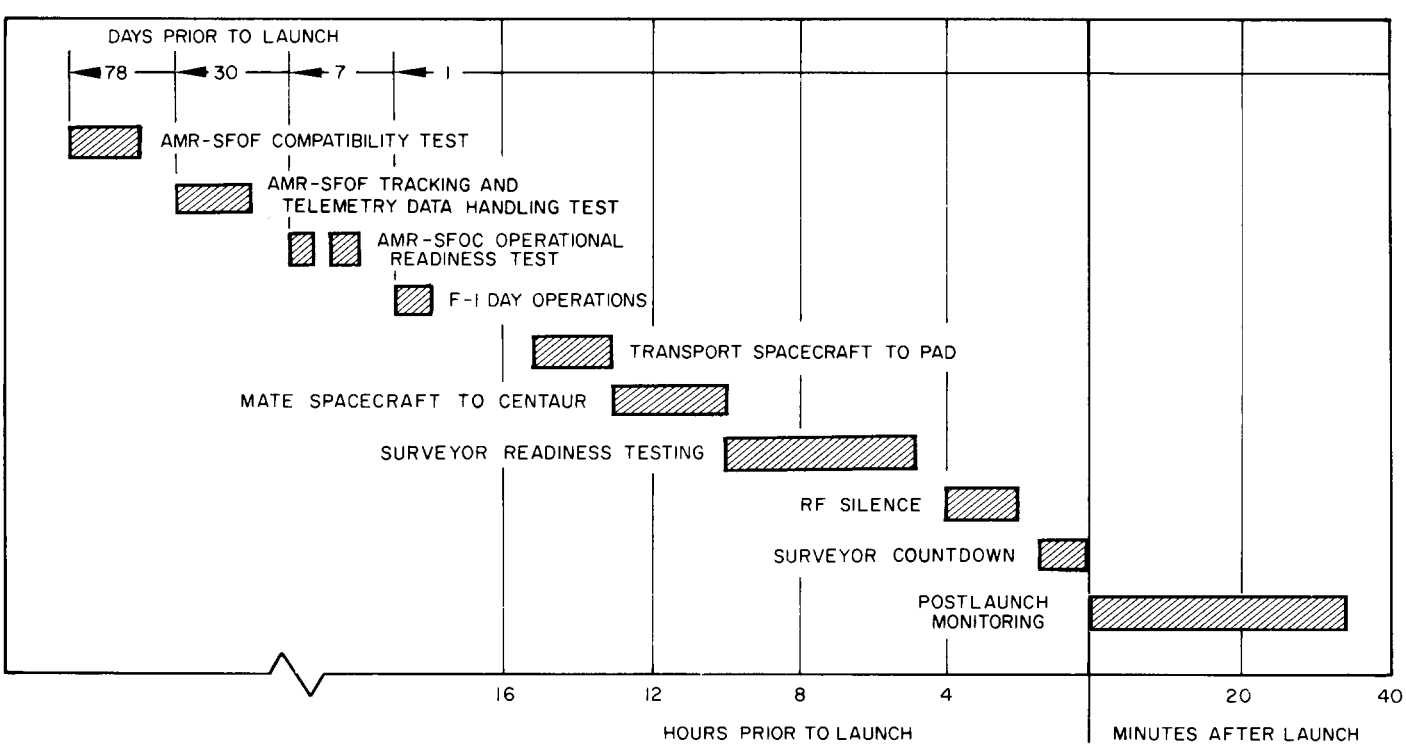

Fig. 93. Launch complex operations

rapid evaluations of all PCM data telemetered from the spacecraft to ascertain *Surveyor* readiness during spacecraft readiness testing and countdown. The PATE system performs this function without the necessity of changing patchboards, the use of overlays for indicator identification, or operator evaluations of displayed data. When utilizing the PATE, each spacecraft parameter is evaluated against known limits in a preprogrammed sequence, and a GO or NO-GO condition is automatically determined. If the comparison demonstrates that the telemetered data is within the specified tolerance, the system proceeds to the next programmed operation. If a NO-GO condition exists, the program is interrupted and a fail indicator is illuminated.

c. PATE input. The PATE system receives its inputs from the CDC decommutator and a preprogrammed punched paper tape. Paper tape is presently being utilized by the CDC to feed a programmed sequence of spacecraft commands to the command generator where they are processed and transmitted. During PATE operations, this tape is replaced by a preprogrammed paper tape which will include PATE information in addition to spacecraft commands. The sequence in which the PATE system will perform comparisons of telemetered spacecraft data to desired system operating parameters is determined by the tape.

PCM data, transmitted from the spacecraft, is received by the CDC and demodulated and decommutated into 10-bit data words. Information contained on the paper tape gates a data word from the telemetry frame in the CDC decommutator into a digital comparator located in the PATE (Fig. 95). The tolerance values required to make a comparison are received from the next block of characters punched on the tape.

d. PATE readout. Readout for visual inspection of the PATE evaluation is accomplished on a digital recorder (printer) in Bay 9 of the CDC. In the present configuration, the printer makes a record of the following:

(1) All commands transmitted to the spacecraft and the time (in GMT) of transmission.

(2) An E in front of the recorded word to identify an emergency command transmission.

(3) An M in front of the recorded word to identify a magnitude command transmission.

(4) A + in front of the recorded word to indicate "mark."

In operation with PATE the printer records additional information as follows:

(1) The decommutator frame word number.

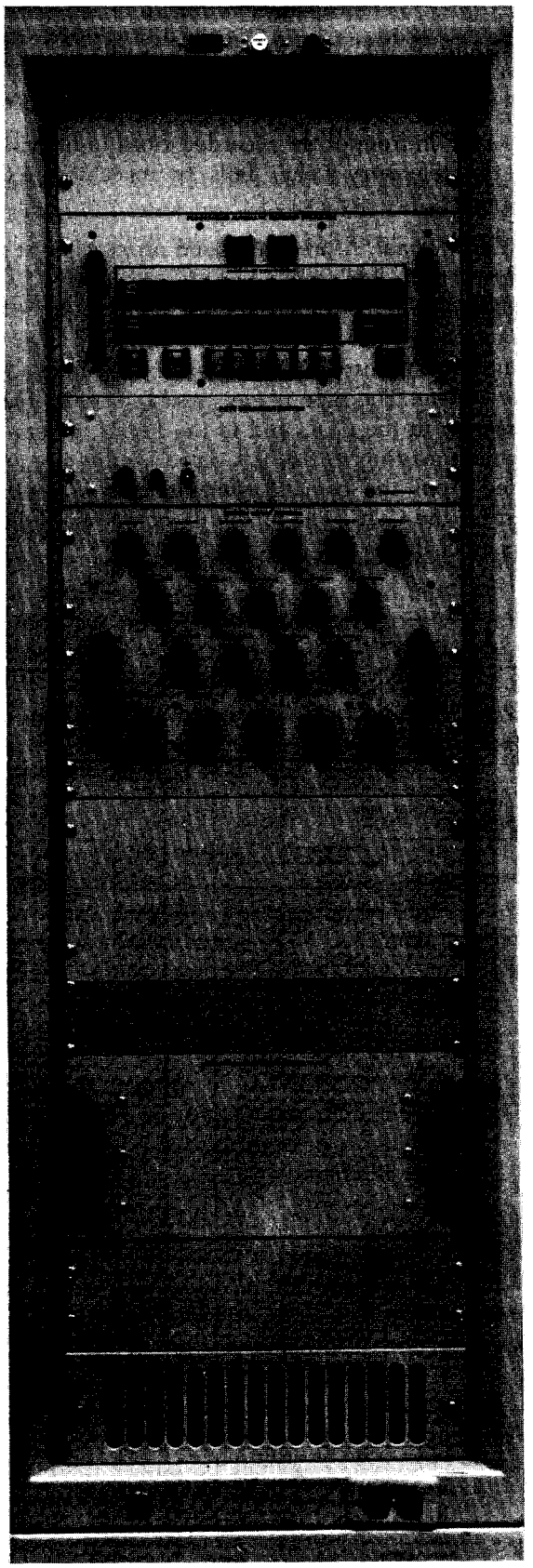

Fig. 94. PATE system control rack

(2) Upper tolerance value (or bits to be compared).

(3) Value of the telemetered data word.

(4) Lower tolerance value (or programmed word).

(5) An F in front of the recorded word to indicate that the telemetry value fails to meet the required limits.

e. Tape format. A predetermined program, best suited for spacecraft data evaluation by the PATE during countdown, will be punched into paper tape utilizing the long range interceptor (LRI) code which is the code presently being used in the *Surveyor* command tape reader system. The tape reader used to serially feed the information to the CDC and to the PATE system is the equipment existing in Bay 9. Control of the tape will be handled from the comand generator as presently designed for the CDC. The tape will include the following sequence of data:

(1) Sequence number.

(2) Spacecraft command.

(3) Sequence number.

(4) Control character.

(5) Telemetry data word select for PATE.

(6) Tolerance values.

(7) Control character.

Sequence numbers are inserted in the tape to incrementally tag each operation of the command generator and the PATE. These numbers will be displayed to the command generator operator, so that he will know exactly which part of the tape program is being performed.

The "command" information on the tape pertains to spacecraft commands which are fed to the command generator, encoded, and transmitted to the spacecraft.

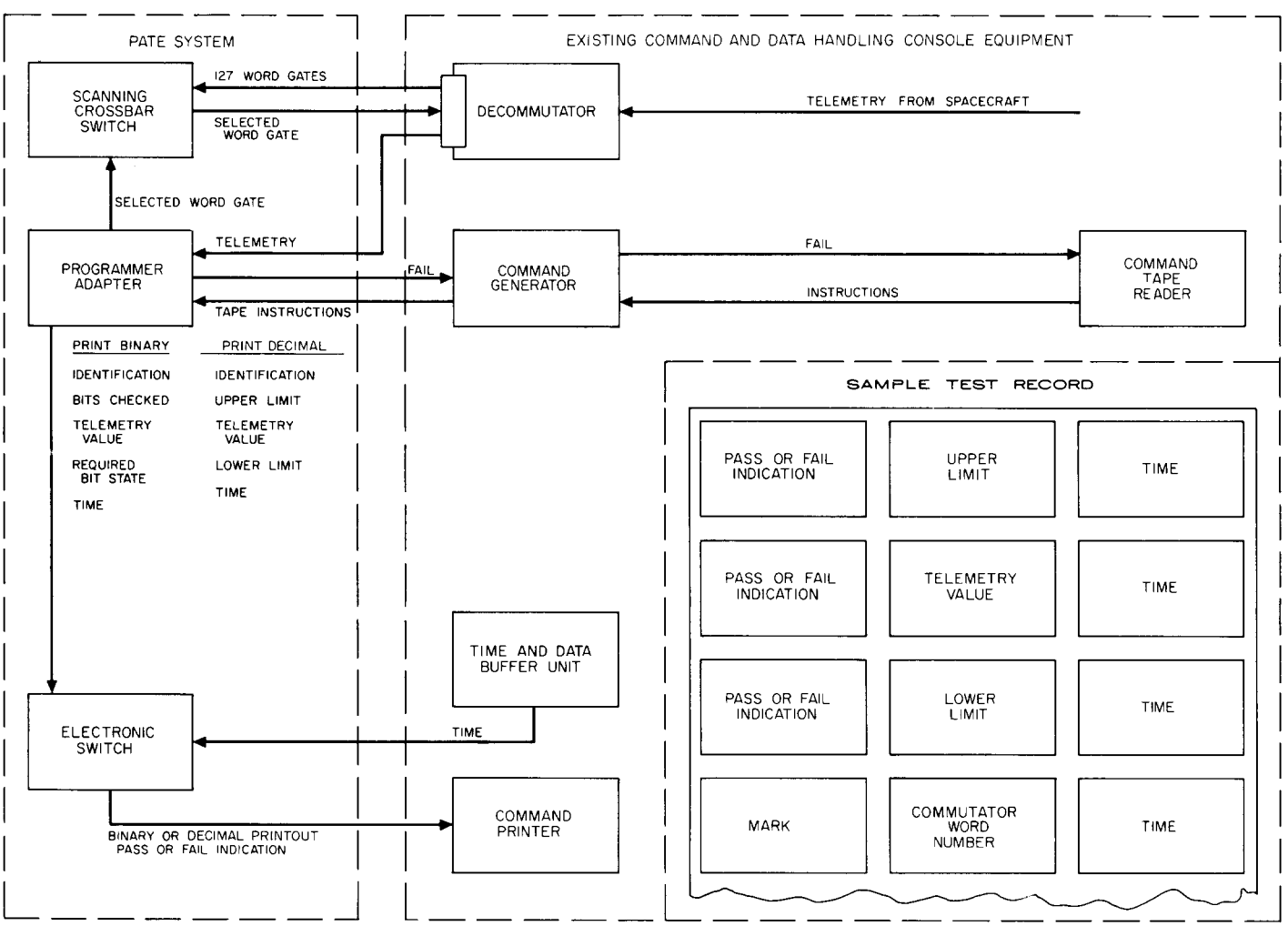

Fig. 95. Programmed automatic telemetry evaluator

A control character, which was not previously used by the command generator, is utilized to indicate that succeeding information on the tape is intended for use by the PATE. This character inhibits the normal information processing in the command generator and the tape data is fed to the PATE registers.

"Telemetry data select" is that information punched on the tape which will gate the desired telemetry word from the decommutator into the PATE comparator for evaluation. This is done by closing the appropriate crosspoint on a crossbar switch which will allow a word gate signal to enter the decommutator channel transfer function and gate its corresponding word of telemetry data into the channel memory. The telemetry word is monitored by the PATE comparator and compared to tolerance values read from the tape.

Tolerance values are the upper and lower limits within which the spacecraft parameter must be operating in order to be functioning properly. These values are precalculated and will be verified by data accrued during spacecraft flight acceptance tests.

Following the data fed to the PATE system, another control character will "enable" the command generator. This character indicates that the next portion of data on the tape will contain command information that is to be processed by the CDC.

f. PATE operation. The PATE system will have three modes of operation: (1) comparison of the magnitude of a 10-bit binary word to upper and lower tolerance values, (2) comparison of arbitrary bits of a 10-bit telemetry word to corresponding bits of a programmed word, and (3) recording of either of the following on the digital recorder: a single telemetry commutator word, or an entire telemetry frame.

The following paragraphs give a general operational description of each mode:

(1) *Mode I (magnitude comparison).* Magnitude information from the *Surveyor* spacecraft such as temperature, voltage, current, etc., is gated into the PATE digital comparator in a 10-bit binary form from the CDC decommutator, where it is evaluated by comparing it to tolerance values received from the punched tape.

A failure of the telemetered data word to fall within the specified limits will result in a NO-GO signal which stops the tape. Also, a red FAIL lamp on the front of the PATE panel will illuminate (Fig. 96). On the PATE readout, an F will be printed in front of the telemetry word. The test operator must then take the necessary steps to correct the unfavorable condition.

To reactivate the automatic operation of the system, the PROCEED button on the command generator must be depressed. This action starts the tape and clears the system for the next sequence of data punched on the program.

A GO signal generated by the PATE indicates that a telemetry data word has been found to have a passing value. In this case, the green PASS lamp on the front of the PATE panel remains illuminated, and the system automatically steps to the next sequence of operations punched on the tape.

(2) *Mode II (bit comparison).* Some of the telemetered commutator words from the spacecraft contain binary (ON-OFF) information on each of its 10 bits. At times, it may be desirable to check the status of only a portion of the data contained within one of these binary words. This is done by comparing the state of only those desired bits in the telemetry word to corresponding bits of a binary word supplied from the punched tape. An indication of PASS or FAIL is generated by the PATE the same way as in Mode I. On the PATE readout, a record will be made of the word compared, the programmed word, and the bits compared. This data will be printed in binary form on the printer, instead of decimal as is the case in Mode I.

(3) *Mode III (single word and sequential printout).* This mode is the manual operation of the PATE system and is utilized when only a printed record is desired of spacecraft data. The binary information selected from the telemetry frame in the PCM decommutator bypasses the digital comparison in the PATE and enters into the print register. The printer monitors the data fed to the register and prints a record of it.

Mode III consists of the selection of either of two manual entries of commutator data into the PATE by the operator: (1) the gating of a single data word from the telemetry frame, or (2) sequentially gating the entire telemetry frame.

Selection of a single data word is done by entering the desired telemetry word number, as it appears in the decommutator, on the keyboard located on the front of the PATE panel. If the selected word contains magnitude information, the decimal lamp should be lit by depressing the appropriate pushbutton on the keyboard. If the word contains binary data, the binary portion of the indicator switch should be illuminated by the operator. This function determines whether the record is to be printed in decimal or binary. When the ENTER button is activated, the selected word will be monitored by the recorder for continuous samples of its telemetered value.

To stop the action, the CLEAR portion of the pushbutton indicator switch should be illuminated by the operator.

To print an entire telemetry frame, the CYCLE pushbutton on the PATE panel should be depressed. The telemetry frame will then be sequentially gated from the decommutator into the PATE print register where a continuous record is made by the recorder. To stop this function, the CYCLE indicator pushbutton switch must again be pressed. This feature gives the system the capability of making a permanent record of all data telemetered from the spacecraft over an extended period.

g. Additional PATE features

(1) *Readout identification.* The number of the telemetry data word, as it appears in the decommutator frame, will be printed in front of each PATE record on the recorder. During the Mode I and Mode II operations of the PATE, this will give the test operator a rapid means of identifying a telemetry word during a FAIL condition so that the trouble can be traced to a specific location in as short a time as possible.

(2) *Intermittent data.* If at any time during the operation of the PATE, the ground support equipment loses rf lock with the spacecraft, the PATE system will be automatically inhibited from receiving input data from the PCM decommutator. This feature will reduce the possibility of faulty data being fed to the digital comparator.

(3) *Printer time share.* At times during the countdown, it will be necessary to send a command to the spacecraft using manual keyboard entry on the command generator at the same time output information from Mode III of the PATE is being recorded. Since it is necessary to have a record of any transmitted commands, the command data will be interposed on the digital recorder output.

(4) *Telemetry console indicator display.* During the operation of the CDC in conjunction with PATE, complete evaluation of telemetered data is no longer performed on the indicators located in the display console (Bay 3 CDC). Analog meter 16 is used to monitor the telemetry data word being routed to the PATE system by crossbar switch selection for a visual inspection of its value. This leaves 15 analog meters, 5 BCD Nixie indicators, and 16 binary indicator lamps for monitoring any desired telemetered data. The data displayed on these indicators is controlled by a switching panel located in the PATE rack (Fig. 97).

(5) *Command-compare tape data.* In the automatic modes of the PATE system for *Surveyor* checkout, the punched paper tape contains the input information to the CDC command generator and the PATE registers. To tell whether data is being fed to the command generator or to the PATE, a COMMAND – COMPARE indicator is illuminated on the front of the PATE panel. COMPARE is lit by the special inhibit control character

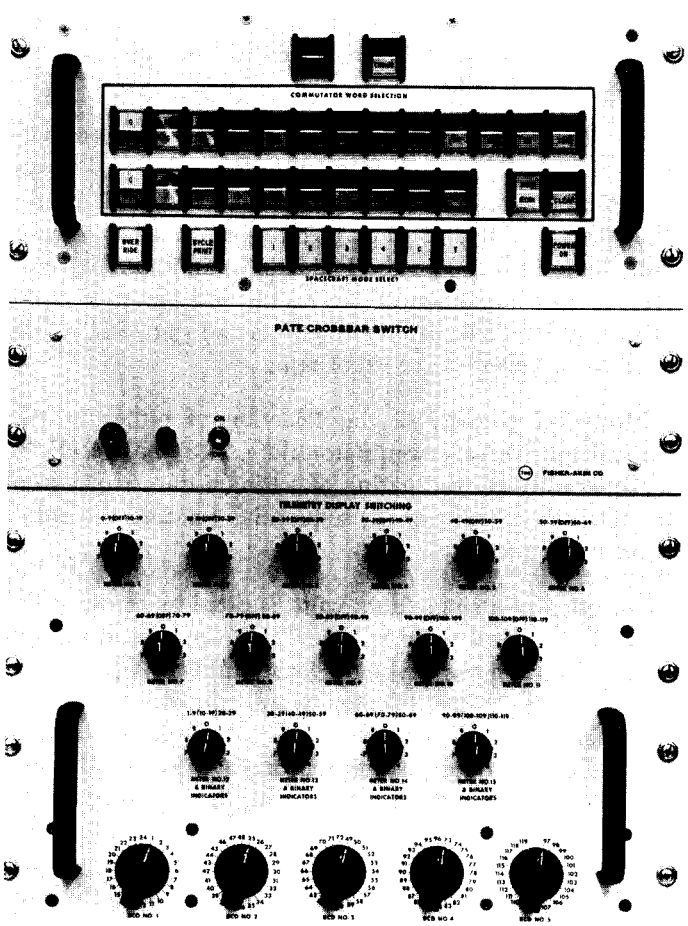

Fig. 96. PATE control panel

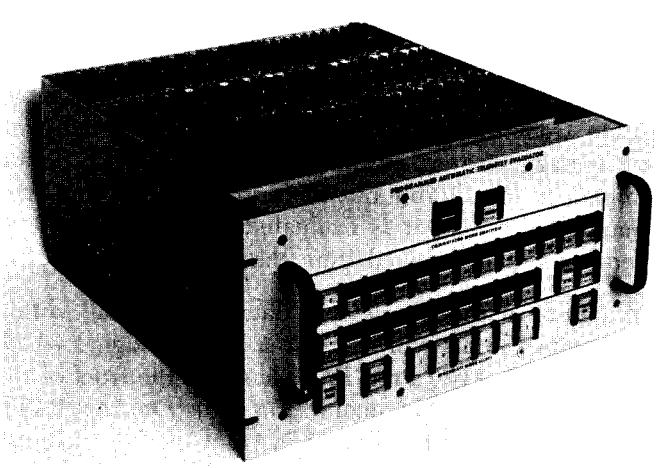

Fig. 97. PATE switching rack

on the tape which indicates that the following information is intended for the PATE. COMMAND is illuminated by the special enable character punched on the tape which indicates command information follows. In this way, the PATE operator will know when a comparison is taking place within the digital comparator.

(6) *Override.* Following spacecraft launch, it will no longer be desirable to have the PATE systems NO-GO signal cause a tape stoppage due to a telemetry word failing the PATE comparison. Therefore, an override signal is generated in the PATE by depressing a push-button switch on the front of the panel. The FAIL indicator will only momentarily illuminate if an unfavorable data word is compared, and the system will continue in its automatic mode of operation. An inspection of the digital recorder tape will reveal any out of tolerance conditions as the fail symbol will still be printed.

h. PATE applications. The PATE system was designed primarily to assist in *Surveyor* readiness testing on the launch pad and during the countdown when test flow and allotted time are most constrained. However, the PATE may also be beneficially employed in other *Surveyor* test operations where the CDC is utilized for central command and control. These tests include the following:

(1) Qualification or "sell-off" testing at the flight acceptance tests.

(2) *Surveyor* readiness and/or simulated countdown tests at the Combined Systems Test (CST), Spacecraft Checkout Facility (SCF), and Explosive Safe Area (ESA).

(3) Engineering interrogations performed from the Deep Space Instrumentation Facility (DSIF) during spaceflight and lunar operations.

The beneficial features of the PATE as applied to these operations are:

(1) To perform rapid evaluations of telemetered data which will provide verification that the spacecraft is functioning properly.

(2) To standardize procedures and minimize operator requirements by utilizing a preprogrammed tape for controlling the spacecraft testing and interrogations.

(3) To provide permanent digital records of the information compiled during the spacecraft testing and interrogations.

Flight acceptance test. During performance of the *Surveyor* flight acceptance test, a qualification or sell-off test is frequently required before the next test increment can be started. The flight acceptance test consists of three basic test phases:

(1) The systems functional test phase.

(2) Vibration test phase.

(3) Thermal–vacuum test phase.

Sell-off tests will be required after the vibration and thermal–vacuum test phases to assure that spacecraft performance has not been compromised as a result of test environments. By utilizing the PATE and the CDC for the major portion of these sell-off tests, the spacecraft can be rapidly examined and compared with predetermined performance standards. The same preprogrammed tape can be utilized for each phase to assure conformity throughout the tests. In this manner a constant performance comparison base that will quickly and automatically alert personnel to possible performance degradation will be provided. The preprogrammed tape will set the limits on allowable changes.

During any of the flight acceptance test phases, the PATE can be utilized to check spacecraft measurements for correspondence to anticipated outputs. For example, a thermal profile yielding projected spacecraft thermal characteristics will have been made in preparation for the thermal–vacuum test. Validity of this profile can be assured automatically by preprogramming the PATE tape with values extracted from the thermal profile.

Testing at the ESA, SCF, and CST. Surveyor readiness and/or simulated countdown tests will be performed at the CST, SCF, and ESA. These tests will be performed utilizing an rf link for command and data transmission. They will all be similarly patterned after the launch countdown test with major portions of the countdown preprogrammed tape utilized. In this manner, a performance standard will be set for the launch countdown, against which previous data can be compared and a valid launch decision rendered.

DSIF spacecraft interrogations. Engineering interrogations of *Surveyor* systems from the Deep Space Instrumentation Facility are performed through the CDC to assure that the spacecraft is functioning properly during all phases of its spaceflight and lunar operations. By utilizing a PATE system in conjunction with the CDC, these interrogations can be greatly enhanced to give rapid, automatic evaluations of the telemetered data.

PATE features can be very advantageous to DSIF operation during certain spacecraft maneuvers where time is a constraining factor. As an example, during lunar descent, all systems connected with this phase of operation must be continually monitored. Manual telemetry

evaluation implies the relatively slow process of checking 16 edge-mounted meters for readings within limits supplied either by an overlay or printed page. No reference is possible to previous readings without replay of the magnetic tape recordings. With the PATE, a much faster evaluation of telemetry data can be made, and a printed record of all sampled telemetry channels can be readily accessible to the test operator for reference to previous readings. With the added ability to automatically verify the status of spacecraft systems during the transit phase, operator requirements at the DSIF stations will be minimized by preprogramming the checkout of the spacecraft during each mode of its operation.

6. Launch Operations Plan

The Launch Operations Plan (LOP), the primary planning document for coordination of all operations and tests required for a *Surveyor* launch, has been released during the reporting period.

The LOP controls the launch operations task by defining the scope and overall objectives of the launch, explaining the actual test philosophies and operational plans that will be used, and describing the equipment required. In addition, the plan describes the manpower organization assigned to accomplish the test and includes charts to show the sequence and interaction of major events.

A supplement to the LOP for each flight spacecraft will document the more detailed program planning required for the launch of a particular vehicle. Each supplement will contain the particular launch objectives, the detailed spacecraft configuration, and a plan to indicate the specific test and/or operations directives which will be employed to process the spacecraft.

The LOP provides the Hughes input to the GD/A Detail Flight Test Plan and will be used in conjunction with the GD/A Flight Test Plan to provide the complete plan for launch operations.

The document also establishes requirements for additional, more detailed documentation in the form of test and operational directives to provide specific direction for a particular test or operational phase of the launch operation. For a particular area of the LOP, each directive will:

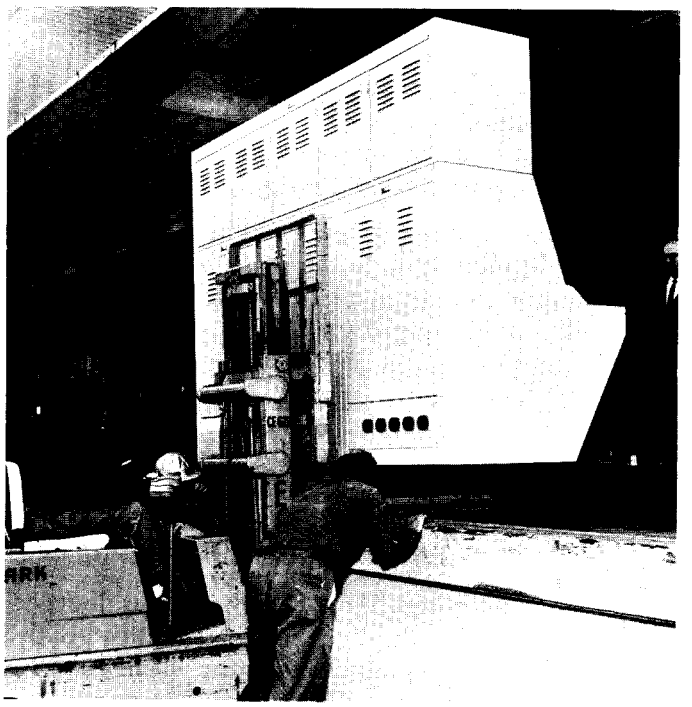

Fig. 98. CDC console being loaded for shipment to Goldstone

(1) Define the purpose, scope, and objectives of a particular test or operational phase.

(2) Provide an operational sequence plan for the various items that constitute the test or operational phase.

(3) Provide a detailed description of the test or operation in question, including equipment, test layout, interconnection diagrams and wiring lists, and basic personnel requirements.

(4) Define the necessary support requirements required during a particular test or operation.

(5) Define the reports and data requirements of the area involved.

7. Command and Data Handling Console (CDC)

The CDC for the Goldstone Deep Space Station was shipped to the station on April 9 (Fig. 98). The CDCs for the other two stations (Canberra and Johannesburg) will be shipped by May 1964.

M. Study on Block II *Surveyor*

1. Introduction

A study on Block II *Surveyor* spacecraft was completed by Hughes Aircraft Company at the request of Jet Propulsion Laboratory and reported in Block II *Surveyor* Study, SSD 4135R, March 1964. The term Block II *Surveyor* refers to spacecraft with as yet unspecified payloads for lunar soft landings in the 1967 through 1969 period. Block I applies to the A-21 and A-21A spacecraft discussed in the preceding sections of this report and scheduled for landing in the 1965 and 1966 period.

The major objective of the study was to evaluate payload capability of the spacecraft, with minimum change to the A-21/A-21A basic bus, under a small number of specific varying conditions. The more significant of these varying conditions were spacecraft separated weight, lunar survival period, trajectory characteristics, and spacecraft propulsion capability. This study did not include formulation of specific configurations.

The basic ground rules employed in the study were as follows:

(1) Minimum change from the Block I spacecraft configuration.

(2) Boost with *Atlas/Centaur* in 1967 through 1969 with injection from a parking orbit.

(3) Midcourse correction capability up to 30 m/sec.

(4) Employment of the Block I *Surveyor/Centaur* interface, including interconnect structure and shroud, without change.

The study assumed an increased spacecraft injected weight capability (2200 to 3200 lb, compared to 2150 lb in Block I). In the study, the lower end of the range (2200 to 2600 lb) was emphasized.

2. Design Alternatives

The major design alternatives considered in the study were as follows:

(1) Two types of vernier engine systems. One system had a restricted throttling range, 3.5:1, with resultant spacecraft thrust-to-weight ratios the same as for *Surveyor* Block I. The other vernier system was assigned an extended thrust range of 20 to 180 lb per chamber.

(2) Two main retro-engine cases. One is the present steel case and the other is a titanium case of improved design.

(3) Two main retro-engine propellants. One is the present propellant with aluminum additive; the other has beryllium additive.

(4) Two transit trajectory classes. They are the 66-hr class used in Block I and the 90-hr class.

The effects of these alternatives on spacecraft dry landed weight are summarized in Table 43.

The maximum and minimum impact velocities are summarized in Table 44. For parking orbit trajectories in the years 1967 through 1969, a range of impact velocities of 2611 to 2687 m/sec for 66-hr transits and of 2512

Table 43. Effect of propulsion and trajectory alternatives on dry landed weight — constant spacecraft injected weight

Alternative	Effect on dry landed weight
Extended throttle range vernier engine system versus restricted throttle range vernier engine system	15- to 16-lb dry landed weight increase for extended throttle range vernier engine system.
Titanium versus steel main retro case	9- to 10-lb dry landed weight increase with titanium case.
Beryllium versus aluminum main retro propellant	Approximately 29-lb dry landed weight increase due to beryllium propellant.
90-hr versus 66-hr transit time	30- to 32-lb dry landed weight increase for 90-hr trajectories at constant injected weight. Approximately 45-lb total dry landed weight increase for 90-hr trajectories with constant Centaur capability.

Table 44. Annual maximum and minimum lunar impact speeds, 1967 to 1969

Year	Time of flight, hr	Impact date	Launch azimuth, deg	Arrival relative to Goldstone operational window	Lunar approach velocity (V_∞), m/sec	Lunar impact velocity (V_I), m/sec
1967	66	2-21-67	90	Early	1128	2629
	66	12-25-67	114	Late	1205	2663
1968	66	12-14-68	114	Late	1231	2675
	66	12-23-68	90	Early	1105	2620
1969	66	8-1-69	90	Early	1085	2611
	66	12-31-69	114	Late	1257	2687
1967	90	3-26-67	114	Late	1020	2585
	90	12-7-67	90	Early	835	2518
1968	90	4-12-68	114	Late	1019	2584
	90	12-26-68	90	Early	826	2515
1969	90	4-2-69	114	Late	997	2576
	90	8-5-69	90	Early	818	2512

to 2585 for 90-hr transits would occur. Spacecraft propellant requirements were determined, based on the maximum velocities of 2687 and 2585 m/sec, consistent with *Surveyor* Block I design practice. The resulting dry landed weights, evaluated parametrically for the injected weight range of 2200 to 2600 lb, ranged from about 620 to 840 lb.

3. Payload Weight Capability

Payload capability was evaluated for 18 combinations of spacecraft design and mission alternatives. The 18 configurations are defined, together with respective weight capability, in Table 45. The payload and injected weights for each configuration are shown graphically in Fig. 99. Table 46 shows weight capability variations at constant spacecraft injected weight.

Maximum payload weight capabilities for the 18 configurations studied range from 157 to 318 lb. The payload weight limit for each of the configurations is established by the maximum volume of main retro propellant that can be accommodated without change of basic spaceframe geometry or *Surveyor/Centaur* interface. Maximum injected weights for the 18 configurations range between 2486 and 2639 lb. The 157-lb payload weight capability is provided when the heaviest power system is combined with the lowest performance propulsion system using a 66-hr trajectory. The 318-lb pay-

Table 45. Summary of configurations

Configuration	Trajectory time, hr	Propulsion design parameters								Electrical power system				
		Main retro-rocket engine						Vernier engine type		Batteries		RTG + two 10-lb batteries	Solar panel	
		Propellant		Nozzle extension		Thermal control								
		Aluminum with steel case	Beryllium with titanium case	0 in.	5.4 in.	Same as A-21A	Modified (additional insulation and heaters)	Extended throttling range	Restricted throttling range	Two large (93 lb)	Two small (45 lb)		Fixed	Movable
A-21A	66	X		X		X			X	See remarks				X
1-A	66	X		X		X			X		X			X
1-B	66	X			X	X			X		X		X	
1-C	66	X			X	X			X			X		X
1-D	66	X			X	X			X	X				X
1-D/90	90	X			X	X			X	X				X
2-A	66	X		X		X		X			X			X
2-B	66	X			X	X		X			X		X	
2-C	66	X			X	X		X				X		X
2-D	66	X			X	X		X		X				X
3-A	66		X	X			X		X		X			X
3-B	66		X		X		X		X		X		X	
3-C	66		X		X		X		X			X		X
3-D	66		X		X		X		X	X				X
4-A	66		X	X			X	X			X			X
4-B	66		X		X		X	X			X		X	
4-B/90	90		X		X		X	X			X		X	
4-C	66		X		X		X	X				X		X
4-D	66		X		X		X	X		X				X

load weight capability is provided when lunar surface survival and wide-band telemetry are not required, and the highest performance propulsion system is combined with a 90-hr trajectory.

4. Power Systems

Power systems considered for Block II fall in two general categories – solar panel-battery, and solar panel-battery-RTG. In all cases, 100% battery redundancy is provided for reliability. Batteries are of the sealed secondary silver-zinc type presently used in Block I, but are sized differently for the landing/limited survival type of mission and for the 30/90-day survival mission with and without RTG. The RTG considered is the SNAP-11. Comparative power source data is summarized in Table 47. For 30/90-day survival missions, the RTG system provides a weight saving of approximately 35 lb, and also permits greater mission flexibility. Because of the use of redundant batteries, the probability of successful flight and landing for all missions considered is in excess of 80%. With the solar panel-battery-RTG system, probability of lunar surface survival is estimated at 0.86 for 30 days and 0.67 for 90 days. A 2-yr survival mission is not considered practicable with present spacecraft design concepts.

5. Landing Accuracy

Landing errors with one midcourse correction are almost entirely a result of errors in the execution of the

Table 45 (continued). Summary of configurations

Configuration	Trajectory time, hr	Telecommunications: High gain antenna: Included	Telecommunications: High gain antenna: Not included	Altitude marking radar: A-21A dish antenna	Altitude marking radar: Modified antenna (planar array)	Spacecraft weight, lb: Injected weight	= weight of expendables	+ dry landed weight: Dry landed weight: Basic bus	Dry landed weight: Payload	Dry landed weight totals	Remarks
						Injected weight	Weight of expendables	Basic bus	Payload		
A-21A	66	X		X		2150	1549	527	74	601	One 46-lb battery on A-21A
1-A	66	X		X		2526	1800	533	193	726	Limited survival
1-B	66		X		X	2568	1829	496	243	739	Limited survival, narrow-band telemetry
1-C	66	X			X	2568	1829	545	194	739	
1-D	66	X			X	2568	1829	582	157	739	
1-D/90	90	X			X	2628	1843	591	194	785	90-hr trajectory
2-A	66	X		X		2563	1811	553	199	752	Limited survival
2-B	66		X		X	2604	1839	517	248	765	Limited survival, narrow-band telemetry
2-C	66	X			X	2604	1839	566	199	765	
2-D	66	X			X	2604	1839	603	162	765	
3-A	66	X		X		2486	1739	536	211	747	Limited survival
3-B	66		X		X	2527	1766	500	261	761	Limited survival, narrow-band telemetry
3-C	66	X			X	2527	1766	549	212	761	
3-D	66	X			X	2527	1766	586	175	761	
4-A	66	X		X		2531	1753	557	221	778	Limited survival
4-B	66		X		X	2572	1779	522	271	793	Limited survival, narrow-band telemetry
4-B/90	90		X		X	2639	1789	532	318	850	90-hr trajectory
4-C	66	X			X	2572	1779	571	222	793	
4-D	66	X			X	2572	1779	608	185	793	

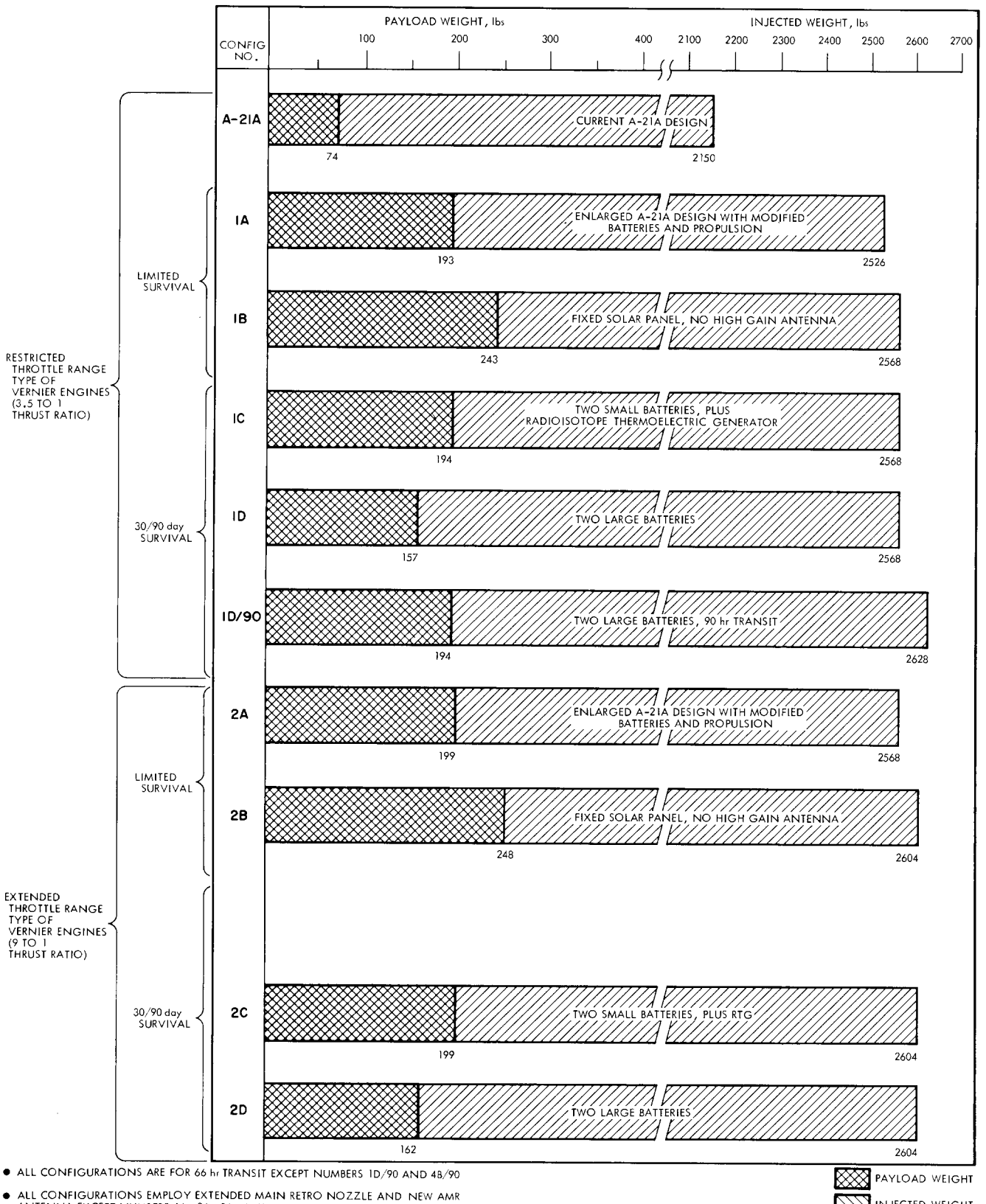

(a) Aluminum propellant, steel retro case

Fig. 99. Maximum payload and injected weight

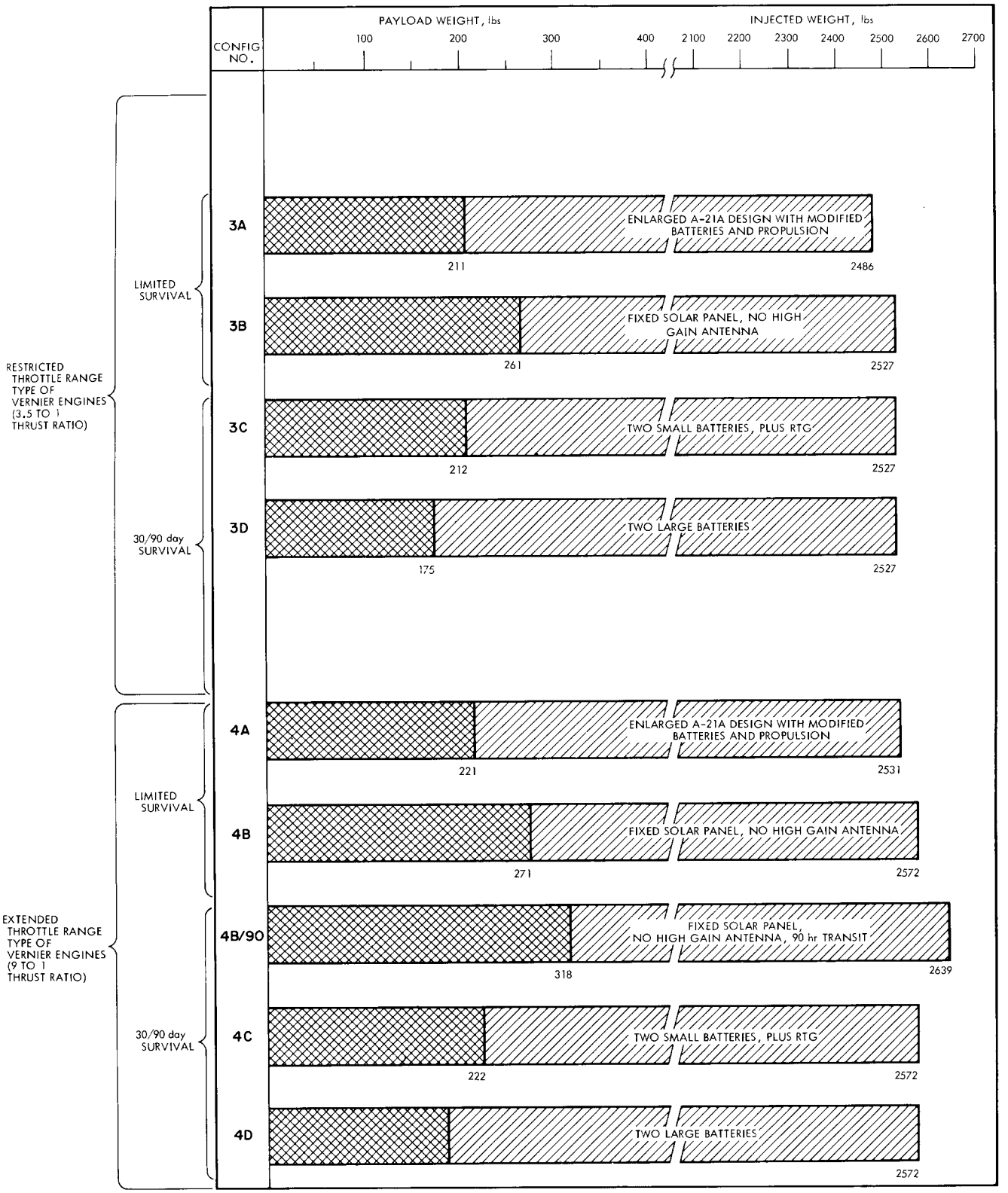

• ALL CONFIGURATIONS EMPLOY HIGH GAIN ANTENNA AND MOVABLE SOLAR PANEL EXCEPT NUMBERS 1B, 2B, 3B, 4B, AND 4B/90.

(b) Beryllium propellant, titanium retro case

Fig. 99 (continued). Maximum payload and injected weight

UNCLASSIFIED

Table 46. Weight breakdown for constant launch vehicle capability corresponding to 2500 lb injected on 66-hr trajectory

Configuration number	Injected weight, lb	Main retro case	Weight of expendables, lb					Total weight expendables	Basic bus, lb						Dry landed weight, lb		Dry landed weight total, lb
			Helium	Nitrogen	Propellant		AMR		Flight control	Electronic	Electrical power	Mechanism	Spacecraft vehicle	Vernier propulsion	Total basic bus	Payload	
					Retro	Vernier											
1-A	2500	153	2.5	4.5	1431	185	8.9	1784.9	48.2	94.8	53.5	27.8	230.6	76.93	531.83	183.2	715
1-B	2500	153	2.5	4.5	1431	185	9.5	1785.5	48.2	85.9	54.8	4.1	223.6	76.93	493.5	221.5	715
1-C	2500	153	2.5	4.5	1431	185	9.5	1785.5	48.2	94.8	66.5	27.8	230.3	76.93	544.5	170.5	715
1-D	2500	153	2.5	4.5	1431	185	9.5	1785.5	48.2	94.8	101.5	27.8	230.6	76.93	579.8	135.2	715
1-D/90	2545	153	2.6	4.5	1424	189	9.5	1782.6	48.2	94.8	101.5	27.8	236.1	77.73	586.1	175.9	762
2-A	2500	153	2.6	4.5	1408	193	8.9	1770.0	48.2	94.8	53.5	27.8	235.9	89.57	549.8	180.2	730
2-B	2500	153	2.6	4.5	1408	193	9.5	1770.6	48.2	85.9	54.8	4.1	228.9	89.57	511.5	218.5	730
2-C	2500	153	2.6	4.5	1408	193	9.5	1770.6	48.2	94.8	66.5	27.8	235.6	89.57	562.5	167.5	730
2-D	2500	153	2.6	4.5	1408	193	9.5	1770.6	48.2	94.8	101.5	27.8	235.9	89.57	597.8	132.2	730
3-A	Not applicable																
3-B	2500	158	2.6	4.5	1385	189	9.5	1748.6	48.2	85.9	54.8	4.1	227.5	77.73	498.2	252.8	751
3-C	2500	158	2.6	4.5	1385	189	9.5	1748.6	48.2	94.8	66.5	27.8	234.2	77.73	549.2	201.8	751
3-D	2500	158	2.6	4.5	1385	189	9.5	1748.6	48.2	94.8	101.5	27.8	234.5	77.73	584.5	166.5	751
4-A	2500	158	2.7	4.5	1359	200	8.9	1733.1	48.2	94.8	53.5	27.8	240.6	90.87	555.8	211.2	767
4-B	2500	158	2.7	4.5	1359	200	9.5	1733.7	48.2	85.9	59.8	4.1	233.6	90.87	517.5	249.5	767
4-B/90	2545	158	2.8	4.5	1348	208	9.5	1730.8	48.2	85.9	64.8	4.1	240.4	92.37	535.8	278.2	814
4-C	2500	158	2.7	4.5	1359	200	9.5	1733.7	48.2	94.8	66.5	27.8	240.3	90.87	568.5	198.5	767
4-D	2500	158	2.7	4.5	1359	200	9.5	1733.7	48.2	94.8	101.5	27.8	240.6	90.87	603.8	163.2	767

UNCLASSIFIED

corrections, and range from 18 km (1σ) at 0-deg incidence to 27 km at 45-deg incidence. The landing error after a second midcourse correction depends in general on both orbit determination and execution errors. For 66-hr trajectories, using doppler and angular data (but not range data), 1σ errors will vary from 2.4 to 8.2 km; with range data, the errors are reduced to 1.8 km to 2.7 km, and result primarily from execution errors. For 90-hr trajectories, the landing errors will be greater than for the 66-hr case if the second maneuver is performed during the second Goldstone pass, but slightly smaller if the maneuver is executed during the third Goldstone pass. To permit the acquisition of range data, modifications must be made in the spacecraft transponder. In addition, provisions must be incorporated to permit use of the spacecraft planar array antenna for receiving to provide ample signal-to-noise ratio of the range-code-modulated signal transmitted from Earth. It is questionable whether the improvements in landing accuracy on the order of two to three provided by ranging justify these spacecraft modifications.

6. Extension of Landing Area

Two methods for extending the *Surveyor* landing area capability were examined (Fig. 100). Method A involves in-flight canting of the AMR antenna. Method B has, in place of canting the AMR, the requirement of a pre-retro attitude maneuver. Both methods also require the addition of a postburnout attitude erection maneuver. It was found that both methods are feasible but Method A has a considerable payload advantage (14.5 lb for a 2150-lb separated weight) over Method B. The equipment additions and changes required for Method A, with the exception of the canting mechanism, are nearly identical with those of B. The reliability estimates favor Method B only very slightly. In-flight canting of the AMR antenna is therefore preferred.

7. Lunar Surface Mobility

It was concluded from a study of liftoff and translation of the *Surveyor* spacecraft along the surface of the Moon that this does not appear to be a feasible means for accomplishing the *Apollo* site certification mission.

Table 47. Energy source and storage considerations

Power system and mission types	Transit time, hr	Transit energy required, w-hr	Transit energy generated, w-hr	Transit energy deficit, w-hr	Recharge time after transit, hr	Lunar night energy required, w-hr	Battery size, w-hr (two each required)	Total battery weight, lb	Total weight of energy sources, lb
Solar panel — battery system	66	6400	5000	1400	20	0	1400	45	54
Limited lunar day survival after landing	90	8600	6800	1800	26	0	1800	55	64
Solar panel — battery system	66	6400	5000	1400	20	~3500 per night	3500	93	102
30- to 90-day survival after landing	90	8600	6800	1800	26	~3500 per night	3500	93	102
Solar panel — RTG-battery system	66	6400	6200	([a])	Less than 3 hr (not required)	~10,500	500	20	67
90-day survival after landing	90	8600	8450	([a])	Less than 3 hr (not required)	~10,500	500	20	67

[a]Insignificant — battery required to supply peak loads only.

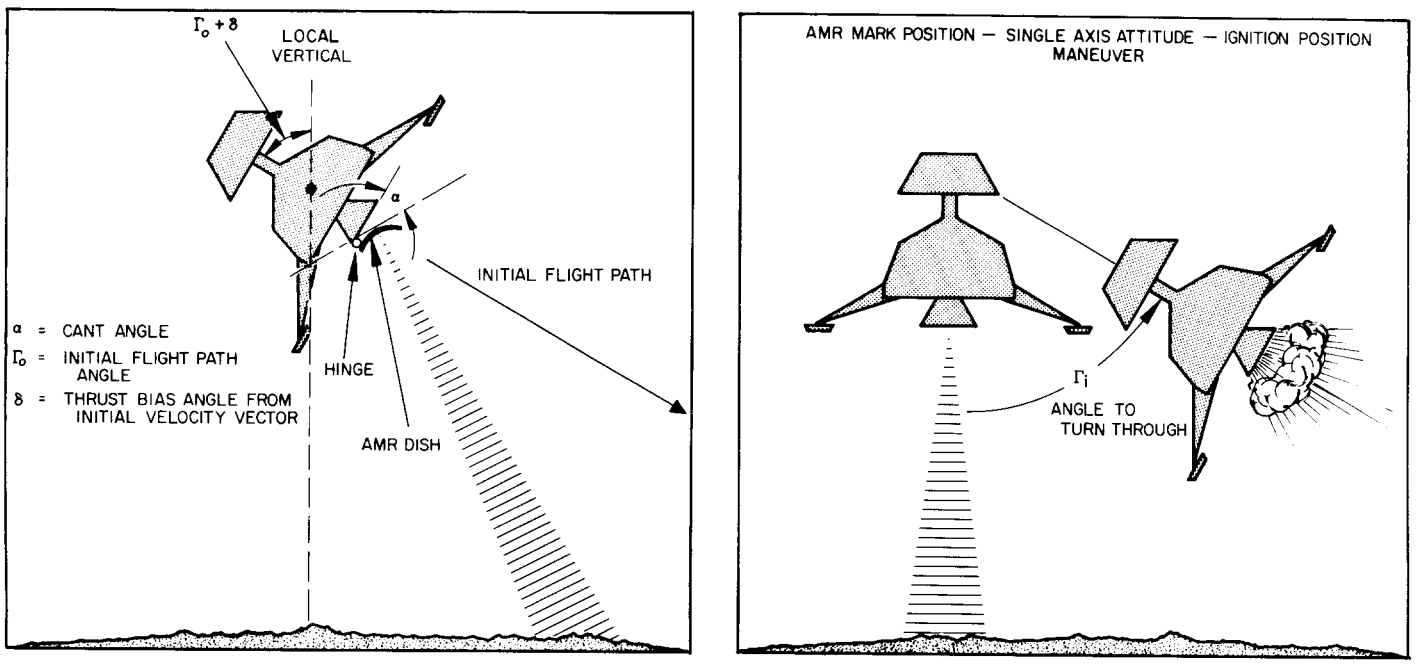

(a) Method A — canting of AMR

(b) Method B — pre-retro maneuver

Fig. 100. Methods of obtaining accurate marking signal